Cross-Layer design for IoT dedicated Healthcare

Namarig Mohemed Taha Abdelrahman Ahmed

Thèse de doctorat

Pour obtenir le grade de Docteur de

l'UNIVERSITÉ POLYTECHNIQUE HAUTS-DE-FRANCE

et de l'INSA HAUTS-DE-FRANCE

UNIVERSITÉ D'AL NEELAIN

Discipline, spécialité selon la liste des spécialités pour lesquelles l'École Doctorale est accréditée :

Sciences et technologies de l'information et de la communication

Présentée et soutenue par Namarig MOHEMED TAHA ABDELRAHMAN AHMED.

Le 24/05/2024, à Valenciennes

École doctorale :
École Doctorale Polytechnique Hauts-de-France (ED PHF n°635)

Unité de recherche :
Institut d'Electronique de Microélectronique et de Nanotechnologie – Site de Valenciennes (IEMN – UMR CNRS 8520)
Laboratoire Télécommunication Engineering - UNIVERSITÉ D'AL NEELAIN

Conception multicouche pour les soins de santé dédiés à l'IoT

JURY

Président du jury
- Mr. Raynald SEVENO. Prof, Université de Nantes.

Rapporteurs
- Mr. Raynald SEVENO. Prof, Université de Nantes.
- Mr. Rabah ATTIA. Prof, University of Tunis.

Examinateurs
- Mr.Iyad Dayoub. Prof, Université Polytechnique Hauts-de-France.
- Mr. Ahmed Mohemed ALhassan. Dr, University Al-Neelain, Sudan.
- Mrs. Khaoula FERCHICHI. Dr, Université du Littoral Cote d'Opale
- Mrs. Tahani Abdalla Attia. Prof, University of Kharthoum.

Directeur de thèse

- Mr. ElHadj Dogheche, Prof, Université Polytechnique Hauts-de-France .
- **Co-directeur de thèse** : Mr.Amin Babiker. Prof, University of Al-Neelain, Sudan.

PhD Thesis

Submitted for the degree of Doctor of Philosophy from

UNIVERSITÉ POLYTECHNIQUE HAUTS-DE-FRANCE

And INSA HAUTS-DE-FRANCE

and, Al NEELAIN UNIVERSITY

Subject:

Information and communication sciences and technologies

Presented and defended by Namarig MOHEMED TAHA ABDELRAHMAN AHMED.

On 24/05/2024, Valenciennes

Doctoral school:

Doctoral School Polytechnique Hauts-de-France (ED PHF n°635)

Research unit:

Institute of Electronics Microelectronics and Nanotechnology – Valenciennes site (IEMN – UMR CNRS 8520)
Telecommunication Engineering Laboratory – Al-NEELAIN University

Cross-Layer design for IoT dedicated healthcare

JURY

President of jury

- Mr. Raynald SEVENO. Prof, Université de Nantes.

Reviewers

- Mr. Raynald SEVENO. Prof, University of Nantes.
- Mr. Rabah ATTIA. Prof, University of Tunis.

Examiners

- Mr. Iyad Dayoub. Prof, Université Polytechnique Hauts-de-France.
- Mr. Ahmed Mohemed ALhassan. Dr, University Al-Neelain, Sudan.
- Mrs. Khaoula FERCHICHI. Dr, Université du Littoral Cote d'Opale
- Mrs. Tahani Abdalla Attia. Prof, University of Kharthoum.

Thesis director
- Mr. ElHadj Dogheche, Prof, Université Polytechnique Hauts-de-France .

Thesis co-director :Mr.Amin Babiker. Prof, University of Al-Neelain, Sudan

Résumé substantiel en langue française

Introduction

L'intégration de l'Internet des objets (IoT) dans le secteur de la santé marque une étape cruciale dans l'évolution des pratiques médicales. L'Internet des objets médicaux (IoMT), qui englobe un réseau de dispositifs médicaux, d'applications logicielles et de services de santé, joue un rôle fondamental pour améliorer les soins aux patients, optimiser le fonctionnement des cliniques et gérer les finances. Avec le nombre d'appareils connectés prévu pour atteindre 22 milliards d'ici 2025, le marché de l'IoMT est sur le point de connaître une croissance significative, annonçant une multitude d'innovations et de tendances dans l'industrie des soins de santé [1]. Cette augmentation de la connectivité facilite non seulement la prolifération des capteurs et des sources de données qui recueillent les informations médicales vitales, mais aussi le développement de passerelles et de réseaux pour une transmission efficace des données, principalement grâce à des réseaux 4G/5G avancés. Les avantages de l'IoT dans les soins de santé, allant de la réduction des coûts et de l'amélioration des résultats du traitement à la surveillance à distance et à l'amélioration de l'efficacité, soulignent sa contribution essentielle à l'avancement des services de santé et des résultats pour les patients.

Ainsi, l'intégration des technologies IoT dans les soins de santé n'est pas seulement un ajout au domaine médical, mais une force transformatrice qui autonomise les patients et les professionnels, favorisant un avenir où les soins de santé sont plus accessibles, précis et centrés sur le patient.

Description du Sujet

L'Internet des objets (IoT) est un concept technologique qui établit la connectivité entre divers appareils et Internet, leur permettant d'échanger des données et de communiquer entre eux. Dans les soins de santé IoT, les réseaux corporels sans fil (WBAN) peuvent être intégrés à d'autres appareils IoT, tels que des passerelles ou des serveurs cloud, pour permettre la surveillance à distance et l'analyse des données de santé des patients. Cette intégration peut offrir aux fournisseurs de soins de santé un accès en temps réel aux données des patients, leur permettant de prendre des décisions éclairées sur les soins aux patients. De plus, l'IoT peut permettre l'application d'analyses de données et d'algorithmes

d'apprentissage automatique aux grandes quantités de données générées par les WBAN, conduisant à une meilleure diagnostic et traitement des affections médicales [2].

Un réseau corporel sans fil (WBAN) utilise des capteurs implantables et portables, placés à la fois à l'intérieur et à l'extérieur du corps humain, dans le but de surveiller les paramètres physiologiques et biochimiques des patients. Les données recueillies sont ensuite transmises à un centre de soins de santé, permettant aux professionnels de la santé de surveiller les signes vitaux. La technologie WBAN a un large éventail d'applications dans les domaines médical, des services d'urgence, de l'électronique grand public, de l'aptitude physique et du suivi du mode de vie, de la défense, du divertissement et de la santé personnelle [3]. La communication WBAN nécessite des attributs spécifiques, notamment des exigences de débit de données minimal, une distance de transmission limitée, une consommation d'énergie réduite et l'évitement des perturbations des autres équipements électroniques et médicaux, tout en assurant une livraison rapide et fiable des données. Les normes PAN existantes ne répondent pas aux demandes uniques des WBAN [3]. La responsabilité de proposer une norme de communication pour le réseau corporel (BAN) a été confiée au groupe de travail 6 de l'IEEE, qui devrait développer la norme IEEE 802.15.6. La norme prendra en compte les exigences de transmission à courte portée et de qualité de service (QoS), notamment la fiabilité et la latence, ainsi que la faible consommation d'énergie des appareils BAN [4].

L'utilisation des WBAN dans les soins de santé IoT présente plusieurs avantages. Les WBAN sont non invasifs et confortables à porter pour les patients sur une période prolongée, permettant une surveillance continue de la santé des patients. La surveillance en temps réel des données de santé des patients peut fournir aux prestataires de soins de santé des informations opportunes et précises, permettant une détection précoce des problèmes médicaux et des interventions en temps opportun. De plus, l'intégration des WBAN avec d'autres appareils IoT peut permettre l'application d'analyses de données et d'algorithmes d'apprentissage automatique aux données, conduisant à une meilleure diagnostic et traitement des affections médicales. L'un des défis critiques dans la conception des WBAN pour les systèmes de soins de santé IoT est d'assurer une transmission de données fiable et économe en énergie. La fiabilité de la transmission des données est essentielle pour garantir que les prestataires de soins de santé reçoivent des informations précises et opportunes sur la santé des patients, tandis que l'efficacité énergétique est cruciale pour prolonger la durée de vie des appareils de soins de santé IoT [5]. La conception multicouche est une approche qui a été proposée pour relever ces défis en permettant la coopération des différentes couches de la pile de protocoles réseau afin d'optimiser les performances du réseau. En utilisant la conception multicouche, les différentes couches de la pile de protocoles peuvent travailler ensemble pour optimiser les performances du réseau plutôt que de fonctionner

indépendamment. Cela peut conduire à une utilisation plus efficace des ressources réseau, à de meilleures performances réseau et à une durée de vie prolongée des appareils.

Objectifs

Les principaux objectifs de cette étude sont :

- Examiner l'état actuel de l'art de la conception multicouche pour les soins de santé IdO et identifier les lacunes et les défis de recherche dans ce domaine.
- Proposer un cadre de conception multicouche pour les soins de santé IdO qui puisse répondre aux exigences de fiabilité, d'efficacité énergétique et de mise à l'échelle de différentes applications de soins de santé IdO.
- Évaluer les performances et l'efficacité du cadre de conception multicouche proposé à travers des simulations et des expériences.
- Comparer les performances de l'approche de conception multicouche proposée avec les approches existantes et identifier les avantages et les limites de l'approche proposée.
- Fournir un aperçu approfondi des défis et des opportunités de la conception multicouche dans les systèmes d'Internet des objets pour les soins de santé, et proposer des solutions permettant d'améliorer ces systèmes.
- Analyser les implications et l'applicabilité en contexte réel des modèles proposés, en tenant compte des défis potentiels et des opportunités d'intégration dans d'autres techniques.

Contributions

- Pour relever ces objectifs, les principales contributions de ce travail sont résumées comme suit :
- Un examen approfondi des techniques de conception multicouche à la pointe de la technologie pour les soins de santé IdO met en évidence les lacunes et les défis de la recherche. Cet examen constituera une base pour approfondir la recherche dans ce domaine.
- Faire progresser le domaine de la conception multicouche pour les soins de santé IdO en fournissant un cadre complet, en évaluant ses performances et en offrant des perspectives sur ses défis et opportunités pour une mise en œuvre pratique.
- Mettre en œuvre et développer le protocole PHY/MAC dans le cadre de la norme IEEE 802.11ah afin d'améliorer l'efficacité du réseau, d'assurer une transmission fiable des données et d'atténuer l'impact des pertes de trajet du corps.

- Améliorer la fiabilité et les performances de la communication entre les appareils portables et les points d'accès, garantissant ainsi une transmission de données précise et opportune.

Etat de l’art dans le domaine

La nature des ressources limitées des appareils IoT présente des défis importants, notamment en termes de consommation d'énergie et de qualité de service (QoS). Les protocoles de communication multicouches ont émergé comme une solution prometteuse pour relever ces défis en optimisant les interactions entre les différentes couches de la pile réseau.

Dans une conception multicouche pour les soins de santé IdO, la couche physique peut être utilisée pour collecter les données des capteurs sur le corps du patient, tandis que la couche réseau peut être utilisée pour transférer ces données aux praticiens de santé en temps réel. La couche application peut ensuite être utilisée pour présenter les données aux fournisseurs de soins de santé d'une manière facile à comprendre et à exploiter.

Cette revue de la littérature explore les avancées récentes dans les protocoles de communication multicouches pour la santé IoT, en se concentrant sur l'efficacité énergétique et la qualité de service

Les auteurs dans [6] ont discuté des défis posés par les réseaux IdO (Internet des Objets) à contraintes énergétiques et peu fiables. Ils ont présenté une conception à couches croisées fiable pour les applications de santé électronique IdO afin d'étendre la durée de vie des appareils IdO et de transmettre les données avec une grande fiabilité. Les auteurs ont proposé d'intégrer la couche liaison de données (MAC) et la couche réseau, en incorporant des paramètres liés à la fiabilité dans le processus de découverte de la route. Cela a renforcé la robustesse du réseau, permettant une surveillance précise des informations de santé des patients. Cependant, l'étude n'a pas pris en compte l'impact de plusieurs appareils IdO ou la mise à l'échelle du réseau. De plus, elle n'aborde pas les problèmes potentiels de confidentialité et de sécurité associés aux applications de santé électronique IdO, qui sont des considérations cruciales dans les milieux de soins de santé.

Dans [7], les auteurs ont proposé une technique d'optimisation de la conception à couches croisées (CLDO) qui dépend de la durée de vie des WBAN (réseaux corporels sans fil) sur plusieurs couches. Ce schéma optimise l'efficacité énergétique, la fiabilité de la transmission et la durée de vie des WBAN en choisissant des nœuds de relais optimisés, en améliorant la puissance de transmission des nœuds et en déterminant des tailles de paquets appropriées pour les différents liens du réseau. Le schéma CLDO améliore la fiabilité de la transmission

de plus de 44,6 % et prolonge la durée de vie jusqu'à 33,2 %. L'article présente une approche globale pour optimiser les performances dans les WBAN. Cependant, le travail n'a pas mentionné les limites du schéma CLDO ou les défis et les inconvénients potentiels associés à sa mise en œuvre.

Dans [6], les auteurs ont proposé un protocole à couches croisées pour les réseaux de l'Internet des Objets (IoT), en particulier dans le domaine des soins de santé, afin de résoudre le problème des interférences causées par le corps humain et les mouvements sur le signal transmis par le nœud capteur. Le protocole utilise des mesures d'énergie de balise dans la couche physique du nœud pour détecter les interférences, qui sont ensuite utilisées par la couche MAC pour prendre des décisions sur la transmission des paquets. Les résultats des expériences démontrent l'efficacité du protocole proposé pour atténuer les interférences causées par le corps humain, ce qui peut améliorer les performances et la fiabilité des réseaux IoT dans le domaine de la santé. Cependant, l'article n'analyse pas l'impact du protocole proposé sur d'autres métriques de performance, comme la consommation d'énergie ou la latence, et les expériences menées pour évaluer les performances du protocole étaient limitées à un scénario spécifique qui ne représente peut-être pas fidèlement les conditions du monde réel.

Selon [7], les auteurs ont proposé la création d'un système d'évaluation de la sécurité en tant que service (SAaaS) pour le secteur des soins de santé, qui peut identifier les vulnérabilités, évaluer et atténuer les menaces dans un écosystème de soins de santé IoT exposé à des appareils et interfaces externes. Le système SAaaS vise à fournir un environnement contrôlé et conscient de la cybersécurité qui assure la confidentialité, la sécurité et la confiance, même dans des appareils et des environnements non fiables. Cependant, le travail n'a pas abordé les limites ou les défis potentiels qui pourraient survenir lors de la mise en œuvre pratique du système SAaaS.

L'enquête dans [8] a passé en revue diverses méthodologies utilisées pour optimiser les performances des WBAN à travers une conception de protocole multi-couches. La recherche a discuté de l'importance des WBAN pour surveiller divers paramètres de santé, tels que la fréquence cardiaque, la température corporelle, la respiration et la pression artérielle, en se concentrant sur l'avantage des WBAN pour surveiller la santé sans affecter l'activité du patient et en insistant sur l'optimisation des performances des WBAN grâce à la conception multi-couches. L'étude présente une étude comparative des méthodologies utilisées pour optimiser les performances et met en évidence la comparaison des performances des protocoles. Cependant, le travail a prêté peu d'attention aux défis et aux limites de la conception de protocoles multi-couches dans les WBAN.

L'enquête [9] se concentre sur les spécifications MAC, PHY et de sécurité de la norme IEEE 802.15.6. La recherche couvre différents modes de communication et mécanismes d'accès. Elle examine les spécifications de communication à bande étroite (NB), à ultra-large bande (UWB) et de communication par le corps humain (HBC) en termes de structure de trame, de modulation et d'autres paramètres essentiels. L'étude met en évidence les services et le paradigme de sécurité de la norme IEEE 802.15.6, fournissant des informations sur les protocoles et les spécifications de sécurité essentielles pour les WBAN. Cependant, l'étude n'a pas fourni d'analyse des performances de la norme IEEE 802.15.6 dans des scénarios réels, ce qui pourrait limiter son applicabilité pratique. De plus, elle n'a pas fourni d'analyse de cette norme par rapport aux autres normes existantes pour les WBAN, ce qui pourrait limiter la compréhension de ses avantages et de ses inconvénients.

Dans [10], les auteurs ont proposé un algorithme de calcul de confiance cross-layer léger pour détecter les attaques Man-in-Middle (MIMA) dans les systèmes de santé IoT. Cet algorithme a deux principales contributions : un regroupement (clustering) efficace sur le plan énergétique et la détection d'attaques cross-layer. L'algorithme de regroupement sélectionne le Chef de Grappe (CH) optimal en utilisant une approche de calcul et d'évaluation de probabilité. L'approche d'évaluation de la confiance cross-layer introduit une évaluation des nœuds pour détecter les attaquants MIMA dans le réseau. Le calcul de la confiance de chaque nœud est effectué en utilisant les paramètres du nœud capteur dans différentes couches, telles que les couches réseau, physique et MAC. La valeur de confiance agrégée de chaque nœud capteur est ensuite comparée à la valeur de seuil pour déterminer si le nœud est un attaquant. L'approche proposée montre que IC-MADS présente de meilleures performances contre les attaques MIMA avec un minimum de surcharge et de consommation d'énergie.

Dans [11], les auteurs ont proposé une approche cross-layer pour la confidentialité de la localisation des appareils cellulaires de e-santé. Cette approche s'appuie sur le beamforming et le bruit artificiel pour protéger la confidentialité de la localisation des appareils cellulaires de e-santé, leur permettant de communiquer de manière sécurisée avec la station de base. Le système proposé comprend un patch de détection, un module d'algorithme, une plateforme cloud et un terminal mobile. Le système proposé peut fournir un niveau élevé de confidentialité de la localisation, même en présence de plusieurs eavesdroppers, et est robuste aux changements environnementaux. De plus, les techniques de beamforming et de bruit artificiel réduisent la consommation d'énergie des appareils cellulaires de e-santé, ce qui se traduit par une autonomie accrue.

Proposition d'une technique d'optimisation de la conception à couches croisées (CLDO) pour les WBAN, optimisant l'efficacité énergétique, la fiabilité de la transmission et la durée de vie des WBAN.

Reference	Description	Routing Mechanism	Energy Effeciency	QoS
[2]	Proposition de conception à couches croisées pour les applications de santé électronique IdO afin d'étendre la durée de vie des appareils et d'assurer une transmission fiable des données.	✓	✓	✗
[5]	Proposition d'une technique d'optimisation de la conception à couches croisées (CLDO) pour les WBAN, optimisant l'efficacité énergétique, la fiabilité de la transmission et la durée de vie des WBAN.	✓	✓	✗
[6]	Protocole à couches croisées pour résoudre les interférences dans les réseaux IoT de santé causées par le corps humain et les mouvements.	✗	✓	✗
[7]	Création d'un système d'évaluation de la sécurité en tant que service (SAaaS) pour le secteur des soins de santé, visant à identifier les vulnérabilités et atténuer les menaces.	✓	✗	✗

[8]	Revue des méthodologies pour optimiser les performances des WBAN via la conception de protocole multi-couches.	✓	✓	✗
[9]	Focus sur les spécifications MAC, PHY et de sécurité de la norme IEEE 802.15.6 pour les WBAN.	✓	✗	✓
[10]	Algorithme de calcul de confiance cross-layer léger pour détecter les attaques Man-in-Middle (MIMA) dans les systèmes de santé IoT.	✓	✗	✓
[11]	Approche cross-layer pour la confidentialité de la localisation des appareils cellulaires de e-santé utilisant le beamforming et le bruit artificiel.	✗	✗	✓
Cette recherche	Création d'un nouveau protocole à couches croisées pour atténuer l'impact de l'affaiblissement du signal dû au corps dans les réseaux IEEE 802.11ah. Amélioration de la fiabilité et des performances de communication entre les dispositifs portables et les points d'accès, garantissant une transmission de données précise et en temps opportun.	✓	✓	✓

References

[1] Mohammad Aminul Islam, Kazi Zehad Mostofa, Hamidreza Mohafez, Md Jakir Hossen, Foo Wah Low, Mikhail Vasiliev, Syed Mohammed Shamsul Islam, and Mohammad Nur-E-Alam. "17 Combination of Sensors-Based Monitoring System and Internet of Things (IoT)." In: Non-Invasive Health Systems based on Advanced Biomedical Signal and Image Processing (2024), p. 413.

[2] Stephanie B. Baker, Wei Xiang, and Ian Atkinson. "Internet of Things for Smart Healthcare: Technologies, Challenges, and Opportunities." In: IEEE Access 5 (2017), 26521–26544. Issn: 2169-3536. DOI: 10.1109/access. 2017.2775180. URL: http://dx.doi.org/10.1109/access.2017. 2775180.

[3] Furqan Jameel, Shurjeel Wyne, Dushantha Nalin K. Jayakody, Georges Kaddoum, and Richard O'Kennedy. "Wireless Social Networks: A Sur- vey of Recent Advances, Applications and Challenges." In: IEEE Ac- cess 6 (2018), 59589–59617. Issn: 2169-3536. DOI: 10.1109/access. 2018.2872686. URL: http://dx.doi.org/10.1109/access.2018. 2872686.

[4] Hadda Ben Elhadj, Lamia Chaari, and Lotfi Kamoun. "A Survey of Routing Protocols in Wireless Body Area Networks for Healthcare Ap- plications." In: International Journal of E-Health and Medical Com- munications 3.2 (Apr. 2012), 1–18. Issn: 1947-3168. DOI: 10 .4018 / jehmc.2012040101. URL: http://dx.doi.org/10.4018/jehmc. 2012040101.

[5] Mohammad Ghamari, Balazs Janko, R. Sherratt, William Harwin, Robert Piechockic, and Cinna Soltanpur. "A Survey on Wireless Body Area Net- works for eHealthcare Systems in Residential Environments." In: Sensors 16.6 (June 2016), p. 831. Issn: 1424-8220. DOI: 10.3390/s16060831. URL: http://dx.doi.org/10.3390/s16060831.

[6] P. Sarwesh, N. S. V. Shet, and K. Chandrasekaran, "Reliable cross layer design for e-health applications—iot perspective," in Cognitive Computing for Big Data Systems Over IoT, pp. 97–113, Springer, 2018.

[7] X. Chen, Y. Xu, and A. Liu, "Cross layer design for optimizing transmission reliability, energy efficiency, and lifetime in body sensor networks," Sensors, vol. 17, no. 4, p. 900, 2017.

[8] P. Sharavanan, R. Kumar, and D. Sridharan, "A comparative study of cross layer protocols in wban," Australian journal of basic and applied sciences, vol. 9, pp. 294–300, 2015.

[9] S. Ullah, M. Mohaisen, and M. A. Alnuem, "A review of ieee 802.15. 6 mac, phy, and security specifications," International Journal of Distributed Sensor Networks, vol. 9, no. 4, p. 950704, 2013.

[10] A. Kore and S. Patil, "Ic-mads: Iot enabled cross layer man-in-middle attack detection system for smart healthcare application," Wireless Personal Communications, vol. 113, no. 2, pp. 727–746, 2020.

[11] S. Tomasin, "Beamforming and artificial noise for cross-layer location privacy of e-health cellular devices," in 2022 IEEE International Conference on Communications Workshops (ICC Workshops), pp. 568–573, IEEE, 2022

ABSTRACT

Wireless Body Area Networks (WBANs) are wireless sensor networks that consist of small, low-power wearable or implantable devices placed on or inside the human body to monitor physiological signals such as heart rate, blood pressure, and body temperature. WBANs have emerged as a potentially transformative technology in healthcare, enabling the continuous monitoring of patient health, remote diagnosis and treatment, and personalized healthcare services. WBANs in IoT healthcare offer several advantages, including noninvasive monitoring, real-time data transmission, and integration with other IoT devices for data analytics and machine learning. However, designing WBANs for IoT healthcare systems presents challenges such as ensuring reliable and energy-efficient data transmission. A cross-layer design is an approach that has been proposed to address these challenges by enabling the cooperation of different layers of the network protocol stack to optimize network performance.

This dissertation aimed to enhance IoT healthcare by implementing and developing a new PHY/MAC protocol within the IEEE 802.11ah framework. This protocol aims to improve the network efficiency, extend the sensor life, and ensure the quality and reliability of data transmission. It adapts to varying data types by modifying the superframe structure based on the adaptive modulation features of IEEE 802.11ah. This study explores the intricacies and potential of cross-layer design in IoT healthcare, offering innovative solutions to boost system performance and efficiency. By conducting simulations and experiments, this study will assess the effectiveness of this approach by comparing it to existing methods. Ultimately, it seeks to provide actionable strategies for developing IoT healthcare systems that fulfil the demands of reliability, energy conservation, and scalability in diverse healthcare scenarios.

RESUMÉ

Les réseaux sans fil pour les zones corporelles (WBAN) sont un type de réseau de capteurs sans fil composé de petits dispositifs portables ou implantables à faible puissance, placés sur ou à l'intérieur du corps humain pour surveiller des signaux physiologiques tels que la fréquence cardiaque, la tension artérielle et la température corporelle. Les WBAN se sont révélés être une technologie potentiellement transformative pour les soins de santé, permettant une surveillance continue de la santé des patients, un diagnostic et un traitement à distance, ainsi que des services de soins de santé personnalisés. L'utilisation des WBAN dans les soins de santé de l'IoT présente plusieurs avantages, notamment la surveillance non invasive, la transmission en temps réel des données et l'intégration avec d'autres dispositifs de l'IoT pour l'analyse des données et l'apprentissage automatique. Cependant, la conception des WBAN pour les systèmes de soins de santé de l'IoT présente des défis, tels que la garantie d'une transmission fiable et économe en énergie des données. La conception en couches croisées est une approche qui a été proposée pour relever ces défis en permettant la coopération entre différentes couches de la pile de protocoles réseau afin d'optimiser les performances du réseau.

Cette thèse vise à améliorer les soins de santé de l'IoT grâce à la mise en œuvre et au développement d'un nouveau protocole PHY/MAC dans le cadre de la norme IEEE 802.11ah. Ce protocole vise à améliorer l'efficacité du réseau, à prolonger la durée de vie des capteurs et à garantir la qualité et la fiabilité de la transmission des données. Il s'adapte aux différents types de données en modifiant la structure de la supertrame en fonction de la fonction de modulation adaptative de l'IEEE 802.11ah. La recherche explorera les subtilités et le potentiel de la conception en couches croisées dans les soins de santé de l'IoT, en proposant des solutions innovantes pour améliorer les performances et l'efficacité du système. En effectuant des simulations et des expériences, l'étude évaluera l'efficacité de cette approche, en la comparant aux méthodes existantes. En fin de compte, elle vise à fournir des stratégies opérationnelles pour le développement de systèmes de soins de santé de l'IoT répondant aux exigences de fiabilité, d'économie d'énergie et de dimensionnement dans divers scénarios de soins de santé..

DEDICATION

I would like to acknowledge everyone who played a role in accomplishing this thesis.

To my beloved parents,

You have been my unwavering pillars of support, guiding me with your wisdom, and showering me with unconditional love. Your sacrifices and devotion shaped me into the person I am today. This thesis is a testament to the values you instilled in me and the beliefs you had in my abilities. Thank you for always being there and for being my constant source of strength.

To my beloved husband,

You have been my partner in every sense of the word. Your unwavering support and understanding your belief in my abilities, even during the most challenging times, have given me the strength to persevere. Thank you for standing on my side.

To my precious children, Roua, Ammar, Amro, and Monzer,

You are the light of my life and my greatest motivation. Throughout this journey, you have been my cheerleader, my reason for pushing boundaries, and my source of boundless joy. Your innocent laughter and unwavering beliefs in me have been my driving forces. I dedicate this thesis to you, my beautiful children, with the hope that it serves as a reminder of the importance of lifelong learning and the pursuit of knowledge. May it inspire you to fearlessly chase your dreams and know that I am forever proud of you.

To all my family,

Each and every one of you has played a significant role in my life journey. Your love, encouragement, and belief in me have been the foundations upon which I built my aspirations. Thank you for always believing me.

To all my dear friend,

Thank you for your unwavering friendship and for standing by me during challenging times.

ACKNOWLEDGEMENT

First of all, I would like to express my deep and respectful gratitude to my PhD supervisors, **Pr. Amin BABIKER**, Professor at Al Neelain University Engineering School of Sudan, and **Pr. El Hadj DOGHECHE**, Professor at Université Polytechnique Hauts-de-France, for the trust they have placed in me by agreeing to supervise my doctoral work. May they find in this work the expression of my deep gratitude.

I would also like to thank **Dr. Ahmed Mohamed ALHASSAN**, assistant professor at Al Neelain University Engineering School of Sudan and **Pr. Iyad DAYOUB**, Professor at Université Polytechnique Hauts-de-France, for their advice, support, patience, and exceptional seriousness. I am also thankful for their assistance.

My deepest thanks go to the members of my defense committee who agreed to judge my thesis. My sincere gratitude goes to **Pr. Raynald SEVENO** Professor at Université de Nantes and **Pr. Rabah ATTIA**, Professor at Université de Tunis for accepting to be the reviewers of this thesis report and for giving me the honor to judge this work with great interest.

Furthermore, I would like to thank **Pr. Tahani Abdallah** Professor at Khartoum University Engineering School of Sudan and **Dr. Khaoula FERCHICHI** , Dr at Université du Littoral Cote d'Opale.

No words can express my gratitude to my colleagues in the Telecommunication and IEMN laboratories for their exchanges and administration help, in addition to the wonderful moments we shared.

Contents

LIST OF FIGURES

LIST OF TABLES

ACRONYMS

AMC	Adaptive Modulation and Coding
AODV	Ad-hoc on-demand distance vector
ARQ	Automatic Repeat Request
AID	Association Identifier
API	Application Programming Interface
AP	Access Point
BER	Bit Error Rate
BLE	Bluetooth Low Energy
BPSK	Binary Phase Shift Keying
BSSID	Basic Service Set Identifier
CAEM	Channel Adaptive Energy Management
CCA	Clear Channel Assessment
CP	Cyclic Prefix
CSMA/CA	Carrier Sense Multiple Access with Collision Avoidance
CLASS	Cross-Layer Signaling Shortcuts
CLD	Cross-Layer Design
CLDO	Cross-Layer Design Optimization
CLS	Clear to-Send
CLRS	Cross-Layer Retransmit Strategy

CLASS Cross-Layer Signaling Shortcuts

CQI Channel Quality Indicator

CW Contention Window

DCF Distributed Coordination Function

DIFS DCF Interframe Spaces

DSP Digital Signal Processing

ECG Electrocardiogram

FEC Forward Error Correction

FPGA Field Programmable Gate Arrays

GMSK Gaussian Minimum Shift Keying

I/Q Phase/Quadrature

HTTP Hypertext Transfer Protocol

IoT Internet of Things

ICU Intensive Care Unit

ISI Inter Symbol Interference

LLN Low Power and Lossy Networks

LOS Line-of-Sight

MH Multi-Hop

MIMA Man-In-Middle Attack

MIMO Multiple-Input Multiple-Output

NLOS Non-Line-of-Sight

NUM Network Utility Maximization

OFDM Orthogonal Frequency-Division Multiplexing

OSI Open Systems Interconnection

PHY Physical- Layer

PDR Packet Delivery Ratio

QPSK Quadrature Phase Shift Keying

QoS Quality Of Service

RAW Restricted Access Window

RFID Radio-Frequency Identification

RTS/CTS Request To Send/Clear To Send

SH Single Hop

SDR Software Defined Radio

SIFS Short Interframe Spaces

SNR Signal to Noise Ratio

STA station

TCP/IP Transmission Control Protocol/Internet Protocol

TDD Time-Division Duplexing

TGah IEEE 802.11ah Task Group

UHD USRP Hardware Driver

USRP Universal Software Radio Peripheral

WBAN Wireless Body Area Networks

WSN Wireless Sensor Network

XLF Cross-Layer Framework

XLM Cross-Layer Module

XLP Cross-Layer Protocol

1

INTRODUCTION

Contents

The integration of the Internet of Things (IoT) into the healthcare sector marks a pivotal evolution in medical practices, enhancing patient care and operational efficiency. The Internet of Medical Things (IoMT), encompassing a network of medical devices, software applications, and healthcare services, plays a fundamental role in patient care, clinic optimization, and financial management. With the number of connected devices projected to reach 22 billion by 2025, the IoMT market is on course to expand significantly, indicating a broad spectrum of innovation and trends within the healthcare industry [1]. This surge in connectivity facilitates not only the proliferation of sensors and data sources that capture vital medical information but also the development of gateways and networks for efficient data transmission, predominantly through advanced 4G/5G networks. The benefits of IoT in healthcare, ranging from cost reduction and improved treatment outcomes to remote monitoring and enhanced efficiency, underscore its critical contribution to advancing healthcare services and patient outcomes. Thus, the integration of IoT technologies in healthcare is not merely an addition to the medical field but a transformative force that empowers patients and professionals alike, fostering a future where healthcare is more accessible, accurate, and patient-centric.

1.1 THESIS CONTEXT

The Internet of Things (IoT) is a technological concept that establishes connectivity between various devices and the Internet, enabling them to exchange data and communicate with each other. In IoT healthcare, wireless body area networks (WBANs) can be integrated with other IoT devices, such as gateways or cloud servers, to enable remote monitoring and analysis of patient health data. This integration can offer healthcare providers real-time access to patient data, enabling them to make informed decisions about patient care. Additionally, IoT can enable data analytics and machine learning algorithms to be applied to the large amounts of data generated by WBANs, leading to improved diagnosis and treatment of medical conditions [2].

A Wireless Body Area Network (WBAN) utilizes implantable and wearable sensors, positioned both internally and externally on the human body, for the purpose of monitoring the physiological and biochemical parameters of patients. The gathered data is subsequently transmitted to a healthcare center, allowing healthcare practitioners to monitor vital signs. WBAN technology has a wide range of applications in the domains of medical, emergency services, consumer electronics, health fitness and lifestyle monitoring, defense, entertainment, and personal health [3].

WBAN communication requires specific attributes, including minimal data rate requirements, limited transmission distance, reduced power usage, and avoidance of disruption to other electronic and medical equipment, coupled with the assurance of prompt and dependable data delivery. The existing PAN standards fall short of meeting the unique demands of WBANs [3]. The responsibility of proposing a communication standard for the Body Area Network (BAN) has been assigned to the IEEE Task Group 6, which is expected to develop the IEEE Standard 802.15.6. The standard will consider the short-range transmission and Quality of Service (QoS) requirements, including reliability and latency, as well as the low energy consumption of BAN devices [4]

The use of WBANs in IoT healthcare has several advantages. WBANs are non-invasive and comfortable for patients to wear for an extended period of time, enabling ongoing patient health monitoring. Real-time monitoring of patient health data can provide healthcare providers with timely and accurate information, leading to early detection of medical conditions and timely interventions. Additionally, the integration of WBANs with other IoT devices can enable data analytics and machine learning algorithms to be applied to the data, leading to improved diagnosis and treatment of medical conditions. One of the critical challenges in designing WBANs for IoT healthcare systems is to ensure reliable and energy-efficient data transmission. The reliability of data transmission is essential to ensure that healthcare providers receive accurate and timely information about patient health, while energy efficiency is crucial to extending the lifetime of IoT healthcare devices [5]. Cross-layer design is an approach that has been proposed to address these challenges by enabling the cooperation of different layers of the network protocol stack to optimize network performance. By using cross-layer design, the different layers of the protocol stack can work together to optimize network performance rather than operating independently. This can lead to more efficient use of network resources, improved network performance, and extended device lifetime.

1.2 MOTIVATIONS

The motivation for this work is to investigate the cross-layer design for IoT healthcare and to develop a cross-layer protocol between the physical layer (PHY) and medium access control (MAC) layer to mitigate pathloss and increase the throughput of the network that relies on the IEEE 802.11ah standard, improve the lifetime of the network and sensor nodes, ensure service quality, and provide reliable transmission. Based on the adaptive modulation supported by this standard, the protocol considers the transmission requirements for various data types and modifies the superframe. The physical (PHY)

and media access control (MAC) refer to two important layers of the OSI (Open Systems Interconnection) reference model, which is a conceptual framework used to describe the functions of a networking system [6].

PHY (Physical Layer)

The Physical Layer (often abbreviated as PHY) is the lowest layer in the OSI model. It is responsible for the physical connection between devices, including the transmission and reception of raw bitstreams over a physical medium. Key functions and characteristics of the PHY layer include:

- Transmission Media: Specifies the physical medium through which data is transmitted, such as copper cables, fiber optics, or wireless signals.
- Data Encoding: Converts data into signals suitable for the transmission medium. This can involve modulation techniques for analog transmission or line coding for digital transmission.
- Bit Rate Control: Manages the speed at which data is transmitted, which can vary depending on the medium and the technology used.
- Synchronization: Ensures the transmitter and receiver are synchronized to interpret the bitstream correctly.
- Interface Standards: Defines electrical, mechanical, procedural, and functional specifications to ensure interoperability between different devices and systems (e.g., Ethernet, USB, Bluetooth).

MAC (Medium Access Control) Layer

The Medium Access Control (MAC) layer is a sublayer of the Data Link layer (Layer 2) in the OSI model. It is responsible for controlling how devices on a network gain access to the medium and permission to transmit data. Key functions of the MAC layer include:

- Access Control: Determines how devices share the medium and avoid collisions, using protocols like CSMA/CD (Carrier Sense Multiple Access with Collision Detection) in Ethernet networks or CSMA/CA (Carrier Sense Multiple Access with Collision Avoidance) in Wi-Fi networks.
- Frame Delimiting: Defines the start and end of frames, which are units of transmission at the Data Link layer.

- Addressing: Uses MAC addresses to uniquely identify devices on a network, ensuring that data is sent to the correct destination.
- Error Detection: Incorporates mechanisms like CRC (Cyclic Redundancy Check) to detect errors in transmitted frames.
- Flow Control: Manages the rate of data transmission to prevent overwhelming a receiver, ensuring efficient and reliable communication.

This study aims to contribute to the development of IoT healthcare by providing insights into the challenges and opportunities in cross-layer design and proposing solutions that can improve the performance and efficiency of IoT healthcare systems. The study also evaluates the performance and efficiency of the proposed cross-layer design approach through simulations and experiments and compares the results with existing approaches. The ultimate goal of this research is to provide practical guidance for the design of IoT healthcare systems that can satisfy the reliability, energy efficiency, and scalability requirements of different healthcare applications.

1.3 OBJECTIVES

The primary objectives of this study are as follows:

- Review of the current state-of-the-art of cross-layer design for IoT healthcare and identify research gaps and challenges in this area.
- Propose a framework for cross-layer design in IoT healthcare that can address the reliability, energy efficiency, and scalability requirements of different IoT healthcare applications.
- Evaluate the performance and efficiency of the proposed cross-layer design framework through simulations and experiments.
- Compare the performance of the proposed cross-layer design approach with existing approaches and identify the benefits and limitations of the proposed approach.
- Provides insights into the challenges and opportunities in cross-layer design for IoT healthcare and proposes solutions that can improve the performance and efficiency of IoT healthcare systems.

- Discussion of the implications and real-world applicability of the proposed models, considering potential challenges and opportunities for integration into other techniques.

1.4 CONTRIBUTIONS

To address these objectives, the main contributions of this work are summarized as follows:

- A comprehensive review of the state-of-the-art cross-layer design techniques for IoT healthcare highlights research gaps and challenges. This review will provide a foundation for further research in this area.
- Advance the field of cross-layer design for IoT healthcare by providing a comprehensive framework, evaluating its performance, and offering insights into its challenges and opportunities for practical implementation.

1.5 THESIS OUTLINE

The remainder of this thesis is organized as follows:

Chapter 2 presents an overview of IoT healthcare and its applications. It reviews existing cross-layer design approaches for IoT healthcare, analyzes the state of the art in cross-layer design, and identifies research gaps and challenges that need to be addressed.

Chapter 3 describes the features of the IEEE 802.11ah standard, which is a pivotal technology in the realm of IoT for healthcare. This study aimed to provide a comprehensive understanding of how this standard can be utilized to address the unique demands of healthcare applications. We examined the standard's network architecture, explored the motivations behind its development, and identified specific healthcare use cases. Additionally, the chapter details the physical (PHY) and medium access control (MAC) layer designs, highlighting how they cater to the requirements of long-range communication, low power consumption, and efficient channel management. The insights gained form the foundation for implementing IoT solutions that are both effective and sustainable in healthcare environments.

Chapter 4 focuses on addressing the challenges posed by body-path loss in 802.11ah networks, particularly in healthcare IoT applications. Our approach involves a novel PHY-MAC cross-layer design aimed at mitigating the effects of body-path loss. This chapter outlines the body path loss problem, introduces the cross-layer design concept, and explores methods for enhancing the performance of 802.11ah networks in this context. We also discuss the assumptions and considerations underlying our approach, followed by a detailed presentation of the simulation results to demonstrate the efficacy of the proposed solutions. The chapter concludes with an analysis of the findings and their implications for future IoT healthcare network designs.

In Chapter 5, we present a practical approach to implementing Cross-Layer Design Adaptive Modulation and Coding (AMC) for IEEE 802.11ah, tailored for IoT healthcare applications, using Universal Software Radio Peripheral (USRP) and GNU Radio. The focus is on bridging the gap between theoretical design and real-world applications. We explore the background and significance of this implementation, describe the architecture of the platform, and delve into the system design and programming. This chapter details the specific steps of the cross-layer implementation and evaluates the prototype through the implementation of different transceivers: BPSK, QPSK, and GMSK.

Finally, the conclusions of this study and some perspectives are presented in section 6.

2

LITERATURE REVIEW

Contents

2.1 INTRODUCTION

This chapter explores the dynamic field of IoT healthcare, beginning with an overview that encapsulates applications revolutionizing patient care and medical processes. We then narrowed our focus to the role of Wireless Body Area Networks (WBANs) as a critical component in IoT healthcare, enabling real-time patient monitoring and data collection. A critical review examined existing cross-layer design approaches that enhance the efficiency and reliability of IoT healthcare systems.

In an analysis of state-of-the-art cross-layer design, we scrutinize the latest methodologies and their contributions to the field. Finally, we identify and discuss the research gaps and challenges that persist, setting the stage for future innovations in IoT healthcare. This chapter comprehensively synthesizes the current trends and future directions in cross-layer design for IoT healthcare applications.

2.2 OVERVIEW OF IOT HEALTHCARE

The Internet of Things (IoT) is a network of interconnected devices that communicate over the Internet without human intervention. It has revolutionized various industries, including healthcare, where it offers cutting-edge solutions for remote patient monitoring, real-time health tracking, and improved healthcare delivery. The IoT-enabled healthcare sector has the potential to revolutionize patient outcomes, enhance care quality, and reduce costs. For instance, a sleep monitoring system device based on IoT can track and analyze sleep patterns, providing valuable insights into sleep quality [7]. Wearable technologies such as fitness trackers and smartwatches can collect data on health metrics, enabling remote monitoring and analysis. The integration of IoT and cloud computing in healthcare has also gained traction, allowing for the digital monitoring, assessment, and secure storage and analysis of health data [8]. Overall, IoT has revolutionized the healthcare sector by enabling a wide range of applications and solutions.

2.2.1 Benefits of IoT in Healthcare

The integration of IoT in healthcare has the potential to enhance the quality of care, improve patient outcomes, and reduce healthcare costs. Table 2.1 represents the different benefits of IoT healthcare [9].

2.2.2 IoT Applications in Healthcare

Integrating the Internet of Things (IoT) into healthcare has led to a paradigm shift in the delivery of medical services, ushering in novel avenues for enhancing patient outcomes and introducing economically viable healthcare solutions. Moreover, the application of IoT in healthcare has catalyzed the emergence of intelligent hospitals, wherein medical apparatus and equipment are seamlessly interconnected via a central network. This interconnected facilitates real-time surveillance and administration of hospital assets, encompassing bed occupancy rates, equipment availability, and patient flow dynamics. In turn, this engenders a more streamlined and effective mode of dispensing healthcare services [10]. Additionally, IoT integration within the healthcare domain engenders the automation of diverse processes and workflows, thereby alleviating the burden healthcare professionals bear while ensuring punctual and accurate execution of tasks. Figure 2.1 shows the different applications of IoT in healthcare.

IoT applications in healthcare can be described as follows [12].

- Remote Patient Monitoring: monitoring of vital signs and health parameters using wearable devices and sensors.
- Telemedicine: Facilitating remote consultations, diagnostics, and treatment through IoT-enabled telehealth services.
- Smart Hospitals: Connecting medical devices and equipment to a central network for real-time monitoring and management.
- Medication Management: Ensuring timely and accurate medication adherence through IoT-enabled reminders and tracking.
- Health and Wellness Tracking: Monitoring fitness, activity levels, and health metrics for proactive health management.

Table 2.1: benefits of IoT healthcare

Improved Patient Outcomes	**Increased Efficiency**	**Cost Savings**
IoT networks can send real-time data to healthcare providers, enabling them to make informed decisions about patient care and treatment options. • Better diagnosis and monitoring of chronic conditions. • Remote monitoring of the patient's vital signs. • Early detection of diseases.	IoT networks can automate many routine tasks, freeing healthcare providers to focus on more strategic initiatives. • Real-time access to patient data. • Automation of administrative tasks. • Reduction of manual data entry.	IoT networks can significantly reduce healthcare costs by streamlining procedures and reducing unnecessary hospital visits. • Preventive care reduces the risk of costly medical procedures. • Automation of administrative tasks reduces staffing requirements.

- Disease Management: Personalized treatment plans based on IoT-generated patient data for chronic disease management.

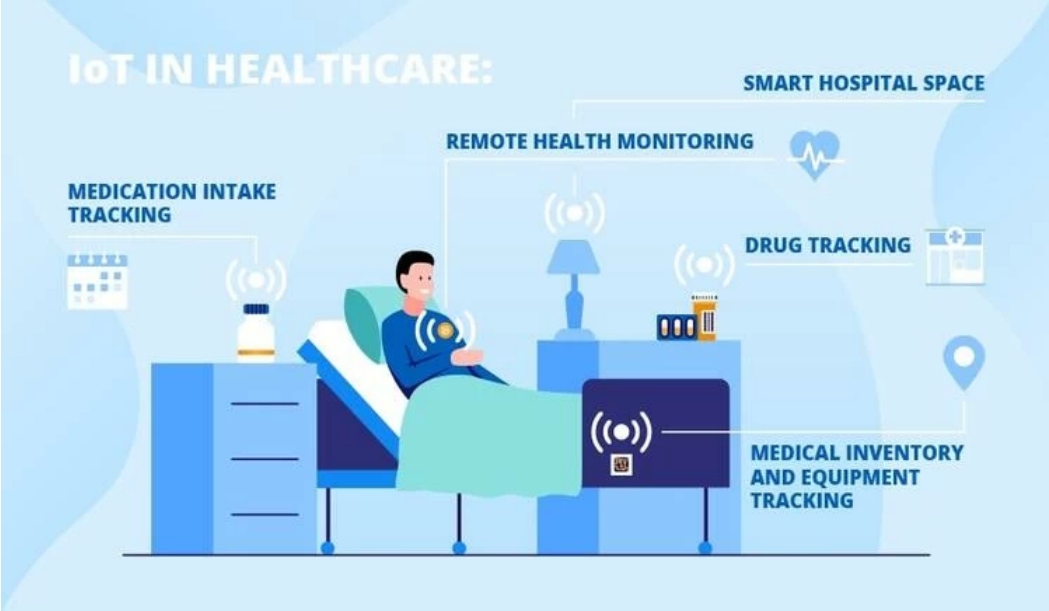

Figure 2.1: Applications of IoT in healthcare [11]

2.2.3 IoT Healthcare Architecture

One promising next-generation technology that provides data-driven insights to improve healthcare systems is health-related IoT [13]. To allow information flow and accurate decision-making, e-health design must incorporate various devices in an interoperability system, apps, and back-end systems. Data flow architecture focuses on data sources, destinations, and paths. The data is saved locally or delivered immediately to the sink without storage. The path includes a gateway that processes and stores the data [14]. The IoT architecture for e-health applications is shown in Figure 2.2.

2.2.4 IoT Network Topology

IoT network topology is divided into three categories: point-to-point network, star topology, and mesh topology. The IoT should be mobile to provide advantages to the system. Most low-power wide-area network (LP-WAN) technologies are used in star network topology, despite the existence of cellular networks and Wi-Fi [15].

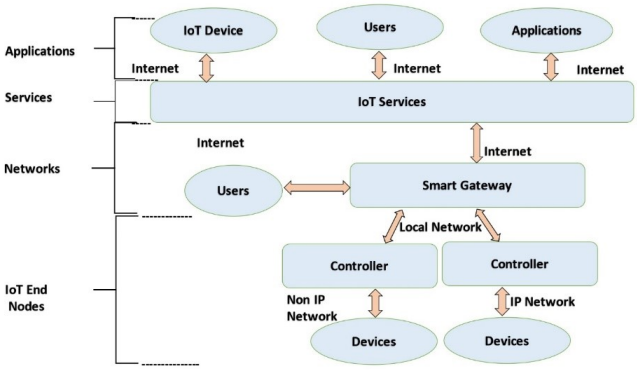

Figure 2.2: IoT architecture for e-healthcare application

- Point-to-point topology is a network configuration in which two nodes are connected directly through a shared link, enabling the transmission between them to utilize the entire bandwidth of the link. This connection can be established using the physical length of a wire or cable; however, it can also be achieved through alternative means, such as satellite or microwave links.

- In star topology, there is a central access point that connects and communicates with all stations in the network. The benefit of this configuration is that the access point manages the intricacies of the network, requiring each station to transmit its signal at an appropriate time or within its designated frequency range. However, one limitation of the star topology is that radio communication between the access point and stations can become lengthy, resulting in increased power requirements for transmitting messages as the distance between a station and the access point increases.

- The mesh topology is a network configuration in which all access points and sensor devices are interconnected. In this topology, the connections between nodes are established randomly. Figure 2.3 illustrates IoT network topologies [15].

2.3 WIRELESS BODY AREA NETWORK (WBAN)

WBAN is a wireless communication network that revolves around the human body as the central focus of communication. Advancements in microelectronics, integrated circuits, system-on-chip design, wireless communication, and low-power sensors have significantly contributed to the development of WBAN. WBAN can be seen as an evolution

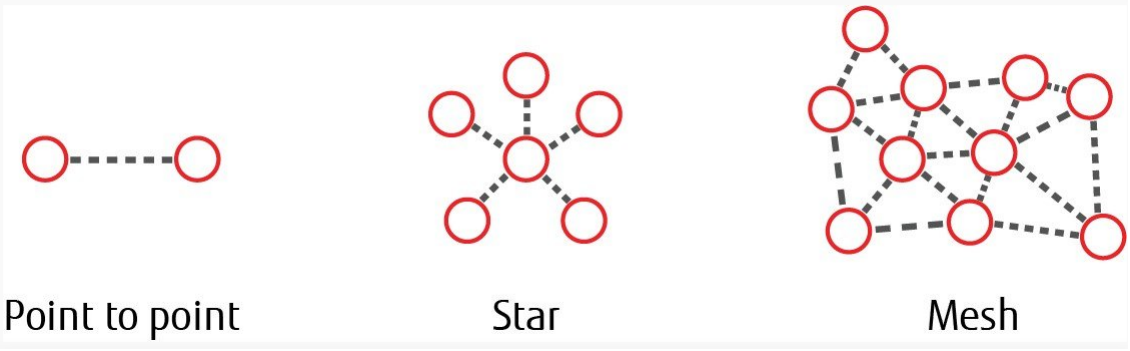

Figure 2.3: IoT network topologyies

of wireless sensor networks, specifically tailored for wearable and implanted technologies, and has become increasingly important in the field of networking. WBAN offers a valuable solution for the remote and seamless monitoring of the human body. Numerous studies and research papers have discussed various aspects of WBAN, including its definitions, architectures, and applications [[16], [17], [18]]. The growth of WBAN has been driven by various trends, such as an increasing population. However, most existing studies in this field have primarily focused on theoretical performance improvements. To standardize WBAN, the IEEE 802 organization established a Task Group known as IEEE 802.15.6 in November 2007. The main objective of this group is to develop a communication standard specifically optimized for low-power and high-reliability applications in BANs (Body Area Networks) [19].

2.4 WBAN ARCHITECTURE

2.4.1 WBAN Components

The development of a Wireless Body Area Network (WBAN) has introduced a novel technology that functions as a three-tier body network, as shown in Figure 2.4. These tiers are:

- Tier 1 (Intra-BAN): Data are collected by the body sensor nodes (BSN) and forwarded to the coordinator in this tier.

- Tier 2 (Inter-BAN): The data received in this tier are processed by the coordinator and transmitted to the sink node.
- Tier 3 (Extra-BAN): In this tier, packets are transmitted from the sink to the health center through the internet [20].

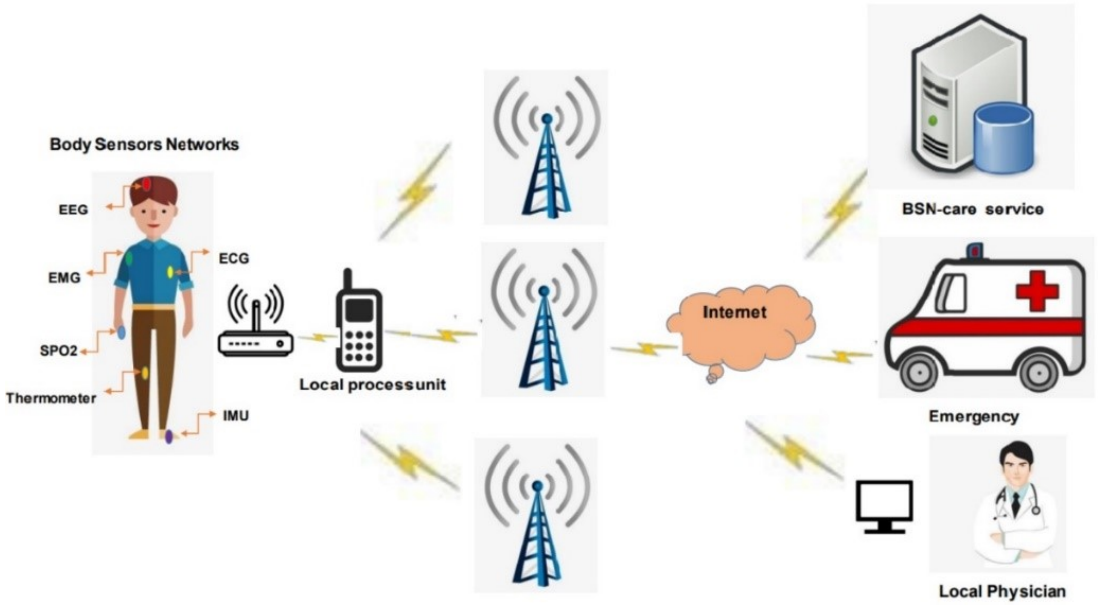

Figure 2.4: WBAN architecture

2.4.2 WBAN Type of Nodes

In WBAN, sensors have the capability to monitor, process, and transmit various information about the human body and vital signs, providing feedback to both the user and the medical entity. There are three types of nodes, based on their functions.

1. Sink or Coordinator: This node serves as the interface between users and sensors/actuators. It acts as a gateway connecting the WBAN to the external world or to another WBAN. It is often referred to as a personal device, such as a watch or phone [179].

2. Sensors: These nodes are responsible for measuring body parameters and forwarding them. Sensors can be placed either inside or on the human body. These can be categorized as end nodes or routers. The end nodes perform specific applications and

communicate directly with the gateway. Routers, however, act as intermediate nodes that relay messages between other nodes and the gateway.

3. Actuators: Actuators are intelligent sensors that are equipped with electromechanical devices. They can perform actions based on the information received from sensors. For example, a system may consist of a sensor that detects blood sugar levels and an actuator that delivers insulin.

2.5 WBAN CLASSIFICATION

WBAN for healthcare systems can be divided into two groups [20].

- **Vital Signs Monitoring:** Sensors that monitor vital parameters are employed in these applications to identify emergencies and allow caregivers to respond efficiently. These sensors are wearable (on-body), implanted (in-body), or mounted on a patient's body (off-body). Furthermore, they are used to monitor various vital indicators, including electromyography (EMG), temperature, electroencephalogram (EEG), electrocardiogram (ECG), heart rate, blood pressure, respiration rate, glucose level, walking and running, and mental status.
- **Remote Health Care Surveillance:** This term refers to non-essential services that do not require the continuous presence of a healthcare expert. For example, body sensors have been used to collect clinically relevant information for rehabilitation, monitor older people, and provide advice and support to people with disabilities [20].

2.6 WBAN TECHNOLOGIES

WBANs are designed for communication between small, low-power devices located on the human body or near it. These networks enable the monitoring and exchange of vital information for healthcare, fitness, and other applications. To support seamless and efficient communication in WBANs, specialized technologies and standards have been developed.

- **IEEE 802.11ah standard**

  This standard operates at frequencies below 1 gigahertz. It is designed for IoT applications that require long-range connectivity, low power consumption, and the ability to support several devices. The standard, also known as Wi-Fi Hallow, provides broader coverage compared to previous Wi-Fi standards like 802.11n or 802.11ac, making it suitable for rural applications, industrial automation, smart homes, and other IoT deployments [21]. IEEE 802.11ah offers improved penetration through walls and other obstacles by utilizing the sub-1 gigahertz frequency spectrum, enabling reliable connectivity over longer distances. It aims to achieve low data rates, allowing devices to conserve power and operate for extended periods on battery power.

- **IEEE 802.15.6 standard**

  The IEEE working group has established a standard for the physical power, (PHY) layer, and data link layer (Medium Access Control (MAC)) for wireless body area networks (WBAN)[22]. This standard was designed for low-power short-range communication in and around the human body. It supports a data rate of 971.4 Kbps across 79 channels. The modulation techniques used in WBAN include binary phase-shift keying (BPSK), quadrature phase-shift keying (QPSK), and Gaussian Minimum Shift Keying (GMSK). WBAN can operate in frequency bands of 400 MHz, 800 MHz, 900 MHz, and 2.4 GHz.

- **IEEE802.15.4 and ZigBee standard**

  IEEE 802.15.4 is a standard designed for low-rate wireless personal area networks (LR-WPANs). It specifies physical layer (PHY) and medium access control (MAC) protocols for low-cost wireless communication between fixed, portable, and moving devices with no batteries or very limited battery consumption. ZigBee is a suite of high-level communication protocols built on top of the IEEE 802.15.4 standard. It was designed to create personal area networks with small, low-power digital radios, such as home automation, industrial control, medical device data collection, and other low-power, low-frequency needs. Devices compatible with ZigBee are sometimes referred to as supporting point-to-point or point-to-multipoint topologies. ZigBee defines the network and application layers for LR-WPANs. The maximum supported data rate using this standard is 250 kbps. It provides a robust communication infrastructure suitable for WBANs[23].

- **Bluetooth Low Energy (BLE) standard**

  Bluetooth Low Energy (BLE) is a set of short-range wireless communication protocols developed by the Bluetooth Special Interest Group (SIG) as a wireless sensor network (WSN) standard with low power requirements, operating within the 2.4 GHz band used by classic Bluetooth [24] [25]. BLE, also known as Bluetooth Smart, is another widely used protocol for WBANs. It is designed for low-power consumption and short-range communication. BLE is particularly well-suited for wearable devices, as it enables seamless connectivity with smartphones and other devices. However, BLE uses different channels and a lower rate of 200 kb/s compared to 1-3 Mbps per second achieved by classic Bluetooth. It should be noted that BLE does not support mesh networks but only supports a single packet type. BLE uses the direct sequence spread spectrum (DSSS) as its spreading technique and provides three profile definitions for applications: healthcare, sports, and consumers. It is important to note that BLE is not compatible with classic Bluetooth. However, Bluetooth 4.0's dual-mode capability facilitates a direct interface between the two standards, where the protocols share a single physical radio and antenna.

- **IPv6 over Low-Power Wireless Personal Area Networks (6LoWPAN standard)**

  6LoWPAN, also known as IPv6 over Low-Power Wireless Personal Area Networks, is a protocol designed to enable the transmission of IPv6 packets over low-power wireless networks, including WBANs (Wireless Body Area Networks). Its purpose is to seamlessly integrate WBANs into the Internet of Things (IoT) ecosystem. By implementing 6LoWPAN, efficient communication is ensured, and interoperability with existing network infrastructure is facilitated. These protocols provide specific specifications for communication, data exchange, and interoperability within WBANs. They are tailored to address the unique challenges presented by low-power, short-range networks. As a result, healthcare professionals, researchers, and consumers can take advantage of the advancements in wearable technology and remote monitoring, benefiting from the capabilities offered by 6LoWPAN [26].

Table 2.2 provides a comparative analysis between these standards In this analysis, we will examine the key features and advantages of IEEE 802.11ah in comparison with other prominent wireless standards used in the IoT ecosystem.

Table 2.2: Comparative Analysis of IEEE 802.11ah and Other Wireless Standards for IoT

Feature	**IEEE 802.11ah**	**Bluetooth Low Energy (BLE)**	**LoRaWAN**	**Zigbee**
Frequency Band	Sub-1 GHz (864-868 MHz, 902-928 MHz)	2.4 GHz	Sub-1 GHz	2.4 GHz
Range	Up to 1 km	Up to 100 m	Up to 15 km	Up to 100 m
Data Rate	Up to 347 Mbps	Up to 2 Mbps	Up to 50 kbps	Up to 250 kbps
Power Consumption	Low	Very Low	Ultra-Low	Low
Network Topology	Star, Mesh	Star, Mesh	Star, Mesh	Star, Mesh, Cluster Tree
Security	128-bit AES encryption	128-bit AES encryption	128-bit AES encryption	128-bit AES encryption
Application Focus	Smart Metering, Surveillance, Industrial IoT	Wearables, Personal IoT	Long-range, Low-power IoT	Home/Building Automation, Personal IoT

2.7 WBAN COMMUNICATION LAYERS

The physical layer

The physical layer in a WBAN has unique characteristics related to radio propagation and mobility that differ from those of typical large-scale sensor networks. These characteristics are influenced by the movement of the human body and the placement of sensors, both on the body and implanted. The wearer's posture and sensor location affect the antenna performance. It is essential to minimize the transmission power to conserve energy and minimize the interference with the wearer. Three factors, namely body path loss (BPL), receiver noise Figure (RNF), and Signal-to-Noise Ratio (SNR), affect the transmission power of sensor nodes when wirelessly transmitting data. SNR depends on

the quality of the communication link, RNF is device-dependent, and BPL is influenced by the antenna type and radiation pattern [27].

The responsibilities of the physical layer include the frequency selection, signal detection, modulation, and encryption. For on-body sensors, frequency bands such as 13.5 MHz, 5-50 MHz, 400 MHz, 600 MHz, 900 MHz, 2.4GHz, and 3.1-10.6 GHz are used. The Federal Communication Commission (FCC) has allocated a frequency band of 402-405 MHz for Medical Implant Communication Services (MICS) [28]. This frequency band was chosen because it is ultra-low power, unlicensed, and does not interfere with other radio spectrum users.

The Media Access Control layer (MAC)

The MAC (Media Access Control) layer plays a crucial role in Wireless Body Area Networks (WBANs). It is responsible for managing the access to the shared wireless medium and ensuring efficient communication between the various devices within the WBAN. The MAC layer coordinates the access to the shared wireless channel among the different devices, such as sensors, actuators, and the central coordinator or gateway, using mechanisms like CSMA/CA or TDMA [29]. Additionally, the MAC layer is responsible for managing the power consumption of the WBAN devices, implementing techniques like duty-cycling to conserve energy. It also provides support for different Quality of Service (QoS) requirements, ensuring low latency for real-time applications and high reliability for critical data. Furthermore, the MAC layer is responsible for maintaining synchronization among the WBAN devices, which is necessary for implementing scheduled access mechanisms and coordinating activities like data collection and transmission. Finally, the MAC layer can also play a role in implementing security measures, such as device authentication and data encryption, to protect the WBAN from unauthorized access and ensure the confidentiality of the transmitted data. The specific implementation of the MAC layer in WBANs can vary depending on the particular WBAN standard or protocol used, but it remains a crucial component for the efficient and reliable operation of Wireless Body Area Networks.

The network layer

The network layer in a Wireless Body Area Network (WBAN) plays a crucial role in the overall functionality and performance of the network. It typically employs specialized routing protocols that consider the unique characteristics of the body-centric environment, such as limited device power, dynamic topology, and user mobility. These protocols aim to optimize energy efficiency, minimize latency, and ensure reliable data delivery. The network layer is also responsible for assigning and managing the unique

addresses of WBAN devices, enabling communication and identification within the network [30]. Additionally, the network layer implements Quality of Service (QoS) mechanisms to prioritize and manage different types of data traffic, ensuring that critical data is delivered in a timely and reliable manner. Given the limited power resources of WBAN devices, the network layer plays a crucial role in managing and optimizing power consumption, using techniques like duty cycling, energy-aware routing, and the coordination of sleep/wake cycles to extend the overall lifetime of the WBAN. Finally, the network layer must enable seamless integration with other networks, such as the Internet or healthcare information systems, to facilitate the exchange of data and the connectivity of WBAN devices, which may involve the use of gateway devices or the implementation of standardized protocols and interfaces.

In WBAN, nodes are typically not required to route packets to other nodes in the network layer. However, recent research suggests that multihop routing in WBAN is more suitable [31] to ensure low transmission power, energy efficiency, and efficient data routing by distributing the routing load across the network. Additionally, routing is possible when multiple WBANs communicate via their coordinators. WBAN coordinators can leverage cooperative and multihop body-to-body communication to extend the end-to-end network connectivity.

2.8 WBAN ROUTING PROTOCOLS

Routing is a significant challenge in WBANs, particularly in critical and emergency scenarios, and has garnered considerable research attention [32]. Over the past decade, numerous routing protocols have been proposed. Many of these protocols are adaptations of the traditional strategies to suit the WBAN context. One of the primary concerns in WBAN is minimizing power consumption when transmitting data between sensors and the sink (or vice versa). Therefore, an efficient routing protocol is crucial for addressing this issue. A comparative analysis of energy-efficient routing in a WBAN was presented in [33]. This analysis can be conducted based on various parameters, and routing protocols can be categorized according to their objectives into different categories [34]: posture-based routing, temperature-based routing (in-body), cluster-based routing, QoS-based routing, and cross-layer-based routing protocols, and cluster-based routing protocols. Moreover, these protocols can be divided into two categories: intra-WBAN routing protocols and inter-WBAN routing protocols [35]. Figure 2.5 shows these protocols.

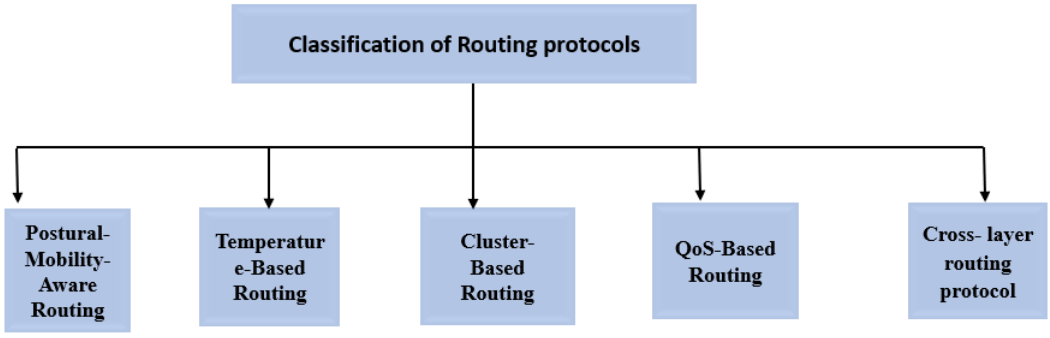

Figure 2.5: Classification of WBAN Routing protocol

2.8.1 Postural-Mobility-Aware Routing Protocols

The structure of Wireless Body Area Networks (WBANs) can experience division as a consequence of body movements or limited transmission ranges of short-range RF signals. Such network division can lead to communication disruptions between nodes and create challenges for data routing. To tackle these issues, researchers have devised various protocols that consider the cost factor of communication. This cost factor evaluates power consumption, which is calculated as the ratio of the total power consumed in the network to the average packets delivered to the sink [36]. These protocols focus on minimizing the cost of data packet transmission between the patient's body and the coordinator. Different protocols contradict advanced and other basic protocols based on power consumption, average access time, mobility, and PDR (Packet Delivery Ratio). These protocols are shown in Table 2.3

2.8.2 Temperature-Based Routing protocols

The increase in temperature caused by the processing and communication in devices can pose a risk to the surrounding tissues and harm the human body. Where The Specific Absorption Rate (SAR) [40] represents the quantity of radiation density that the tissue absorbs per unit weight, as calculated by a specific equation 2.1.

Table 2.3: Postural-Mobility-Aware Routing Protocols

Ref	**Protocol**	**Objective**	**Energy consumption**	**Avg. Latency**	**PDR**
[35]	Posture aware-dynamic data delivery (PA-DDD)	Efficient and dynamic data delivery	0.1 mW	Very low	Average 73.63%
[36]	Distance vector routing postural link costs (DVRPLC)	average latency decreasing	0.75 mW	2.38 s	81-89%
[37]	Opportunistic	Enhancement in the network lifespan	1.5 mW	Not applicable	Not applicable
[38]	Prediction-based secure and reliable (PSR) routing framework	Reduction in security and reliability	2 mW	High	Up to 80%
[39]	Network management cost minimization framework (NCMD)	Dynamic environment topological fracture treatment	0.5 mW	High	Not applicable

$$\text{SAR} = \frac{\sigma |E|^2}{\rho} \text{(W/Kg)} \tag{2.1}$$

Where σ refers to the electrical conductivity of the tissue. E relates to the electric field that is generated as a result of radiation, and ρ is the tissue's density.

Additionally, prolonged exposure to high temperatures can damage devices used for long-term monitoring. To address this issue, a set of protocols [[41], [42]] has been proposed to minimize the heat generated by these devices. Thermal-aware routing protocols are specifically designed to ensure that the temperature increase remains within a predefined threshold. This means that data transmission among sensors should be dispersed across the network rather than relying on a single route. The primary objective of the temperature-based routing method is to prevent nodes from experiencing temperature increases or promptly lowering their temperature. This was achieved by avoiding high-temperature nodes and establishing suitable paths. Figure 2.6 shows a routing schematic.

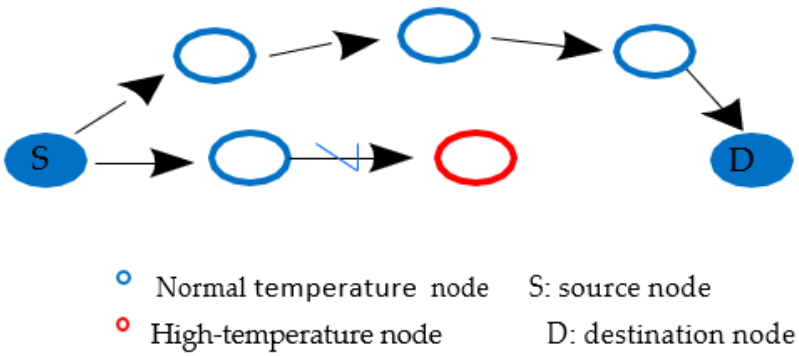

Figure 2.6: Temperature-sensing routing

In conclusion, every temperature-sensitive routing protocol aims to minimize the temperature increase in implanted body nodes. Table 2.4 presents a comparison with other advanced techniques based on factors such as temperature rise, latency, packet discarding mechanism, address scheme, packet distribution ratio, and energy usage.

Table 2.4: Temperature-Sensitive Routing

Reference	**Protocol**	**Objective**	**Energy consumption**	**Temperature rise**	**Delay**
[40]	Thermal aware routing algorithm (TARA)	Reducing the overheating	1.6 mW	High	High
[43]	Adaptive least temperature routing (ALTR)	Reducing latency	0.4 mW	Low	Medium
[44]	Trust thermal routing protocol (TTRP)	Avoid hotspot creation	0.5 mW	low	Low
[45]	Mobility adaptive threshold thermal multihop protocol (MATTEMPT)	Reducing energy usage and rise in temp	0.32 mW	Low	Low

2.8.3 Cluster-Based Routing protocols

Clustering is a method of dividing a network into distinct subnetworks or clusters, with each cluster having a designated cluster head responsible for gathering sensor data from its cluster and transmitting it to the sink node [46]. Cluster-based routing in Wireless Body Area Networks (WBANs) is inspired by Wireless Sensor Networks (WSNs) and has proven effective in addressing global constraints. Through clustering, network connectivity is ensured, energy consumption is managed, and overall network robustness is improved. In this approach, body nodes are divided into groups based on specific criteria, with a designated cluster head in each group responsible for collecting data from nodes and transmitting it to the coordinator. Communication between body nodes is only possible through the cluster head. The comparison of cluster-based protocols is provided in Table 2.5.

2.8.4 QoS-Based Routing

QoS routing is vital in resource-constrained WBANs, addressing challenges and considering various quality criteria such as data prioritization, energy efficiency, link and transmission reliability, low latency, node temperature, and data security. The objective of QoS-aware routing protocols in WBAN is to enhance the QoS for specific network traffic. Therefore, routes are selected based on traffic priorities, and the highest priority packets are allocated more reliable routes. Table 2.6 presents a comparative overview of recently developed routing protocols that consider quality criteria such as network size, network throughput, mobility, congestion, PDR, and energy utilization.

2.8.5 Cross-layer Routing Protocol

The concept of cross-layer design involves exchanging data between different layers to enhance the adaptability of the model and make efficient use of network resources. It has several advantages, including improved network design, scalability, interoperability, and flexibility [53]. In cross-layer design, each layer in a system has its own specific parameters and control elements. These parameters are utilized by the layers to determine the most suitable adaptation rules for their respective control elements considering the current network conditions. Cross-layer design often requires solving an optimization

Table 2.5: Cluster-Based Routing

Reference	**Protocol**	**Objective**	**Energy consumption**	**Delay**	**PDR**
[47]	CBBAP - Cluster Based Body Area Protocol	Reduced node-to-sink communication	0.316	low	Not applicable
[48]	Dual Sink Clustering Protocol (DSCP)	Reduce shadow effect impact	Low	0.5 s	90-95 %
[49]	EERDT - Energy Efficient and Reliable Data Transfer Protocol for WBAN	Energy efficiency and reliable data transfer	0.528 mW	low	Not applicable

Table 2.6: QoS-Based Routing

Reference	**Protocol**	**Objective**	**Energy consumption**	**Delay**	**PDR**
[50]	Localized Multi-objective Routing (MOR) protocol	Assistance for data design QoS	0.72mW	low	Low
[51]	Energy peering routing (EPR) protocol	Reducing network congestion	0.5 mW	Not applicable	High
[52]	Quality of Service aware Routing Protocol (IM-QRP)	QoS based on priority routing	0.48 mW	Not applicable	Medium

problem that incorporates the variables and constraints from multiple layers. By solving this problem, the optimal values of the control components in each layer can be obtained. Although cross-layer design offers many benefits, it is important to recognize that it may not be a universal solution for all network-design challenges. While there are significant advantages to departing from the traditional architecture, improvements in network speed must be weighed against potential compatibility issues that may arise from the successful implementation of these solutions. The interactions between the layers change, but the decision to move away from the standard paradigm should be justified based on the benefits and comprehensive evaluation of the potential drawbacks. [54].

Methods of Cross-layer Design for IoT

The cross-layer architecture enhances security levels compared to the simple-tiered approach. Cross-layered methods utilize connectivity across different layers, whether adjacent or non-adjacent, to improve energy efficiency and routing decisions. Recent research has demonstrated that cross-layer design significantly impacts the performance of IoT networks [53]. The primary methods used in cross-layer design are as follows:

1. Creation of New Interfaces
   In this strategy, the layer makes judgments based on the parameters in the lower layer to improve performance. This approach can be classified into three types:

   - Upward flow
     In the flow approach, the higher layer of the system must obtain information from the lower layer during runtime. To facilitate this, a new interface was created from the lower to the higher layer.

   - Downward flow
     In this approach, the new interface transfers data from a higher layer to a lower layer to configure the parameters of the lower layer.

   - Forth and Back Flow
     At runtime, the two layers collaborate to complete separate duties in this method. This is observed in an iterative loop between layers [55]. For example, as part of the overall QoS, a MAC layer can connect directly to the application layer to transmit latency requirements and establish packet priority.

2. Merge Adjacent Layers
   This approach generates a new layer by combining multiple levels [56]. The conventional stack structure is still used for cross-layer techniques between the MAC and physical layers. Creating a layer that unifies the functionality of these

layers without overhead is an efficient technique for boosting efficiency. This union relies on the existing protocol stack interfaces between two-layer services and does not require new interfaces.

3. Vertical Calibration
   This approach modifies the parameters that extend across the layers of the protocol stack. The parameters of all layers determine any specific layer's performance increase. Co-optimization boosts the individual performance benefits of this strategy. The authors of [57] proposed incorporating AMC into the PHY layer to reduce transmission rates and boost reliability through error control codes. The author proposed using an automatic repeat requests (ARQ) mechanism at the MAC layer to restrict the number of re transmissions to alleviate channel fading and improve system throughput. When the ARQ at the MAC layer and AMC at the PHY layer are considered separately, the CLD can outperform the ARQ and AMC, which operate in isolation across their layers.

4. Layering Optimization Decomposition
   This method decouples the traditional stack effectively and changes it to a single integrated solution by providing a CLD framework. According to [58], this theory implements asynchronous parallel processing over a network to indirectly handle a modeling optimization problem in the network. The links between layers reveal multiple techniques for modulating and disseminating centralized computers. The connections of the layers are mapped to separate the vertical decomposition function of the optimization problem in terms of Network Utility Maximization (NUM).

5. Vertical Decomposition
   The protocol stack is decoupled from network protocol services, such as routing, congestion management, energy sensing, and error control, as part of the modules that execute the same activities as distinct layers. Vertical decomposition was utilized by the authors of ref [58] to improve and control the interaction between distinct levels. Vertical calibration occurs throughout the layers in this method, defining the past knowledge collected from the layers or updated depending on the runtime parameters. The decomposition process entails the creation of modules that maintain layer connections, which may help explain why a cross-layer design is required. Figure 2.7 presents different cross-layer design methods.

Cross-layer Interactions Approaches

The approaches of cross-layer interaction implementation are classified as follows.

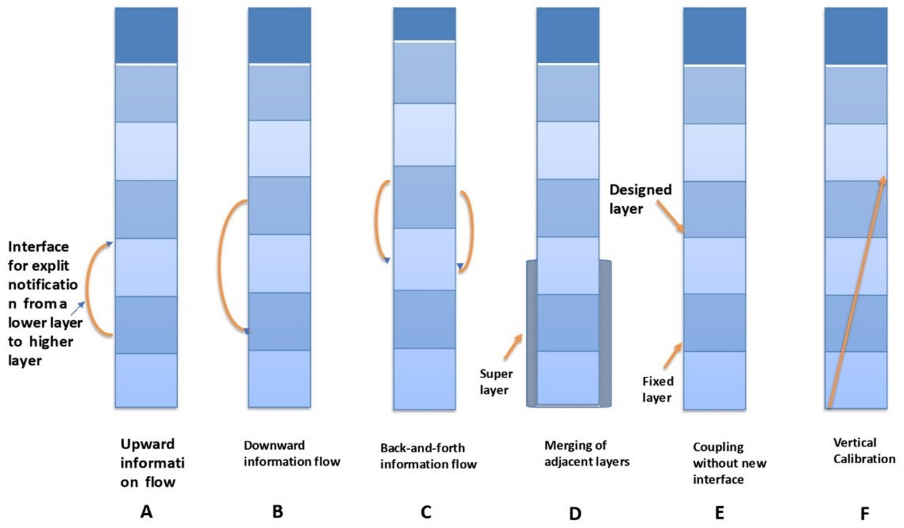

Figure 2.7: Cross-layer design methods for IoT

1. Direct Communication
   This method is appropriate when running-time information exchange between layers is required, as in CLD, which relies on dynamic vertical calibration or new interfaces. Direct communication includes creating variables in one layer during run time. Furthermore, in a multilayered design, each layer manages variables that are irrelevant to the other layers. In refs [59], the authors propose CLASS (Cross-Layer Signaling Shortcuts) as a direct communication technique. These concepts are intriguing when only a few cross-layer data points are required. The problem with implementing this method is determining how to deal with the memory locations shared between the layers.

2. Shared Database Across-Layers
   This approach is particularly suitable for vertical calibration across layers, as it enables simultaneous communication between all layers through a shared database using an optimization program [60]. Similarly, a shared database can construct interfaces between the layers.

3. Completely New Abstractions
   The new operating mechanism of this method was designed without additional protocol layers. This method is adaptable and allows for interactive communica-

tion. The authors of ref [61] propose a novel method for organizing protocols. This protocol organization is desirable because it allows interactions among basic blocks. Consequently, they have the potential to provide considerable flexibility in terms of design and runtime. However, because of how protocols are built, they change the fundamental nature of the situation and may necessitate an entirely new system-level implementation. Figure 2.8 shows different cross-layer interaction methods.

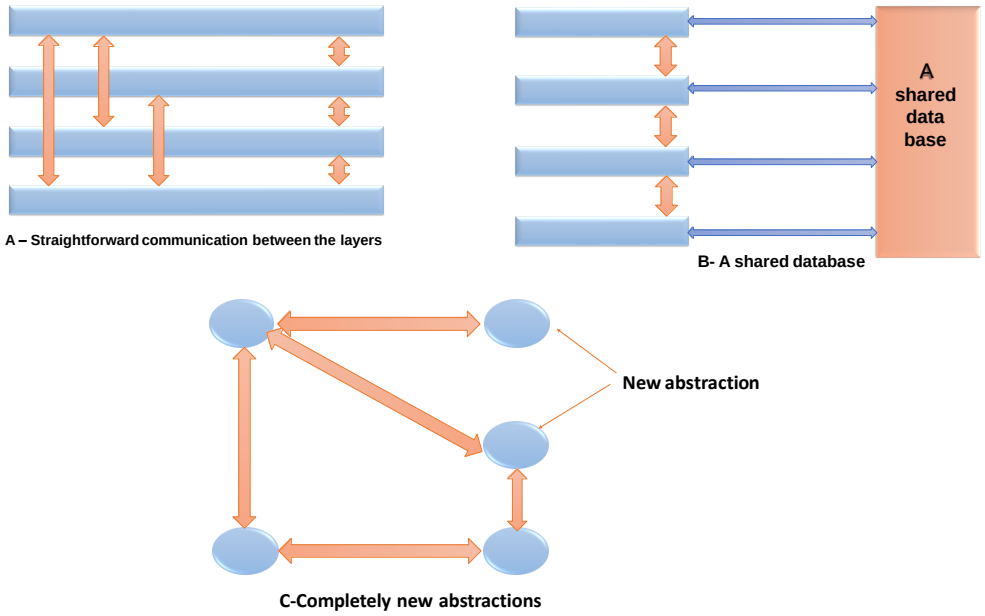

Figure 2.8: Cross-layer interaction methods

Cross-layer design for IoT healthcare

Cross-layer design for IoT healthcare refers to an innovative approach in networking, where interactions and optimizations are made across different layers of the networking protocol stack, rather than strictly adhering to the traditional layered architecture (such as the OSI model). This method allows for more flexible and efficient communication protocols, which is particularly beneficial in the context of Internet of Things (IoT) healthcare applications. The primary goal of cross-layer design in IoT healthcare is to enhance the performance, reliability, and energy efficiency of healthcare systems that utilize IoT devices for patient monitoring, data collection, and delivery of healthcare services [62].

A cross-layer design in IoT healthcare increases the efficiency of healthcare services by integrating several layers of communication protocols. An example is the use of a cross-layer design in IoT healthcare to improve patient monitoring and management. Different levels of communication protocols are combined in this technique to enable real-time patient health monitoring and to allow healthcare personnel to respond swiftly to any changes in the patient's condition. For example, the physical layer may collect data from sensors on a patient's body. In contrast, the network layer may transfer these data to healthcare practitioners in real time. The application layer can then be utilized to offer data to healthcare providers in an easy-to-understand manner. A few cross-layer approaches include the application layer, and even fewer have the entire protocol stack to provide a customized solution for real-time applications [63].

Many schemes can demonstrate significant energy-efficiency improvements by optimizing more layers classified as loosely and tightly coupled. Loosely coupled protocol designs optimize the parameters at the lower layer to improve performance at the higher layer. For example, as part of the routing algorithm, the network layer can use channel conditions from the physical layer. In the protocol stack, the parameters are accessible only to the next layer to make better decisions and increase performance gains. Tightly coupled designs should outperform loosely coupled designs because they do not incur communication overhead [64].

Objectives of cross-layer design for IoT healthcare

Several issues have led to questioning the standard layered design strategy of networks, particularly in relation to the specific requirements of cross-layer design for IoT e-health.

- Channel Conditions
  The link capacity in WBANs may vary due to conventional wireless links issues such as node interference and other variables. However, due to RF signals' characteristics, such as attenuation and absorption signals in and around the human body, route losses vary depending on the propagation direction. Channel conditions can be affected by antenna orientation, physical stature, patient posture, and garment type [65].Cross-layer approaches can adapt to variations in channel conditions by incorporating link adaptation to accommodate changes in the channel characteristics.

- Network Heterogeneity
  A heterogeneous IoT system comprises different sub-systems, including constrained resources and powerful nodes. Regarding integration into a defined structure, the protocol stack standard may adequately satisfy the needs of heterogeneous

networks, but this affects energy efficiency and performance. For example, if routing paths are built between nodes via different networks, the protocol selects the available path based on the lowest cost or the shortest distance. However, the routing protocol considers MAC-layer interactions if the node wants to discover a path with sufficient bandwidth. A standard protocol stack does not support this form of cross-layer interaction [66].

- Performance
  The tightly coupled standard layer maintains protocol interoperability, although this may affect performance. The data are transmitted between layers, regardless of the role of the protocol in data transmission or reception [67].

- Quality of Service
  Data transmission without delay is referred to as QoS. This term refers to real-time communication, in which on-time delivery and reception are critical. Owing to their applications, WBANs have a distinct demand for QoS level. A high packet delivery ratio, short packet transmission latency, reduced collisions, an effective balance of energy efficiency, retransmissions, and dependable transmissions are all crucial in the WBAN context [68]. Traditional layered systems may be unable to ensure certain service levels, limiting the QoS. Consequently, the cross-layer design is regarded as a superior solution for meeting all these objectives.

Cross-layer Design Methodologies in IoT Healthcare

The primary goal when designing IoT healthcare networks is to increase the lifetime of a node and reduce power consumption. Therefore, a cross-layer design methodology can be employed to ensure optimal performance by considering the interlayer protocol stack interactions. This approach achieves energy conservation, network reliability, and reduced latency. For example, the cross-layered protocol between PHY and MAC can potentially create an optimal solution because the design between them is more typical. The principal goal of the MAC layer can take the form of link adaptation or channel modulation techniques to coordinate access to the PHY layer [69].

The principle method of cross-layer design routing protocol must address all individual strategies and requirements because there are numerous constraints when dealing with IoT systems, particularly healthcare ones. In terms of power consumption, performance, memory, and traffic matching, as well as the ability to deal with changes and conserve transmitter power [70]. According to the literature, the cross-layer approach can be used with WBANs. Collaboration across layers

can save energy, provide tailored services, better serve priority data, and achieve higher performance.

Routing Mechanism

Routing is one of the most effective ways to address network requirements. By incorporating two or more levels, the cross-layer routing protocol is utilized in WBANs to boost the efficiency and compatibility between techniques and protocols. The cross-layer concept is critical in routing and power control strategies. To compute a reliable path utilizing a cross-layer, the standard (AODV) routing protocol can be utilized along with a reliability-related parameter [71].

The Expected Transmission Time (ETT) is a metric used in networking and communication systems to estimate the time it takes for a data packet to be transmitted from a source to a destination. It is a routing indicator that provides insight into network quality.

The ETT is calculated as the ratio of the forward packet delivery rate (Pdr) to the reverse packet delivery rate (Pvr). This calculation takes into account factors such as the packet size and available bandwidth, as well as link quality measurements like the Expected Transmission Count (ETX) and Signal-to-Noise Ratio (SNR) [72]. The ETT defines by the equation 2.2:

$$ETT = ETX \cdot t = ETX \cdot \left(\frac{P_{fs}}{BL}\right) = ETX \cdot \left(\frac{P_{fs} \cdot (Ts_s - Tl)}{Pls}\right) \tag{2.2}$$

Where: ETX (Expected Transmission Count) is a metric that represents the expected number of transmissions required to successfully deliver a packet. t is the time it takes to transmit a single packet. P_{fs} is the frame size in bits. BL is the link bandwidth in bits per second. Ts_s is the time to send a single frame. Tl is the time for the link layer protocol to process a frame. Pls is the physical layer rate in bits per second. The ETX is defined by equation 2.3:

$$ETX = \frac{1}{P_{dr} \cdot P_{vr}} \tag{2.3}$$

ETT modifies the ETX value based on link fluctuations. ETT information is contained in an AODV (Ad-hoc On-Demand Distance Vector) protocol control packet, specifically the RREQ (Route Request) packets. After the ETT information was found through RREQ, and nodes adjusted their transmission range by modifying their transmission power. Figure 2.9 depicts this process.

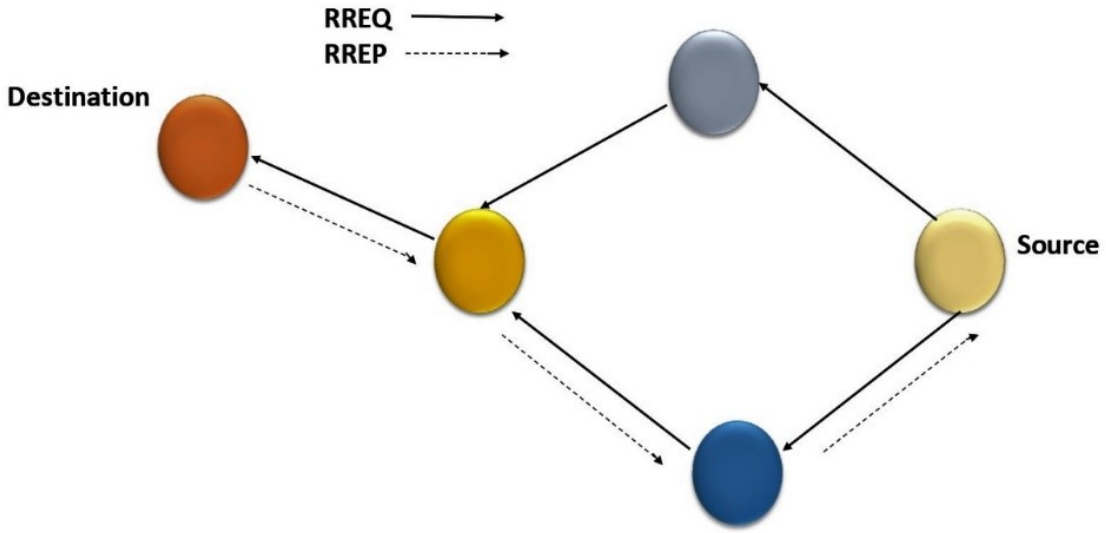

Figure 2.9: The route discovery process

Cross-Layer Routing Parameters

Cross-layer routing relies on multiple protocol levels to exchange information, achieving the desired network performance advantages [73]. The three lower layers are involved in the cross-layer routing decision. By incorporating the characteristics of the network (NET), MAC, and PHY layers during routing decisions, the routing protocol becomes more robust against interference and congestion. Wireless channel characteristics, such as (SINR) are available at the PHY layer play a significant role in determining interference. At the MAC layer, node characteristics factors such as the re transmission count [74] and buffer space may help reduce packet loss and congestion. These metrics and traditional path characteristics, such as ETE and hop count, must be considered to achieve high network performance. Consequently, picking the next hop or route at the NET layer mitigates the above mentioned issues.

Cross-Layer Routing Methods

Increased average life and health costs and developments in downsizing electronic devices, sensors, batteries, and wireless communication technology, have fueled the development of WBANs. Routing protocol design is a critical component

of IoT e-health systems, notably in WBAN, where it plays a critical role in the communication stack and impacts performance. Through a summary and analysis of the literature, the WBAN routing protocols are classified into temperature, posture, QoS, cluster, and cross-layer-based routing [75]. In this study, we focused on cross-layer and QoS-based routing protocols. Figure 2.10 shows the cross-layer WBAN protocol.

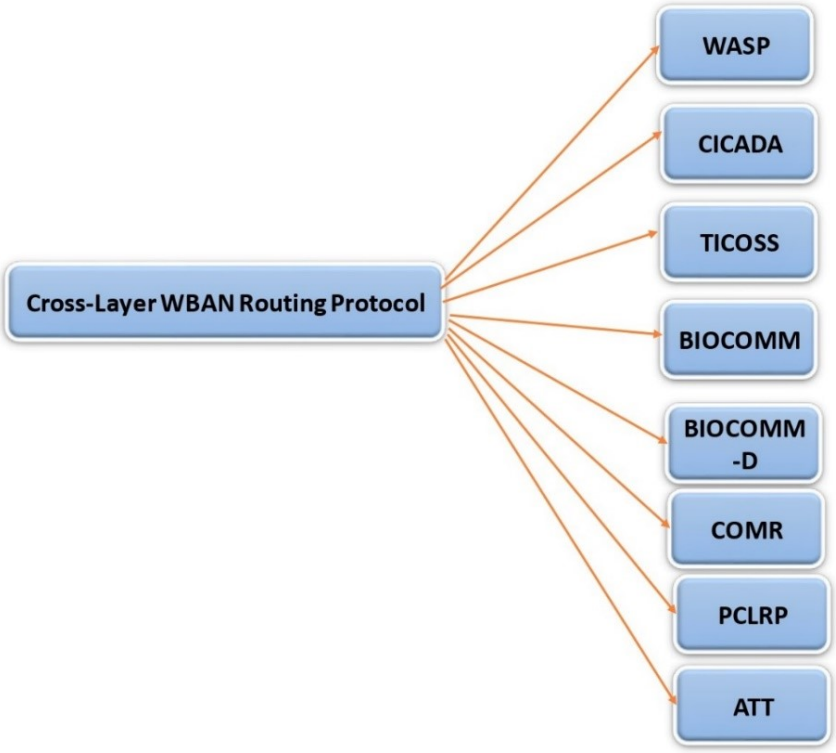

Figure 2.10: Cross-layer WBAN protocol

Wireless Autonomous Spanning Protocol (WASP)

The WASP protocol employs a spanning tree to avoid loops in network topologies, thereby improving throughput and reducing delay in WBANs. This tree allocates slots and routes data to the sink. The protocol uses cross-layer techniques to enable the efficient distribution of wireless links. The authors in ref [76] proposed a (WASP) protocol that incorporates slotted MAC and the automatic setup of different nodes.Every node utilizes a unique WASP message to communicate with its children regarding the time slots available for transmitting their data. The node receives the Listening scheme from its parent node (higher level), whereas the child

nodes provide all the necessary information for the node to construct this scheme (lower level). Figure 2.11 shows the different elements of the WASP scheme.

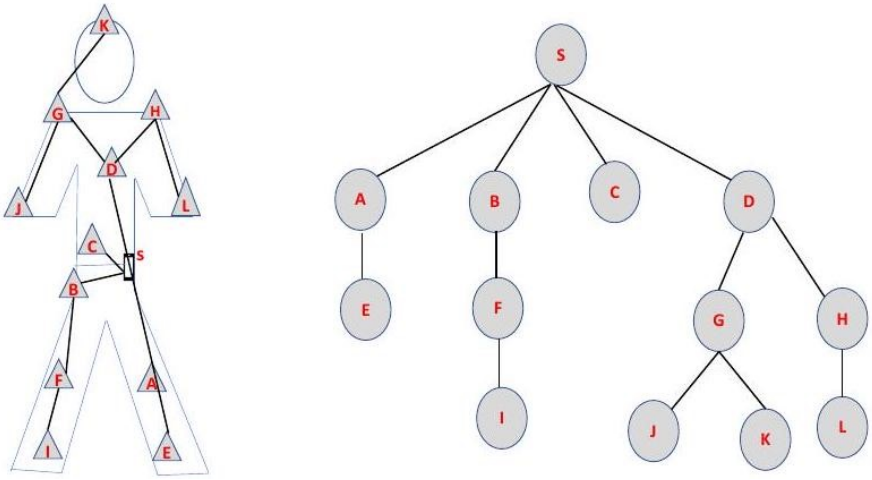

Figure 2.11: WASP protocol, redrawn from [76]

The network topology is indicated by the lines connecting the nodes. All communication was performed wirelessly. A tree is constructed so the nodes can only hear each other (children, siblings, and parents). The network traffic is controlled by building a broadcast message scheme and spanning a tree, which the children and parents use.

Cascading Information Controlling Access Dynamic Slot Assignment Protocol (CICADA)

CICADA is a cross-layer protocol designed for TDMA scheduling depending on the multi-hop in the MBAN. This protocol was built on a spanning tree, similar to the WASP protocol in Ref. [76]. The authors of [77] proposed the CICADA system for WSN energy efficiency; each node in this protocol executes two guesstimates to obtain data from child nodes; for sending data, the time slot number and wait duration are computed. This protocol separates the transmission cycle into two sub-cycles: data and control. The data sub-cycle specifies the duration of the data and the waiting period. The control sub-cycle specifies the length of the sub-cycle, tree depth level, and sequences used to communicate the control schemes to the nodes. The data period is utilized to deliver packets to the parental contract based on the waiting period and sub-nodes (position- sleep) to save power. This

protocol distributes a spanning tree to transfer data access without collisions. Due to each cycle's specified length, the time slots are spread and allocated, simplifying slot synchronization. When child nodes communicate, the parent nodes must be notified.

Time-zone Coordinated Sleeping Scheduling (TICOSS)

TICOSS is a cross-layer protocol that connects the routing and MAC layers [56]. This system is based on the MAC efficient routing localization integrated (MERLIN) protocol, explained in ref [78], and enables multi-hop transmission in the 802.15.4 standard by separating a network into separate time zones. The benefits of the TICOSS protocol are as follows:

- To save energy, A node can alternate between active and inactive times.
- It eliminates packet collisions caused by the hidden terminals.
- It finds the shortest routing path for packets to the nearest gateway. Time is given to the network nodes to reduce power consumption, which exchange basic information with the network. The authors of [79] employed TICOSS in WBAN to determine the shortest path by manipulating sensor nodes as FDD (Full Functional Devices). The timetable conserves the sensor node energy while minimizing closed-end collisions. Furthermore, this strategy promotes mobility in high-traffic areas and increases service life.

BIOCOMM and BIOCOMM-D

BIOCOMM, a cross-layer protocol designed for biomedical networks, offers several benefits such as preventing hotspot formation, reducing network traffic, and prolonging the lifespan of implanted biomedical sensor nodes [80]. The protocol achieves improved network performance through a Cross-layer Messaging Interface (CMI), which facilitates communication and information exchange between the network and MAC layers. The Neighbor Status Table (NST) is used to keep track of the status of neighboring nodes in both the MAC and network layers. The MAC layer determines whether a neighboring node is blocked (B) or free (F), and notifies the network layer of any changes in status by sending corresponding messages (BLOCKED or FREE) through the CMI.

Likewise, the network layer informs the MAC layer about the available free slots through the CMI, enabling the MAC layer to transmit frames. Each node in the network employs a hop-count algorithm to determine the shortest path for packet

transmission. To prevent infinite routing, the hop count is associated with the packet; if the number of hops exceeds a predefined threshold, the packet is dropped. A modified version of BIOCOMM, called Biocomm-D, was introduced to address delays in transmitting sensitive data packets. Figure 2.12 shows the BIOCOMM protocol.

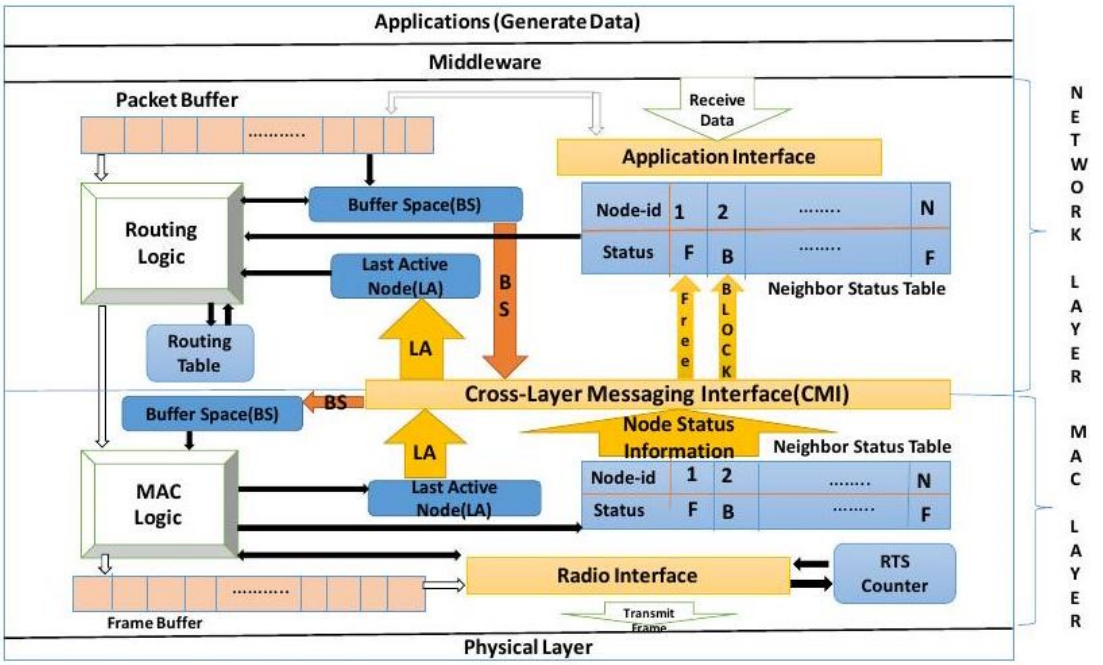

Figure 2.12: BIOCOMM protocol architecture, redrawn from [80]

Priority Cross-Layer Routing Protocol (PCLRP)

Delay is a critical concern in WBAN networks for high-priority data. PCLRP has consistently shortened the time it takes to allocate and transmit vital data between patients and processing units [81]. The PCLRP includes communication between the PHY, MAC, network, and application layers. The active healthcare application's physical parameters and QoS standards were considered in this protocol by configuring the MAC slot for routing protocols. Elhadj et al. [64] proposed a PCLRP combined with a PCLMAC protocol for various healthcare applications. This protocol divides the data into three categories based on priority: emergency data (EM), delay-sensitive data (DS), and general data (GD). Data are transmitted based on importance, where priority is given to the critical data. This protocol provides tailored QoS for latency, power consumption, and PDR. The beacon mode is the protocol's operating mode and is transmitted at the start of the super frame.

A back-off mechanism was employed throughout the competition stage to reduce the data emergency time. Figure 2.13 depicts the MAC super frame division stage, which includes the following components: beacon (B), Downlink Period (DL), Children Contentions Free Phase (CCFP), Children Competition Access Period (CCAP), Neighbor Contention-Free Period (NCFP), Neighbor Contention Access Period (NCAP), and INACTIVE period. The PCLRP protocol uses cooperative relay mode during the routing phase. During the beacon phase, the coordinator uses ACK information to determine the relay node, node location, time slot, and energy. The authors of ref [82] developed a priority routing algorithm to save energy by avoiding congestion depending on queue length and hop number. However, the algorithm reduces energy waste and ensures less path loss. However, transmission delays in non-emergency data have not been examined.

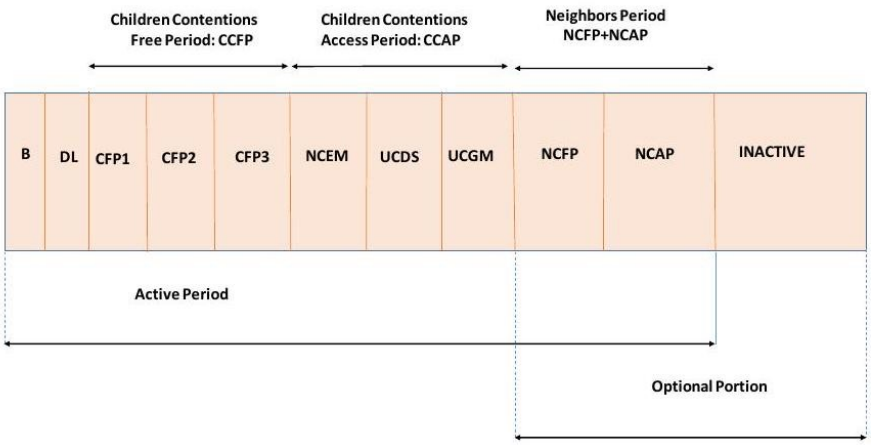

Figure 2.13: Super frame structure of the PCLRP protocol, redrawn from [83]

Cross-Layer Opportunistic MAC/Routing Protocol (COMR)

The COMR protocol was introduced to enhance power efficiency, minimize latency, and improve the Packet Delivery Ratio (PDR) during node data transmission. In their work cited as a reference [82], the authors proposed the COMR protocol, which utilizes a timer-based selection approach to enhance network reliability. The timer values were determined based on signal strength indicators and residual energy. Among all nodes, the relay node selected in this protocol is the node closest to the sink and possesses the highest residual energy. Any node in the network can serve as a relay node. Data transmission in the COMR protocol is achieved

through a handshake mechanism involving request-to-send (RTS) and clear-to-send (CTS) messages. As the payload size increases, the PDR decreases, but the overall lifetime of the network increases. In addition, the energy consumption is higher in the receiving or idle states than in the transmission mode. Figure 2.14 provides a visual representation of the COMR protocol.

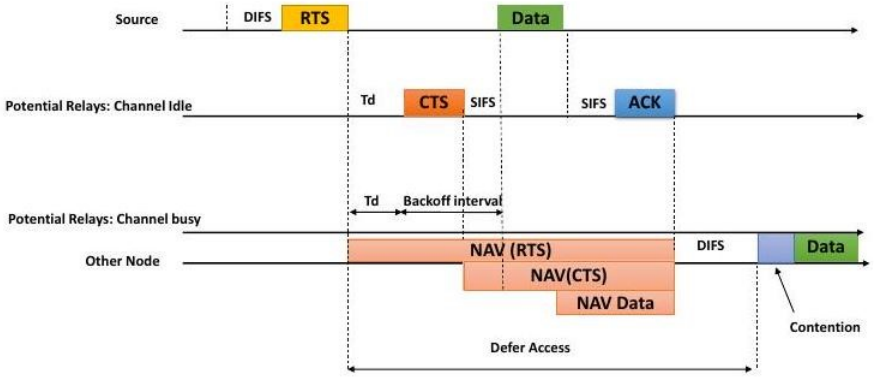

Figure 2.14: COMR protocol architecture, redrawn from [82]

Cross-Layer Re-Transmit Strategy (CLRS)

CLRS is a cross-layer protocol based on the IEEE 802.15.6 standard, as proposed in reference [100]. Unlike previous Body Area Network (BAN) routing systems, this protocol focuses on retransmitting lost packets. The main causes of data transmission failures in CLRS are shadow and collision effects [82]. In the Medium Access Control (MAC) layer, packet failures are detected by analyzing the waveform characteristics of the data frames, which then triggers the retransmission technique. The superframe structure of the protocol is illustrated in Figure 2.15.

During the MAP1 phase, modes B and D are employed to prevent high-priority data from consuming all available transmission resources. The Time Division Multiple Access (TDMA) technique is utilized in the MAP1 phase to enhance transmission by allowing channel access. In the case of data transmission failure owing to collisions, the resources for retransmission are allocated based on the superframe structure.

If data transmission fails during MAP, the data will be retransmitted in the subsequent period. Similarly, in the EAP and RAP phases, if data transmission fails, retransmission occurs and the priority of the data determines the random time

back-off. In the event of a communication failure caused by human shadows, the retransmission of data is suspended until the shadow effect ends, after which the data can be retransmitted.

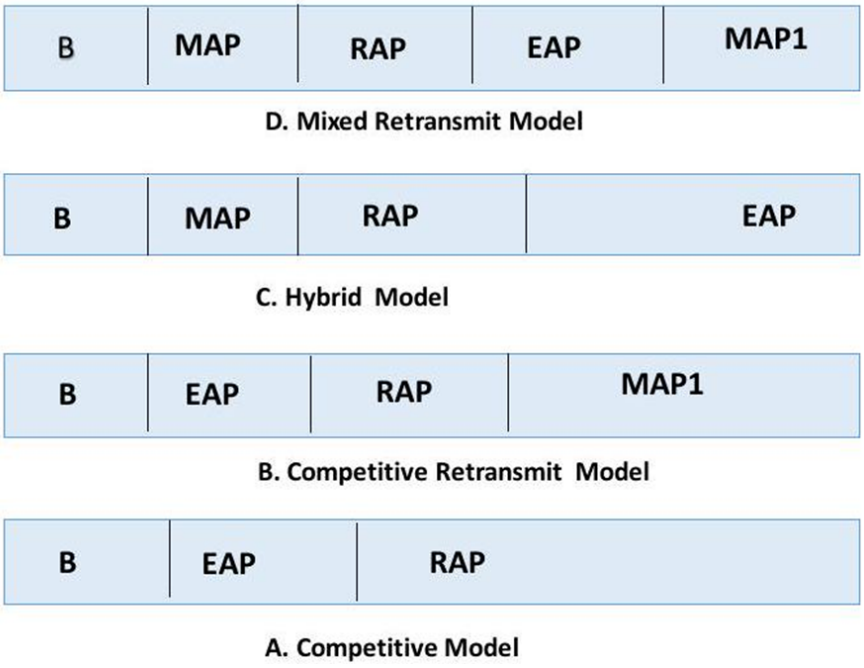

Figure 2.15: CLRS protocol super frame classification, redrawn from [100]

Cross-Layer Design Optimal Protocol (CLDO)

The CLDO scheme was designed to enhance the reliability of transmission and energy efficiency in WBANs by optimizing the MAC/PHY and network layers. In their work cited as a reference [84], the authors introduced the CLDO approach, which focuses on improving network parameters through collaboration between these layers. This approach involves determining the optimal packet size, relay-node selection, and transmission power. The authors demonstrated that selecting the best relay node leads to successful packet delivery while reducing the energy consumption and errors. In the routing stage, the selection of the next hop considers the power consumption and efficiency rate of the node. If the residual energy of a node falls below a certain threshold, the node transmits its own information to ensure transmission reliability.

Simple Opportunistic Routing Protocol (SOR)

The SOR protocol is a wireless sensor network (WSN) model designed to select the node closest to the target node for forwarding data. This protocol takes advantage of the broadcasting capabilities of WSNs, which helps to improve the efficiency, throughput, and reliability of sensor networks. In the SOR scheme, a nearby node assists the source node by relaying packets to the sink node. Data transmission often requires multiple hops, and relay nodes are selected using a handshake method. The source node broadcasts an RTS packet, and a relay node that successfully contends for the transmission responds randomly. In a study by the authors of [37], they proposed a straightforward opportunistic routing method that supports the mobility of Wireless Body Area Networks (WBANs) to prolong their lifespan. This algorithm involves the use of a sensor node, sink node located on the wrist, and relay node positioned on the waist. As a person walks, the wrist moves back and forth. If the sink node is in front of the body, the sensor node directly sends data through a single-hop path known as line-of-sight (LOS). However, if the sink node is on the back side of the body, the relay node is used to forward the data from the sensor to the sink node. If the sink node relies on LOS communication, a low-power RTS packet is sent such that only the sensor node can receive it. When a sensor node is available, it sends an acknowledgement (ACK) and establishes a connection with the sink node. After successful communication, received acknowledgement (RACK) was provided to the sensor node. If RACK is not received, the operation is repeated. In another study by the authors of [85], they investigated SOR techniques for WBANs. They analyzed the selected node and relay selection approaches to determine whether these metrics can enhance the reliability of WBAN networks.

Auto correlation-based Adaptive Transmission (ATT)

The auto-correlation-based Adaptive Transmission scheme (AAT) is a technique designed to enhance the reliability of transmission and reduce the power consumption in Wireless Body Area Network (WBAN) systems. In a study conducted by the authors of [86], they proposed a method that combines multi-hop cooperative transmission, autocorrelation coefficient, and dynamic scheduling for cross-layer adaptive power transmission. This technique involves three stages: link quality prediction, transmit power control, slot sequence rearrangement for the shortest path, and relay node selection. The hub node dynamically adjusts the transmission power based on the expected channel state to achieve optimal energy efficiency. The MAC superframe structure of the ATT protocol is illustrated in Figure 2.16. The carrier sense multiple access with collision avoidance (CSMA/CA) mechanism was em-

ployed to gain access to RAP1 (Relay Access Point 1). The multi-hop access point (MAP) is divided into two phases: the Data Transmission Phase (DTP) and Relay Transmission Phase (RTP). Each node completes information transmission within an appropriate slot. If data are sent, the relay node continuously transmits in the RTP slot and receives it in the DTP slot. In terms of power consumption and rate of successful data delivery, this protocol demonstrates a high level of transmission reliability compared to other protocols.

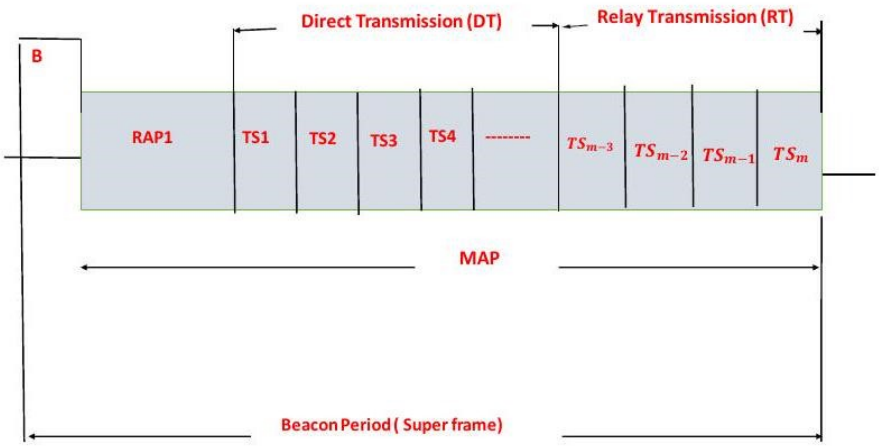

Figure 2.16: ATT protocol

Cross-Layer Optimization Protocol Guaranteed CLOPG

The CLOPG protocol was introduced in ref [87] as a cross-layer protocol based on bandwidth allocation and an adaptive routing system that includes topology discovery and load balancing. During the topology discovery step, each sensor sends a welcome message to the neighbor and maintains the neighbor's schedule based on requests for communication, data transfer, and termination information. The sensor transmitter chooses high-power sensors, which is the quickest way for the coordinator. Priority data are used to allocate high bandwidth. During transmission to the sink, a high bandwidth allocates emergency data and terminates non-emergency data. In the load-balancing routing phase, accepted and unaccepted messages are used, where sensors get the other sensors' requests for forwarding data. The wastage of power in this protocol is exceptionally high because of table maintenance and route selection, which reduces network performance.

Cross-Layer Optimization Based on Prediction (CLOBD)

This protocol promotes seamless communication and interaction between different layers. In [88], the authors presented an approach for cross-layer optimization based on link quality prediction. Considering the capacity disparity between coordinators and nodes, two types of link quality prediction algorithms were devised, each with varying levels of complexity. These algorithms are specifically designed to predict the link quality between any two nodes and the connections between coordinators and nodes. The equations representing these algorithms are shown in Equation 2.4.

$$R_{ij}(t) = \beta(R_{ij}(t-1) + (1-\beta)(R_{ij})) \quad | \quad R_{is}(t) = R_{is}^{(t)} - ECF_t \quad (2.4)$$

In this context, $R(t)$ represents the link quality between coordinators s and i. $ECF_{(t)}$ denotes the error correction factor and β is a weight factor. This protocol uses a multihop mode to accommodate a mobile network environment. Because using a fixed transmission power in a mobile context can result in packet loss or excessive energy consumption, this study incorporates adaptive transmission power adjustment for nodes. When the expected link quality value surpasses a threshold, the transmission power is reduced to conserve energy. Additionally, by increasing the data priority and combining the random back-off duration of the MAC layer with higher power transmission, the protocol ensures the reliable transfer of high-priority data.

Cross-Layered Broadcast Protocol (CLBP)

The cross-layer broadcast protocol (CLBP) was developed for Wireless Body Area Networks (WBANs) to enhance node synchronization and medium access, as described in [89].

This protocol is designed to be more adaptable to different human body postures and is well suited for multi-hop topologies and mobile scenarios. The operation of this technique is illustrated in Figure 2.17.

Before initiating the broadcast process, the sink node undergoes a prepossession step, where it allocates transmission slots and defines a communication graph, as illustrated in Figure 2.18. In the network, the nodes are identified as those whose links have transmission probabilities greater than 0.5. Broadcast packets consist of both data and control information, including slot assignments and synchronized data. Only sender nodes that have been assigned a current slot are allowed to transmit previously approved packets. The sink node is responsible for sending

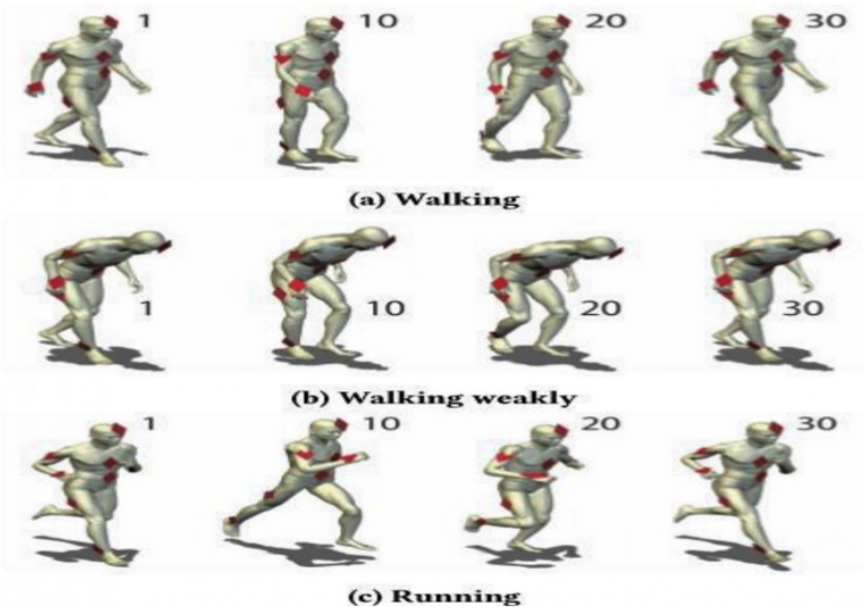

Figure 2.17: Different postures WBAN protocol [89]

data, synchronizing the strategy packets, and managing medium access. A slot assignment technique was employed to mitigate issues such as idle listening, collisions, overheating, and energy consumption. This technique aims to optimize the utilization of slots and reduce undesirable effects.

Comparison and Analysis

The proposed protocols, known as cross-layer protocols, have been suggested to enhance the efficiency of wireless networks. These protocols aim to coordinate multiple protocols and integrate additional layers without disrupting their original functionality. This section compares between these protocols.

As described by Braem [76], the WASP protocol establishes fixed intervals for data transmission. However, owing to the unlimited resources required for on-demand requests, this protocol exhibits relatively high power consumption. In addition, WASP necessitates the provision of faulty frame acknowledgements to the sender node. Although it does not facilitate end-to-end package delivery, it allows for the

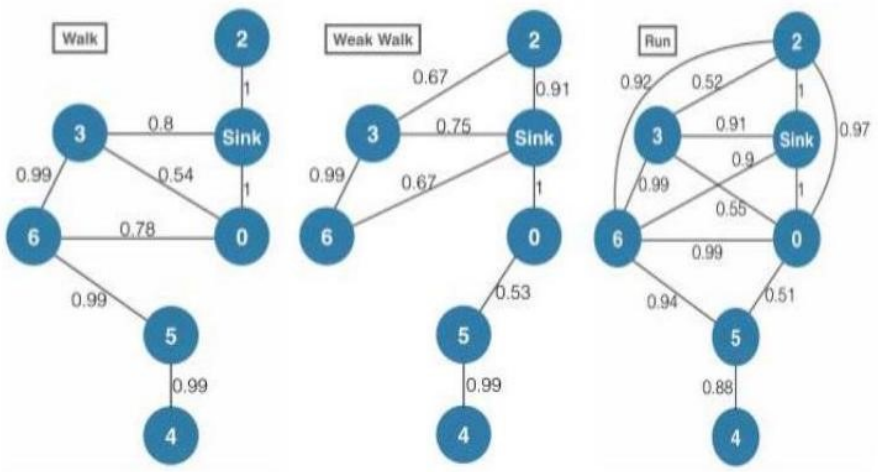

Figure 2.18: Communication graph per poster [89]

inclusion of new nodes in the network. One limitation of this protocol is that any node within the network can exit without notifying others.

The CICADA protocol, which is an extension of the WASP protocol as presented by Latrémolière [90], utilizes a technique called "waiting period" to keep the radio signal off while the node is waiting. As a result, the power consumption in this protocol is moderate compared to that of WASP. However, both the WASP and CICADA protocols face the same challenge when a child or parent node leaves the network without alerting the sink node, as mentioned in Braem [76].

The TICOSS [78] protocol follows the MERLIN protocol [56], the concept of scheduling time slots, and all nodes in this protocol ensure the exact moment to wake up to save power while sending and receiving data. TICOSS outperforms the CICADA protocol regarding PDR and power usage [90] . The protocol's drawbacks include latency and lower data reliability. The Biocomm [80] protocol architecture was proposed to communicate routing and the MAC layer through the CMI. This protocol avoids dropping data, keeps it away from congested nodes, and assigns reliable pathways to higher-priority data. In addition, [80] indicates the linkages and hotspot nodes before data transmission, in contrast to [WASP [[91]–TICOSS [78]]. The Biocomm-D protocol expands the Biocomm [80] protocol, which delivers good energy consumption results. The CLOPG [92] protocol uses more energy when choosing pathways. In the emerging data case, this causes network performance degradation [80]. CICADA, BIOCOMM, and TICOSS operate

in the MAC and network layers. The BIOCOMM protocol outperformed the other cross-layer protocols, but the CICADA protocol mitigated the power consumption over packet delivery ratio. AAT [93]and CLDO [92] have an edge regarding reliability measures. In theoretical studies, CLDO provides dependability; however, this approach adds latency and fails to deliver improved performance. The PCLRP [64] and CLRS [88] protocols use a back-off time technique in the MAC layer based on data priority, ensuring reliable transmission and minimal latency. The distinction is that the CLRS addresses data dependability and reduces transmission time. Consequently, the CLRS protocol outperforms the PCLRP protocol in terms of reliability and latency. The downside of CLRS is that the transmission ceases due to the shadow effect, resulting in a long delay. Therefore, adaptive power management is critical. This is mentioned in the CLRS, COMR, and AAT protocols. AAT is determined by the channel state estimate, COMR by the transmission state, and CLRS by link quality prediction. Each strategy is worth investigating; its purpose is to improve energy efficiency and reliability through power regulation. CLBP enhances media access and node synchronization. The advantages of SOR are realized successfully by providing high efficiency and various concurrent flows.

Cross-layer Challenges and Future Research Directions

A cohesive communication protocol is necessary for a cross-layer design to ensure dependable and efficient communication in IoT networks. This protocol should take into account routing, transport, and MAC (Media Access Control) characteristics, while also considering the effects of the physical layer. However, several research challenges remain open to the development of systematic approaches to cross-layer design problems.

Some of these issues include security and privacy concerns in Wireless Body Area Networks (WBANs), the necessity for increased standardization, accurate modeling of delays, and mobility considerations. In the following section, we discuss specific cross-layer design problems that require further investigation.

1. **Lack of Standardization**

   Standardization involves implementing and developing technical specifications to ensure compatibility, interoperability, and the quality of services and systems. Standardization is essential for cross-layer design in IoT, which aims to optimize the performance and reliability of IoT applications by integrating layers such as physical, data link, network, transport, and applications.

However, there needs to be more agreement on which standards best support the individual layers or IoT scenarios. Although various standards exist for communication, data handling, security, and service discovery, no framework unifies or harmonizes these protocols and standards for cross-layer design. This can cause compatibility and interoperability issues among heterogeneous IoT devices and platforms using different technologies [94].

2. **Hard to Redesign**

   Developing cross-layer protocols and algorithms that strike a balance between the advantages and drawbacks of cross-layer design is crucial. This entails considering the limitations of IoT devices and networks, such as resource constraints and heterogeneity. One approach is to employ lightweight or distributed cross-layer solutions, which can reduce the computational and communication costs associated with the cross-layer design. Another option is to utilize cooperative or collaborative cross-layer solutions by leveraging the diversity or redundancy of IoT devices or networks to enhance the performance or reliability of the cross-layer design. Given that most IoT protocols follow a traditional design integrated with wireless devices, it is necessary to introduce a dynamic cross-layer design to optimize the transmission of data between layers. However, this is a complex problem to address because it has implications for other subsystems and requires redesign or adaptation, as mentioned in the study by [95].

3. **Connectivity with the Realistic Physical Layer**

   Recent experiments have demonstrated that the impact of wireless channel impairments on the upper layer of communications cannot be ignored. In particular, channel fading plays a significant role in determining link availability, which directly affects wireless transmissions. In addition, the mobility of nodes must be considered. The network is prone to frequent reconfiguration owing to events such as node join, node mobility, and node departure. Consequently, connections are formed and dissolved on a regular basis. In light of these factors, there is a need for new analytical models that incorporate both mobility and fading channels to accurately estimate connection conditions.

4. **Accurate Delay Modeling**

   In the context of IoT e-health applications, a cross-layer design can help solve the problem of accurate delay modeling by integrating the network layer and data link layer (MAC layer). In the proposed cross-layer model, reliability-related parameters are included in the route discovery process, and MAC-based power control techniques make use of routing information to obtain suitable transmission power [96]. This approach helps to prolong the lifetime of IoT devices and ensures reliable data transfer in IoT e-health applications.

   Therefore, the development of a model for describing end-to-end delays caused by interactions between different layers is required. This is crucial for IoT e-health applications that require real-time data transfers

5. **Context Awareness**

   The context concept refers to the patient's condition and environment (mental state, temperature, humidity, and other information that helps to characterize the patient's position). Context awareness in the MAC and application layers is an open research question regarding WBANs. The authors of [97] proposed applying context-aware techniques employing a cross-layer design to handle mission mistakes, power consumption, and QoS limits via efficient parameter communication between the application layer and MAC. The authors state that more research is required on this topic.

6. **Adaptive Duty Cycles**

   The cross-layer design can help optimize adaptive duty cycles for IoT in e-health applications by enabling physical layer parameters, such as signal strength and interference levels, to dynamically adjust sensor sampling schedules based on real-time connectivity conditions. MAC layer protocols can also prioritize low-latency transmissions of critical alerts and alarms over more efficient uploads of non-urgent data. Network routing algorithms can leverage application insights into treatment plans and disease progression to select the best paths for the timely delivery of important patient readings according to clinical context and needs. An adaptive MAC protocol for Wireless Body Area Networks (WBANs) was proposed in several studies. This protocol aims to address the challenges of fluctuating business traffic and energy consumption in WBANs. The proposed protocol sets data priorities based

on the type of service, and adjusts the superframe structure accordingly [98]. It also utilizes a TDMA approach and well-defined synchronization scheme to avoid collisions and improve network performance [99]. Most solutions establish a duty cycle fixed for sleep frames, and a poor duty cycle choice increases the delay and power consumption. Therefore, future cross-layer systems should develop algorithms that are capable of predicting sleep and wake times.

7. **Security In WBAN**

   Transferring patient data and vital signs necessitates a highly secret and protective method which requires various encryption algorithms and more data processing and energy consumption. Practical cross-layer solutions for WBAN must meet security and privacy requirements while ensuring the network's longevity. A few articles reviewed in this survey discussed security issues and data management in WBAN, such as [100], where the authors presented a cross-layered CICADA-S security protocol with low power consumption based on the CICADA protocol. The authors proposed controlling authentication codes to address security concerns such as intrusive nodes joining the network while preserving power consumption and WBAN throughput. Therefore, these issues are critical for WBAN networks and warrant further investigation.

8. **Cross-Layer Simulators**

   Current network simulator technologies, such as NS-2, OPNET, Omnet++, GloMoSim, and J-Sim, may make it challenging to develop a cross-layer protocol. Consequently, new simulator software based on the development paradigm is required to facilitate the creation and testing of algorithmic solutions for cross-layer protocol solutions.

9. **Coexistence With Other Wireless Protocols**

   The coexistence of numerous cross-layer implementation ideas with diverse wireless protocols and the proliferation of cross-layer routing protocols have generated problems. These concerns affect the stability and reach of the network. In an across-route network, several methods are deployed across multiple locations. However, covering a dynamic network is difficult. As a result, the availability of numerous incompatible protocols is inappropriate for various applications [101].

2.9 CONCLUSION

This chapter provides a comprehensive overview of the burgeoning field of IoT in healthcare, focusing particularly on its applications and the pivotal role of Wireless Body Area Networks (WBANs) in revolutionizing patient monitoring and care. Through a thorough review of existing cross-layer design approaches for IoT healthcare, we explored the advancements and state-of-the-art methodologies that underscore the potential for enhancing network efficiency, reliability, and energy conservation in healthcare applications. Moreover, our analysis highlighted the innovative strides made in cross-layer design, showcasing its significance in addressing the multifaceted demands of IoT healthcare systems. Despite these advancements, this chapter also identifies several research gaps and challenges, including the need for more robust security measures, greater scalability, and improved interoperability among IoT devices. These identified gaps underline the necessity for ongoing research and development to fully harness the transformative power of the IoT in healthcare, ultimately paving the way for more personalized, efficient, and accessible patient care solutions.

3

IEEE802.11AH PROTOCOL PERFORMANCE EVALUATION

Contents

3.1 INTRODUCTION

This chapter presents a detailed examination of the IEEE 802.11ah standard, a pivotal advancement tailored for the Internet of Things (IoT) sector. It begins with an outline of the standard's network architecture, which supports many IoT devices and applications. The motivation for the IEEE 802.11ah development is scrutinized, highlighting its role in overcoming the constraints of previous wireless technologies. The chapter then dissects the Physical (PHY) layer, emphasizing operation in the sub-1 GHz bands for extended range and penetration, essential for IoT connectivity.

Furthermore, we analyze the PHY layer's design features that enable long-distance communication and power efficiency. The MAClayer discussion follows, addressing innovations such as Time-Slotted Channel Hopping for interference mitigation, Restricted Access Window for improved channel access, and Target Wake Time for enhanced power management. These sections offer a comprehensive understanding of the design considerations of the IEEE 802.11ah protocol and its operational benefits in IoT environments.

3.2 IEEE 802.11AH OVERVIEW

IEEE 802.11ah, also known as Wi-Fi HaLow, is a wireless networking protocol introduced in 2017. It operates on the 900 MHz frequency, which doesn't require licensing, and offers extended range compared to traditional Wi-Fi networks using the 2.4 GHz and 5 GHz channels. Wi-Fi HaLow is energy-efficient, allowing multiple stations or sensors to connect and share signals, making it suitable for the Internet of Things (IoT). It has comparable power consumption to Bluetooth, LoRa, and Zigbee, but provides faster data speeds and wider coverage range [102]. This chapter provides a comprehensive overview of the key features of the IEEE 802.11ah standard, with a focus on the physical (PHY) and medium access control (MAC) layers.

3.2.1 IEEE802.11ah Architecture

The architecture of the IEEE 802.11ah standard maintains the structure of earlier IEEE 802.11 systems. This preservation of network architectures ensures compatibility and allows for the use of existing network configurations. Additionally, the IEEE 802.11ah standard supports various applications, including point-to-multipoint, fixed, and outdoor applications [103, 104].

Moreover, it introduces support for a relay architecture, where the Access Point (AP) is expanded through a two-hop relay approach. Figure 3.1 provides a simplified representation of this approach. The diagram illustrates that the relay consists of a relay-STA connected to the Root AP and a relay-AP connected to the end STAs. This configuration enables the transmission of frames in both directions. These relays extend the coverage area of the Basic Service Set (BSS) and can reduce energy consumption and packet delivery time.

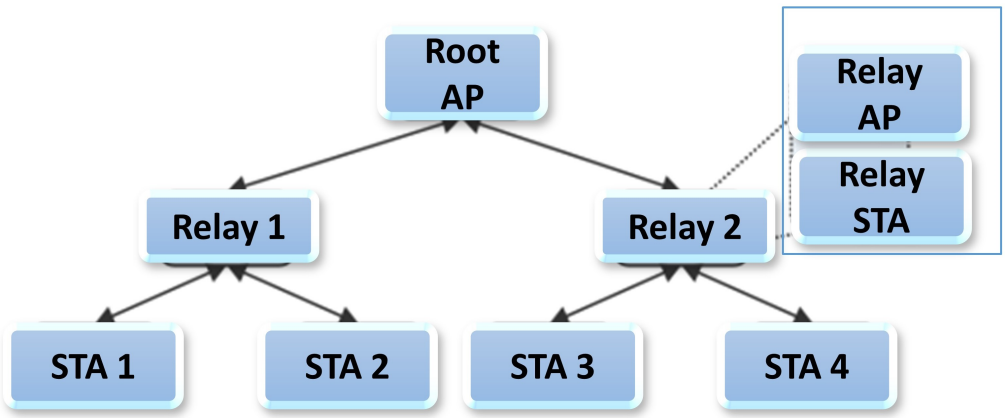

Figure 3.1: IEEE 802.11ah Relay Architecture [104]

The 802.11ah standard allows for the establishment of multiple Basic Service Sets (BSSs) that can operate on either the same or different carrier frequencies.

The specific frequencies used are determined by the regulatory guidelines in the region where the system is deployed. Additionally, these BSSs have the flexibility to operate on different channel bandwidths ranging from 1MHz to 16 MHz, in accordance with the channelization policy of the respective country.

3.2.2 Motivation of IEE802.11ah Development

The wireless sensor network market has experienced significant growth, leading to the need for new standards that can address requirements not covered by the existing IEEE 802.11 amendments. Owing to its focus on personal computers (PCs), the original 802.11 standard did not adequately support low-powered devices. This necessitated the use of amendments.

The IEEE 802.11ah standard aims to achieve several goals. It seeks to provide long-range transmission capabilities of over 1 km at speeds exceeding 100 kbps, while minimizing energy consumption and supporting large networks. In addition, it aims to offer cost-effective wireless sensor network solutions for various applications, including building automation, smart metering, surveillance, and challenging environments.

IEEE 802.11ah aims to achieve these goals by minimizing changes to the existing IEEE 802.11 standard. The physical (PHY) and medium access control (MAC) layers presented in this study are built upon the IEEE 802.11ac amendment, which focuses on enhancing the efficiency by reducing the control frames and shortening the MAC header.

Standardizing sub-1GHz WLANs offers several advantages.

- It is highly user-friendly in outdoor settings and exhibits exceptional signal transmission properties at lower frequencies across various installation scenarios within the Industrial, Scientific, and Medical (ISM) bands.
- A high sensitivity and a high link margin enhanced the reliability of the standard.

3.2.3 IEEE 802.11ah Use Cases

The support provided by IEEE 802.11ah encompasses various applications, such as industrial and home automation, healthcare, smart metering, and agriculture. These applications typically involve wireless sensor nodes that monitor the environment and collaborate to transmit aggregated data to the network. Figure 3.2 illustrates the architecture of IEEE 802.11ah for different use cases. This standard introduces an efficient scheduling and polling method to ensure scalability for a large number of stations (STAs) that operate in infrastructure mode only. Additionally, an advanced power-saving mechanism has been proposed to address the power consumption issue found in traditional Wi-Fi technologies. [105].

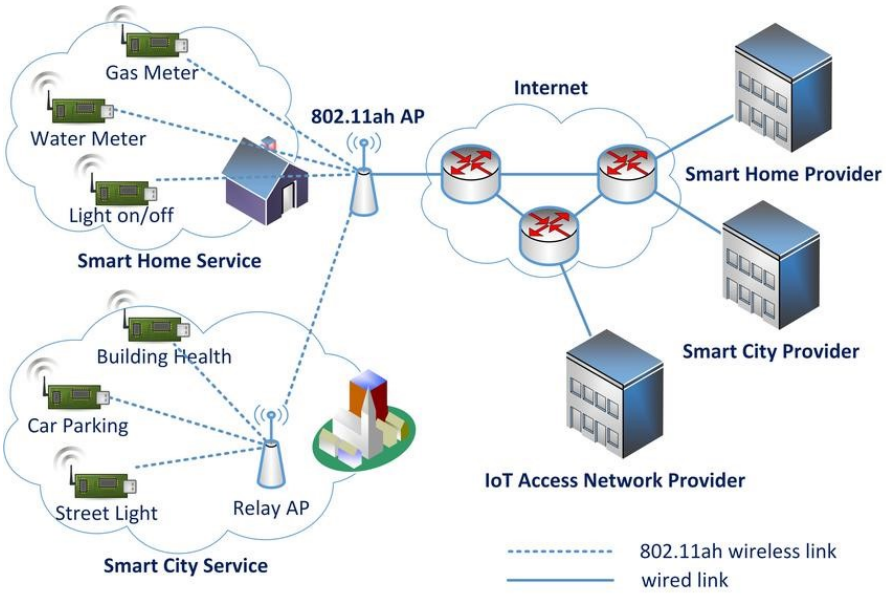

Figure 3.2: IEEE802.11 ah uses [106]

1. Smart sensors and meters

   The performance of the battery is an important factor in selecting a standard when a large number of nodes are deployed to cover large areas. Sensor networks are among the use cases endorsed by TGahs. Owing to increased penetration through obstacles and other walls at low frequencies, more nodes deployed in a single leap. The diversity provided by IEEE 802.11ah benefits many sensor network applications [106, 107] such as: smart meters,

smart grids, indoor healthcare and fitness system, automation of industrial processes, and environmental monitoring.

2. Backhaul networks

   The IEEE 802.11ah TGah standard also addresses the establishment of a backhaul network that connects sensor devices to remote servers. The extensive coverage of frequencies below 1 GHz enables a simple network configuration for connecting access points (APs) operating within this frequency range, such as wireless mesh networks. These networks typically operate in a multi-hop system, where traffic loads are unevenly distributed. Nodes located closer to the sink node experience higher uplink traffic loads. Consequently, power consumption and traffic load are influenced by location, and nodes with heavy traffic loads can limit the network's lifespan as they require more power consumption [108].

3. Extended range of Wi-Fi for traffic off-loading

   Mobile carriers have faced a significant surge in traffic loads due to the widespread usage of mobile devices. This increased consumption necessitates a higher capacity in wireless networks to meet user demands for high-speed access anytime and anywhere. To enhance bandwidth, operators have implemented technologies like HSPA and LTE. However, achieving higher speeds may not always be cost-effective due to limited bandwidth availability, even with 4G networks [109].

   The IEEE 802.11ah task group has adopted cellular traffic offloading as a use case. While 802.11n technology could improve offloading by providing higher bandwidth, the low power consumption and long-range capabilities of IEEE 802.11ah make it particularly suitable for supporting battery-powered mobile devices. As a result, the technical requirements for a WiFi-based solution are effectively met by IEEE 802.11ah, which led to its selection by the task group over alternative amendments.

4. M2M communication

   With the proliferation of M2M (machine-to-machine) standards being developed in different standardization bodies, IEEE 802.11ah can play a vital role in establishing a foundation for M2M standards that incorporate cloud computing capabilities [110]. This standard is particularly relevant for applications like smart metering, security sensing, and fleet management. IEEE

802.11ah addresses the necessary functionalities for these applications, including support for a large number of devices, low power consumption, and both short- and long-range data transmission.

3.3 PHY LAYER DESIGN

The physical layer design for the 802.11ah standard is based on the previous modifications of the 802.11 standard. Building upon the design of 802.11ac, which operates at bandwidths of 20MHz, 40MHz, 80MHZ, and 160MHz, IEEE 802.11ah's PHY was adapted to support these bandwidths. A 1 MHz channel was specified in addition to 802.11ah for extended coverage. In the next section, we will present the features of the 802.11ah PHY layer concerning the modulation and transmission schemes described by the authors in [111].

3.3.1 Channelization

The allocation of channels varies by country, leading to distinct sub-1 GHz ISM bands for 802.11ah across countries [111], such as Europe, the United States, Singapore, China, South Korea, and Japan. Figure 3.3 illustrates the accessibility of frequency spectrums and channel allocation in significant geographical locations. In South Korea, the operational ISM bands extend from 917.5 MHz to 923.5 MHz, providing a 6 MHz band with a 0.5 MHz for offset to avoid disruption to older wireless systems operating at lower frequencies. Europe is allocated a 5 MHz frequency range, from (863 MHz to 868 MHz), with a guard band equal to 600 KHz. China implements a channelization model that spans from (755 MHz to 787 MHz). The Effective Radiated Power (ERP) in the range of 755 MHz to 779 MHz is restricted to a limit of 5 mW, while the limit increases to 10 mW in the range of 779 MHz to 787 MHz. Consequently, a total bandwidth of 32 MHz is available within this range. In Japan, the channelization model covers a frequency range of 916.5 MHz to 927.5 MHz, resulting in a bandwidth of 11 MHz. This model includes 0.5 MHz allocation for designating center frequencies instead of using start/stop bands.

The channelization model in Singapore allows for the operation of the standard within specific frequency bands, namely (866 to 869) and (920 to 925), which

adds up to a total of 8 MHz bands. The United States leads to band availability by adopting a range of 26 MHz bands, specifically from ‘902 MHz to 928 MHz). As a result, the U.S. is the only country that can operate using a 16 MHz bandwidth.

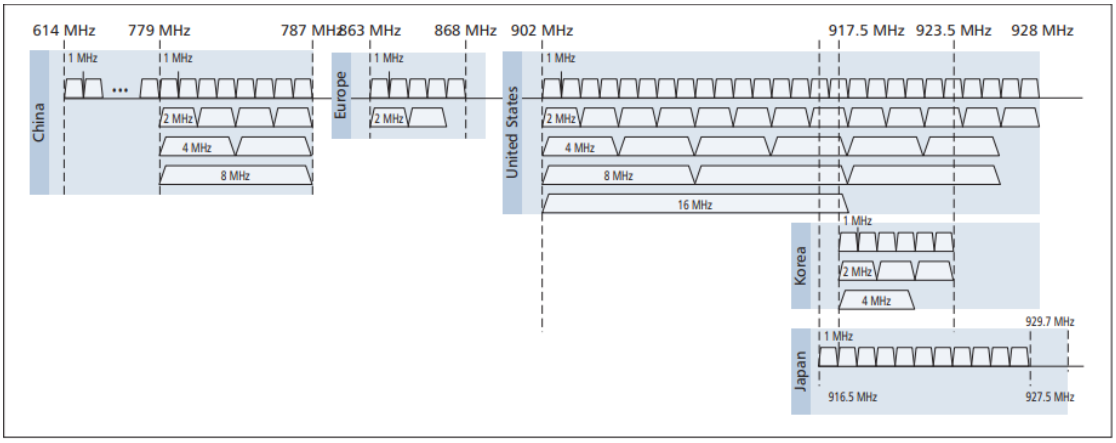

Figure 3.3: Sub-1 GHz Bandwidth in Strategic Locations [111]

3.3.2 Transmission Modes

The PHY layer design is addressed according to the framework specified in the standard (TGah group) in two groups:

- Transmission bandwidth setting for a 1 MHz channel
  In this scenario, the modulation methods used were identical to those found in IEEE 802.11ac’s Fast Fourier Transform (FFT). The physical layer makes use of a 64-subcarrier OFDM waveform separated by 31.25 KHz.

- Transmission bandwidth setting for a 2 MHz channel
  In this case, the spacing of the subcarrier is 31.25 KHz, and the OFDM consists of 32 tones.

Table 3.1 describes the PHY layer specifications.

These transmission patterns are considered to operate in various (MCS) to attain two performance scenarios: communication for long-range and capabilities for high data rate. The standard supports different modulation such as BPSK, QPSK, and QAM. It takes 64 FFT to construct the OFDM symbol for a 2 MHz through a

Table 3.1: PHY Layer Specifications

Characteristics	**Value**
Clear Channel Assessment(CCA) Time	40 μs
Short Inter-frame Space(SIFS) Time	160 μs
Slot Time	52 μs
Air Propagation Time	6 μs

single spatial stream, but only 52 of those subcarriers are used for data transmission. Table 3.2 lists the different modulations (MCSs) for 2MHz Bandwidth Channels with the data rates transmission mode.

Table 3.2: MCS Index Modulation and Coding Scheme

MCS Index	**Modulation**	**Coding Rate**	**NSS SS**	**N SCDT**	**N DBPSCS**	**N DBPS**	**OFDM SD**	**CP**
MCS-0	BPSK	1/2	1	52	1	26	40 μs	0.65
MCS-1	QPSK	1/2	1	52	2	52	40 μs	1.3
MCS-2	QPSK	3/4	1	52	2	78	40 μs	1.95
MCS-3	16-QAM	1/2	1	52	4	104	40 μs	2.6
MCS-4	16-QAM	3/4	1	52	4	156	40 μs	3.9
MCS-5	64-QAM	2/3	1	52	6	208	40 μs	5.2
MCS-6	64-QAM	3/4	1	52	6	234	40 μs	5.85
MCS-7	64-QAM	5/6	1	52	6	260	40 μs	6.5
MCS-8	256-QAM	3/4	1	52	8	312	40 μs	7.8
MCS-9	256-QAM	5/6	-	-	-	-	-	-

3.4 MAC LAYER DESIGN

The MAC layer of IEEE 802.11ah has been designed to enhance the MAC protocols and frame formats, with the primary objective of reducing the power consumption of client devices. It also supports a large number of clients for sensing applications and Internet of Things (IoT) deployments in both indoor and outdoor environments. The specific MAC layer features are discussed in the subsequent section.

3.4.1 Organization of Associated Stations

According to the IEEE 802.11ah standard [110], three types of stations are specified, and each type has its own set of rules to govern their access to the shared channel. The station types were as follows:

- **Traffic Indication Map (TIM) Stations:** These stations receive traffic indication maps, which inform them of the presence of data frames destined for them in the access point's buffer. TIM stations have specific rules to follow when accessing the shared channel.
- **Non-TIM Stations:** These stations did not receive traffic indication maps. They have different rules for accessing shared channels compared with TIM stations.
- **Non-scheduled Stations:** These stations operate in a contention-based manner without a specific timing schedule. They contend for channel access using contention protocols such as Carrier Sense Multiple Access with Collision Avoidance (CSMA/CA).

  Each station type in IEEE 802.11ah has unique characteristics and access rules to ensure efficient and fair utilization of the shared channel.

3.4.2 MAC Frame Types

The conventional MAC frame structure follows a consistent arrangement of fields in all frames. A typical MAC frame is depicted in Figure 3.4. The frame consists of

several fields, including the Frame Control field, Duration/ID field, address fields, and the concluding field known as the Frame Check Sequence (FCS). These fields form the basic frame format that is shared by all frames, encompassing different subtypes and types. However, there are additional fields specific to particular frame types and subtypes [112].

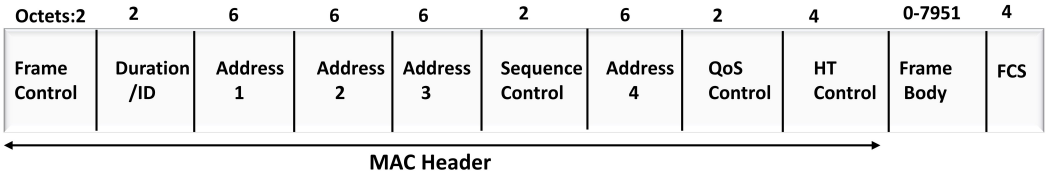

Figure 3.4: MAC format

In the 802.11ah standard, modifications have been made to the elements within the Frame Control field, particularly concerning combinations of type and subtype. Notably, a significant alteration was implemented in PS-Poll format. The original IEEE 802.11 format along with the format adopted by TGah illustrates Figure 3.5.

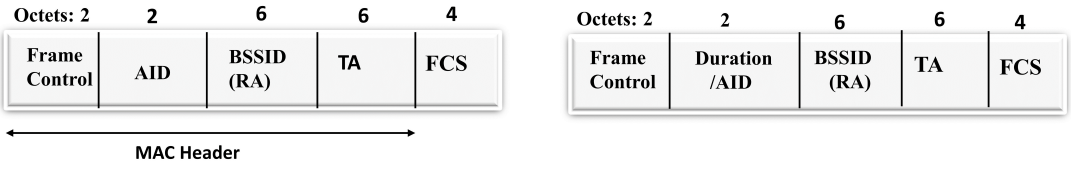

Figure 3.5: Frame formats for PS-Poll in IEEE 802.11 and IEEE 802.11ah

The duration/ID field serves different purposes depending on the context in which the PS-Poll frame is sent. When the PS-Poll is the first frame in a Speed Frame exchange initiated by a station (STA), the duration/ID field holds the duration value. However, in other cases, the duration/ID field contains an Association Identifier (AID). In addition to the existing frame types, IEEE 802.11ah introduces a novel frame called the Null Data Packet (NDP). The NDP is designed to reduce the MAC protocol overhead within an IEEE 802.11 Basic Service Set (BSS).

3.4.3 Support of Large Number of Associated Stations

A significant challenge in adopting the traditional IEEE 802.11 is the limited capacity for multiple stations to be concurrently associated with a single AP. Therefore, TGah introduced an innovative hierarchical approach that organizes stations into groups, enabling support for more devices. The configuration of each device group may vary based on the specific application, power requirements, or targeted Quality of Service (QoS) (TGah).

- The creation of a novel (AID) system that categorizes stations into blocks (referred to as TIM groups) sub-blocks, pages, and station indexes within sub-blocks.
- The subdivision of a partial bitmap is associated with the TIM element into bitmaps, each corresponding to a TIM group.

During the association phase, the AP assigned a unique AID to stations. The structure of AID is illustrated in Fig. 3.6. This AID, consisting of 13 bits, significantly enhances the maximum supported stations from (2,007) in 802.11 to (8,191) in 802.11ah.

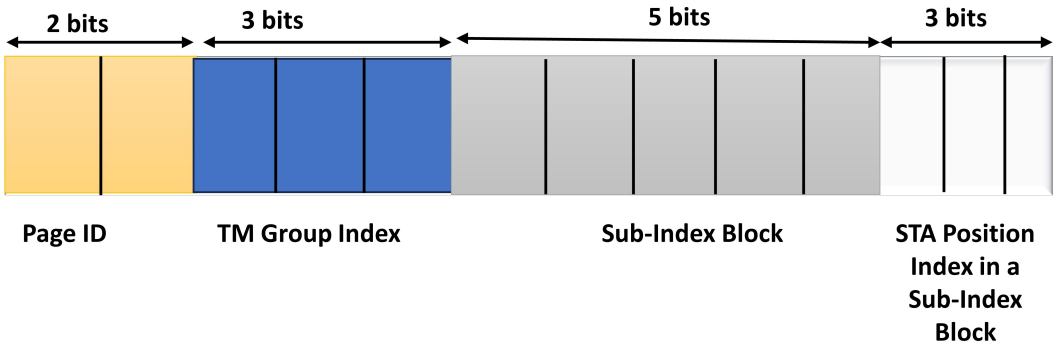

Figure 3.6: structure of AID frame

3.4.3.1 Relay

The IEEE 802.11ah standard supports relay mechanism which enhances the access point (AP) coverage area through a two-hop relay mechanism. As depicted in the Figure 3.1, the relay comprises a relay station and relay access point (relay-AP) [113]. The relay is linked to Root AP, while the relay-AP linked to the STAs end. This allows for bidirectional transmission of frames. Including relays expands the area coverage of the basic service set (BSS) and reduce energy consumption and transmission time and when delivering packets successfully.

3.4.3.2 Sectorization of Group

Group Sectorization uses spatial division multiple access (SDMA) with time division multiple access. It divides the coverage area of BSS into subregions (geographical areas), with each subregion including a subset STAs to mitigate hidden station problems, interference and traffic congestion. This division is achieved by transmitting or receiving the Montreal Protocol through multiple air links encompassing multiple sectors of the enterprise support system.

3.4.4 TIM stations Power Saving

IEEE 802.11ah includes a power-saving mode, often referred to as awake or sleep mode, which aims to minimize energy consumption in sensor devices. This mode utilizes power-saving features of the network interface by turning off the radio module during periods of low traffic.

During awake mode, the radio is active, allowing the wireless interface to establish data connections or remain idle. On the other hand, in the sleep state, the radio is deactivated, rendering the wireless interface unable to monitor or detect network activity. This power-saving mode is defined as Power Saving Mode (PSM) in the IEEE 802.11 standard.

In the PSM, the Access Point (AP) buffers incoming frames for mobile stations until the stations wake up and request the delivery of the buffered traffic. Once the

reception is complete, the station returns to the PSM. The IEEE 802.11ah standard incorporates two types of signaling-beacon frames to address this functionality.

- The Delivery-Traffic Indication Map (DTIM) provides information about sets of STAs that have pending data.
- Traffic Indication Map (TIM): The TIM and DTIM beacons inform a group of STAs at the AP about which STAs have pending data. The structures of the TIM and DTIM beacons are based on the Short Beacon Frame (SBF) and Information Elements (IE), each serving specific purposes. Figure 3.7 represented these structures.

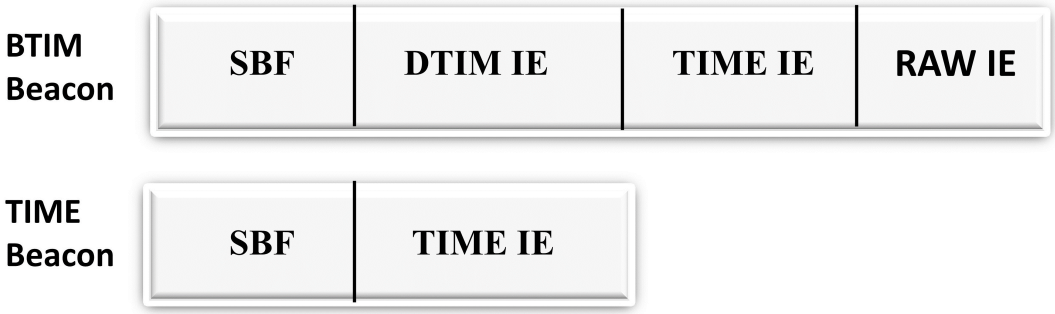

Figure 3.7: Structures of DTIM and TIM.

- SBF: The primary purpose of the AP is to announce its presence and synchronize the stations (STAs) within its network.
- DTIM IE: The capability enables stations (STAs) to determine their allocation within Traffic Indication Map (TIM) groups and the intervals at which they should wake up.
- TIM IE: The Access Point (AP) partitions the partial bitmap associated with one or multiple TIM Groups to indicate which stations within the TIM Group have pending data to receive.
- RAW IE: The RAW IE (Restricted Access Window Information Element) is responsible for signaling important information regarding the periods in which selected STAs contend for the channel. This Information Element, known as the RAW IE, includes details such as the duration from the beacon

to the Restricted Access Window (RAW), the duration of the RAW itself, and the methods used for creating sub-slots within the RAW period.

TGah has categorized STAs For 802.11ah into three types[111]:

- TIM STAs: STAs listen to TIM and DTIM beacons to enable efficient data transmission and reception, similar to IEEE 802.11 Power Saving Mode (PSM) concept.
- Non-TIM STAs: STAs listen to beacons of DTIM for data exchange. TIM IE excludes buffering, assuming that there is no periodic requirement for them to awaken for beacon receiving.. This design allows STAs to remain in the Power Saving Mode (PSM) for extended periods without the concern of beacon reception, indicating an ultralow power mode.
- Unscheduled STAs: STAs are not required to listen to beacons and can engage in data transmission or reception at all times

In the IEEE 802.11 Power Saving Mode (PSM), the TIM beacon contains an Information Element (IE) field that provides information about the buffered packets for STAs in PSM. STAs in PSM periodically wake up upon receiving beacons to check if there are packets addressed to them. When data is present, the STA sends a Power Saving (PS)-Poll Frame to the AP to request the transmission of the buffered packets. Any STA can enter PSM when it determines from the TIM beacon that no data is specifically intended for it.

3.4.4.1 Page Segmentation and TIM

IEEE 802.11ah uses a TIM and Page Segmentation technique to reduce channel contention time and maximize inactivity for stations. It organizes stations into hierarchical TIM groups (TGah) for scheduling, signaling, and channel resource allocation. This allows only TIM groups to compete simultaneously, resulting in energy savings. The system includes TIM beacons for station-level signaling.

- DTIM beacons are utilized for signaling purposes and indicate that TIM groups, whether unicast or multicast, have pending data at the AP. These beacons also provide detailed information about the properties of the Restricted Access Window (RAW), including the duration of segments and sub-slotting methods.

– TIM beacons enable stations to enter a power-saving state during a restricted access window if they have no packets to transmit. This is possible when the station detects no incoming traffic addressed to its TIM group or detects incoming traffic aimed at its TIM group but not indicated in its TIM beacon.

3.4.4.2 Advanced Modes of Signaling

The IEEE 802.11ah standard includes two advanced signaling modes in the TIM and Page Segmentation scheme, which are activated when there are more than one network pages [106]:

– Non TIM offset: In this mode, the signaling for a specific TIM group is repeatedly transmitted within the same beacon, with each repetition corresponding to the number of network pages. This mode is the default in IEEE 802.11ah.

– TIM offset: In this mode, a 5-bit field is included in the DTIM beacon, allowing for the scheduling of TIM groups from separate pages using their own TIM beacons. Although the TIM offset mode consumes less energy compared to the non-TIM mode, it may have limitations in terms of the maximum number of supported stations, network efficiency, and packet delivery ratio (PDR).

3.4.5 Channel Access

The 802.11ah standard uses TIM stations' channel access method, which combines AP-centralized time allocation with CSMA/CA mechanism of Distributed Coordination Function. The limited access window, consisting of downlink, uplink, and multicast segments, restricts access between consecutive TIMs [114]:

– Uplink: In IEEE 802.11ah uplink transmission, stations monitor TIM groups to determine channel contention time, using Distributed Coordination Function (DCF) mechanism. Primary access method and handshaking technique can be used for channel access and collision avoidance.

– Downlink: IEEE 802.11ah requires stations to monitor their TIM beacons and initiate contention using the Distributed Coordination Function (DCF).

When a station's backoff period expires, it sends a Power Saving (PS)-Poll frame to request relevant data, as illustrated in Figure 3.8.

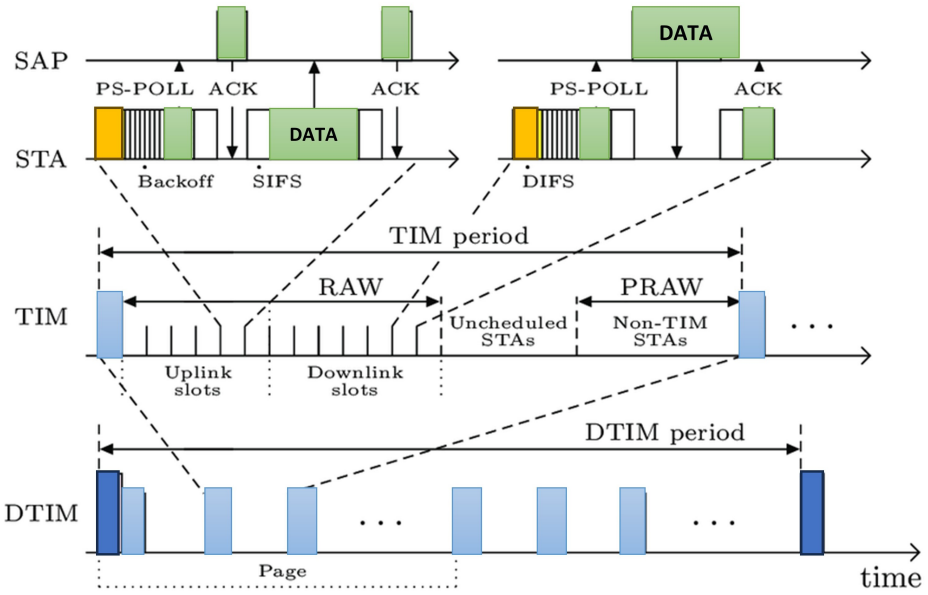

Figure 3.8: IEEE 802.11ah access mechanism.

3.4.5.1 Target Wake Time(TWT)

Non-TIM STAs are permitted by the access point (AP) to either send uplink traffic or request buffered downlink traffic upon waking up. However, this simplistic approach can lead to network performance issues, particularly when many STAs wake up simultaneously, resulting in uncontrolled traffic and contention that may cause excessive collisions or access delays[115]. To address this challenge, TGah has introduced an approach where AP coordinates the of STAs waking up at predefined times, temporally spreading out channel access. This mechanism relies on a newly defined function called TWT (Target Wake Time). This time allows the access point (AP) to designate precise time intervals for each station (STA) to utilize the communication channel. The AP transmits TWT data to each STA using a newly introduced Information Element (IE) known as TWT IE, as seen in

Figure 3.9. The structure of the Request Type field is depicted in Figure 3.10. The interchange of these elements occurs during the association request and response frames, and they dictate the timing and frequency at which STA wakes up for uplink and transmissions.

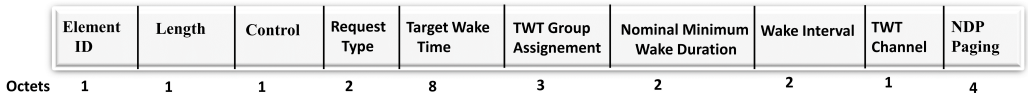

Figure 3.9: TWT format.

Figure 3.10: Request Type format.

When a TWT (Target Wake Time) element is sent from a TWT requesting station to a TWT responding station, the TWT Request subfield is set to 1. Conversely, if the TWT element is sent from a TWT responding station to a TWT seeking station, the TWT Request subfield will have a value of 0.

In cases where the Access Point (AP) has buffered packets for a Station (STA), it can send a Null Data Packet (NDP) frame to the STA, allowing the STA to request the delivery of the buffered data. If the AP does not send the NDP paging frame, the STA can still transmit uplink frames.

3.4.5.2 Restricted Access Windows

The TGah standard retains existing contention-based channel access procedures for TIM STAs, but introduces a new contention-free strategy to address hidden node

problems. The Restricted Access Window (RAW) optimizes medium utilization by minimizing collisions, providing exclusive access to specific STAs, reducing contention and improving performance[116].

The Resource Allocation (RA) frame is proposed to optimize medium utilization and reduce collisions by dynamically learning the designated time slot for medium access for STAs. This approach allows STAs to transmit only ready-to-transmit stations, avoiding unnecessary allocation to all TIM stations. The structure and timing diagram are illustrated in Figure 3.11.

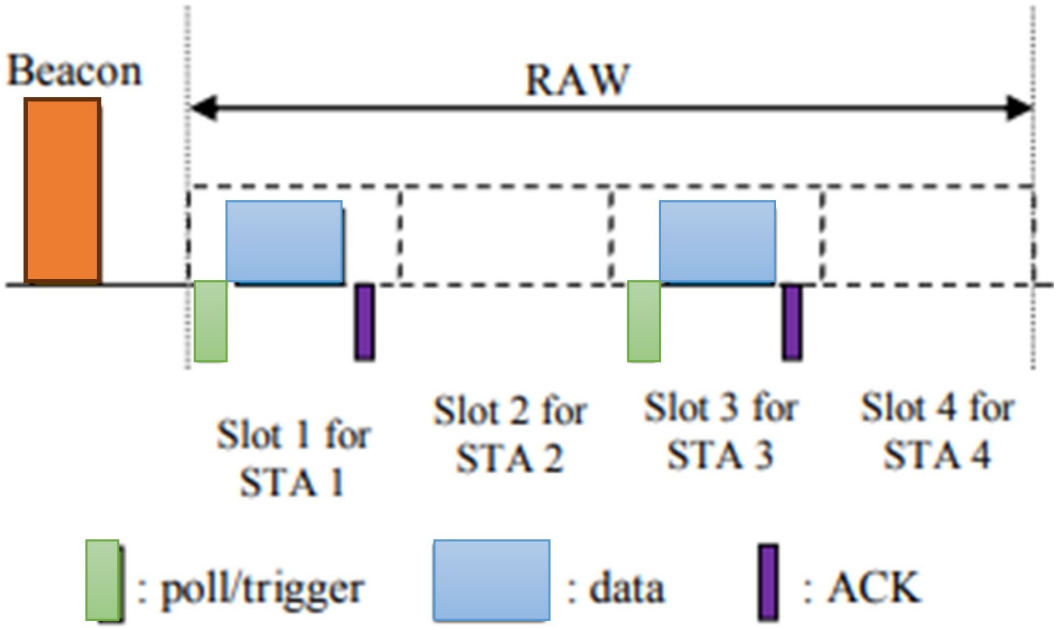

Figure 3.11: RAW Mechanism.

3.4.5.3 Distributed Coordination Function (DCF)

The DCF in IEEE 802.11 ah uses Basic Access and RTS/CTS techniques for packet transmission as shown in Figure 3.12. A station monitors a channel and

sends a new packet if it remains unused for a specific period. The back-off time is a random integer multiple of a primary time slot, preventing collisions. If the channel becomes busy, the countdown is paused until another idle DIFS period is observed. The back-off rules determine the next available time slot for transmission.

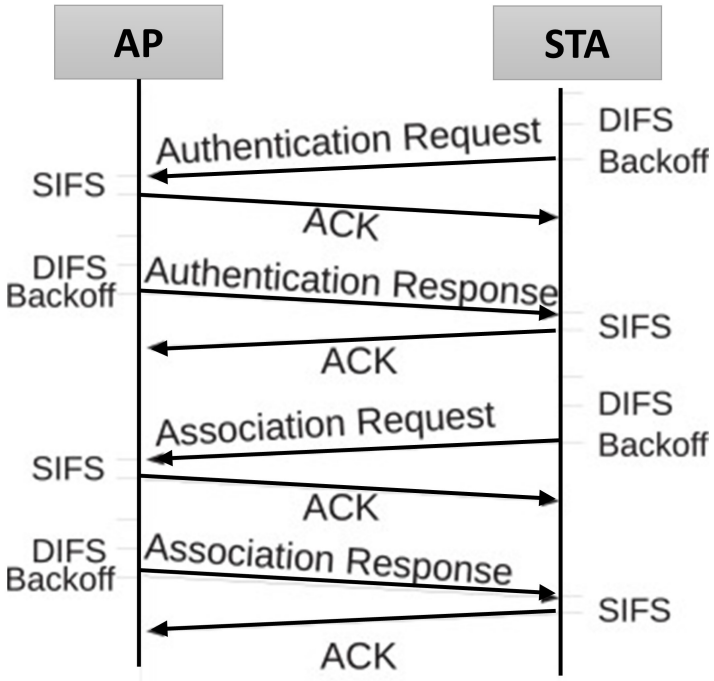

Figure 3.12: Distributed coordination function (DCF) mechanism

3.4.5.4 Long Sleeping Periods

Stations that operate under the Page Segmentation and TIM scheme are obligated to listen to DTIM beacons, even during extended periods when they are unlikely to send or receive data. In IEEE 802.11ah, all types of stations are allowed to set substantially longer doze times, particularly during their primary interaction with the Access Point (AP) [117]. However, these extended doze times can lead to significant clock drift, which presents a challenge for synchronization. To mitigate

potential synchronization delays with the network, a station needs to wake up earlier as the duration of its inactivity (sleep) increases. This ensures that the station remains synchronized with the network and avoids any detrimental impact caused by clock drift.

3.4.5.5 Support for Small Transmission

To mitigate the impact of high overheads and low performance associated with small data transmissions in wireless sensor networks, TGah introduces three key enhancements. IEEE 802.11ah decreases the size of the MAC header from 28 to 18 bytes by using association IDs instead of regular MAC addresses, in contrast to IEEE 802.11. Furthermore, TGah specifies many null data packet frames that consist solely of a single PHY header. These frames are used to condense the existing IEEE 802.11 signaling frames, including ACKs, block ACKs, CTSs, and PS-Polls. Finally, a speed frame exchange method is implemented to indicate the successful receiving of frames by broadcasting a data frame instead of a conventional acknowledgment (ACK) [118].

3.5 IEEE802.11 AH SIMULATION AND PERFORMANCE EVALUATION

In this section, the PHY/ MAC layers of the 802.11ah are analytically modelled using MatLab. The goal is to provide a rationale for the advancement of this technology. Employing various performance metrics on diverse real-life scenarios makes assessing the network's performance feasible.

3.5.1 Model Environment

This section aims to assess the infrastructure of the Basic Service Sets (BSSs). We assume there is one access point (AP) at least in the network, which it serving a number of stations (STAs).

3.5.2 Network Topology

The topology suggested is point-to-point, where stations (STAs) directly exchange packets with the access point (AP) without intermediate nodes. By using this strategy, the AP is certain to receive packets in a single hop. Single-hop transmissions have reliability compared to multi-hop transmissions because they introduce less delay, which is particularly critical for applications in the medical field. In this evaluation, we assume an ideal channel without consideration for hidden nodes.

3.5.3 Access Mechanism

The 802.11ah standard, designed for low-power and long-range IoT applications, employs the DCF as fundamental access mechanism, utilizing CSMA/CA with a random backoff timer. DCF incorporates enhancements tailored to these applications, such as a longer contention window, reduced inter-frame space (IFS), and power-saving capabilities [119]. Additionally, 802.11ah supports the RTS/CTS methods to mitigate collisions caused by hidden nodes to improve the overall performance of the network. The IEEE802.11ah evaluation employs DCF with two access mechanisms: basic, and RTS/CTS access. as illustrated in Figure 3.13 and Figure 3.14.

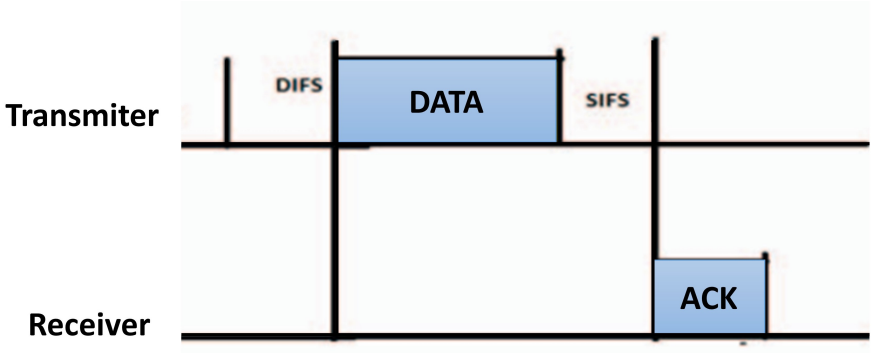

Figure 3.13: Basic Access Mechanism

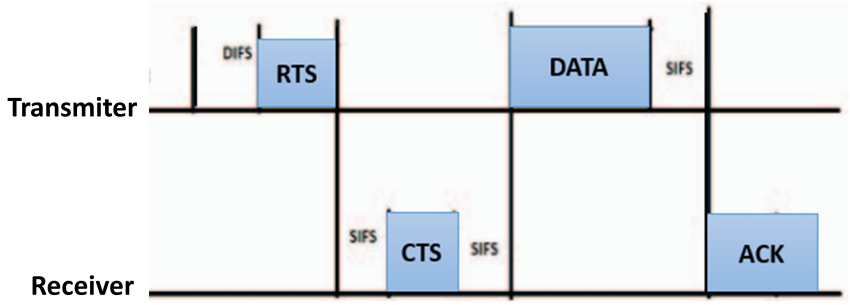

Figure 3.14: RTS/CTS Mechanism

3.5.4 Channel model

A channel model is crucial for wireless communication system design, as it characterizes the effects of various environmental factors on a transmitted signal. IEEE 802.11ah, intended for various applications ranging from in-home to outdoor urban environments, needs a versatile channel model to represent the diverse deployment scenarios.

The standard path loss model for 802.11ah is based on the TGah model as referenced in articles [120–122], and can be represented by equation (3.1), presuming an antenna height of 15 meters above for the outdoor scenario.

$$P_{\text{loss}} = 8 + 37.6 \log_{10}(d) \tag{3.1}$$

Where d is the distance between the transmitter and receiver at a frequency of 900MHz. A correction factor $21 \log_{10}\left(\frac{f}{900\text{MHz}}\right)$ should be applied for other frequencies.

The path loss for the outdoor scenario after correction is calculated as:

$$P_{\text{loss}} = 23.3 + 36.7 \log_{10}(d) \tag{3.2}$$

Where the distance and frequency are the same as the conditions regarding equation (3.1).

The TGah path loss model for the indoor is derived by scaling down the frequency operations in TGah. It comprises a model for free space with a slope of up to 2 for a specific distance known as the breakpoint distance (d_{BP}). Beyond this distance, the model transitions to a slope of 3.5. Two scenarios are considered: one is a large indoor with (NLoS) conditions for open space (Model C) and a breakpoint distance of 5 meters, and the other is a scenario with (LoS) conditions represented by (Model D) and a breakpoint distance of 10 meters. Both channel models are for indoor environments.

$$L(d) = \begin{cases} L_{\mathrm{FS}}(d) = 20\log_{10}\left(\frac{4\pi f_c}{c}\right), & \text{if } d \leq d_{\mathrm{BP}} \\ L_{\mathrm{FS}}(d_{\mathrm{BP}}) + 35\log_{10}\left(\frac{d}{d_{\mathrm{BP}}}\right), & \text{if } d > d_{\mathrm{BP}} \end{cases} \tag{3.3}$$

Where c is the speed of light in m/s, and f_c is the center of the carrier frequency in MHz. Figure 3.15 shows theoretically the path loss expected in an outdoor envi-

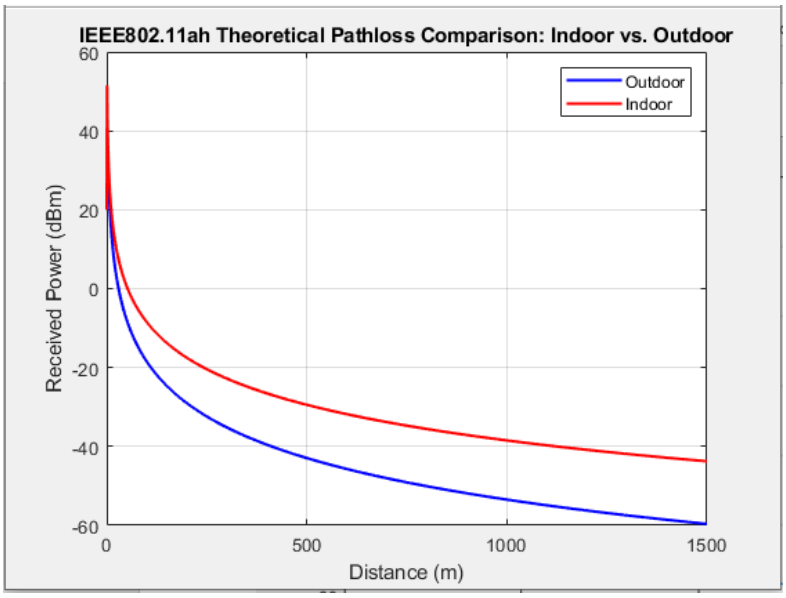

Figure 3.15: Comparison IEEE802.11ah path loss for indoor and outdoor

ronment compared to an indoor one for the IEEE 802.11ah standard, where path loss is associated with increasing distance between the transmitter and receiver.

3.6 PERFORMANCE METRICS

Performance metrics for network evaluation are essential for the QoS. The primary objective of utilizing these metrics is optimizing user satisfaction by effectively utilizing the existing resources to support various applications with specific QoS demands. The subsequent section will assess the following performance metrics.

- Average delay
- Theoretical Maximum throughput(TMT).
- Saturation throughput.
- Energy efficiency.

3.6.1 Average Delay

The theoretical delay provides insights into a node's time from transmitting a request (RTS) to beginning transmission to acknowledgment receiving, assuming ideal conditions. Figure 3.16 illustrates that MCS1 exhibits significant delays compared to MCS4 as the size of the data packet increases.

A higher MCS (Modulation and Coding Scheme) index corresponds to higher data rates, resulting in shorter frame transmission durations (lower delay) and reduced energy consumption.

3.6.2 Theoretical Maximum Throughput(TMT)

The theoretical maximum throughput (TMT) refers to the highest possible data transfer rate that can be attained in an IEEE 802.11 network. It focuses exclusively on the actual data transfer rate offered by the MAC layer. Hence, the TMT can be precisely described as the upper limit of MAC service. The TMT is calculated for different access mechanisms, such as RTS/CTS and Basic Access, under ideal conditions for transmission [123]. Then, the throughput expression: To calculate

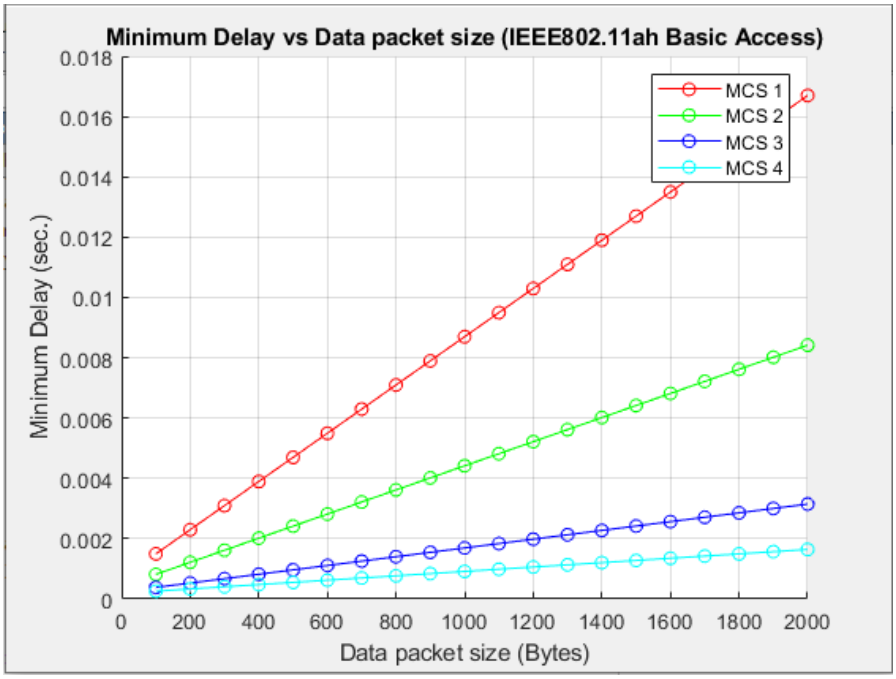

Figure 3.16: Average delay

the TMT for 802.11ah , the MAC SDU (MSDU) divides by the time required for its transmission.

$$TMT = \frac{\text{MSDU size}}{\text{Delay per MSDU}} \tag{3.4}$$

Control frames are consistently transmitted at 1Mbps to maintain compatibility with older systems. Figures 3.14 and 3.15 mentioned above explain the transmission of data packets using Basic access and RTS/CTS methods. This pattern repeats in a definite cycle when consecutive traffic is sent from the transmitting node. It is important to note that the timing diagram differs between these access methods, and the duration of the block varies based on the spread spectrum technology and introductory data rates in use. The contention window (CW) does not grow exponentially in scenarios without collisions. Instead, the CW always remains equal to the CW_min, which can vary depending on the specific spread spectrum technology employed [124]. The backoff time is determined randomly, following a uniform distribution between 0 and CW_min, resulting in an expected

CW_min$\hat{2}$ value. Equation (3.5) illustrates how to calculate this backoff delay as a constant.

$$T_{BO} = \frac{CW_{min}}{2 \times \text{SlotTime}} \tag{3.5}$$

The overall delay is determined by adding up all the individual delay elements within a complete transmission cycle using the access scheme. The delay for CSMA/CA and RTS/CTS can be computed using equations (3.6) and (3.7), respectively.

$$\text{Delay per MSDU}_{\text{Basic}} = T_{BO} + \text{DIFS} + \text{ACK} + \text{DATA} + \text{SIFS} \tag{3.6}$$

$$\text{Delay per MSDU}_{\text{RTS/CTS}} = T_{BO} + \text{DIFS} + \text{RTS} + \text{CTS} + \text{ACK} + \text{DATA} + (3 \times \text{SIFS}) \tag{3.7}$$

We can calculate TMT by taking the ratio of the number of bits in MSDU to the combined delay for the access mechanism.

$$TMT_{\text{Basic}} = \frac{L_{\text{payload}}}{T_{BO} + \text{DIFS} + \text{ACK} + \text{DATA} + \text{SIFS}} \tag{3.8}$$

$$TMT_{\text{RTS}} = \frac{L_{\text{payload}}}{T_{BO} + \text{DIFS} + \text{RTS} + \text{CTS} + \text{ACK} + \text{DATA} + (3 \times \text{SIFS})} \tag{3.9}$$

According to IEEE 802.11ah, it is specified that control frames should be transmitted using the most MCS available. However, any available MCS can be used for data packets, so the data rate is considered when determining the data packet duration. The control frames' duration and data were calculated using the method described in the reference [125].

$$T_{\text{control\_frames}} = \left\lceil \frac{L_{\text{control\_frames}}}{L_{\text{basic\_datarate}}} \right\rceil \times T_{\text{sym}} + \text{PHY} \tag{3.10}$$

The length of the DATA frames is calculated by:

$$T_{\text{DATA}} = \left\lceil \frac{L_{\text{payload}} + \text{MAC}}{\frac{R}{\text{basic\_datarate}} \times L_{\text{basic\_datarate}}} \right\rceil \times T_{\text{sym}} + \text{PHY} \tag{3.11}$$

Where R represents the data rate according to the MCS, and $L_{\text{basic\_datarate}}$ represents the data bits per OFDM symbol. Table 3.3 represents these values.

Table 3.3: Variable Definitions

Variable	CW1	CW2	CW4	CW8	CW16	Description
N_{SD}	24	52	108	234	468	Subcarriers in OFDM symbol
N_{ST}	26	56	114	242	484	Total number of useful subcarriers in OFDM symbol
N_{SP}	2	4	6	8	16	pilots Number per OFDM symbol
N_{SR}	13	28	58	122	250	Highest subcarrier per OFDM
Δ_F					$31.25kHz$	Frequency spacing

Figure 3.17 presents the computed TMT (Throughput Metric) for the Basic Access and RTS/CTS mechanisms across five distinct Modulation and Coding Schemes (MCS) within the IEEE 802.11ah standard. The figures demonstrate the benefits of the Basic Access mechanism over the RTS/CTS system under ideal conditions without collisions or errors. This advantage stems from the RTS/CTS mechanism necessitating the transmission of a larger number of control frames compared to the Basic Access mechanism, thereby enhancing overall performance.

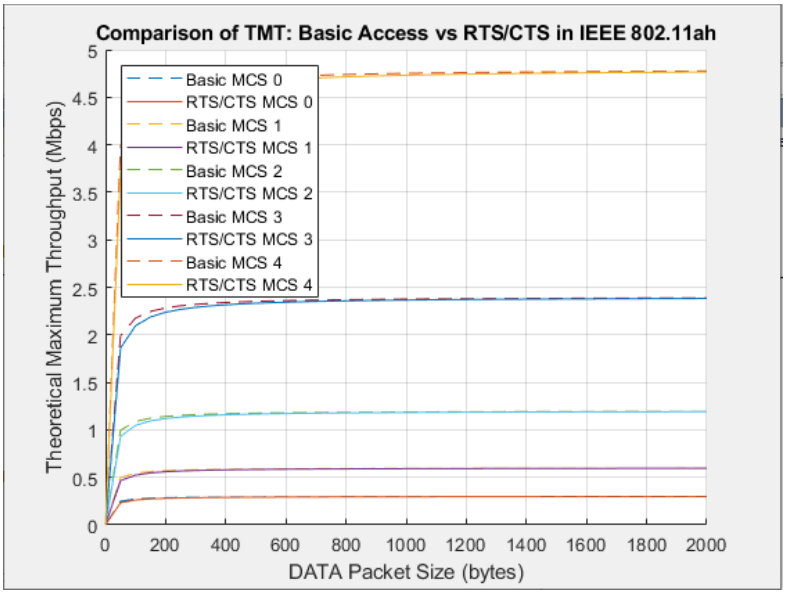

Figure 3.17: Comparison of IEEE 802.11ah Maximum Theoretical Throughput

3.6.3 Performance analysis for IEEE802.11ah

This analysis aims to assess the performance quality of the IEEE802.11ah standard when the network is operating at its maximum capacity and utilizing all available resources. This scenario holds significance as it allows us to evaluate the network's capabilities under heavy load, particularly relevant for real-world applications. Throughout this analysis, we will explore different performance indicators, including throughput, latency, and energy efficiency. These metrics will measure how well IEEE802.11ah manages a substantial amount of data traffic, the speed of data packet processing, and the efficiency of energy resource utilization.

• **Markov model:** is a mathematical model representing system progression at discrete time intervals. It is used in IEEE 802.11ah networks to address issues like the mobility of nodes, traffic patterns, and node quantities. It provides accurate representation, examination, and enhancement of network activity, enhancing performance and quality. However, its effectiveness depends on model precision and network algorithm execution [126]. In this section, we used the Markov model suggested in the references [127], [124] to analyze and improve the performance of IEEE 802.11ah in various network situations. This model is represented in Figure 3.18.

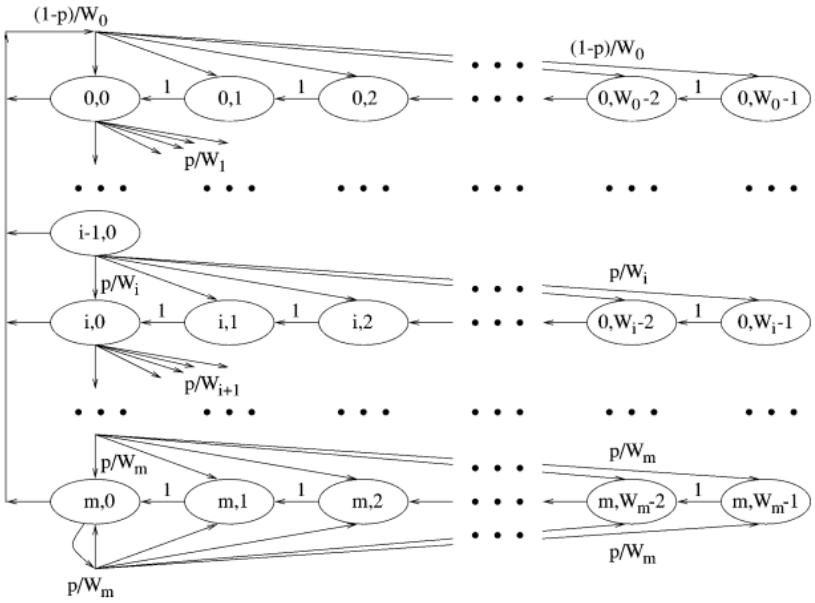

Figure 3.18: Model Markov chain. [126]

Figure 3.18 illustrates a discrete-time Markov chain. All nodes have access to the medium, but when the medium is occupied, the system duplicates the contention window (CW) and calculates the backoff time [127].

From the model, we can define the parameters as follows:

- m': represents the maximum number of backoff stages.
- W: denotes the contention window (CW).
- ρ: represents the probability of transmission failure.

The IEEE 802.11ah parameters include a CW_{min} value of 15 and a CW_{max} value of 1023. As a result, we can conclude that:

$$W_i = \begin{cases} 2^i W & \text{if } i \leq m' \\ W_i - 2^{m'} W & \text{if } i \geq m' \end{cases} \tag{3.12}$$

Where

$$\begin{aligned} W &= CW_{\min} + 1 \\ 2^{m'}W &= CW_{\max} + 1 \end{aligned} \tag{3.13}$$

For IEEE 802.11ah, the value of m is set to 6. It's important to note that, unlike Bianchi's approach [127], m' represents the maximum backoff stage in this context. According to 802.11, this value is more significant than m.

In this case, the parameter m also represents the maximum count of retransmission, which varies for data frames (5) and RTS frames (7). This is a distinction from Bianchi's approach [127]. which needs to differentiate between these two cases. The critical difference lies in our Markov model based on [128], which considers the impact of the frame retransmission limit. From the Markov model, we can represent the transition probabilities of only non-null one-step by:

$$\begin{cases} P_{i,k|i,k+1} = 1 & \text{if } k \in [0, W_i - 2], i \in [0, m] \\ P_{0,k|i,0} = \dfrac{(1-p)}{W_0} & \text{if } k \in [0, W_0 - 1], i \in [0, m-1] \\ P_{i,k|i-1,0} = \dfrac{p}{W_1} & \text{if } k \in [0, W_i - 1], i \in [1, m] \\ P_{0,k|m,0} = \dfrac{1}{W_0} & \text{if } k \in [0, W_0 - 2] \end{cases} \tag{3.14}$$

These transition probabilities correspond to the following factors: 1. The transition probabilities affect the back-off timer. 2. The back-off timer for the new packet begins from the current back-off stage. We also consider that after a successful transmission. 3. In an unsuccessful transmission case, the transition probabilities reflect the increase in back-off stages. 4. When the back-off stage reaches its maximum value, the transition probabilities indicate that the contention window (CW) will reset if the transmission fails; conversely, if the transmission succeeds, the new packet's back-off stage restarts.

Let the Markov chain stationary distribution be denoted as $b_{i,k}$. So:

$$\begin{aligned} b_{i-1,0} \cdot p &= b_{i,0} && \text{for } 0 < i \leq m \\ b_{i-1,0} &= p^i \cdot b_{0,0} && \text{for } 0 \leq i \leq m \end{aligned} \tag{3.15}$$

Due to the symmetry of the Markov chain, we can observe that for every $k \in (0, W_{i-1})$, the following holds:

$$b_{i,k} = \frac{W_i - k}{W_i} \begin{cases} (1-p) \sum_{j=0}^{m-1} b_{j,0} + b_{m,0} & \text{for } i = 0 \\ p b_{i-1,0} & \text{for } 0 < i \leq m \end{cases} \tag{3.16}$$

From equation (3.14) and considering chain transitions, we can simplify equation (3.15) as:

$$b_{i,k} = \frac{W_i k}{W_i} \quad b_{i,0} \quad \text{for } 0 \leq i \leq m \tag{3.17}$$

Hence, by applying the normalization condition to the stationary distribution, we obtain:

$$1 = \sum_{i=0}^{m} \sum_{k=0}^{W_i-1} b_{i,k} = \sum_{i=0}^{m} b_{i,0} \sum_{k=0}^{W_i-1} \frac{W_i - k}{W_i} = \sum_{i=0}^{m} b_{i,0} \frac{W_i + 1}{2} \tag{3.18}$$

The τ probability of a station (STA) transmitting in a randomly selected slot time is represented as follows:

$$\tau = \sum_{i=0}^{m} b_{i,0} \quad = \frac{1 - p^{(m+1)}}{1 - p} \cdot b_{0,0} \tag{3.19}$$

In the stationary-state, the probability that a station (STA) transmits a packet, denoted as p, can be expressed as:

$$p = 1 - (1 - \tau)^{n-1} \tag{3.20}$$

Where:

$$b_{0,0} = \begin{cases} \frac{2(1-p)(1-2p)}{W(1-(2p)^{m+1})(1-p)+(1-2p)(1-p^{m+1})} & \text{for } m \leq m' \\ \frac{2(1-p)(1-2p)}{W(1-(2p)^{m'+1})(1-p)+(1-2p)(1-p^{m+1})+W2^{m'}p^{m'+1}(1-2p)(1-p^{m-m'})} & \text{for } m > m' \end{cases} \tag{3.21}$$

We can write the above equation in simpler terms as:

$$b_{0,0} = \frac{2(1-\rho)(1-\rho)}{(1-2p)(W+1)+\rho W(1-(2\rho)^m)} \tag{3.22}$$

And the probability of τ as:

$$\tau = \frac{b_{0,0}}{1-\rho} = \frac{2(1-\rho)}{(1-2p)(W+1)+\rho W(1-(2\rho)^m)} \tag{3.23}$$

Moreover, the calculation of the ρ value is performed using the following equation:

$$\rho = 1 - e^{-\rho_i} \tag{3.24}$$

Where ρ_i is calculated as:

$$\rho_i = \lambda T \tag{3.25}$$

Where T represents the time required to transmit the packet, while λ denotes the average packet length within a one-second interval.

Performance analysis:

This section evaluates the 802.11ah performance under saturation conditions. The evaluation focuses on various metrics, including the saturation throughput, representing a maximum system load achievable under stable conditions as the offered load increases. Energy efficiency, average delay, and packet error rate.

1- **Saturation throughput analysis:**

The saturation throughput refers to the maximum system throughput that can be achieved under stable conditions when the system is operating at maximum load. In order to evaluate the throughput, we utilized the model proposed by [127] to analyze the behavior of a single station (STA) and determine the probability of successfully transmitting a packet within a randomly chosen slot time. This probability remains unchanged regardless of the specific access mechanism used, whether it is Basic or RTS/CTS. The throughput of both access modes is determined by examining the possible events that can occur within a slot time and is presented as a function of the calculated value of .

In this model, it is assumed that there are multiple competing STAs. The stochastic process b(t) represents the back-off window size for a particular station at a given slot time t. The slot time is denoted by the constant value , which represents the variable time interval between two consecutive reductions of the back-off time counter. One of the fundamental assumptions in this model is that the states of the STAs, represented by states(t), do not affect the probability p of a packet collision occurring.

We can represent the normalized throughput (S) of the system as the ratio:

$$S = \frac{L_{\text{Payload}}}{\text{Length of a slot time}} = \frac{P_{\text{tr}} P_s L_{\text{Payload}}}{(1 - P_{\text{tr}})\sigma + P_{\text{tr}} P_s T_s + (1 - P_s) P_{\text{tr}} T_c} \quad (3.24)$$

where: S is the throughput, is the slot duration, Tc is the Collision Time, and Ts is the time of successful transmission. P_{tr} = Transmission probability, P_s = transmission success. And calculated from equations below:

$$P_{\text{tr}} = 1 - (1 - \tau)^N \quad (3.25)$$

$$P_s = \frac{N\tau(1 - \tau)^{N-1}}{1 - (1 - \tau)^N} \quad (3.26)$$

The average interval during which the channel is occupied due to either a successful transmission or a collision. The payload refers to the mean length of a packet, while represents the duration of a time slot that is not occupied. T_c, T_S: represent the average times the channel is sensed as busy due to a successful transmission or collision. The Payload refers to the average packet length, and denotes the duration of an empty time slot.

The time for basic access is calculated as:

$$T_s^{\text{basic-mechanism}} = \text{DIFS} + T_{\text{DATA}} + T_{\text{ACK}} + T_{\text{PHY}} \tag{3.27}$$

$$T_c^{\text{basic-mechanism}} = \text{DIFS} + T_{\text{DATA}} + T_{\text{PHY}} \tag{3.28}$$

And for RTS/CTS mechanism calculated as:

$$T_S^{(\text{RTS/CTS})} = \text{DIFS} + T_{\text{RTS}} + T_{\text{CTS}} + T_{\text{DATA}} + T_{\text{ACK}} + (3 \times \text{SIFS}) + \text{Timeout} + T_{\text{PHY}} \tag{3.29}$$

$$T_c^{(\text{RTS/CTS})} = \text{DIFS} + T_{\text{DATA}} + \text{Timeout} + T_{\text{PHY}} \tag{3.30}$$

From the above equations, the interval of control frames $(T_{\text{RTS}}, T_{\text{CTS}}, \text{and } T_{\text{ACK}})$ and the Data frame duration (T_{DATA}) are determined as:

$$T_{\text{control-frame}} = \left\lceil \frac{L_{\text{control\_frames}}}{L^{\text{basic-data rate}}} \right\rceil \times T_{\text{sym}} + \text{PHY} \tag{3.31}$$

$$T_{\text{DATA}} = \left\lceil \frac{L_{\text{payload}} + \text{MAC}}{R_{\text{basic data rate}} \times L^{\text{basic data rate}}} \right\rceil \times T_{\text{sym}} + \text{PHY} \tag{3.32}$$

2. **Average delay**: This refers to the time delay while transmitting data from the source to the destination. When analyzing the frame transmission process, we define the start of transmission as when the frame becomes the head STAs queue. The transmission is considered complete upon receiving a positive acknowledgment

[129]. This analysis assumes the frame drop probability to be extremely low and negligible. Under the assumption that the probability of frame drops is extremely low and disregarded, the average frame delay can be expressed as:

$$\text{Average delay} = \left(\text{slot time length} \sum_{i=0}^{m-1} p^i \frac{W_{i+1}}{2} + \frac{p^m}{1-p} \frac{W_m + 1}{2} \right) \quad (3.33)$$

We can write the average delay in a simplified form:

$$\text{Delay} = \frac{P_{\text{tr}}(1 - P_s)T_c + (1 - P_{\text{tr}})\sigma + (P_s P_{\text{tr}} T_s)}{P_s P_{\text{tr}}} \quad (3.34)$$

3. **Energy efficiency**: Energy calculations are a crucial performance metric in the Wireless of Area body area networks (WBANs). Since the radio component of a WSN node typically accounts for a significant portion of its energy consumption, energy efficiency becomes particularly important. The energy consumption required to transmit a data packet can be determined using the following formula:

$$E_{\text{eff}} = \frac{P_{\text{tr}}(1 - P_s)T_c + (1 - P_{\text{tr}})\sigma + (P_s P_{\text{tr}} T_s)}{P_s P_{\text{tr}} l_{\text{payload}}} \quad (3.35)$$

Development of a New Markov model: The Markov parameter was integrated with a Poisson distribution for traffic load to assess the performance and analysis of the 802.11ah standard network in real-life scenarios. According to the model [127], we assume that each station can send one packet, and there is a consistent probability q that at least one packet will arrive per state. In this new model, we create states (0, k) for k [0, W-1]. These states reflect a node that has dispatched a packet but currently has no packets waiting. It is worth noting that in these states, (0, k) is always equal to 0 since any i = 0 indicates a collision, and thus, there must be a packet waiting for transmission. Next, we establish relationships between the collision probability, the stationary distribution, the transition matrix of the Markov chain, and the probability of transmission per station. We can predict the network throughput by solving these relationships for p and . Authors in [127], considering the probability of the medium being idle equal to $(1-)^{(}n-1)$. Consequently, our probabilities of transition rely solely on q and p values.

$$\left(\frac{1}{b_{(0,0)}}\right) = (1-q) + \frac{q^2W(W+1)}{2\,(1-(1-q)^W)} + \frac{q(W+1)}{2(1-q)}\left(\frac{q^2W}{1-(1-q)^W} + p(1-q) - q(1-p)^2\right) + \frac{pq^2}{2(1-q)(1-p)}\left(\frac{W}{1-(1-q)^W} - (1-p)^2\right)\left(2W(1-p-p(2p)^{m-1}) / (1-2p) - (1-p)\right) \quad (3.36)$$

And

$$\tau = \frac{b_{(0,0)}q^2}{1-q}\left(\frac{W}{(1-p)(1-(1-q)^W)} - (1p)\right) \quad (3.37)$$

By considering specific values for W and q, we obtain the values of p and by solving equations (3.36) and (3.37).

System Evaluation

The evaluation was conducted through three simulation scenarios:

1) Variations in the number of nodes and slot duration. 2) Changes in the distance. 3) Considering collision probability.

The analysis includes the delay, energy consumption, and throughput. These parameters offer valuable insights into the performance analysis of the IEEE 802.11ah network for real-life networks.

Result and Discussion:

This section evaluated the parameters of delay and throughput based on the performance of IEEE 802.11ah. The goal was to develop a protocol suitable for real-life applications in Wireless Body Area Networks (WBANs).

(1) Average delay

• Delay with distance change:

The average delay of IEEE802.11ah depends on the variations in distance and the node number described in Figure 3.19.

The result showed that we obtained a minor delay equal to 0.01025 s for the number of nodes 50 when the distance between the node and AP was 100 m. The highest

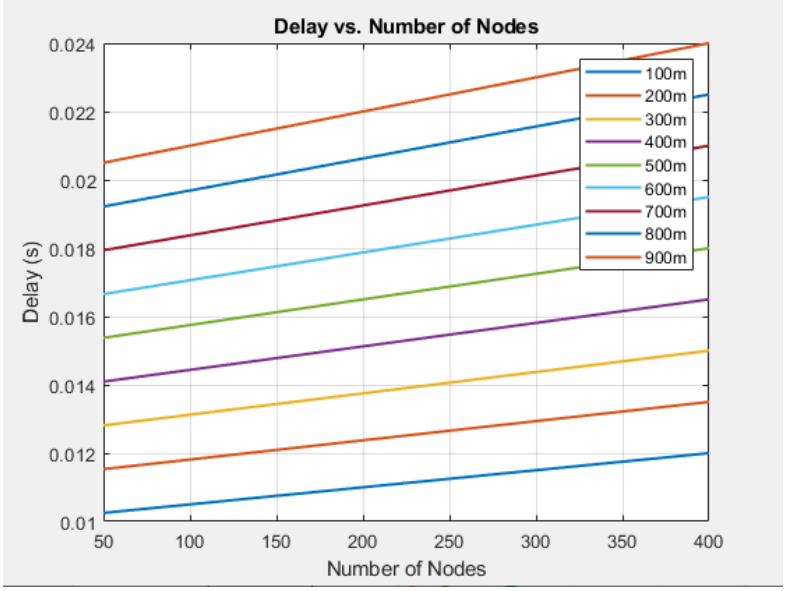

Figure 3.19: Average Delay with changes in node and AP distance

delay value is 0.24 s for the number of nodes 400, at a distance equal to 900 m. This demonstrates that a queue forms when the number of nodes connected to the AP increases, leading to eventual delays. Additionally, when the distance between the AP and nodes increases, the time required for communication with the AP also increases, resulting in further delays. It can be inferred that both the number of nodes and the distance between the nodes and AP significantly impact the average delay value.

• Delay with RAW Slot Duration Change

Figure 3.20 illustrates how variations in the time of RAW slots and the number of nodes impact the delay.

From the figure we can observed that the smallest delay value was 0.041 s, occurring when there were 50 nodes and the 100 ms slot duration of RAW. Conversely, the maximum value of delay was 743,128 s, observed when there were 400 nodes and RAW was 400 ms. The findings indicate that, as the number of transmitted packets increases and the RAW slot length, nodes experience queuing in the RAW, leading to delayed packet transmission and subsequent delays. It is crucial to observe that there is a relationship between the number or density of nodes and

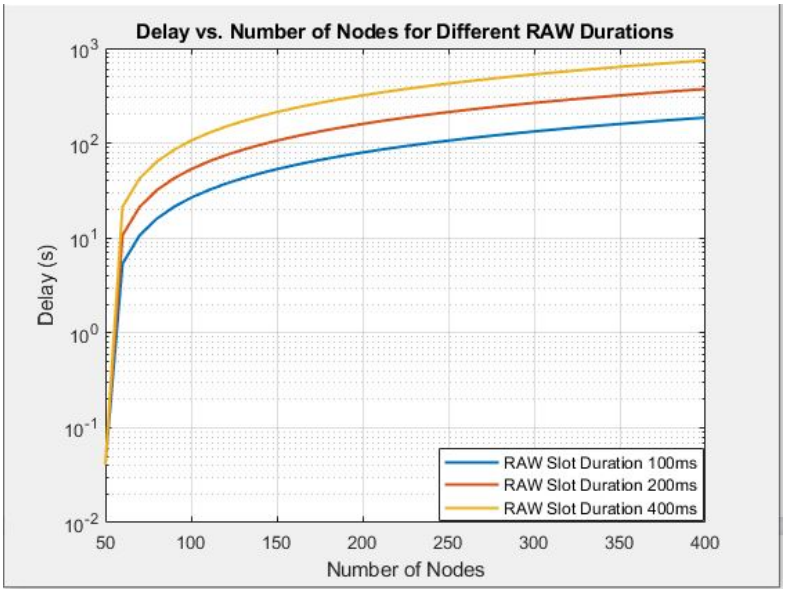

Figure 3.20: Delay with RAW slot duration change

the length of the RAW slots. As the number of connected nodes increases, the duration of the RAW slot tends to be extended. Hence, the number of nodes and the time of each RAW slot exhibit a direct correlation with the delay parameter. The differences in the duration of RAW and the number of nodes have a major impact on the performance of the IEEE 802.11ah network, especially in terms of the delay value.

2. Throughput

• Throughput with changing RAW slot duration:

The figure 3.21 illustrates the relationship between the throughput and the number of nodes in a network for different RAW (Restricted Access Window) slot durations. The three curves represent different RAW slot durations: 100 milliseconds (blue line), 200 milliseconds (red line), and 400 milliseconds (yellow line). We can observe that For all three slot durations, throughput decreases as the number of nodes increases. This suggests that the network becomes less efficient as more nodes are added, likely due to increased contention and collisions. For a given number of nodes, the throughput is highest for the 100 ms slot duration and lowest for the 400 ms slot duration. This indicates that shorter RAW slot durations result in higher throughput. At 50 nodes, the throughput for all slot durations starts at approximately 2.1×10^5 bps. As the number of nodes increases to 400, the throughput for the 400 ms slot duration drops below zero, indicating a highly

inefficient network. The throughput for the 100 ms slot duration remains the highest throughout the range of nodes, suggesting it is the most efficient among the three configurations.

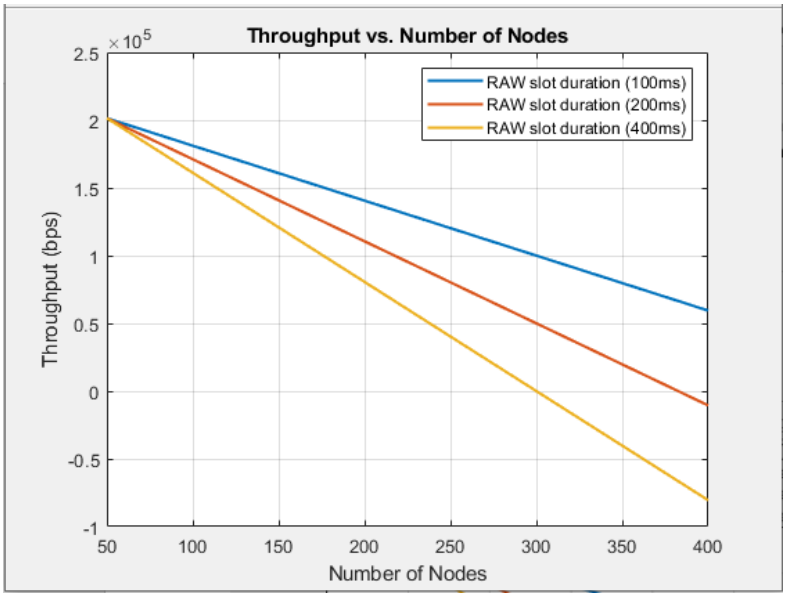

Figure 3.21: Throughput with RAW Slot Duration change

From equation (3.23), the duration value of the RAW slot is found in the denominator, indicating an inverse relationship with throughput. In simpler terms, increasing the slot duration RAW leads to a throughput decrease. Considering Equations (3.25) and (3.26), both Ps and Ptr values are also found in the denominator. This suggests that when the node's number increases, Ps Ptr also tends to increase, resulting in a drop in throughput due to their inverse correlation with it. In conclusion, the number of nodes and the duration value of the RAW slot significantly impact the performance of the IEEE 802.11ah network.

• Throughput with change of distance:
The Throughput of IEEE802.11ah depends on the variations of distance and the number of nodes is described in Figure 3.22. According to Figure 3.23, the highest throughput recorded was 201396.2 bps at a distance of 100 m, and the node number was equal to 50. Conversely, the most minor decrease of 1901286.3 bps in throughput was observed when there were 400 nodes and the distance between the node and AP was 900 m. These findings indicate that the node's quantity and also the distance impact the throughput value. Specifically, the throughput value tends to decrease as the node's quantity increases. As the number of nodes rises,

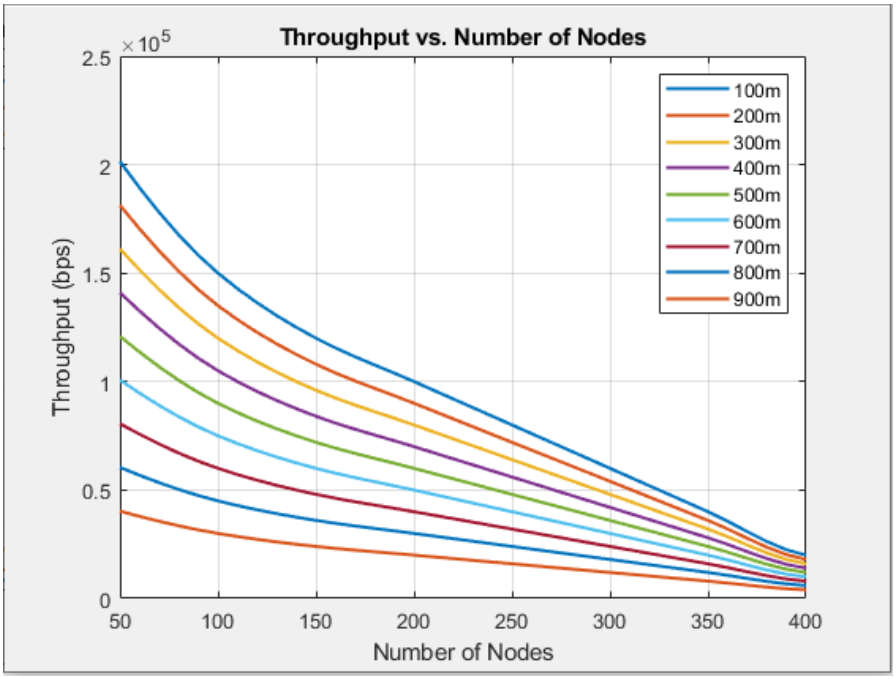

Figure 3.22: Throughput with changes in node and AP distance

the channel becomes congested, making it more challenging to enable node access to the channel, thus reducing the overall throughput value. Furthermore, when the distance between increases, the value of throughput decreases due to delayed data transmission caused by the longer distance.

3.7 CONCLUSION

This chapter focused on evaluating the characteristics of the IEEE 802.11ah where the standard offers extensive coverage, extremely low power usage, and the capability to accommodate a significant (STAs) number, with 100 kbps data rates of at least. The next chapter will build upon this foundation to propose and evaluate cross-layer design principles tailored to the IEEE 802.11ah standard in the context of Wireless Body Area Networks.

4

PHY-MAC CROSS-LAYER DESIGN FOR BODY PATHLOSS MITIGATION

Contents

4.1 INTRODUCTION

This chapter introduces a focused investigation into improving the performance of the IEEE 802.11ah protocol by addressing the body path loss problem, which is a significant challenge in wearable and implantable healthcare devices. The chapter progresses by outlining a PHY-MAC cross-layer design that promises to mitigate path loss issues and enhance data transmission efficiency. An overview of this design sets the foundation for understanding its application in the healthcare IoT.

The enhancements proposed for the 802.11ah standard are then thoroughly examined, with explicit assumptions and considerations considered to ensure the relevance and applicability of the improvements. Simulation methodologies are described, and empirical results are presented to substantiate the effectiveness of the proposed cross-layer design enhancements. The chapter culminates with a conclusion that synthesizes the findings, reaffirming the potential of cross-layer strategies in advancing IoT healthcare communications.

4.2 BODY PATHLOSS PROBLEM

WBAN is a developing technology that can be seamlessly integrated with innovative sports and e-health using wearable devices. Enhancing the user experience and quality of service (QoS) is vital for a wearable network. The limited energy available from batteries and the path loss during body mobility are significant research challenges in extending the lifetime of the WBAN network [130]. IEEE 802.11ah provides expanded range and power efficiency. This feature enables direct communication between sensor nodes and an access point, eliminating the requirement for a coordinator device. One of the main challenges for IEEE 802.11ah for WBAN is to achieve high throughput and reliability due to shadowing, fading, and path loss. Prior research has suggested techniques to enhance energy efficiency and mitigate path loss to increase the life of these networks [131, 132]. However, there are still constraints on effectively handling the dynamic adaptive features of channel conditions and energy distribution. In this chapter, we describe the development of a cross-layer PHY/MAC protocol to mitigate path loss and increase the throughput of the network that relies on the IEEE 802.11ah standard. This protocol aims to improve network and sensor nodes' lifetime, ensure service quality, and provide reliable transmission. Based on the adaptive modulation that is supported by this standard, the protocol considers the transmission requirements for various data

types and modifies the superframe. In several ways, the human body can influence wireless signals. The presence of a sizable human body between the antennas of the transmitter and receiver may impair radio frequency (RF) performance. Primarily composed of water, the human body is a highly efficient absorber of radio frequency (RF) radiation, which increases with body mass (Pos) [133]. Attenuation occurs when wireless signals pass through or are near the human body; this phenomenon is called body path loss. This effect is especially pronounced in environments with high human activity, where communication channels become degraded and unstable. It is critical to resolve this concern because 802.11ah-compliant IoT devices may be worn or placed near humans [92].

4.2.1 Cross-Layer Design Overview

Cross-layer design facilitates collaboration and information sharing between protocols from different layers [134]. This includes transmission power, available resources, and link interference. The objective is to select the optimal route by considering energy consumption and performance requirements. For example, information from the physical layer about the BER and neighboring node's signal strength can help routing algorithms at the network layer figure out which node is following the path. The PHY and MAC layers' functions are traditionally kept apart. While the MAC layer controls access to the transmission medium, the PHY layer handles the actual transmission and receiving of signals. On the other hand, a cross-layer design promotes the exchange of data and capabilities between these layers to increase flexibility and adaptability.

4.2.2 Enhancing 802.11ah Performance using CLD

4.2.2.1 System Model

The model makes the assumption that the AP in the network and the STA (sensor) only have a single antenna and are unable to send and receive simultaneously. This model also assumes optimal feedback channels and perfect channel state information (CSI); Figure 4.1 illustrates this model.

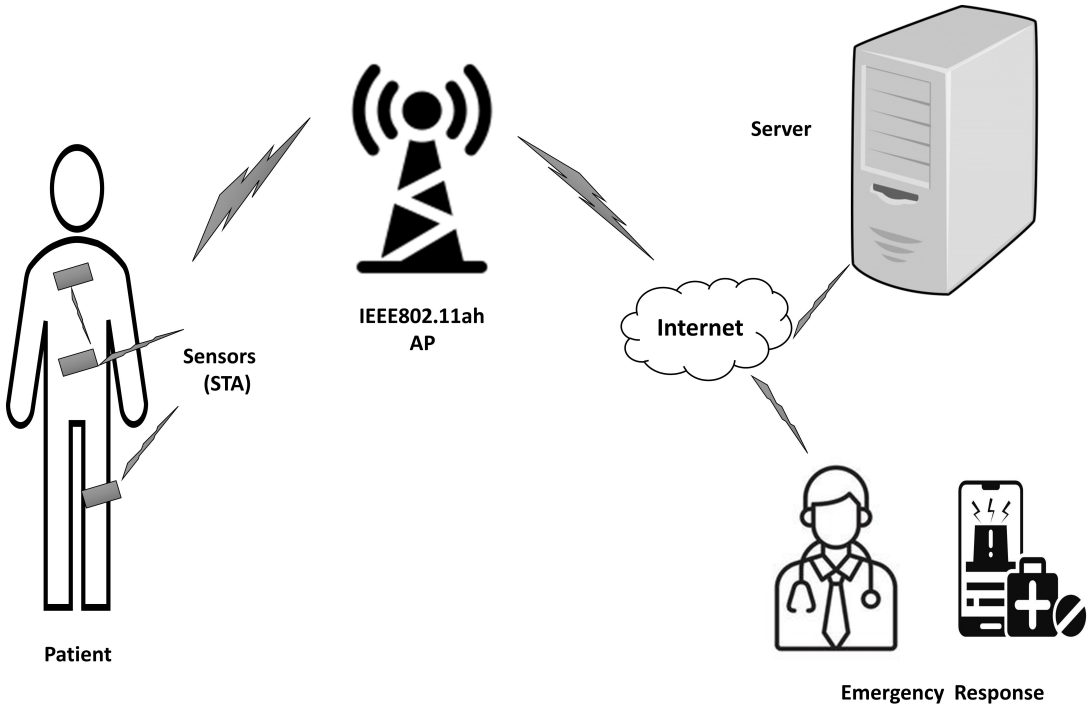

Figure 4.1: The Model

4.2.2.2 Network topology

In this model we consider the point-to-point topology, where stations (STAs) directly exchange packets with the access point (AP) without any intermediate nodes. This approach ensures packets travel to the AP or STA in a single hop. Single-hop transmissions are favored over multi-hop transmissions in terms of reliability because they introduce less delay, which is particularly critical for applications in the medical field. In this evaluation, we assume an ideal channel without consideration for hidden nodes.

4.2.2.3 Body pathloss model

To analysis body path loss, the TG6 In 2010 established WBAN channel models comprising seven scenarios depend on the positions of transceiver nodes [135]. These scenarios include Implant to Implant, Implant to Body, Implant to External,

Body to Body (Line and Non-Line of-Sight), Body to External (Line and Non-Line-of-Sight) scenarios. Table 4.1 shows the possible scenarios.

Table 4.1: The possible scenarios. TG6

Scenarios	Description	Frequency Band	Channel Model
S 1	Implant to implant	(402-405) MHz	CM1
S 2	Implant to body	(402-405) MHz	CM2
S 3	Implant to external	(402-405) MHz	CM2
S 4, S 5	Body to Body (LOS) and (NLOS)	(13.5, 50, 400, 600, 900) MHz (2.4, 3.1-10.6) GHz	CM3
S 6, S 7	Body to external (LOS) and (NLOS)	13.5, 50, 400, 600, 900 MHz 2.4, 3.1-10.6 GHz	CM4

Each of these scenarios comes with an explanation and the associated frequency range. These situations are organized according to where the communicating nodes are situated, encompassing the implant, the body's surface, and external nodes. Additionally, these situations are clustered into groups that can be described using identical Channel Models (CM).

The TG6 group has established three categories of nodes to describe the characterization of the propagation of electromagnetic waves originating from devices in proximity to or within the human body:

- Implant node: A node located within the body. This can be immediately under the skin's surface or deeper within the bodily tissue.
- Body surface node: A node located on the human skin or no more than 2 cm away.
- External node: A node not in contact with the skin of the human and is located between a few centimeters and 5 meters from the human body.

Four types of channels between different nodes are possible. Figure 4.2 describes these potential types (TG6).

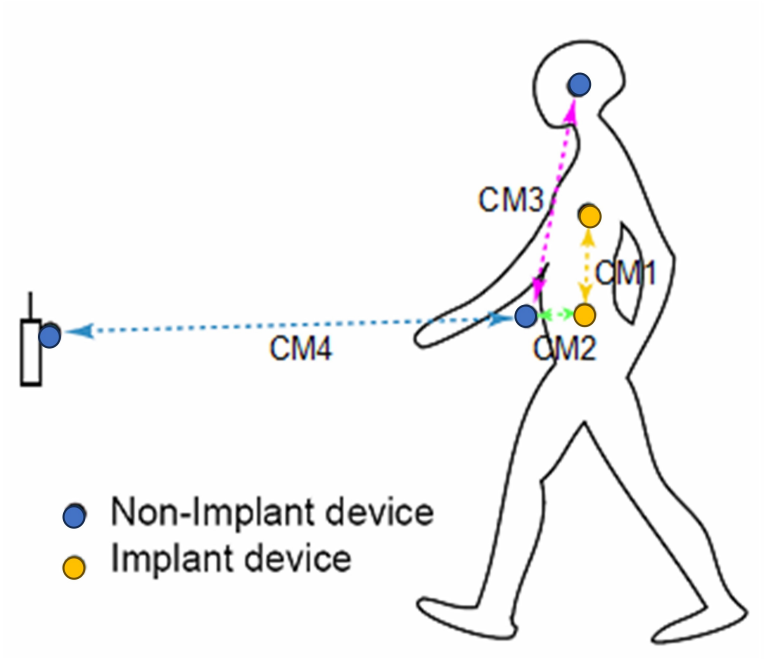

Figure 4.2: The potential types (TG6).

In this research, we studied the path loss models of body surface to external CM4 for 900MHz . The path loss model expressed in decibels (dB) between the transmitter and receiver as a function of the distance (d), is defined using Friis formula, just as it would be in free space [136, 137]. The body path loss represent as:

$$PL(d) = \frac{P_t \cdot G_r}{P_r} \tag{4.1}$$

Where:

P_t : The transmit power
G_r : The receive antenna gain
P_r : The received power

The path loss (PL) between the transmitter and receiver, which depends on the distance (d) between them, is calculated as:

$$PL(d) = PL_0 + 10n \log_{10}\left(\frac{d}{d_0}\right) + S(f,d) \tag{4.2}$$

Where:

PL_0 : The path loss at a reference distance d_0

n : The path-loss exponent, which can be much larger than traditional models

n can be much larger than traditional models, often in the range.

$S(f,d)$ is a body-small shadowing (fading) term that depends on the frequency and distance. The body shadowing is more complex as it takes into account the reflection, absorption, and diffraction by the human body. Small-scale fading is characterized by the Ricean distribution, where the K factor diminishes as the path loss increases. The distribution of the delay spread follows a normal distribution. Table 4.2 concisely overviews the model and its relevant parameters [138].

Table 4.2: Delay Spread Parameters

Parameter	**Value**
K_0	30.6
m_k	0.43
σ_k	3.4
Mean value delay spread parameters	
Distance [cm]	t_{rms} [ns]
45	16
15	6
Parameters of the 90% cumulative value of the delay spread	
Distance [cm]	t_{rms} [ns]
45	22
15	11

$$\text{Scale fading } (K_{\text{dB}}) = K_0 - P_{\text{dB}} m_k + n_k \sigma_k \tag{4.3}$$

where: K_0: The correlation between the measured data and K factor for the path loss.
$P_d B$: Path loss mk : The correlation between K and the data measured
n_k: Zero mean random variable with Gaussian distribution
k: The variance of the data measured between K factor and path loss in logarithmic form.

Figure 4.3 represents the delay spread, a measure of time dispersion in signals due to multipath propagation, and the cumulative probability of observing a delay spread where the cumulative distribution function (CDF) values range from 0 to 1. The delay spread is generally lower for the 15-cm distance compared to the 45-cm.

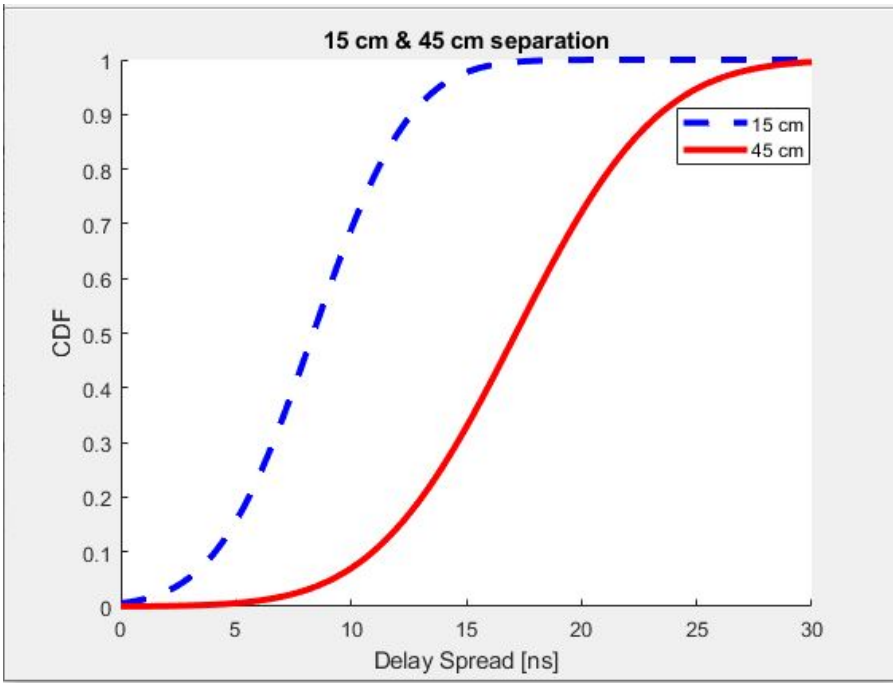

Figure 4.3: The CDF vs delay spread

As a result, increasing the distance between the STA and AP may lead to more pronounced multipath effects, resulting in higher delay spreads.

Figure 4.4 illustrates a clear inverse relationship between scale fading and path loss, with additional variability caused by the delay spread, which conforms to a normal distribution.

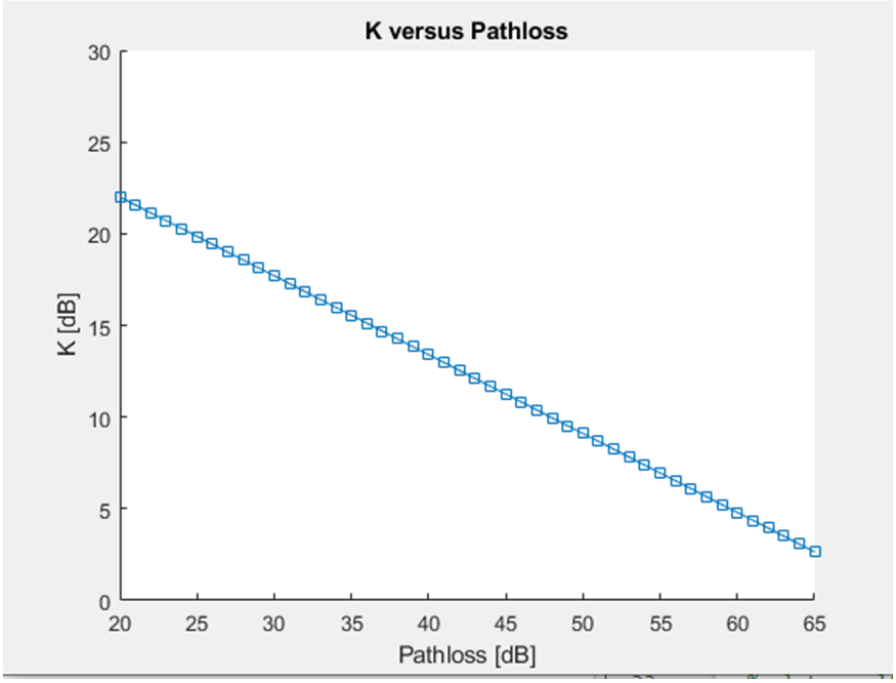

Figure 4.4: The relationship between scale fading and path loss

This emphasizes the interaction that impacts the strength of wireless signals.

Equation 4.4 presents a body propagation loss model that integrates two types of propagation channels: the on-body channel and the free-space channel [[139].

$$P_l = 10(n-2)\log_{10}(d_1) + 20\log_{10}(d) + S + C \tag{4.4}$$

Where d_1 is the distance within the body, d is the air distance. S is a constant for body shadow, and C is the system loss constant.

In order to utilize this path loss model for the 802.11ah standard operating at a frequency of 900 MHz, it is necessary to modify it by incorporating a correction factor that accounts for the specific frequency.

$$P_l = 10(n-2)\log_{10}(d_1) + 20\log_{10}(d) + S + C + 20\log_{10}\left(\frac{f_{0.9}}{f_{2.4}}\right) \tag{4.5}$$

Where $20\log_{10}\left(\frac{f_{0.9}}{f_{2.4}}\right)$ is the correction factor for IEEE802.11ah. $f_{0.9}$ and $f_{2.4}$ are specific frequencies (0.9 GHz and 2.4 GHz respectively). It represents the frequency of the transmitted signal in the lower frequency band (The carrier frequency used in IEEE 802.11ah can vary within the Sub-1 GHz band. However, the standard specifies a few specific center frequencies that are commonly used [140]: 902 MHz: This is one of the center frequencies defined in the IEEE 802.11ah standard. It is often used as a carrier frequency in the Sub-1 GHz band for Wi-Fi HaLow applications. 928 MHz: Another center frequency specified in the standard, 928 MHz is also commonly used in IEEE 802.11ah deployments. The carrier frequency used in a specific IEEE 802.11ah implementation may depend on factors such as the region of deployment, available spectrum, and local regulations [106].

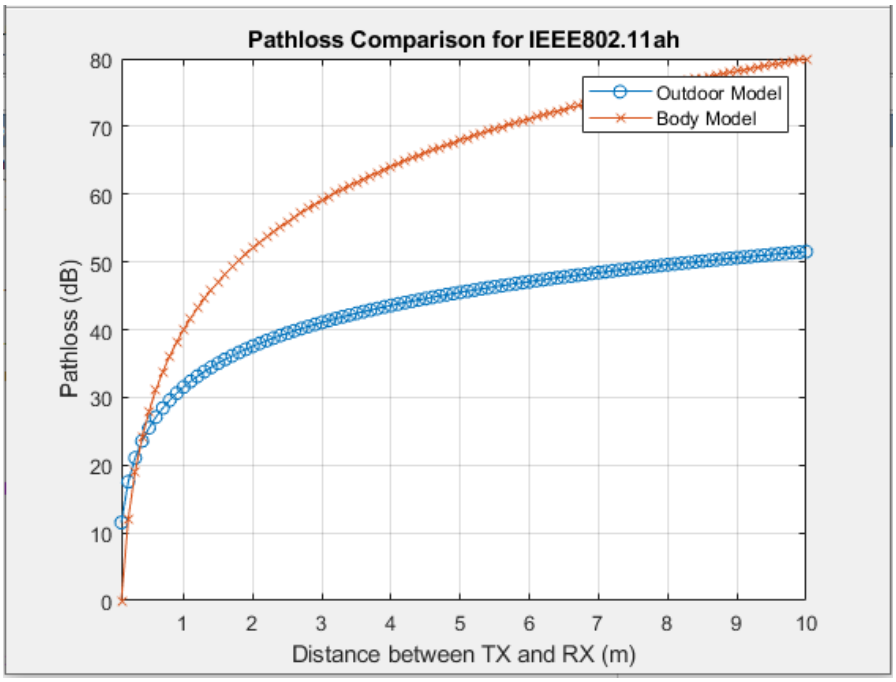

Figure 4.5: Pathloss Body model and IEEE802.11ah outdoor model.

Figure 4.5 illustrates a comparison between the body pathloss and the original pathloss from IEEE802.11 ah depend on the distance between the transmiter (TX) and the receiver (Rx). The body pathloss is evidently greater by 25 dB than the typical pathloss specified by TGah by assumes that all other parameters remain constant.

4.3 CROSS LAYER DESIGN USING ADAPTIVE MODULATION AND CODING SCHEME

To enhance 802.11ah performance, we proposed a cross-layer adaptive modulation model that integrates Adaptive Modulation and Coding (AMC) with the Automatic Repeat Request (ARQ) protocol for the IEEE 802.11ah standard. The goal is to maximize throughput by minimizing the packet error rate (PER). This model enables the exchange of specific parameters across different layers.

Specifically, as depicted in Figure 4.6, the design process will determine specific parameters in the PHY layer, denoted as $X_{\text{PHY}}^{\text{opt}}$ (AM switching thresholds or a set of useful AM modes), whereas at the MAC layer, denoted as $Y_{\text{MAC}}^{\text{opt}}$ (average packet arrival rate). The aim is to increase the average system throughput (η) while simultaneously satisfying predefined Quality of Service (QoS) requirements.

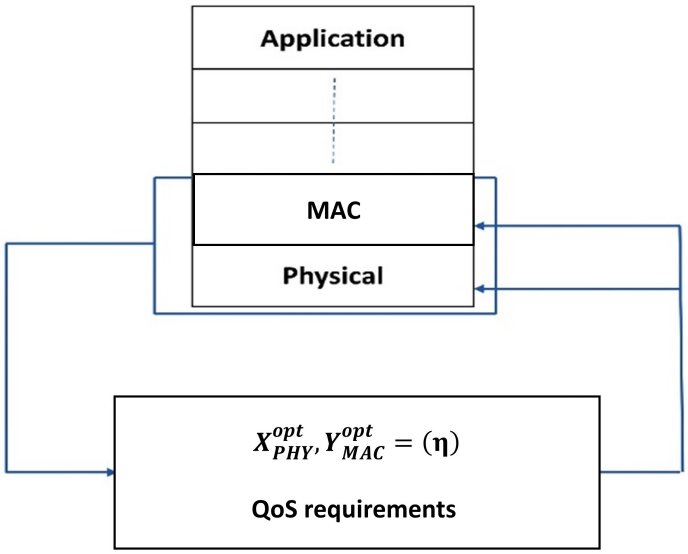

Figure 4.6: Cross-layer perspective

4.3.1 Adaptive Modulation and Coding (AMC)

The primary goal of AMC is to optimize the data rate by adapting transmission parameters to channel fluctuations while simultaneously ensuring a predetermined packet error rate. By manipulating transmission parameters at the PHY layer, we may adapt to changes in the channel and ensure that the BER remains below a specific, predetermined threshold. The IEEE 802.11ah standard has a physical layer that can accommodate data rates from 150 kbps to 78 Mbps, covering a distance of up to 1 km. The system can operate in various modes, each utilizing different coding rates.

4.3.2 Automatic Repeat Request (ARQ)

Automatic Repeat Request (ARQ), also called automatic repeat query, is an error-control technique for transmitting data reliably over an unreliable communication channel. It relies on acknowledgements sent by the receiver to confirm the correct reception of a message, as well as timeouts that define the maximum time allowed for receiving an acknowledgement. ARQ is particularly useful in situations where the capacity of the communication channel is uncertain or fluctuates [141]. If the sender does not receive an acknowledgement within the specified timeout period, it initiates a retransmission of the message. This process continues until the sender either receives an acknowledgement or reaches a predetermined limit on the number of retransmissions. Different variations of ARQ protocols exist, including Stop-and-wait ARQ, Go-Back-N ARQ, and Selective Repeat ARQ. These protocols typically employ sliding window mechanisms to assist the sender in determining which packets, if any, need to be retransmitted. These ARQ protocols are typically implemented at the OSI model's data link or transport layers (layers 2 and 4).

4.3.3 Physical layer design

For physical layer design, we can consider different transmission modes; these modes and the coding rate depend on IEEE 802.11ah and are listed in Table 4.3.

Table 4.3: The different transmission modes

	Mode 1	Mode 2	Mode 3	Mode 4	Mode 5	Mode 6
Modulation Schemes	BPSK	QPSK	QPSK	16 QAM	16 QAM	64 QAM
Coding Rate R_C	$\frac{1}{2}$	$\frac{1}{2}$	$\frac{3}{4}$	$\frac{9}{16}$	$\frac{3}{4}$	$\frac{3}{4}$
a_n	1.1378	0.3451	0.2297	0.2181	0.1836	0.1987
b_n	7.5656	3.2643	1.5343	0.6350	0.3584	0.0971
Rate R_n (bits/sym.)	0.5	1.0	1.5	2.25	3.0	4.5

From Table 4.3: a_n and b_n, the coefficients used in the calculations relate to the modulation schemes. Different modulation schemes have varying coding rates and corresponding a_n and $b_n$values. The table provides a comparison of the efficiency and performance of each modulation scheme based on the rate R_n.

• Signal -to-Noise Ratio calculation

The received SNR for each block is treated as a random variable that follows a gamma function as described in ref [142]. The gamma function that characterizes the probability of receiving SNR per block as a random variable is as follows:

$$p(\gamma) = \frac{m^m \gamma^{m-1}}{\Gamma(m)\gamma} \exp\left(-\frac{m\gamma}{\gamma}\right), \quad \text{for } \gamma \geq 0 \tag{4.6}$$

Where: - γ represents the average received SNR ($\mathbb{E}[\gamma]$) - $\Gamma(m)$ represents the Gamma function and is calculated by $\int_0^\infty e^{-t} t^{m-1} dt$ - m is the parameter of Nakagami fading and is greater than or equal to $\frac{1}{2}$ The Rayleigh fading channel can be considered as a specific instance of the Nakagami-m model, where the value of m is equal to 1.

4.3.4 MAC layer design

At MAC layer, we used the Automatic Repeat Request (ARQ) protocol to mitigate the negative impact of a high Frame Error Rate (FER) caused by body pathloss and shadow effects on the throughput by combining Automatic Repeat Request (ARQ) that are supported by IEEE 802.11ah and Forward Error Correction (FEC). We use the notation FSN to represent the serial number for the data frame being sent and FRN to represent the serial number for the data frame being received at STA and AP, respectively. The incremental redundancy frame serial number that the STA transmitted is denoted as IN (Increment redundancy). This process are explained as follows: The STA transmits a new frame with a sequence number (FSN) of i. If the AP successfully receives and decodes this frame, it sends an acknowledgement (ACK) frame back to the STA with a sequence number (FRN) of i+1 , indicating a successful transmission. The STA will transmit the next new frame with a sequence number of i+1 in the next time slot. However, suppose the AP receives the frame but fails to decode it correctly. In that case, it will discard the frame and send a negative acknowledgement (NACK) with a sequence number of i requesting the STA to retransmit the data frame with sequence number i. The access point (AP) will drop the frame with serial number FSN= i if it cannot decode it accurately before reaching the maximum number of retransmissions, denoted as L. Figure 4.7 is shown the flow chart of this process.

The joint outage probability of the STA-AP link is:

$$\mathrm{PR(STA\text{-}AP)} = \mathrm{Pr}^{L}\left\{\log_2(1+\mathrm{SNR}|h_{\mathrm{STA\text{-}AP}}|^2) < R\right\} = \mathrm{Pr}^{L}\left\{|h_{\mathrm{STA\text{-}AP}}|^2 < \frac{2^R-1}{\mathrm{SNR}}\right\} \tag{4.7}$$

Where: L is the maximum number of bits transmitted, R is the rate, and $h_{\mathrm{STA\text{-}AP}}$ is the coefficient of channel gain. We used convolutional code as error correction code, which are typically defined by their base code rate and the encoder's depth or memory, denoted as: [n,k,K]. The base coding rate is commonly expressed as n/k, where n represents the raw data rate for input and k represents the data rate for output channel encoded stream. n is smaller than k due to the inclusion of redundant information in the input bits through channel coding. A binary convolutional code, abbreviated $C_{(}i)$ is used at the MAC layer as the error-correcting technique for

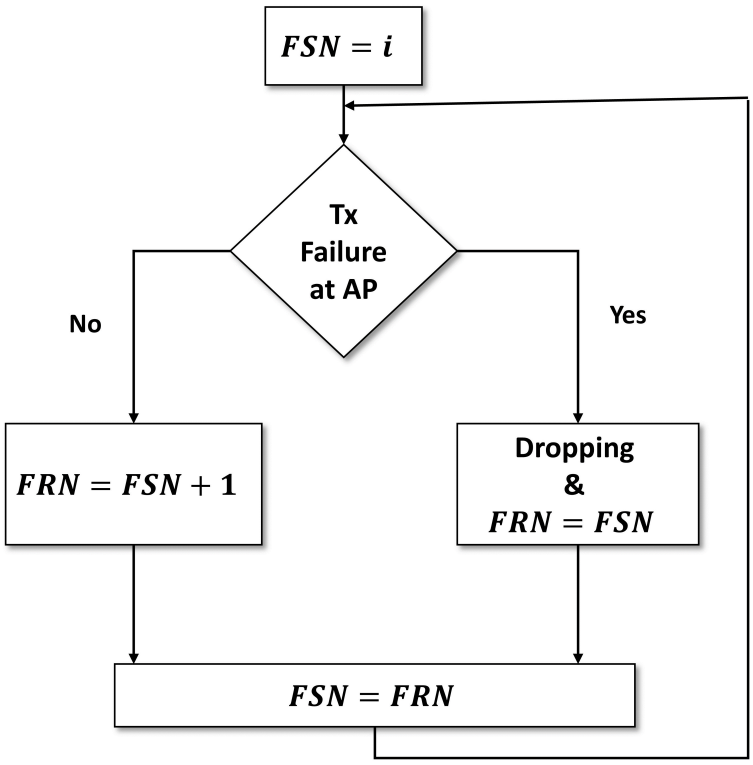

Figure 4.7: ARQ process

ARQ [143]. The code has a coding rate of RH. The total bits in the packet, including the added CRC bits, is represented as L.

$$N_c = \frac{L}{RH} \tag{4.8}$$

Where: L: The bits transmitted. Once modulation and coding are applied using mode n with a rate of R_n, the codeword packet is then mapped toward symbol frame that consists of N_c / R_n symbols. Finally, the frame is sent at the physical layer together with pilot symbols and additional control information.

4.3.5 Cross-layer design

4.3.5.1 Design requirements

To meet specific QoS requirements, we need to impose some constraints on the design: - C_1: The maximum number of retransmissions $N_{\text{retransmit}}^{\max}$ allowed for each packet. - C_2: The packet loss probability after $N_{\text{retransmit}}^{\max}$ is limited to P_{loss}.

The $N_{\text{retransmit}}^{\max}$ can be determined by equation (4.9):

$$N_{\text{retransmit}}^{\max} = \frac{\text{The maximum allowable system delay}}{\text{delay required for each transmission}} \tag{4.9}$$

P_{loss} can be determined based on the required BER and the packet size (L), using the following equation:

$$P_{\text{loss}} = 1 - (1 - \text{BER})^{L} \tag{4.10}$$

Given that the average bit error rate (BER) after decoding is P, if the packet is not accurately received after $N_{\text{retransmit}}^{\max}$ transmissions, we establish the assumption that the packet is considered dropped. For C_2, the following inequality needs to be fulfilled:

$$P^{\left(N_{\text{retransmit}}^{\max}\right)} \leq P_{\text{loss}} \tag{4.11}$$

Where P_{loss} depends on the body path loss model described by equation (4.5). In particular,

$$P \leq P_{\text{loss}}^{\left(\frac{1}{N_{\text{retransmit}}^{\max}}\right)} = P_{\text{target}} \tag{4.12}$$

To fulfill equation (4.11), the desired value of P_{target} imposes a specific BER requirement for the mode selected at the physical layer. As the C_i codeword

only comprises information bits, whereas C_i ($i > 2$) codewords include both redundancy and information bits, so the BER imposed by P_{target} on the AMC scheme at the PHY layer has two separate scenarios: one for C_1 and another for C_i ($i > 2$).

In case 1: concerning C_1, we suppose that each bit in the output after the process of demodulation and decoding with AMC has an equal Bit Error Rate (BER). Given that C_1 only consists of information bits, we can express the relation of the Packet Error Rate (PER) to the BER by the following equation:

$$P^{(1)} = 1 - (1 - \text{BER}^{(1)})^L \tag{4.13}$$

$P^{(1)}$ represents the PER of C_1. $\text{BER}^{(1)}$ is the Bit Error Rate after the process of demodulation and decoding. If $P^{(1)}$ equals $\text{BER}_{\text{target}}$, then the BER target required on AMC for code C_1 is determined by the following equation:

$$\text{BER}_{\text{target}}^{(1)} = 1 - (1 - P_{\text{target}})^{(1/L_1)} \tag{4.14}$$

In case 2: In the case of C_i ($i > 2$), due to the non-independence of errors arising from the decoder associated with C_i, it becomes challenging to find a particular relationship between BER and PER following C_i decoding. To address this, we employ an upper bound on PER as provided in [144]. The upper bound on PER for a packet of length L encoded by C_i is determined by:

$$P^{(i)} \leq 1 - (1 - P_u^{(i)})^L = P_{\text{bound}}^{(i)} \tag{4.15}$$

$P^{(i)}$ represents the PER decoding using C_i code. $P_u^{(i)}$ denotes the error probability of the first event union bound associated with code C_i. The union bound can be approximated as [145]:

$$P_u^{(i)} = \sum_{d=d_{\text{free}}}^{\infty} P_d a_d \tag{4.16}$$

Where: d_{free} represents the free distance of code C_i. P_d is the incorrect path probability at a distance d. a_d is the total count of error events characterized by a weight of d. The probability P_d can be expressed as follows:

$$P_d \approx (4\rho(1-\rho))^{(d/2)} \tag{4.17}$$

From equations (4.14), (4.15), and if the:

$$P_{\text{bound}}^{(i)} = P_{\text{target}} \tag{4.18}$$

We can achieve the desired Bit Error Rate (BER) for AMC at the physical layer.

4.3.5.2 AMC Mode Selection

The mode selection depends on the feedback from the MAC layer, which is determined by:

$$\text{MCS} = f(P_{\text{re}}) \tag{4.19}$$

where P_{re} is the probability of packet retransmission reported by the MAC layer. The function f determines the modulation method based on the rate of retransmission. Since feedback on retransmissions is provided by the MAC layer, we may modify our modulation using the following function:
Algorithm 1: AMC Adjustment

Input: An index P_{re}

```
Begin
    Define constant 'THRESHOLD_LOW'
    Define constant 'THRESHOLD_HIGH'
    If \( P_{\text{re}} \) is less than 'THRESHOLD_LOW'
    Then Return '16-QAM'
```

```
    Else If \( P_{\text{re}} \) is less than 'THRESHOLD_HIGH'
    Then Return 'QPSK'
    Else
    Return 'BPSK'
End
```

Output: A modulation scheme ('16-QAM', 'QPSK', or 'BPSK')

Similar to references [142, 143], the entire range of SNR is obtain by:

$$\mathrm{BER}_n(\gamma) \approx a_n \exp(-b_n \gamma) \tag{4.20}$$

The index n corresponds to the AMC mode. The parameters a_n and b_n can be determined by appropriate equation (4.20) to the actual Bit Error Rate (BER) of mode n. From (4.20), we obtain:

$$\begin{aligned} \gamma_0^{(i)} &= 0, \\ \gamma_n^{(i)} &= \frac{1}{b_n} \ln\left(\frac{a_n}{\mathrm{BER}_{\text{target}}^{(i)}}\right), \quad n = 1, \ldots, N, \\ \gamma_{N+1}^{(i)} &= +\infty. \end{aligned} \tag{4.21}$$

With $\gamma_n^{(i)}$ specified by the above equation, AMC will work with the real BER fulfilling:

$$\rho_n^{(i)} \leq \mathrm{BER}_{\text{target}}^{(i)} \tag{4.22}$$

4.3.5.3 Summary of steps of cross-layer design:

Step 1: Calculate the value of P_{target} based on equation (4.12), by using C_1 and C_2 as inputs.

Step 2: To obtain the desired P_{target}, calculate the corresponding $\text{BER}_{\text{target}}^{(i)}$ for the i-th transmission using equations (4.12), (4.13), (4.14), and (4.15).

Step 3: To calculate the $\text{BER}_{\text{target}}^{(i)}$, determine $\gamma_n^{(i)}$ of AMC mode n from equation (4.22).

4.3.6 Performance Analysis and results

This section focuses on obtaining the SNR, BER, average system Packet Error Rate (PER), spectral efficiency, and throughput of our cross-layer design.

4.3.6.1 SNR Estimation

The transmitter sends N symbols during each frame interval using BPSK, QPSK, 16-QAM, or 64-QAM modulation. This means that $N \cdot k$ bits are sent in each group, where k can be 1, 2, 4, or 6. The system adjusts itself to maintain a desired level of performance. The specific switching levels $\{l_1, l_2, l_3, l_4\}$ are selected for different modulation schemes to achieve a target Bit Error Rate (BER) in a channel affected by Additive White Gaussian Noise (AWGN). The receiver estimates the signal-to-noise ratio (SNR) and provides this information to the transmitter, allowing it to select the appropriate modulation scheme. The assumption is that the channel experiences slowly varying Rayleigh fading.

4.3.6.2 Bit Error Rate Analysis

The performance of adaptive modulation, considering the perfect estimation of Signal-to-Noise Ratio (SNR), can be represented by the Bit Error Rate (BER) as described in reference [121].

$$
\begin{aligned}
P_e(\Gamma) = \frac{1}{\beta}\Bigg[& \int_{l_1}^{l_2} P_{\text{bpsk}}(\gamma) f(\gamma \mid \Gamma) d\gamma \\
& + 2\int_{l_2}^{l_3} P_{\text{qpsk}}(\gamma) f(\gamma \mid \Gamma) d\gamma \\
& + 4\int_{l_3}^{l_4} P_{\text{16qam}}(\gamma) f(\gamma \mid \Gamma) d\gamma \\
& + 6\int_{l_4}^{l_5} P_{\text{64qam}}(\gamma) f(\gamma \mid \Gamma) d\gamma \Bigg]
\end{aligned}
\tag{4.23}
$$

where Γ represents the average Signal-to-Noise Ratio (SNR), $f(\gamma \mid \Gamma)$ denotes the probability distribution of SNR for a specific average value, P_{bpsk}, P_{qpsk}, P_{16qam}, and P_{64qam} represent the probabilities of bit error for BPSK, QPSK, 16-QAM, and 64-QAM, respectively, at a given SNR value. Additionally, β represents the average number of bits per symbol, given by [146].

$$
\beta = \frac{1}{\int_{l_1}^{l_2} f(\gamma \mid \Gamma) d\gamma + 2\int_{l_2}^{l_3} f(\gamma \mid \Gamma) d\gamma + 4\int_{l_3}^{l_4} f(\gamma \mid \Gamma) d\gamma + 6\int_{l_4}^{l_5} f(\gamma \mid \Gamma) d\gamma}
\tag{4.24}
$$

In equation (4.23), it is assumed that the signal-to-noise ratio (SNR) is perfectly known. We can express equation (4.23) in an alternative form as follows:

$$
\begin{aligned}
P_e(\Gamma) = \frac{1}{\beta}\Bigg[& \int_{0}^{\infty} P_{\text{mod}}(\text{bpsk} \mid \gamma) P_{\text{bpsk}}(\gamma) f(\gamma \mid \Gamma) d\gamma \\
& + 2\int_{0}^{\infty} P_{\text{mod}}(\text{qpsk} \mid \gamma) P_{\text{qpsk}}(\gamma) f(\gamma \mid \Gamma) d\gamma \\
& + 4\int_{0}^{\infty} P_{\text{mod}}(\text{16qam} \mid \gamma) P_{\text{16qam}}(\gamma) f(\gamma \mid \Gamma) d\gamma \\
& + 6\int_{0}^{\infty} P_{\text{mod}}(\text{64qam} \mid \gamma) P_{\text{64qam}}(\gamma) f(\gamma \mid \Gamma) d\gamma \Bigg]
\end{aligned}
\tag{4.25}
$$

The probability of selecting modulation scheme k (where k can be BPSK, QPSK, 16QAM, or 64QAM) given a specific SNR value γ is denoted as $P_{\text{mod}}(k \mid \gamma)$. When the SNR estimation is perfect, the probability of using BPSK can be expressed as:

$$P_{\text{mod}}(\text{bpsk} \mid \gamma) = [u(\gamma - l_1) - u(\gamma - l_2)] \tag{4.26}$$

The unit-step function $u(x)$ is used in perfect SNR estimation, while imperfect SNR estimation requires different modulation schemes and spectral efficiency. The probabilities of utilizing different modulation schemes can be formulated using a similar approach, considering the corresponding switching levels. Additionally, the spectral efficiency, represented by β, is adjusted to accommodate these adaptations.

$$\begin{aligned}\beta = 1 &\int_0^\infty P_{\text{mod}}(\text{bpsk} \mid \gamma) f(\gamma \mid \Gamma) d\gamma \\ &+ 2 \int_0^\infty P_{\text{mod}}(\text{qpsk} \mid \gamma) \cdot f(\gamma \mid \Gamma) d\gamma \\ &+ 4 \int_0^\infty P_{\text{mod}}(16\text{qam} \mid \gamma) f(\gamma \mid \Gamma) d\gamma \\ &+ 6 \int_0^\infty P_{\text{mod}}(64\text{qam} \mid \gamma) f(\gamma \mid \Gamma) d\gamma\end{aligned} \tag{4.27}$$

Now, we can establish the probability of employing modulation scheme k as the likelihood that the estimated SNR, $\hat{\gamma}$, falls within the range associated with that specific scheme, assuming the actual SNR is γ. To illustrate, consider the case of BPSK.

$$P_{\text{mod}}(\text{bpsk} \mid \gamma) = \int_{l_1}^{l_2} f(\hat{\gamma} \mid \gamma) d\hat{\gamma} \tag{4.28}$$

Here, $f(\hat{\gamma} \mid \gamma)$ represents the probability of the SNR estimate, $\hat{\gamma}$, given that the actual SNR is γ.

Figure 4.8 represented the probability density compared to the estimated signal-to-noise ratio (SNR).

The figure illustrates how the probability density function (PDF) of the SNR estimate varies with changes in pilot length and the number of noise samples. The actual SNR is assumed to be 5 dB.

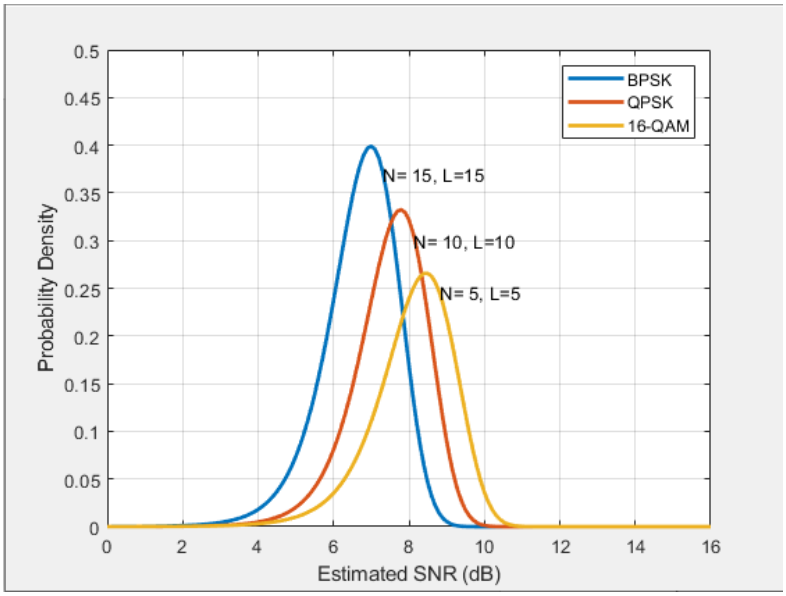

Figure 4.8: Probability density vs estimated SNR

The figure 4.9 shows the Bit Error Rate (BER) performance of different modulation schemes for IEEE 802.11ah wireless communications, plotted against the Signal-to-Noise Ratio (SNR). The modulation schemes shown are BPSK (Binary Phase-Shift Keying), and 16-QAM (16-Quadrature Amplitude Modulation).

The key observations from this figure are that BPSK consistently demonstrates superior BER performance across all SNR values, achieving a BER of $10^{-}4$ at 10 dB SNR, owing to its simple and robust modulation scheme. QPSK follows with slightly degraded performance, reaching approximately $10^{-}3$ BER at 10 dB SNR, while 16-QAM exhibits the highest BER among the three. This performance hierarchy illustrates the fundamental trade-off between spectral efficiency and error resilience in wireless communications. While BPSK offers the lowest BER, it provides the least spectral efficiency. Conversely, 16-QAM enables higher data rates at the cost of increased susceptibility to noise and interference, particularly at lower SNR values. These distinct performance curves underscore the potential benefits of adaptive modulation in IEEE 802.11ah systems, allowing for dynamic optimization between reliability and throughput as channel conditions vary.

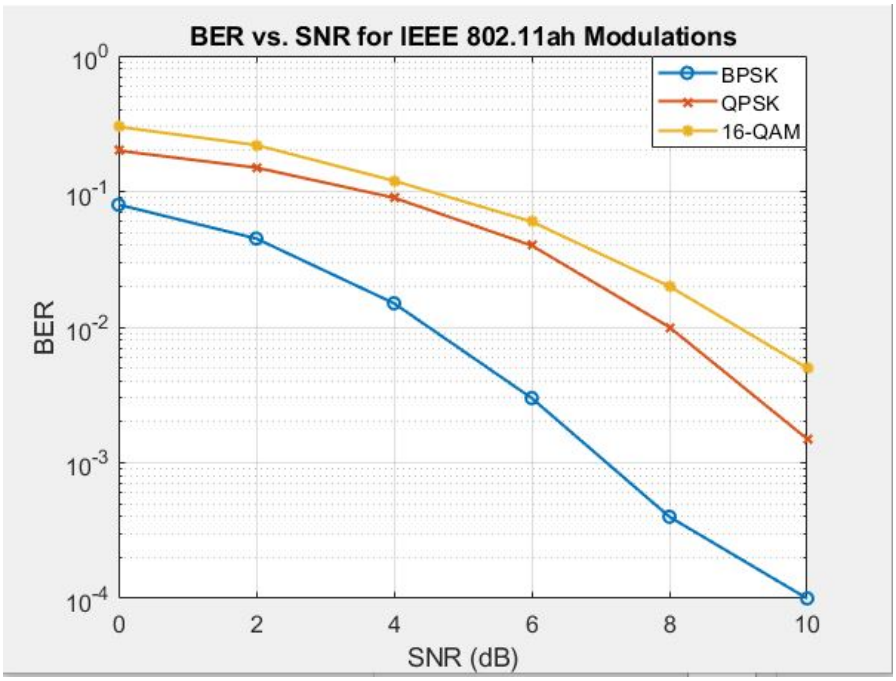

Figure 4.9: BER vs. SNR for IEEE 802.11ah Modulations

4.3.7 Packet Error Rate Analysis

Analyzing packet error rates in fading channels helps assess the dependability and throughput of systems. An appropriate PER model should be used, depending on how fading impacts the signal transmission. Distinct symbols from each packet with N symbols in fast-fading channels undergo particular fading effects [121].

The average packet error rate, denoted as $\overline{\text{PER}}$, is calculated based on the symbol error rate, denoted as $\overline{\text{SER}}$ [146], as:

$$\overline{\text{PER}}(\overline{\gamma}) = 1 - (1 - \overline{\text{SER}}(\overline{\gamma}))^N \tag{4.29}$$

$\overline{\gamma}$ represents the SNR on the receiver, and $\overline{\text{SER}}$ is based on the modulation used. Conversely, in fading conditions, the value of the packet error rate is determined by calculating the average of the instantaneous $\overline{\text{PER}}$ in an AWGN channel, considering all values of the SNR (γ).

Given a distribution of γ, denoted as f_γ:

$$\overline{\text{PER}}(\overline{\gamma}) = \int_0^\infty \text{PER}(\gamma) f_\gamma(\gamma) d\gamma \tag{4.30}$$

As stated in reference [20], the average PER for uncoded schemes in a Rayleigh block fading channel may be accurately estimated using the equation:

$$\overline{\text{PER}} = 1 - \exp\left(-\frac{\gamma_{\text{th}}}{\overline{\gamma}}\right) \tag{4.31}$$

where $\overline{\gamma}$ denotes the average SNR at the receiver, and γ_{th} represents the SNR threshold, depending on the decoding algorithm.

The average PER for uncoded schemes in the case of Rice block fading can be determined using the following formula [121]:

$$\overline{\text{PER}} = 1 - Q_1\left(\sqrt{\frac{2K}{\sqrt{2(K+1)}}}\frac{\gamma_{\text{th}}}{\overline{\gamma}}\right) \tag{4.32}$$

where Q_l represents the Marcum Q function, whereas K represents the Rician fading factor.

For an AMC system, the SNR threshold γ_{th} is necessary to determine the average PER, which is calculated from [146]:

$$(1 - \text{SER}(\gamma_{\text{th}}))^N = \frac{1}{2} \tag{4.33}$$

Where N is the number of symbols per packet, and SER represents the symbol error rate of the modulation.

The results from Figure 4.10 demonstrate the correlation between packet size, transmit powers, and PER performance.

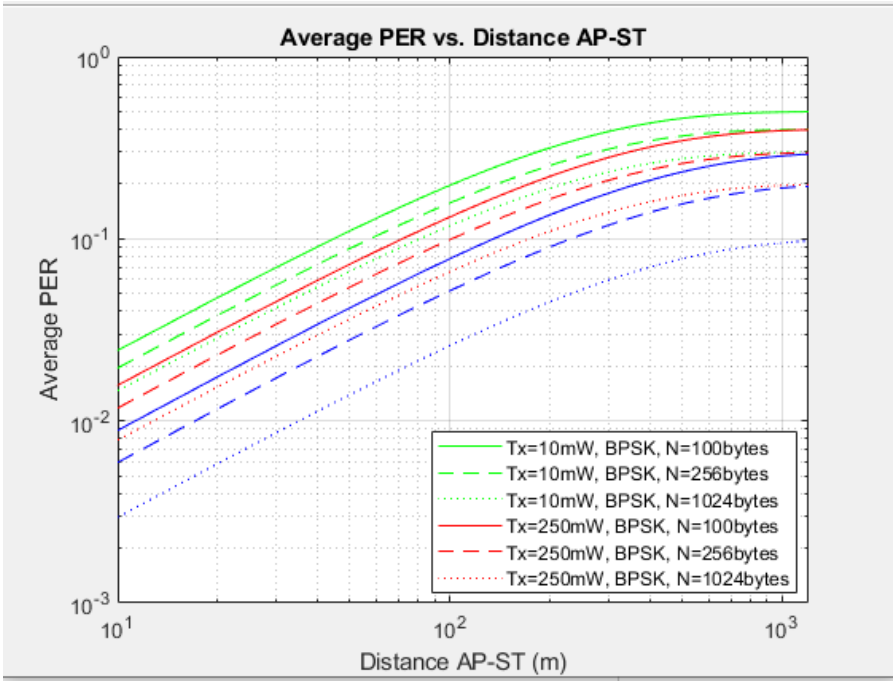

Figure 4.10: 802.11ah PER performance

As anticipated, the PER performance decreases as the packet size increases, and the transmit power decreases. The PER performance requirement is met for distances less than 450m when using a transmit power of 10 mW. However, with transmit powers of 250 mW and 1W, the standard is met over all distances up to 1 km.

4.3.7.1 Spectral Efficiency

By utilizing the mean PER obtained from the physical layer, we can now assess the spectral efficacy of the cross-layer design. Given that the upper limit on retransmissions is $N_{\text{retransmit}}^{\max}$, the typical amount of data sent per packet $\overline{N}_t$ can be obtained from:

$$\overline{N}_{\text{transmission}} = 1 + \overline{P} + \overline{P}^2 + \ldots + \overline{P}^{N_{\text{retransmit}}^{\max}} = \frac{1 - \overline{P}^{N_{\text{retransmit}}^{\max}+1}}{1 - \overline{P}} \tag{4.34}$$

Furthermore, the AMC mode n will be selected with a probability as [147]:

$$P_n = \frac{\Gamma(m, m\gamma_n/\overline{\gamma}) - \Gamma(m, m\gamma_{n+1}/\overline{\gamma})}{\Gamma(m)} \tag{4.35}$$

The average spectral efficiency is determined by the maximum transmission number for each packet, which is equivalent to the average of transmissions per bit and calculated as:

$$\overline{S} = \frac{1}{P_T} \frac{\sum_{n=1}^{N} R_N P_n}{\overline{N}_t} \tag{4.36}$$

Where $R_N = R_H R_C \log_2(M_n)$ represents the rate of the transmitted symbol.

Figure 4.11 displays the average spectral efficiency of a cross-layer system, with variation in the maximum retransmission number $N_{\text{retransmit}}^{\max}$.

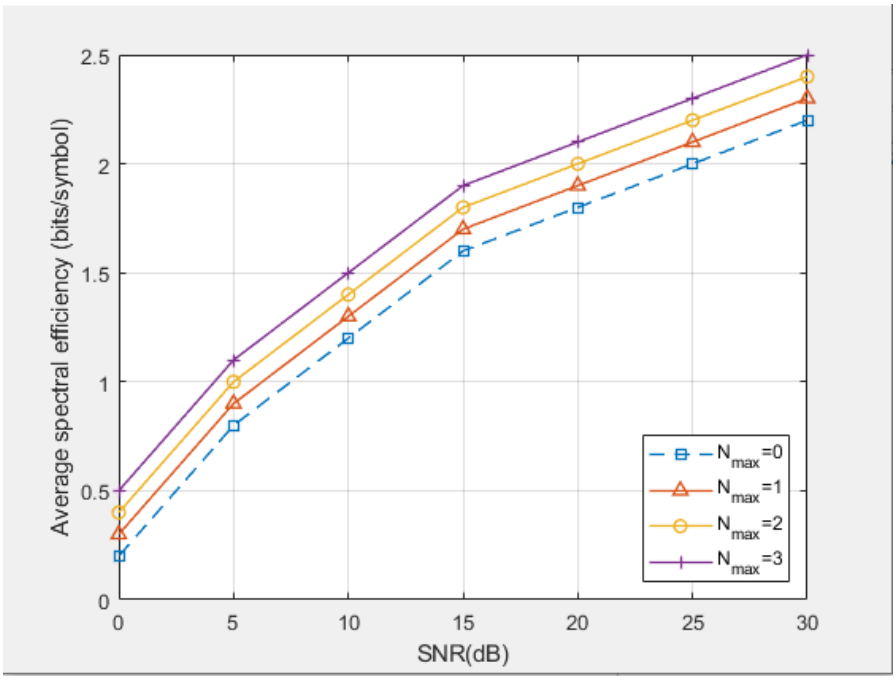

Figure 4.11: Average spectral efficiency vs SNR

The spectral efficiency is improved as $N_{\text{retransmit}}^{\max}$ increases. A higher value of the maximum number of retransmissions $N_{\text{retransmit}}^{\max}$ results in a reduced bit error rate

(BER) requirement. A system with a higher $N_{\text{retransmit}}^{\max}$, while maintaining the same SNR, can select an AMC mode with a higher rate.

4.3.7.2 Beacon Signal Utilization

The IEEE802.11ah standard has two modes for managing power consumption: activation and low power consumption [120]. During activation mode, the STA allows for continuous transmission of data. Conversely, in low power consumption mode, the STA alternates between sleep and activation mode. During sleep, the STA deactivates and ceases to receive signals. Consequently, even if AP need to transmit data to the STA, the data can only be temporarily stored by the AP. Upon awakening, the STA transitions to active mode and initiates a request, prompting the AP to relay the stored data to the STA. The ah STA average power consumption calculated as:

$$P_{\text{average}} = (T_{\text{tx}} \times P_{\text{Total}}) + T_{\text{rx}}(P_{\text{MC}} + P_{\text{rx}}) + T_{\text{sleep}} \times P_{\text{sleep}} \tag{4.37}$$

The IEEE 802.11ah in sensor network applications is in sleep mode for 99.8% of the time. Within the remaining 0.2%, the majority of the time, 0.1% is spent on transmitting, 95.7% is spent on receiving, and 4.2% is spent in idle states [110].

In our model, and using the AMC function above, the physical layer continuously examines the power of beacon signals received from the 802.11ah Access Points (AP). Through the analysis of these beacon signals, we can gather information about the current channel conditions and determine the impact of body pathloss. Table 4.4 represented the physical layer parameters.

In the MAC layer of the sensor node employ the beacon received power from the PHY layer. The STA will measure the power received from the beacon, denoted as P_{re}. If the power received is less than the threshold, that means we have body pathloss, and STA will delay its transmission to avoid packet loss. When the level of received power exceeds the threshold, STA will have a much greater likelihood of reaching the access point (AP). The transmission of STA will recommence [148]. The probability of body path loss was examined by [131, 138], which is determined by the attenuation resulting from body shadowing. Where the placement of sensor nodes (on the wrist, neck, or head) impacts the likelihood of body attenuation.

Table 4.4: PHY Model Parameters

Parameter	Values
Carrier frequency	900 MHz
Noise Figure (F)	3 dB
N	100
Modulation	MCS 0: BPSK
	MCS 1-2: QPSK
	MCS 3-4: 16-QAM
	MCS 5-7: 64-QAM
	MCS 8-9: 256-QAM
Bandwidth (B)	1 MHz
Fade margin	3.84 dB

Table 4.5 displays the parameters that determine the likelihood of body shadowing according to the 802.11ah standard [149]. We can determine the average packet error rate (PER_{avg}) during transmission under pathloss as [147]:

$$\text{PER}_{\text{avg}} = (P_{\text{body pathloss}} \times \text{PER}_{\text{BPL}}) + ((1 - P_{\text{pathloss}}) \times \text{PER}_{\text{SPL}}) \quad (4.38)$$

Where: PER_{avg} is the packet error rate when AP transmission during body pathloss. PER_{BPL} is the packet error rate of the system during body pathloss.

The PER is derived using the Block Rayleigh approximation, as explained in reference [149]. It is a function of the symbol error rate (SER) and signal-to-noise ratio (SNR). The receiver has a noise temperature of -145.22 dB, noise figure of +5 dB, and gain of +3 dB.

Due to the larger body pathloss compared to the standard pathloss, the PER_{BPL} (Packet Error Rate of Body Pathloss) is higher than the PER_{SPL} (Packet Error Rate of Standard Pathloss). Consequently, an increase in $P_{\text{body pathloss}}$ will result in a greater PER_{avg}.

Table 4.5: Displays the parameters

Parameter	Values
Time slot	52 μs
TSIFS	160 μs
DIFS	264 μs
CW_{max}	1023
CW_{min}	31
L_{Data}	100 bytes
R_{max}	7
PS-POLL	14 bytes
Body Shadow Probability (p_{body})	Glucose Monitor: 5%
	ECG: 7%
	Blood Pressure: 10%

The performance of our cross-layer solution implemented is assessed by measuring the throughput between the Access Point (AP) and theStation (STA) using equation :

$$S = \frac{8L_{\text{data}}}{T_{\text{message}}} \cdot (1 - p_{\text{body}}) \cdot (1 - \text{PER}_{\text{avg}}) \tag{4.39}$$

$$T_{\text{DATA}} = T_{\text{Preamble \& Header}} + (T_{\text{Sym}} \cdot N_{\text{sym}}) \tag{4.40}$$

Figure 4.12 illustrates the relationship between the average Packet Error Rate (PER) and the distance between the Access Point (AP) and Station (STA).

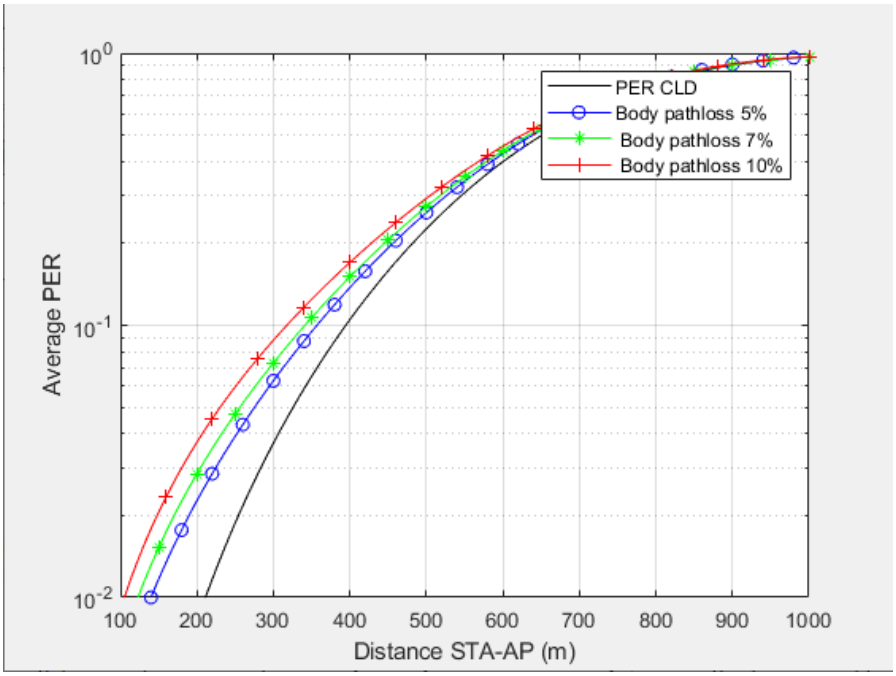

Figure 4.12: PER analysis with different pathloss

The graph compares the performance of the cross-layer method to the non-cross-layer method using various probability of body (loss) values. It is postulated that the AP will emit its beacon at 20-millisecond intervals. The duration of the simulation is one thousand seconds. Whether or not there is body attenuation is determined by calculating the probability of body path loss. PER and throughput

are computed per beacon interval and distance in meters. Pathloss is interchanged between regular pathloss and body pathloss according to the outcomes of random probability calculations. In the simulation, body pathloss is set to 5%, 7%, and 10%. A marginal enhancement of 70% is attainable for a distance of 220 meters. However, this enhancement will incur expenses due to a decline in throughput. Figure 4.13 depicts a simulation of throughput for the values of these values of body pathloss. A throughput reduction of 4% occurs at a distance of 220 meters and 7% for the probability of pathloss = 10%.

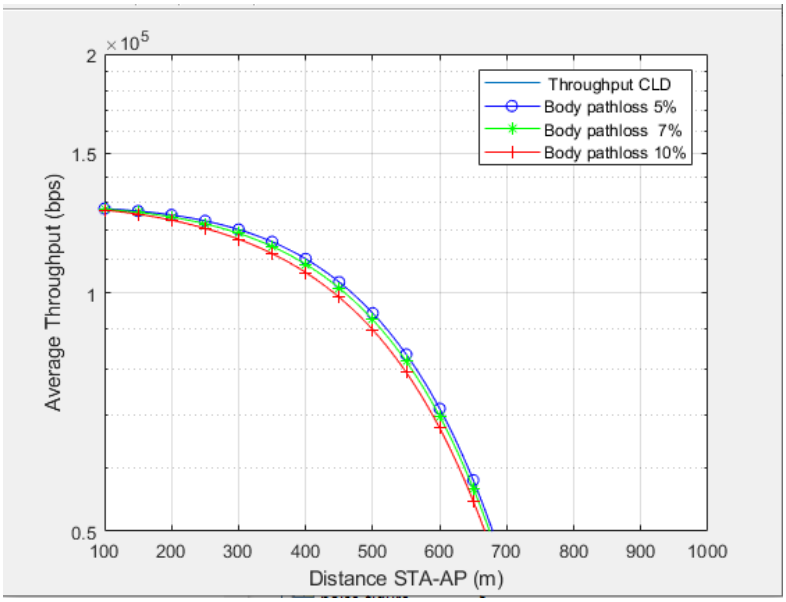

Figure 4.13: The throughput with different pathloss

From Figure 4.12 and Figure 4.13, the PER can decrease by 70% at a distance of 220 meters and a body of 7%. This improvement is because the cross-layer method avoids sending data when there is a high probability of packet errors. However, it is important to understand that this Packet Error Rate (PER) reduction comes at the cost of a decrease in throughput. The outcomes for other sensors exhibit a comparable pattern.

Figure 4.14 presents the relationship between average throughput (in kbps) and the distance between the station and access point (STA-AP) for three different healthcare communication scenarios: CLD for blood pressure, CLD for ECG, and CLD for glucose monitoring. At a distance of 300 meters, the throughput values for the three scenarios are approximately 92 kbps, 81 kbps, and 73 kbps, respectively.

As the distance increases to 1000 meters, the throughput values decline to around 36 kbps, 33 kbps, and 31 kbps, respectively. This decline in throughput with increasing distance is an expected phenomenon due to signal attenuation and path loss in wireless communication systems.

The CLD for blood pressure scenario consistently maintains the highest throughput across the entire distance range, followed by the CLD for ECG and the CLD for glucose monitoring scenarios. This suggests that the communication requirements and the underlying data transmission protocols for these healthcare applications have varying sensitivity to the distance between the STA and AP. The rate of throughput decline is not uniform across the scenarios, with the CLD for blood pressure scenario experiencing a relatively steeper decline compared to the other two scenarios.

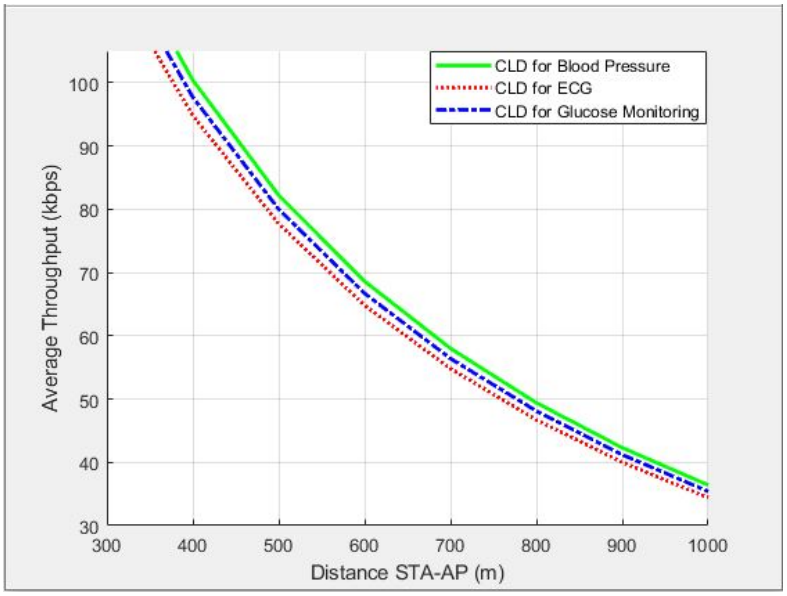

Figure 4.14: Throughput for ECG, Blood pressure, and Glucose monitoring

In conclusion, the results indicate that the proposed cross-layer method can reduce PER by approximately 85%.

4.3.7.3 Cross-layer for CW Optimization

Our method involves modifying the contention window function (CW) of the DCF protocol at the MAC layer. The MAC layer adjusts the CW based on feedback from

the PHY layer. This ensures reduced collisions and retransmissions, especially during high body path loss conditions. The proposed modification to the DCF procedure revolves around mechanisms that lead to packet loss and consumption of bandwidth, where packet loss occurs due to collisions in the channel contention process. After these collisions, retransmissions happen, which use more bandwidth and cause packet latency.

Within the DCF procedure, the backoff mechanism serves to mitigate the occurrence of collisions [149]. However, it does not eliminate this issue. In the event of a collision (indicated by the absence of an ACK packet response), a backoff will be created randomly. After each collision, the window size is increased to decrease the likelihood of future collisions. The CW values in the conventional solution will vary within the specified range of $\mathrm{CW}_{\mathrm{min}}$ and $\mathrm{CW}_{\mathrm{max}}$ values. Upon successful transmission of a packet, the congestion window (CW) is reset to its minimum value.

The foundation of our solution rests upon two key concepts. Increasing the contention window (CW) will result in a larger CW and a subsequent larger backoff, leading to higher overhead. However, a decreased CW value will result in a smaller CW and increased collisions.

The basic DCF backoff time is given by: $\beta_i \cdot \mathrm{SlotTime}$, where β_i is calculated as:

$$\beta_i = 2^{(k+i)} - 1 \tag{4.41}$$

Here, i is the transmission attempt number, originally set to 1. The value of k is determined by the PHY layer kind, and SlotTime is a function that depends on the parameters of the physical layer. The flow chart in Figure 4.15 represents the proposed solution algorithm. Once the i value reaches a predetermined upper limit, the range of CW_max remains constant. Additionally, when a packet is sent successfully, the contention window (CW) is reset to its minimum value, CW_min. The variable i ranges from 1 to 6, specifically taking the values $\{1,2,3,4,5,6\}$. For instance, when i equals 6, the corresponding value of CW is 1023 [TGah].

Figure 4.16 illustrates the capacity of the IEEE 802.11ah MAC technology across various Contention Window (CW) sizes. It indicates a clear trend where capacity, measured in bits per second (bps), increases as the transmit power, measured in dBm, is raised from -50 dBm to 20 dBm. The curve shows that the rate of

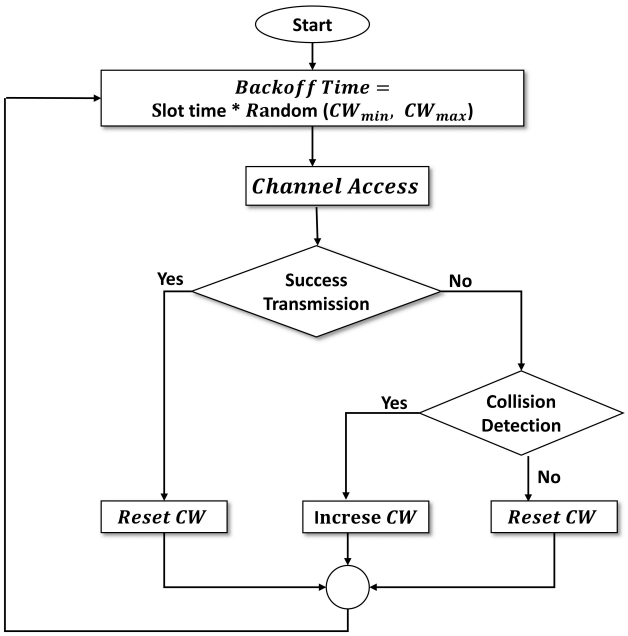

Figure 4.15: Flowchart of algorithm

capacity increase becomes more pronounced as the transmit power approaches higher values. Increased power improves signal quality up to a certain threshold.

To increase throughput, modifications in the 802.11ah standard apply to the header include a reduction of 4 bytes in MAC addressing and 2 bytes for AID (Association Identifier). The throughput of DCF determines by equation 4.42 [147].

$$S = \frac{8L_{\text{data}}}{T_{\text{message}}} \tag{4.42}$$

The L_{data} represents the size of the payload in bytes. Equation (4.43):

$$T_{\text{DATA}} = T_{\text{Preamble}} + (T_{\text{Sym}} \cdot N_{\text{sym}}) \tag{4.43}$$

where N_{sym} represents the number of symbols in different MCS, and T_{Sym} is the duration of a symbol using convolution code.

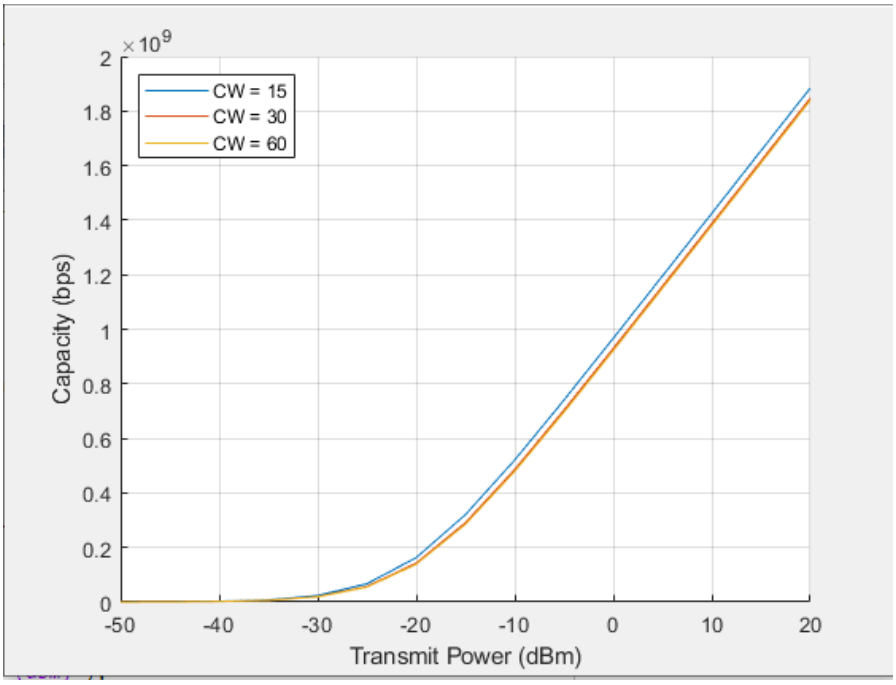

Figure 4.16: IEEE 802.11ah MAC capacity

Equation (4.44):

$$N_{\text{symAH}} = \left\lceil \frac{8 \cdot K \cdot (L_{\text{Header}} + L_{\text{data}}) + 14 + (K-1) \cdot (L_{\text{deli}} \cdot 8)}{6} \right\rceil \quad (4.44)$$

where N_{symAH} represents the number of symbols in AH, K is a constant, L_{Header} and L_{data} represent the sizes of the header and data in bytes, respectively, and L_{deli} represents the size of the delimiter in bytes.

$$T_{\text{message}} = \text{DIFS} + \text{SIFS} + T_{\text{data}} + T_{\text{ACK}} + T_{\text{BACKOFF}} + 2\delta \quad (4.45)$$

where DIFS and SIFS are specific time intervals, T_{data}, T_{ACK}, and T_{BACKOFF} represent the transmission times for data, ACK, and backoff signals, respectively, and δ represents the time of propagation.

Equation (4.45) shows that in an ideal scenario, the contention window (CW) doesn't grow exponentially. However, real-world scenarios involve errors, increas-

ing throughput, and the Packet Error Rate (PER), causing retransmission and exponential increase in CW as shown in equation (4.46) [147].

$$T_{\text{BACKOFF}} = \sum_{i=0}^{\infty} PDR(i) T_{\text{backoff}}(i) \tag{4.46}$$

where $T_{\text{backoff}}(i)$ is defined by Equation (4.47):

$$T_{\text{backoff}}(i) = \begin{cases} \frac{2^{(i-1)}(CW_{\min}+1)-1}{2} \cdot T_{\text{Slot}}, & \text{for } 1 \leq i < m \text{ or } CW_{\max}/2 \\ CW_{\min} \cdot T_{\text{Slot}}, & \text{for } i \geq m \end{cases} \tag{4.47}$$

Equation (4.47):

$$PDR(i) = (1 - \text{PER}) \cdot \text{PER}^{(i-1)} \tag{4.48}$$

where $PDR(i)$ represents the Packet Delivery Ratio for i attempts, and PER represents the Packet Error Rate. The value of m, representing the maximum back-off attempts, is 6. Figure 4.17 shows the curve of the throughput results as a function of payload size.

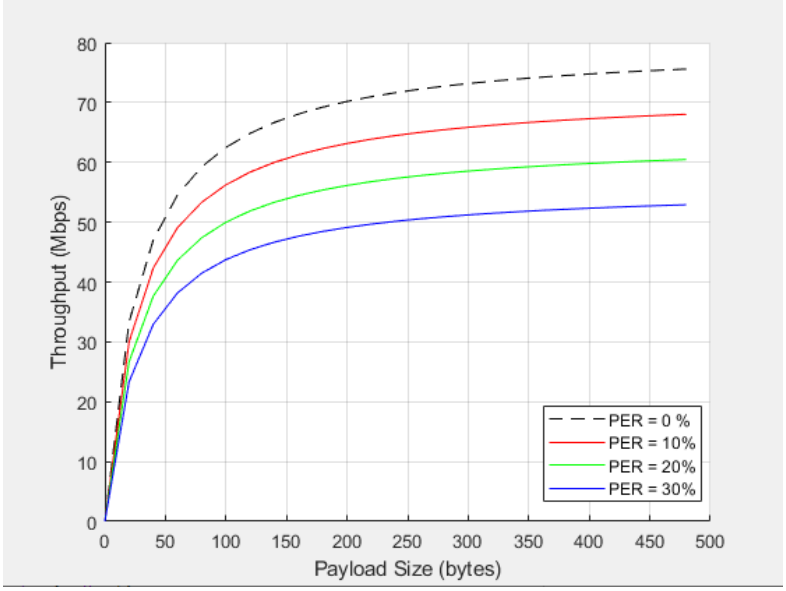

Figure 4.17: Throughput vs Payload size for 802.11ah

Using IEEE 802.11ah allows for reduced overhead by implementing shorter MAC headers. However, when employing these shortened headers along with NDP ACK,

we observed only marginal improvements in throughput, specifically less than 2%. The figure depicts the throughput results using long headers and regular ACK. The throughput of IEEE 802.11ah increases as the payload size grows, reaching a peak of 70 Mbps with a 0% error rate and subsequently declining to 40 Mbps with a 30% error rate. Error rates significantly influence this performance, emphasizing the importance of effective error management in network design. The findings indicate that adopting robust error-correction techniques is crucial when interference levels fluctuate.

4.4 CONCLUSION

This chapter has highlighted the dynamic nature of the Medium Access Control (MAC) layer, which is engineered to adjust the Contention Window (CW) in response to feedback from the Physical (PHY) layer. This adaptive mechanism is instrumental in reducing collisions and the subsequent need for retransmissions, particularly in high-body path loss scenarios. The Distributed Coordination Function (DCF) and its application to Wireless Body Area Networks (WBANs) have been scrutinized for their efficiency in addressing packet loss that leads to bandwidth waste and increases packet latency between nodes. The DCF is based on the CSMA/CA protocol and has two access methods: the primary access method and the Request to Send/Clear to Send (RTS/CTS) procedures. The RTS/CTS procedures control the STA's transmission times through a back-off algorithm based on the Contention Window (CW). The PHY-MAC cross-layer design emerges as a potent strategy for overcoming the challenges of body path loss in 802.11ah networks. This allows the network to become more agile in response to fluctuating conditions and ensures that the full potential of the 802.11ah standard is harnessed. This augments the network's responsiveness and fortifies the efficiency and robustness of IoT communications, establishing a solid foundation for the future of interconnected devices.

5

CROSS-LAYER DESIGN USING USRP AND GNU RADIO

Contents

5.1 INTRODUCTION

In this section, we discuss the development of a cross-layer AMC system for 802.11ah using Software Define Radio (SDR) and GNU Radio for the physical layer, along with a custom MAC layer. The effectiveness of the prototype was evaluated by implementing BPSK, QPSK, and GMSK transceivers. A comparative analysis measures the platform against existing standards. The chapter concludes by addressing challenges and suggesting directions for future research to enhance the platform's capabilities in the healthcare technology landscape. Some of the challenges encountered include synchronizing the software and hardware components, managing timing constraints, and evaluating performance over realistic channel models.

5.2 BACKGROUND AND SIGNIFICANCE

Technological advancements, such as software-defined IEEE 802.11b receivers and Channel Impulse Response (CIR) measurement tools, have emerged to address the increasing need for channel analysis in cross-layer wireless networks. An example of this progress is a system using USRP and GNU Radio, which proves the feasibility of integrating such technologies in complex network environments [150]. The combination of GNU Radio and USRP has been pivotal in developing various protocol layers, as evidenced by its application in IEEE 1609.3 and 1609.4 standards for managing applications and the physical layer akin to 802.11p [151]. Furthermore, GNU Radio has been instrumental in constructing a comprehensive orthogonal frequency-division multiplexing (OFDM) receiver for IEEE 802.11a/g/p networks, a crucial development in IoT applications in healthcare [152]. The development of a testing framework based on GNU Radio and USRP for IEEE 802.11p is vital for tackling challenges such as high Doppler frequency shifts and rapid handoffs, which are significant concerns in IoT healthcare settings [153]. Additionally, a cross-layer protocol for PHY/MAC designed for body path loss in IEEE 802.11ah IoT networks is of particular importance in healthcare. This protocol enhances Packet Error Rate (PER) performance while maintaining throughput, demonstrating its potential in healthcare IoT applications [154].

5.3 ARCHITECTURE OF THE PLATFORM

This section describes the platform used for the implementation. GNU Radio, a freely available software toolkit, was chosen as the platform for implementing the SDR system. GNU Radio operates under the GNU General Public License and is primarily used by academics, researchers, hobbyists, and commercial companies for prototyping and testing various implementations. It was initially developed in 2001 by John Gillmore and Eric Blossom, and has since gained popularity, attracting a growing number of contributors and an extensive source code base. GNU Radio modules are designed to handle infinite streams of data, with complex, short, and floats being the most common types. GNU Radio boasts a vibrant and engaged community, offering numerous examples, reference systems, and applications for various communication technologies such as the Global System for Mobile Communications (GSM), OFDM, and High-definition television (HDTV).

Requirements of GNU Radio

1. Software-defined radio (SDR) Software-defined radio (SDR) is a radio communication system that replaces traditional analog hardware components, such as mixers, filters, amplifiers, modulators/demodulators, and detectors, with software implemented on a computer or an embedded system [155]. Software-defined radio (SDR) applications aim to replace traditional signal-processing systems with software running on standard computers. However, these applications require interfaces for wireless data transmissions. As depicted in Figure 5.1, the primary element of the Software-Defined Radio (SDR) system is the baseband processor.

   A basic SDR system typically consists of a personal computer with a sound card or an analog-to-digital converter, along with an RF front-end. Instead of relying on specialized hardware circuits, a significant portion of the signal-processing tasks are offloaded to a general-purpose processor. The radio functionalities, including receiving and transmitting different radio protocols or waveforms, are determined solely by the software employed.

   GNU Radio (GR) is specifically designed to address the demands of complex applications involving real-time signal processing, which is crucial for effective SDR implementations. Although simple GNU Radio applications can run on any computer, more advanced applications often require additional

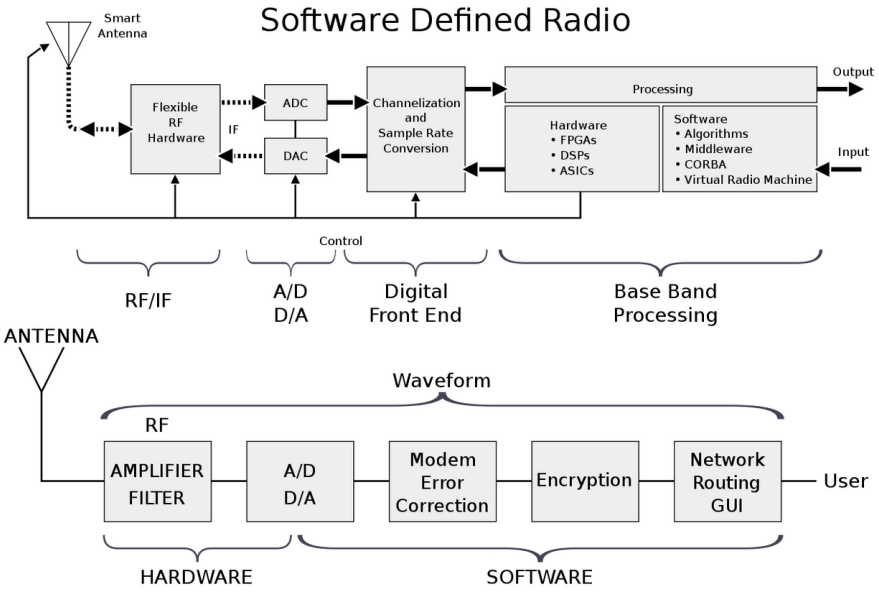

Figure 5.1: Software-defined radio concept [155]

hardware to convert the software-generated digital signal into an analog signal at the desired frequency.

2. The USRP (Universal Software Radio Peripheral) USRP is a hardware component that is used together with the GNU Radio software to build software radios, Figure 5.2 reresnts the USRP B200. It consists of two boards: the motherboard and the RF daughterboard. When an RF signal is received by the USRP daughterboard, it is down-converted to an intermediate frequency (IF), which can then be digitized by oversampling using the ADC on the motherboard.

   The received complex signal is then processed by the FPGA, which acts as a digital down converter (DDC). Subsequently, the I and Q signals were decimated to match the data-rate capabilities of the USB. The processed signal was then transmitted to the host computer via the USB. This process is reversed when transmitting from the host computer to the USRP. In this case, the complex signal is interpolated from the USB, digitally upconverted by the digital upconverters (DUCs) on the mixed-signal processor, converted into analog form by the DAC, and eventually transmitted as an RF signal. A

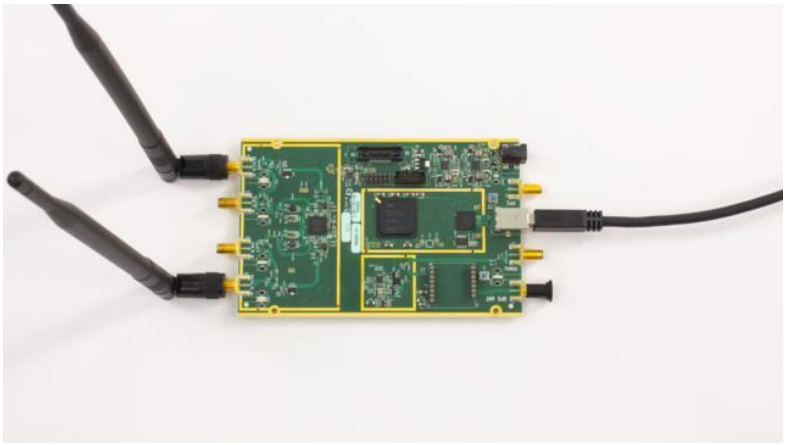

Figure 5.2: USRP B200

visual representation of the signal flow within the USRP is shown in Figure 5.3, which illustrates the main components of the USRP motherboard.

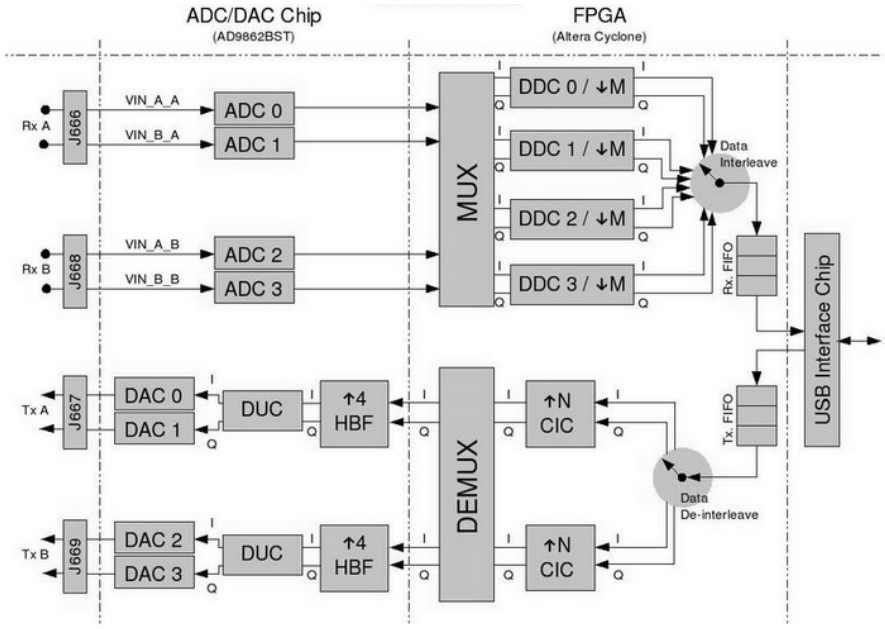

Figure 5.3: The USRP motherboard

3. GNU Radio's graphical interface
   The GNU Radio Companion (GRC) is an extension of GNU Radio (GNU) that offers a graphical user interface (GUI) for creating GNU Radio applications. This provides a visual environment in which users can easily

add modules, configure their parameters, and interconnect them. GRC is a time-saving tool that helps prevent errors by simplifying the system setup and providing real-time verification of parameters. This also facilitates the testing of the new modules. However, it is important to note that GRC is primarily focused on working with pre-existing modules and their parameters, and does not provide extensive customization options. Therefore, it is not recommended to implement entirely new modules, because making modifications to enable control from GRC requires adjustments to the underlying files. GRC has particular utility in educational settings, where quick learning and successful application creation are desired. However, in research environments where researchers typically add and customize modules, GRC may be less suitable. GRC can serve as a valuable tool for constructing test applications and generating Python code, which can be used as a starting point for more intricate and customized applications.

5.4 SYSTEM DESIGN AND PROGRAMMING

5.4.1 System description

Our system aims to develop a system that can monitor vital signs such as ECG and SPo2 (saturation oxygen in the blood) in real-time, the processed data will be displayed to healthcare professionals, and this system will provide healthcare professionals with a simple, cost-effective, and accurate method for monitoring vital signs in real-time, ultimately leading to improved patient outcomes. One way of solving this problem is that monitoring these signals is difficult if not appropriate cross-layer designs are designed. For instance, if I have 1000 sensors all of them will collide, then cross-layer designs avoid collisions, and consequently, the monitoring is possible. Perhaps this is important because we are developing a testbed to assess different cross-layer designs. The need for such a system arises from the fact that vital sign monitoring is a crucial aspect of healthcare, particularly in critical care settings such as intensive care units (ICUs). Timely and accurate information on a patient's vital signs can help healthcare professionals identify any abnormalities and take appropriate action to prevent adverse outcomes. However, traditional vital sign monitoring systems are often complex, expensive, and require specialized expertise to operate. This project aims to develop a system that is simple, cost-effective, and can be easily integrated into existing healthcare

workflows. The system uses a Universal Software Radio Peripheral (USRP) device to collect data from ECG and SpO2 sensors, which will be processed and analyzed using GNU radio (software developed in Python). The processed data will be displayed to healthcare professionals in a user-friendly format, allowing for quick and accurate assessment of the patient's vital signs. The use of USRP in the system design offers several advantages. Firstly, USRP devices are relatively inexpensive and can be easily configured to interface with various sensors.

Secondly, USRP devices can handle large amounts of data, making them ideal for real-time data transfer and analysis. Finally, USRP devices are highly versatile, allowing for customization and development of software to suit specific requirements.

5.4.2 System Objective

The main objective of this experiment is to design and evaluate a wireless communication module that allows integrating different sensors and a receiver USRP that allows collecting these data from sensors. This module recreates a realistic environment and allows one to carry out experimental evaluations because we have control and repeatability features. The experimental evaluation of cross-layer design requires all these features.

The problem

Using a pulse oximeter commercial device to transmit the data to the USRP is not feasible and more complicated, and we also have no control over the parameters of the commercial device. Because we need to collect 1,000 packets, this process takes a lot of time (sensing with the finger, waiting to get variables, and seeing if signals are collecting or not).

The solution

The proposed solution uses a prototype that emulates the transmitter of this kind of signal by controlling the experiment's parameters for transmitting it and selecting the best one because the experiments have been repeatable many times. For this reason, we will use real commercial devices in the last step once I check the prototype working with our approach for one case (because it doesn't allow changing the length of the packet, channel frequency, sample rate, or time configuration)

to show that our approach is also working with commercial devices in real-time. Figure 5.4 depicts typical components of our system.

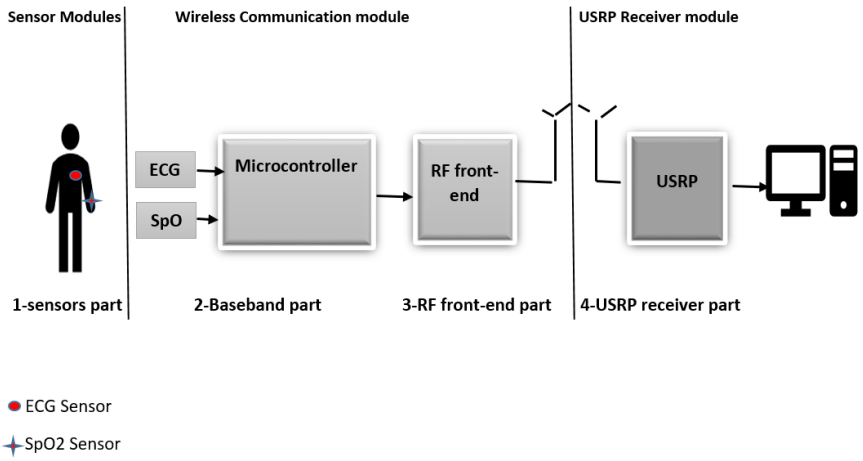

Figure 5.4: system block diagram

From figure 5.4, the microcontroller senses the signal of SpO2 and converts it to a digital signal (using an ADC with a given sample rate), then adds a header and sends it to the RF front-end, which uses another sample rate and carrier frequency. The data are formatted as a Protocol Data Unit (PDU) for the MAC layer. The sensor data stream occupies the MAC buffer for transmission (Tx). As the MAC layer program runs, data from the buffer are selected and sent to the access point using the 802.11ah network. Finally, the USRP (receiver side) sets the sample rate and carrier frequency equal to those used by the RF front-end.

The SpO2 sensor operates in a specific frequency range, typically approximately 1–3 MHz, with a sample rate of approximately 100 samples/s (SPS) and a few ksps. We set the sample rate and bandwidth of the SDR to capture the SpO2 signal (the SpO2 signal is a low-frequency signal typically ranging from 1-3 MHz). Therefore, if we need to capture this signal, a sample rate of at least 10–20 MHz is typically required with a bandwidth of 2–4 MHz. The SDR filter settings determine the range of frequencies captured and filtered by the SDR. We must select a filter that is appropriate for the frequency range of the SpO2 signal. The appropriate filter for the SpO2 signal depends on the specific characteristics of the signal. In general, a low-pass filter is commonly used to filter out high-frequency noise and interference while preserving the low-frequency SpO2 signal. We can use a Butterworth or Chebyshev filter with a cutoff frequency of approximately

3–5 MHz to capture the SpO2 signal. The filter settings vary depending on the characteristics of the SpO2 signal and the noise level in the environment.

5.5 CROSS-LAYER IMPLEMENTATION

5.5.1 Physical layer

In the IEEE 802.11ah standard, the PHY layer converts MAC frames into signals and transmits or receives them through the communication medium. The PHY layer of IEEE 802.11ah utilizes orthogonal frequency-division multiplexing (OFDM) for data communication. The TGah PHY incorporates several features such as Forward Error Correction (FEC), OFDM modulation, and receiver synchronization [156]. In the physical layer, the data handling process involves environmental signal collection, scrambling, convolutional encoding, and data interleaving. Data interleaving is designed to enhance the effectiveness of Forward Error Correction (FEC) by spreading burst errors over time. This is achieved through a two-step permutation process, in which adjacent coded bits are mapped to distant subcarriers and alternated on significant bits. The first step is defined by the following equation :

$$m_k = \left(\frac{N_{cbps}}{12}\right) \cdot k \bmod 12 + \left\lfloor \frac{k}{12} \right\rfloor \tag{5.1}$$

The second variation is defined by :

$$j_k = \left\lfloor \frac{m_k}{S} \right\rfloor + \left[m_k + N_{\text{cbps}} - \left\lfloor \frac{12 \cdot m_k}{N_{\text{cbps}}} \right\rfloor \right] \mod (s) \tag{5.2}$$

For $k = 0, 1, \ldots$, where N_{cbps} denotes the count of coded bits per subcarrier, corresponding to values 1, 2, 4, or 6 for modulation schemes BPSK, QPSK, 16-QAM, or 64-QAM; k represents the coded bit's index before the initial permutation; m_k signifies the index post the first but before the second permutation; and j_k is the index after the second permutation, immediately before modulation mapping.

5.5.2 MAC Layer

To incorporate the cross-layer functionality, channel access was maintained using CSMA/CA. The MAC layer implementation was modified by integrating the algorithms from [154] and [157]. This integrated approach combines the idle-to-receive state transition of the original MAC protocol and the acknowledgment mechanism with the enhanced backoff algorithm and the continuous medium monitoring of the proposed method. This ensures efficient data transmission while conserving energy, minimizing signal collisions, and reducing delays resulting from body bath loss. The proposed method can be summarized as follows: Figure 5.5 the initial design of the MAC layer in a broad sense, along with our specific alterations.

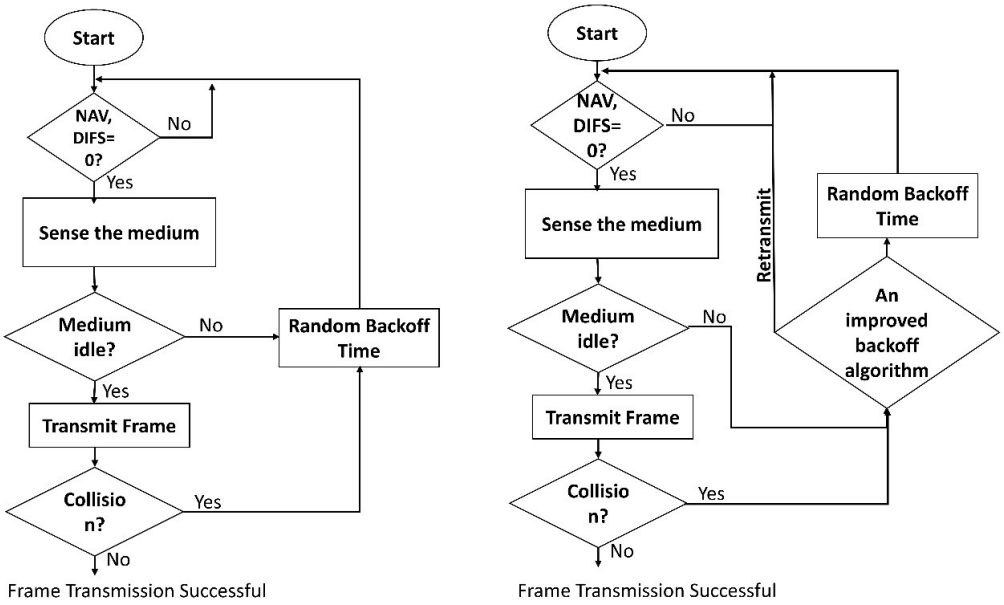

Figure 5.5: cross layer algorithm

An enhanced backoff algorithm improves the data transmission ability compared with the original method, which involves retransmission and random backoff time in the DCF protocol. The proposed method can be summarized as follows:

- The system started in an idle state and monitored the status of the medium.
- If a new packet is ready for transmission, the system checks if the medium is busy.

    * If the medium is idle, the system checks the PHY layer buffer for received data.

    * If data are found, they are saved in the receiver buffer, and an acknowledgment is sent.

    * If no data is found, the system initiates packet transmission.

- If the medium is busy, the system waits for the Network Allocation Vector (NAV) and distributed interframe space (DIFS) to prevent signal collisions.
- Once the medium becomes idle, the system starts measuring the time in units of slot time.
- If the second carrier sense indicates that the medium is not idle, a collision occurs.

    * The system applies an enhanced backoff algorithm function, freezing the original random backoff time.

    * Transmission uses an enhanced backoff algorithm. All other operations continue to use the original random backoff time function

- In the case of transmission, the Wi-Fi physical hierarchy module in GNURadio receives data from the MAC and other transmitting stations/APs.

The original MAC protocol starts in an idle state and transitions to the receiving state. MAC checks the PHY layer buffer for the received data, saves it in the receiver buffer, and sends an acknowledgment. If no data are found, the system returns to an idle state. If data are found, MAC initiates the CSMA/CA protocol. The system waits for the Network Allocation Vector (NAV) and distributed interframe space (DIFS) to conserve energy and prevent signal collisions. The cross-layer modification introduces an if-else selection before checking the MAC Tx buffer for transmission, in our cross-layer design, we merged the transmitter and receiver into a single transceiver unit. The primary GNU Radio module employed is the Wi-Fi physical hierarchy, which can receive data from the MAC layer and external transmitting stations or access points. Figure 5.6 illustrates the transceiver design, adapted from the source [158], with frequency, encoding, and sample rate modifications to align with the 802.11ah standard. The frequency was below 1 GHz and varied according to the regional frequency ranges. We adapted Bastian's basic 802.11/a/g/p WiFi OFDM source code to align it with the 802.11ah standard.

This involved altering the bandwidth choices to 1 MHz, 2 MHz, and 4 MHz, with 2 MHz being mandatory and 1 MHz and 4 MHz being optional. Additionally, changes were made to the transmitter code MCS uses.

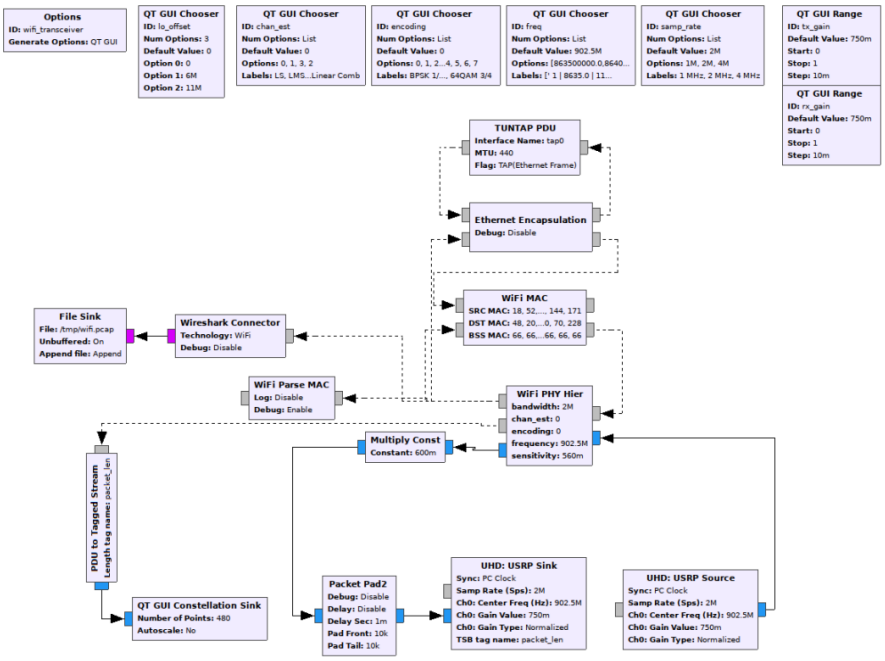

Figure 5.6: transceiver design

The OFDM modulator in the Python file ofdm.py connects C++ blocks and produces a complex modulated signal at the baseband. It has a send function that facilitates the transmission of payloads. The send function converts the payload into a data packet using make packet, which adds the Cyclic Redundancy Check (CRC) and header. The send function does not return any value but invokes insert tail, placing the data at the end of the queue. The modulator's initial components include the "pkt input" module, which maps bytes to complex symbols, the preambles module, the iFFT module, and the "cpadder" module [159]. The OFDM signal is transmitted through the uppermost layer of the application using the USRPs at a 2.5 GHz transmit frequency. An OFDM-based transceiver is realized using real-time signal processing frameworks (IEEE 802.11ah Blocks) in GNU Radio Companion (GRC), with the Ettus USRP N200 processing symbols over the wireless radio channel. The FER Error Rate (FER) is assessed for each sub-carrier using standard OFDM modulation techniques like BPSK, QPSK, 16, and 64-QAM, coupled with various punctuated coding rates. This setup also allows for the obser-

vation of real-time signal constellations and OFDM signal spectra to analyze the impact of multipath signal propagation through both flat and frequency-selective fading channels. Techniques such as least squares (LS) and training-based adaptive least mean square (LMS) algorithms are employed in the receiver. The simulation is practically demonstrated in GRC, transforming it into a set of Software-Defined Radios (SDR) functioning as a concurrent transceiver[159]. The OFDM block produces OFDM symbols depending on parameters such as fft length, occupied tones, cp length, and the chosen modulation type, among others. The voltage of the signal transmitted to the antenna, as a function of time for any given OFDM symbol, is characterized as.

$$S(t) = e^{j2\pi f_c t} \sum_{k=-\frac{N_{\text{used}}}{2}}^{\frac{N_{\text{used}}}{2}} a_k \cdot e^{j2\pi k\Delta f(t-T_g)} \tag{5.3}$$

Where t represents the time elapsed from the start of the specific OFDM symbol, constrained by $0 < t < T_s$, a_k denotes a complex number corresponding to the data transmitted on the carrier with a frequency offset index of k during the aforementioned OFDM symbol. This complex number a_k maps to a point in a QAM constellation. T_g is the guard time, T_s is the total duration of the OFDM symbol inclusive of guard time, and Δf signifies the spacing between carrier frequencies.

The frequency offset index is determined based on its carrier index, as outlined in equation 5.4.

$$k_{f_{oi}} = \begin{cases} k_{ci} - \frac{N_{\text{used}}}{2}, & \text{if } k_{ci} < \frac{N_{\text{used}}}{2} \\ k_{ci} - \frac{N_{\text{used}}}{2} + 1, & \text{if } k_{ci} \geq \frac{N_{\text{used}}}{2} \end{cases} \tag{5.4}$$

The frequency offset index is determined based on its carrier index, as outlined in the following equation.

$$\text{out}[nD + k] = \text{symbol table}[\text{in}[n]D + k], \quad k = 0, 1, \ldots, D-1 \tag{5.5}$$

The sequence of `gr_packed_to_unpacked_XX` and `gr_chunks_to_symbols_XY` is used to convert a stream of bytes or shorts into floats or complex symbols.

The polyphase Resample block functions as a filtering mechanism, receiving a complex stream and producing a singular complex stream, thereby obviating

the necessity for additional connecting elements. It aligns with other polyphase filter banks (PFBs), adeptly handling multi-rate signal processing tasks. This block facilitates arbitrary resampling through the use of N filters and rational resampling, achieving an arbitrary rate by interpolating between two points. Table 5.1, estimation of SNR with changes in the multiplied constant value. The channel

Table 5.1: Delay Spread Parameters

Multiply Constant value	**Estimated SNR Value**
1	1.00134
10	10.3085
50	52.209883
100	108.347

model block is a fundamental simulator for channel modeling, useful in assessing, designing, and experimenting with different signals, waveforms, and algorithms. It allows users to adjust the voltage of an AWGN noise source, set a normalized frequency offset and a sample timing offset, and use a noise seed to randomize the AWGN noise source. In this model, the estimation of multipath effects is possible through the use of a filter that represents the multipath delay profile. The MPSK SNR estimator is a block dedicated to calculating the signal-to-noise ratio (SNR) of a signal. This block is useful for monitoring and obtaining SNR estimates of the signal. It's designed to integrate into a flow graph, transmitting all received data to its output. The estimated SNR value tends to rise with an increase in the multiply constant block value, as shown in Table 5.1. The frequency lock loop uses a band-edge filter to cover digitally modulated signals' upper and lower bandwidths, determined by the modulated signal's excess bandwidth. The filters are large for accurate comparisons and have a flat-phase response. The Polyphase Clock Sync block executes timing synchronization for PAM signals, enhancing signal-signal noise ratio (SNR) and reducing Inter-Symbol Interference (ISI) [160]. The Costas loop is capable of producing two types of output streams. The first stream consists of the baseband I and Q signals, while the second stream displays the loop's normalized frequency. The digital version of the Costas loop includes several key components: a Direct Digital Synthesizer (DDS), a Low Pass Filter (LPF), a Phase Discriminator (PD), and a Loop Filter (LF). It's important to note

that this setup assumes the input signal to be a baseband signal, which is modulated by an intermediate frequency carrier [161].

$$x(t) = M(t) \cdot \cos(w_c t) \tag{5.6}$$

The outputs of the in-phase and quadrature branches from the local Direct Digital Synthesizer (DDS) are as follows, respectively:

$$\begin{aligned} V_{oi} &= \cos(w_c t + \Delta\phi) \\ V_{oq} &= \sin(w_c t + \Delta\phi) \end{aligned} \tag{5.7}$$

Where $\Delta\phi$ represents the phase difference between the input signal and the local signal of the DDS. Subsequently, the outputs from the multipliers in both the in-phase and quadrature branches are as follows:

$$\begin{aligned} Z_i(t) &= M(t) \cdot \cos(w_c t) \cdot \cos(w_c t + \Delta\phi) \\ Z_q(t) &= M(t) \cdot \cos(w_c t) \cdot \sin(w_c t + \Delta\phi) \end{aligned} \tag{5.8}$$

Following the low-pass filtering process, the respective outputs are as follows:

$$\begin{aligned} y_i(t) &= \frac{1}{2} k_{l1} M(t) \cos(\Delta\phi) \\ y_q(t) &= \frac{1}{2} k_{l2} M(t) \sin(\Delta\phi) \end{aligned} \tag{5.9}$$

Where k_{l1} and k_{l2} represent the coefficients of the low-pass filter. Once $y_i(t)$ and $y_q(t)$ have been processed through the phase discriminator and loop filter, the following equation is used:

$$V_c(t) = \frac{1}{8} k_p k_{l1} k_{l2} \sin(2\Delta\phi) = k_d \sin(2\Delta\phi) \tag{5.10}$$

5.5.3 Channel Coding

In digital communications, channel code refers to the combination of forward error correction code and interleaving used in scenarios where the medium of

communication or storage is treated as a channel. The purpose of a channel code is to safeguard the data transmitted across it or stored within it, even in the presence of disturbances like noise (errors). The concept of channel coding applies to both the transmitting and receiving ends of a digital communications system. Channel coding encompasses three main strategies: randomization, FEC (Forward Error Correction), and interleaving.

5.6 EVALUATION OF PROTOTYPE

A real-time software-defined radio (SDR) system was set up using laptops equipped with 8 GB RAM and an Intel Core™ i7 operating at 2.50 GHz, as illustrated in Figure 5.7. The USB 3.0 connection interface of the system was connected to a USRP N210 device.

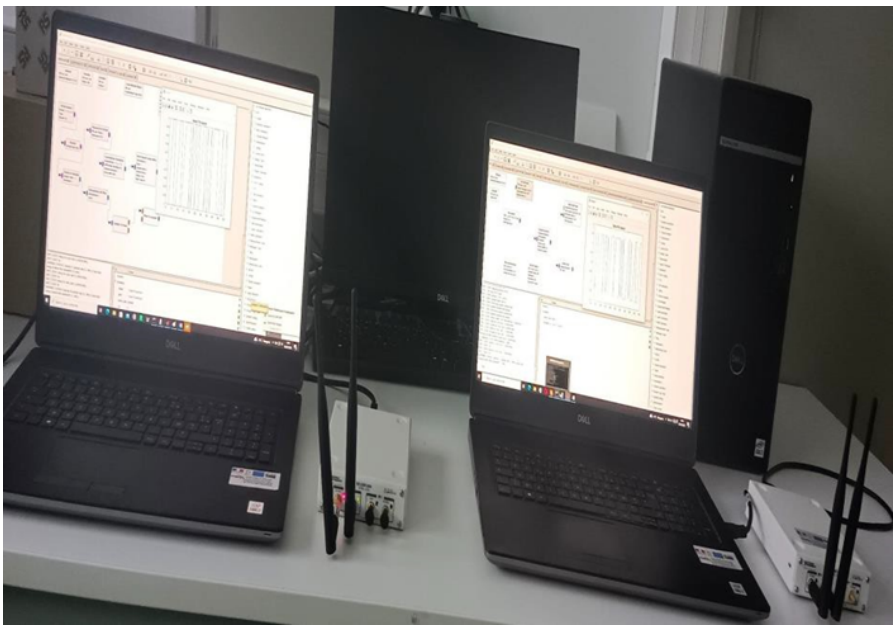

Figure 5.7: Test Bed Setup for Software-Defined Radio Development.

The concatenated OFDM signal is transmitted over the air in a lab environment using the TX/RX antenna of the USRP RF front end and received by the RX2 antenna. Incorporated one-way and two-way data file transmissions, employing modulation technologies supported by TGah, including BPSK, QPSK, and GMSK. We conducted a detailed analysis of the effectiveness of each transmission mode

through the configuration and execution of the software-defined radio environment. This part goes into more detail about how the experiment was set up and how our findings have affected the creation of energy-efficient transmission methods for IoT e-health using IEEE802.11ah, which is a key part of making healthcare delivery systems last longer and work better. The figure 5.8 presents the results of an experimental evaluation of an IEEE 802.11ah transceiver implementation using the GNU Radio software-defined radio platform and USRP.

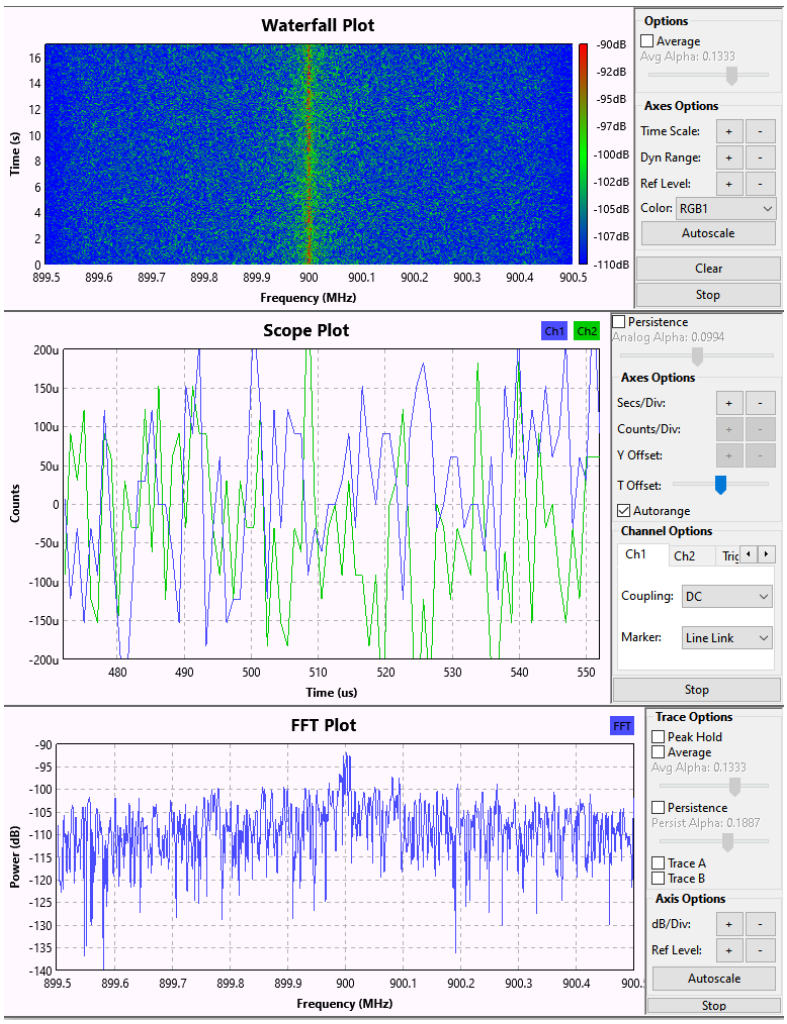

Figure 5.8: Spectrum in 900 MHz; (a) Signal frequency domain; (b) Signal in time demain.

The top panel shows a waterfall plot, which visualizes the time-frequency characteristics of the 802.11ah signal. The y-axis represents time, the x-axis shows frequency, and the color scale indicates the signal power. This plot allows the

identification of the occupied frequency bands, as well as the temporal evolution of the signal's spectral content, which is crucial for verifying compliance with the 802.11ah channelization and modulation schemes.

The middle panel displays the time-domain waveform of the 802.11ah signal, captured using an oscilloscope-like scope plot. This representation enables the analysis of the signal's amplitude, frequency, and potential distortions in the time domain, complementing the frequency-domain information provided by the waterfall plot.

The bottom panel shows the Fast Fourier Transform (FFT) of the 802.11ah signal, which provides a detailed view of its frequency spectrum. The x-axis represents frequency, and the y-axis shows the signal power. This FFT plot is essential for validating that the frequency content of the implemented 802.11ah transceiver matches the expected channel allocations and modulation characteristics defined by the standard.

The various trace colors and labels in the figures correspond to different test configurations or parameter settings, such as the use of different 802.11ah physical layer modes e.g., OFDM.

802.11ah operates within a frequency range of 863.5 MHz to 927.5 MHz, although the specific allocation of frequencies may differ between countries. Numerous groups use this sub-GHz frequency range, with cellular systems and amateur radio operators being two notable examples. To ensure a seamless experiment, we opted to select a frequency range that is relatively free from other signals that could potentially interfere with our own signal. In order to identify a suitable channel with minimal interference, we conducted a spectrum sweep. We used a step size, considering that the B200 device has a maximum bandwidth of 56MHz. In our laboratory environment, we discovered that the 900MHz frequency exhibited less congestion compared to other frequencies.

5.6.1 BPSK Tranceiver

BPSK is used in many communication systems, especially in IoT applications, due to its simplicity, low cost, and good performance under noise. In order to implement BPSK using SDR and GNU radio, the signal must first be generated. The signal is generated using a signal generator or a computer with a sound card. In this experiment, we generate signals in a Matlab program. The BPSK GNU flow

graph shown in Figure 5.9 represents the steps in implementing a Binary Phase Shift Keying (BPSK) modulation system. The graph consists of four main blocks:

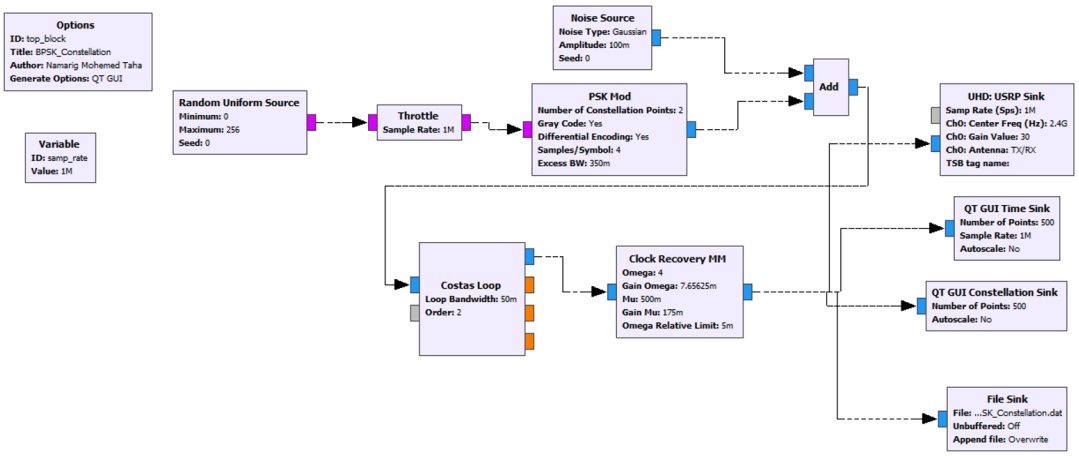

Figure 5.9: The BPSK flowgraph.

a source block, a modulator block, a channel block, and a demodulator block. The source block generates a binary signal, which is then sent through a modulator to produce the BPSK signal. The BPSK signal is transmitted through a channel, which introduces noise and interference. Finally, the demodulator block decodes the received signal and recovers the original information. The BPSK modulator was created using USRP. With the help of MATLAB and GNU radio software. The GNU tool has signal processing blocks built in other processing software, which are used to construct the modulator as data flow graphs. Its crucial feature permits real-time data processing with a high sampling rate and quick computation, SPO2 DAT files were investigated and effectively implemented. The system was tested in a laboratory environment and was able to successfully transmit and receive medical data with a low bit error rate. The constellation diagram of the receiver is shown in figure 5.10. We also demonstrated the ability to adapt to changing environments and interference by adjusting the receiver's gain and frequency. In this figure, because we used an attenuator, an ideal channel, and raised cosine filtering (to avoid spectral spreading), we can observe that the symbol error rate = 0, BER = 0, and PDR =100% at gain above 10 dB. This is very important in IoT health applications.

Figure 5.11 represents the performance of BPSK modulation. From the figure, we observed that with the BER decreasing rapidly as the SNR increases until it

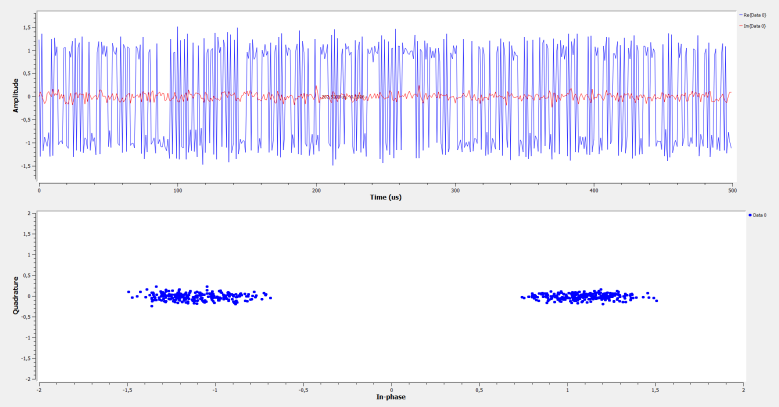

Figure 5.10: Constellation diagram of receiver.

reaches a minimum value, which is affected by the modulation scheme, channel characteristics, and receiver design.

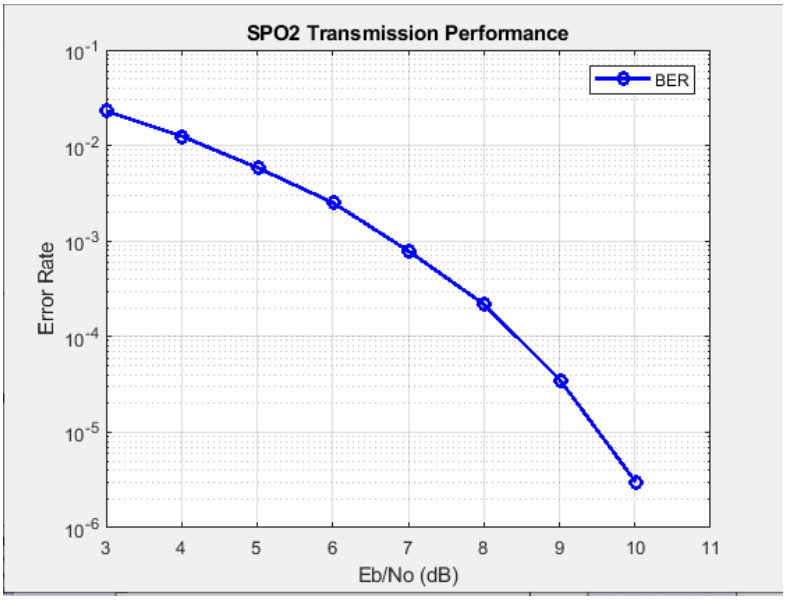

Figure 5.11: The performance of BPSK modulation.

Our implementation has effectively attained a minimum bit error rate (BER) and higher signal-to-noise ratio (SNR) values, indicating the reliability and efficiency of the communication system. Moreover, implementation demonstrates robustness against radio-frequency interference, ensuring improved quality in transmitting medical information.

The figure presents a graph illustrating the Bit Error Rate (BER) performance of SPO2 transmission using BPSK modulation over a range of E_b/N_0 values. The figure shows that as the E_b/N_0 ratio increases, the BER decreases significantly, indicating an improved performance. Around an E_b/N_0 value of 10 dB, the BER approaches 10^{-5}, which is considered a good performance for our system.

5.6.2 QPSK Transceiver

Quadrature Phase Shift Keying (QPSK) is a widely used digital modulation scheme in wireless communication, known for its balance between spectral efficiency and robustness. QPSK modulates the phase of a carrier wave to transmit two bits per symbol, with four distinct phase states (0, 90, 180, and 270 degrees) representing four possible bit combinations (00, 01, 10, 11).

- The key aspects of QPSK theory include:

  1. Phase Modulation: Unlike BPSK, QPSK uses four phase shifts to represent data, doubling the bit rate for a given bandwidth.

  2. Spectral Efficiency: QPSK is more spectrally efficient than BPSK while maintaining a comparable level of robustness to noise and interference.

  3. Symmetry: The four-phase states of QPSK are symmetrically spaced, offering a uniform error probability.

- Designing QPSK GNU Flow Graph

  Figure 5.12 shows the QPSK flow graph. The first stage entails the transmission of a QPSK signal. This process involves the creation of a sequence of binary digits and converting this sequence into a complicated pattern of points in space.

  Figure 5.13 shows the performance of QPSK using a matched filter.

  The Qpsk_stage1.grc flowgraph transmits a signal using Quadrature Phase Shift Keying (QPSK) modulation (Barry Dugan). It visually represents the transmitted signal and elements of the receiving chain through time-domain, frequency-domain, and constellation diagrams. The Root Raised Cosine (RRC) filter is applied to constrain the signal's transmit bandwidth within the

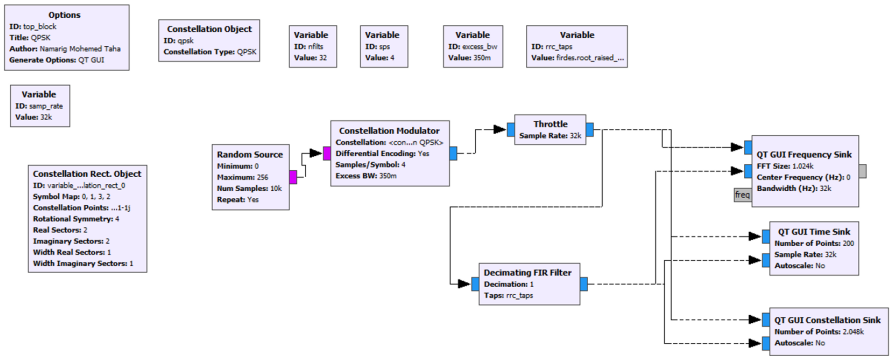

Figure 5.12: The QPSK flograph.

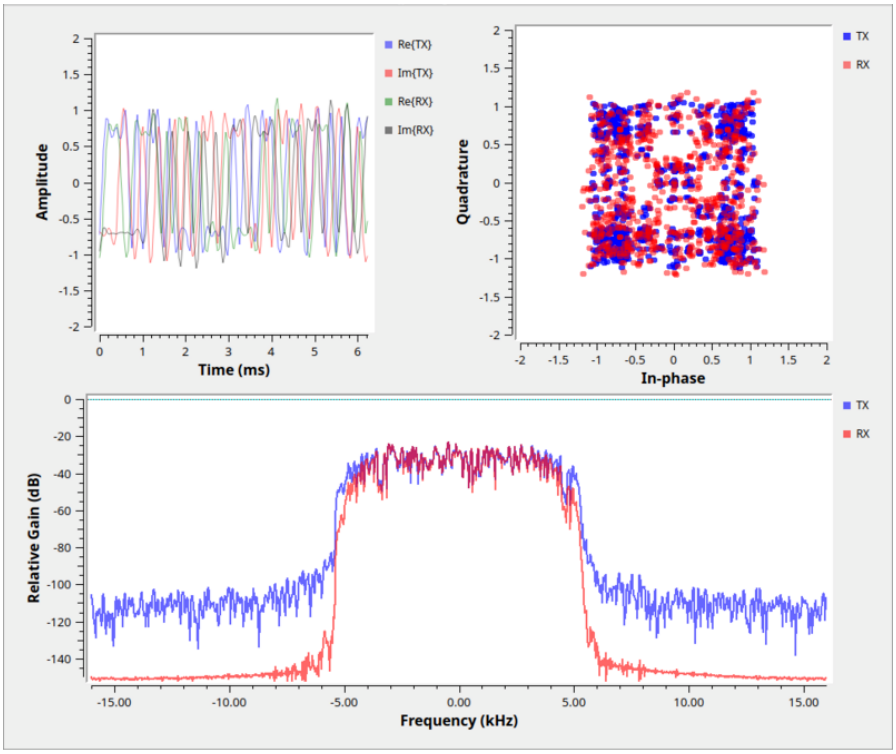

Figure 5.13: QPSK performance.

preferred range. Without a shaping filter, the transmitted signal would resemble square waves, causing significant energy spillage into adjacent channels. However, a consequence of using the RRC filter is the introduction of intersymbol interference (ISI), which degrades the quality of the received signal by merging symbols together. This aspect will be further analyzed in the timing recovery section.

– Channel Impairments

The initial phase of the simulation involved transmitting a Quadrature Phase Shift Keying (QPSK) signal and analyzing the impact of channel and signal distortions during the transmission and reception processes. This incorporates noise, specifically Additive White Gaussian Noise (AWGN), and differing clocks. Due to these imperfect clocks, the received signal deviates from its target, Figure 5.14. Determining the ideal sampling point is also challenging because the two radios operate at dissimilar speeds, rendering the precise sampling point indeterminate. In the simulation's second phase, adjustments can be made to additive noise, frequency offset, and timing offset, enabling observations of the signal under various levels of these disturbances.

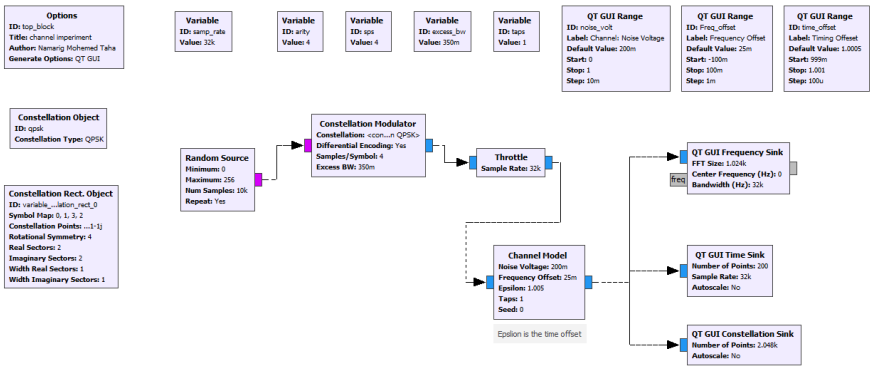

Figure 5.14: Channel Impairments.

– Polyphase Clock Sync
The Polyphase Clock Sync serves three primary roles. 5.15 represents the performance of using polyphase filter.

Initially, it executes clock recovery. Next, it acts as the receiver's matched filter to eliminate intersymbol interference (ISI). Finally, it down-samples the signal, decreasing the samples per symbol.

The constellation exhibits residual noise due to intersymbol interference (ISI) even after passing through the 32 filters. However, this noise is attenuated by increasing the channel's noise voltage setting beyond 0,

- Body pathloss during multipath
Multipath occurs because, in many communication settings, there is not just one path for the signal to travel from the transmitter to the receiver. In our model, the

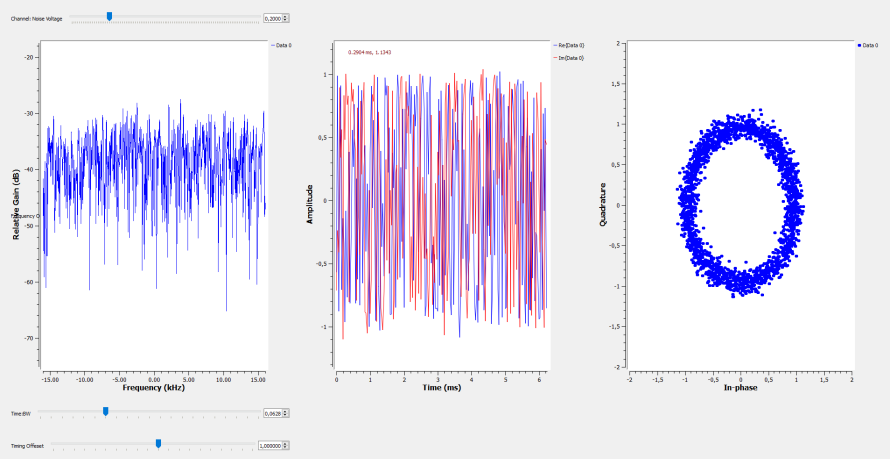

Figure 5.15: Polyphase filter performance.

multipath effect arises from body path loss due to the shadow effect. This leads to new paths between the sensor node (STA) and the access point (AP), depending on the distance between the transmitter and receiver. To counteract the impact of multipath, we employed an adaptive algorithm. This algorithm utilizes the Constant Modulus Algorithm (CMA) type, a blind equalization effective only on signals with a constant amplitude or modulus. Consequently, digital signals such as QPSK are suitable for this algorithm, as their characteristics include points solely on the unit circle.

- Description algorithms
  The Constant Modulus Algorithm (CMA), developed by Godard in 1980, is the foremost technique in blind equalization. Blind equalization, or self-recovering equalization, entails independently setting equalizer taps without using a training sequence or symbol decisions. CMA closely resembles the Least Mean Square (LMS) algorithm. The critical difference between them lies in the performance function. While the LMS algorithm uses the squared error as its performance function, CMA adopts an alternative approach [162]. In various equalizers, like maximum likelihood sequence estimation, the channel response is known at the receiver (Rx) through a channel estimation process that depends on a training sequence. For adaptive equalization methods such as Least Mean Square (LMS) equalizers or Decision Feedback Equalization (DFE), the tuning of equalizer taps initially uses training sequence symbols and subsequently symbol decisions. However, in many cases, the receiver must obtain equalizer coefficients without assistance from the transmitter (Tx) regarding known symbols. This non-data-aided

approach is essential in mobile communication systems where the receiver might lose the signal due to channel fading or

blockage, necessitating blind acquisition once the signal is restored. Other applications include general-purpose radios for demodulating various wireless signals, military radios, signal monitoring, and point-to-multipoint networks. The equation depicted in the image is as follows:

$$\left(\frac{1}{N}\sum_{m=1}^{N}\left(|y[m]|^2-1\right)\right)^2 \tag{5.11}$$

The expression $|y[m]|^2$ represents the energy of the symbol-spaced samples distributed over the constellation. The value 1 represents the intended energy concentrated within a circle in the constellation, Figure 5.16. The latter stages of the derivation strongly resemble the LMS algorithm.

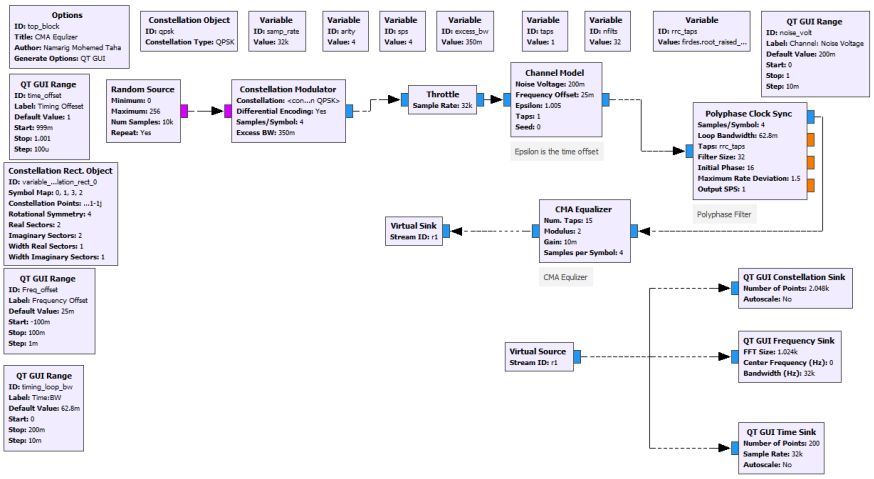

Figure 5.16: CMA equalizer.

From figure 5.17 the convergence of the CMA algorithm can be observed. It is important to note that since the clock sync and equalizer blocks operate concurrently, they converge independently, yet the convergence of one influences the other. This results in an interaction as both blocks lock on the signal. Ultimately, we can discern the impact on the time-aligned multipath signal and post-equalization.

Pre-equalization, the signal appears distorted, even in the absence of noise. However, the equalizer compensates for and neutralizes the channel effects, producing a clear signal. Additionally, the channel's response can be examined, revealing how it becomes notably more uniform following the equalization process.

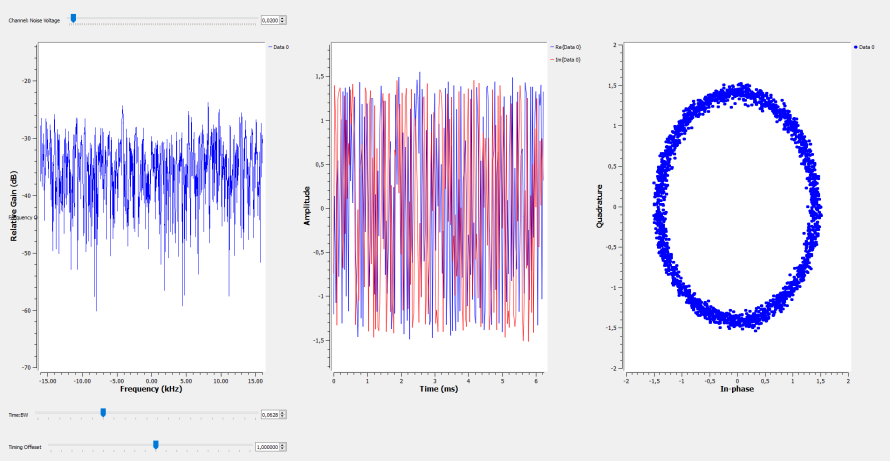

Figure 5.17: CMA equlizer performance.

After equalizing the channel, we still face the challenge of phase and frequency offsets. Equalizers typically have a slow adaptation rate, making them less effective against rapid frequency changes. Additionally, using only the CMA equalizer, which aims to converge to the unit circle, does not provide phase accuracy. It needs constellation awareness; it may lock onto any phase during convergence. Thus, we must address both phase and frequency offsets. This stage involves two considerations. Firstly, a second-order loop tracks both phase and its time derivative, frequency. Secondly, this stage is designed for fine frequency correction, presupposing that the frequency is already reasonably close to the ideal. If the discrepancy is too large, the loop will fail to converge, causing continuous drift. Coarse frequency adjustments can be made using tools like the FLL_Band-Edge block.

- Frequency and Phase Correction

  We employed the Costas Loop for this operation. The Costas Loop block can synchronize BPSK, QPSK, and other signals Figure 5.18 representss the QPSK flowgraph using Costas loop. It operates on a second-order loop, determined by a loop bandwidth parameter, and it requires the specification of the PSK modulation

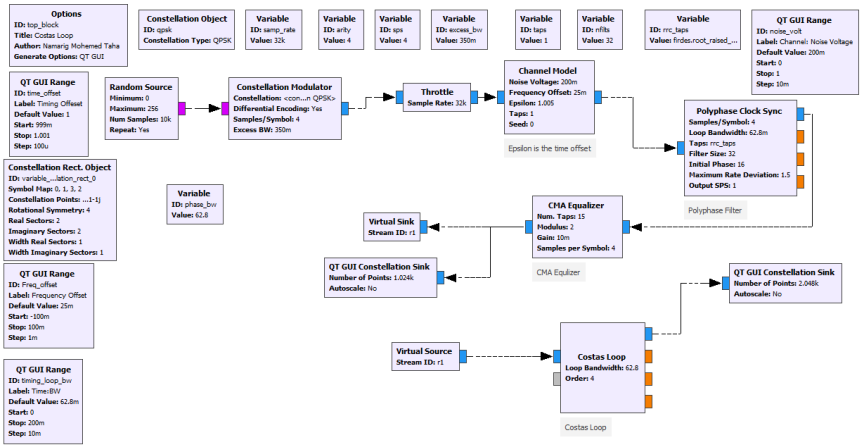

Figure 5.18: Costas loop.

order. Figure 5.19 represents the constellation plot of QPSK after using Costas loop.

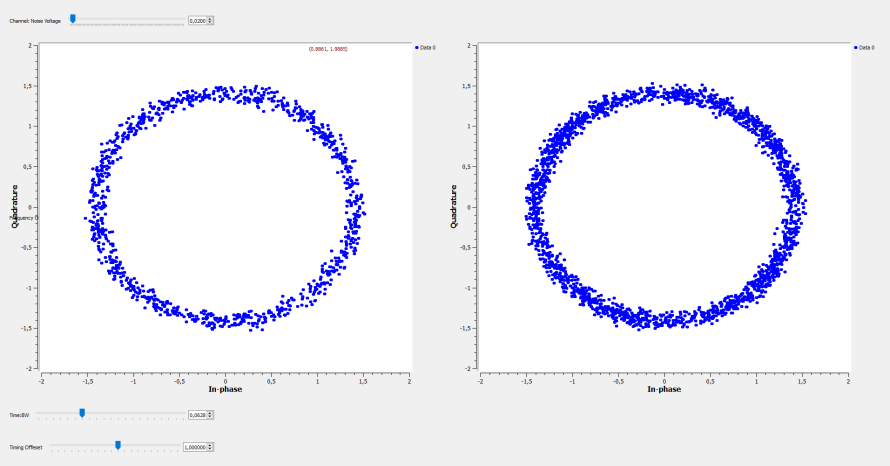

Figure 5.19: Costas loop performance .

Following the equalization process, the symbols are positioned on the unit circle; however, they are subject to rotation owing to the frequency offset. Once processed through the Costas loop block, the constellation is observed to be stable and locked, similar to its original state, except for some added noise. Figure5.20 represent the constellation block.

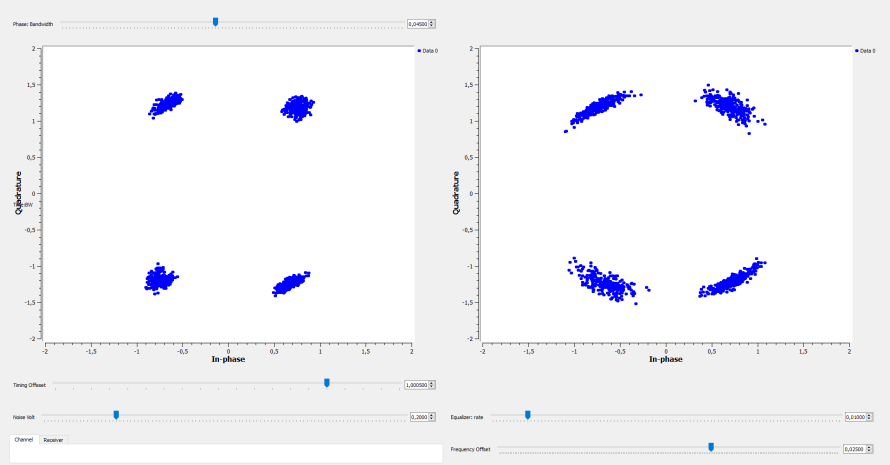

Figure 5.20: constellation plot

- Decoding

The final stage is shown in Figure 5.21. The signal decoding involves placing a Constellation Decoder post-Costas loop, which may cause ambiguity within the constellation.

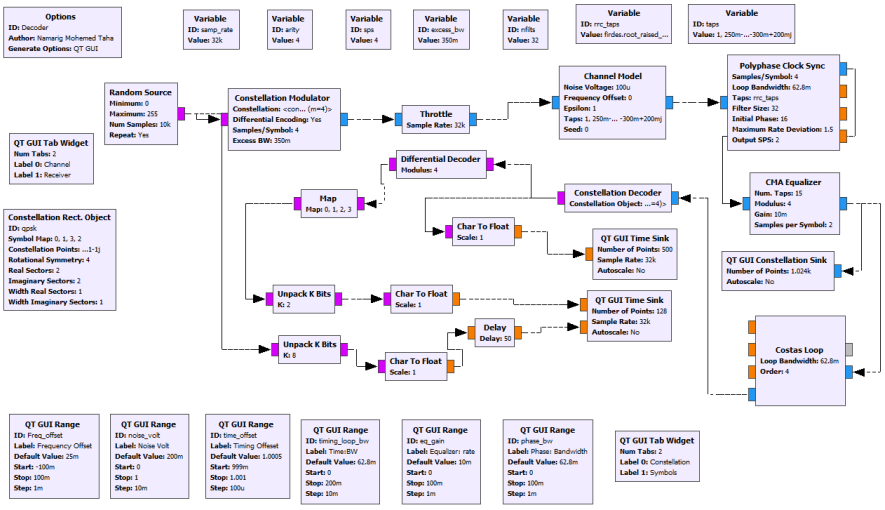

Figure 5.21: Decoding flowgraph .

To address this, differential symbols are transmitted instead of constellation points. A differential decoder converts the differentially coded symbols back to their original state, but post-decoding accuracy isn't guaranteed. Demodulation involves

interpreting symbols based on established mappings. Figure 5.22 represents the constellation plot of QPSK after decoding signal.

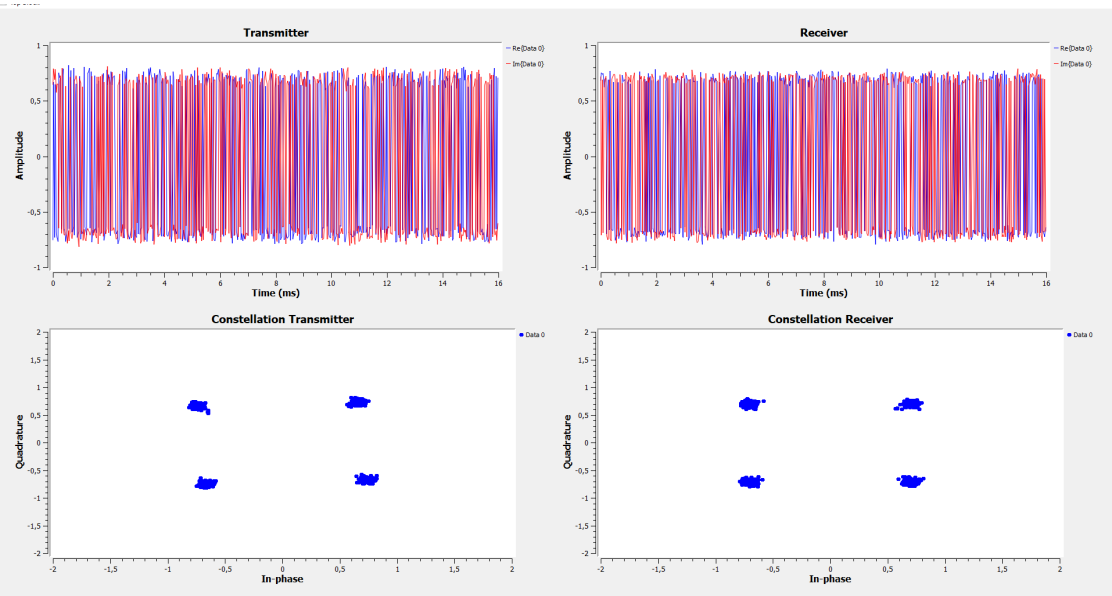

Figure 5.22: conestellation plot .

Figure 5.23 presents the Bit Error Rate (BER) performance of a QPSK modulation scheme for SPO2 data transmission over a range of E_b / N_0 values. The results show a clear inverse relationship between the BER and E_b / N_0; as the E_b / N_0 increases from 6 to 15 dB, the BER correspondingly decreases from approximately 10^{-1} to below 10^{-5}. This indicates a significant improvement in transmission quality with increasing signal-to-noise ratio.

The performance curve demonstrates that the system achieves a lower error rate as the energy per bit relative to the noise power spectral density (Eb/No) is increased, which is characteristic of a well-implemented modulation scheme in a digital communication system. The steep slope of the curve between 6 dB and 10 dB suggests that within this region, even small improvements in Eb/No yield significant gains in reducing the BER. Beyond 10 dB, the improvements continue but at a slower rate, indicating that we are approaching an error floor or other system limitations that are not improved by further increasing the Eb/No. This behavior is typical for digital modulation schemes where, after a certain point, factors other than signal-to-noise ratio begin to dominate error performance. For healthcare applications where data integrity is critical, operating in the region where BER is minimized is

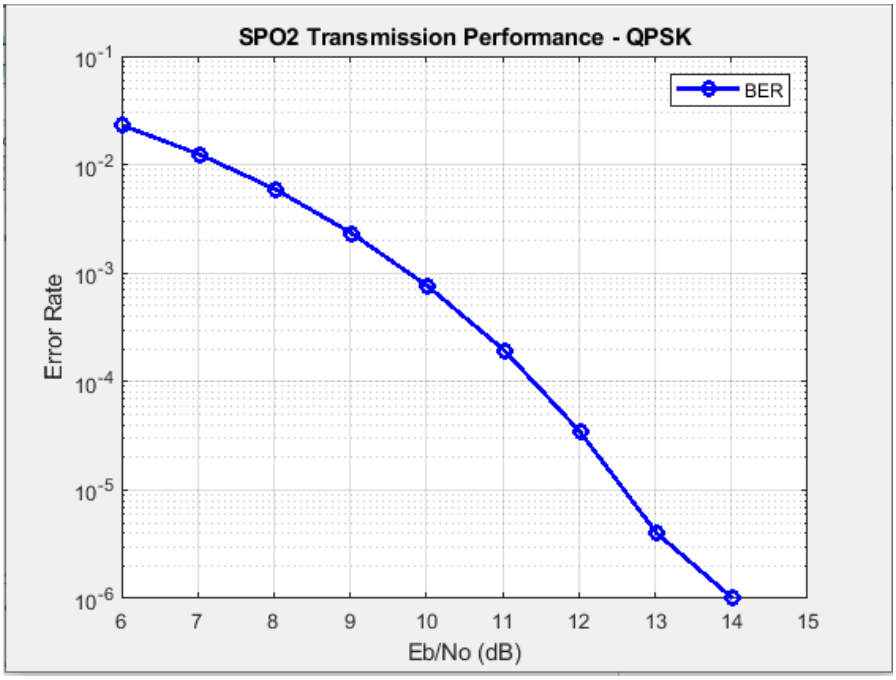

Figure 5.23: BER performance of a QPSK modulation scheme for SPO2 data.

essential, and these results can inform system design for SPO2 data transmission in an IoT healthcare environment

5.6.3 GMSK Transceiver

Gaussian Minimum Shift Keying (GMSK) is a modulation technique that resembles the standard minimum phase shift keying method. The main distinction is that a Gaussian filter shapes the digital data stream before applying it to a frequency modulator. GMSK belongs to the category of continuous-phase frequency-shift keying (FSK), wherein a constant envelope is achieved through phase changes between symbols. In the context of SPO2 data transmission, GMSK modulation was employed to transmit the packetized SPO2. The GNU Radio tool allows for the convenient reconfiguration of data transmission parameters, such as data size, transmission rate, and gain, owing to its flexibility. To implement GMSK using an SDR and GNU Radio, we used the GNU Radio Companion (GRC) to create a flowgraph that includes blocks for the GMSK Modulation and Demodulation. Figure 5.24 shows a flow graph. A "Variable Frequency Oscillator" block was

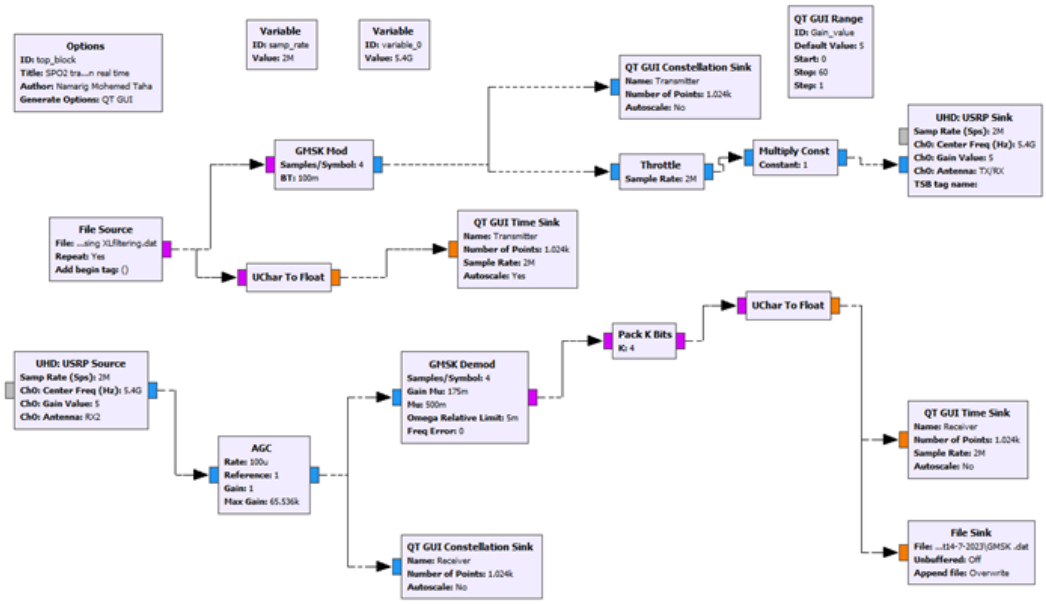

Figure 5.24: GMSK transceiver flow graph.

added and set the frequency to the desired center frequency of the GMSK signal, a "GMSK Modulator" block, and connected the output of the VFO to the input of the modulator, a "USRP Source" block. Moreover, the modulator output is connected to the input of the SDR. A "USRP Sink" block was added on the receiver side, and the frequency and gain were set. Furthermore, a "GMSK Demodulator" block connects the SDR output to the demodulator input. Last, a "Sink" block was added and connected to the demodulator's output.

- **Result and Discussion**

  The GNU Radio and USRP platforms are used to transmit the SPO2 signal in real time by employing GMSK modulation. The first step entails receiving the SPO2 signal from the sensor, then creating packets using MATLAB software. Figure 5.25 provides a visual representation of the transmitted SPO2 signal generated by the GNU Radio. The figure shows the captured SPO2 signal obtained directly from the sensor.

  From Figure 5.26, 5.27, and 5.28 the utilization of the GMSK modulation technique ensures that the only parameter that undergoes change is the phase, while the amplitude remains constant. This is evident in Figure 5.26, where it can be ob-

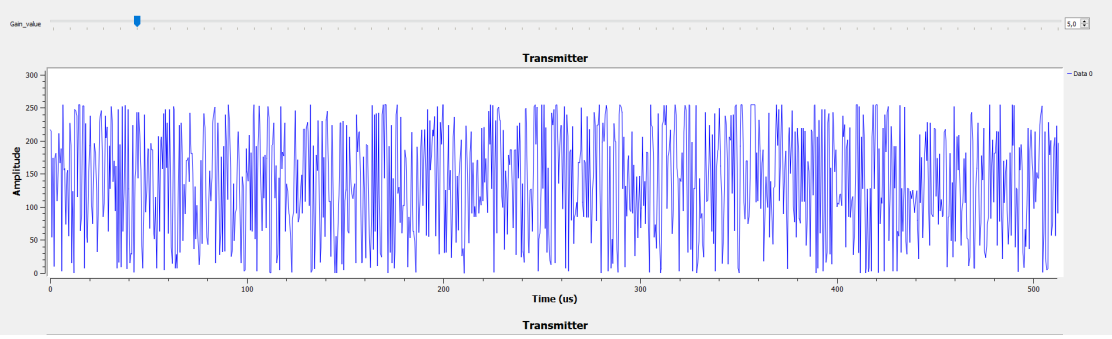

Figure 5.25: Input SPO2 signal from transmitter end.

served that the amplitude remained consistent throughout, the frequency exhibited variation, and there were no interruptions in the phase.

The time-domain representation of the SPO2 signal depicted provides valuable insights into the impact of the GMSK modulation technique on the signal parameters. By employing this modulation technique, the amplitude of the SPO2 signal remains constant while the phase varies. Maintaining a constant amplitude

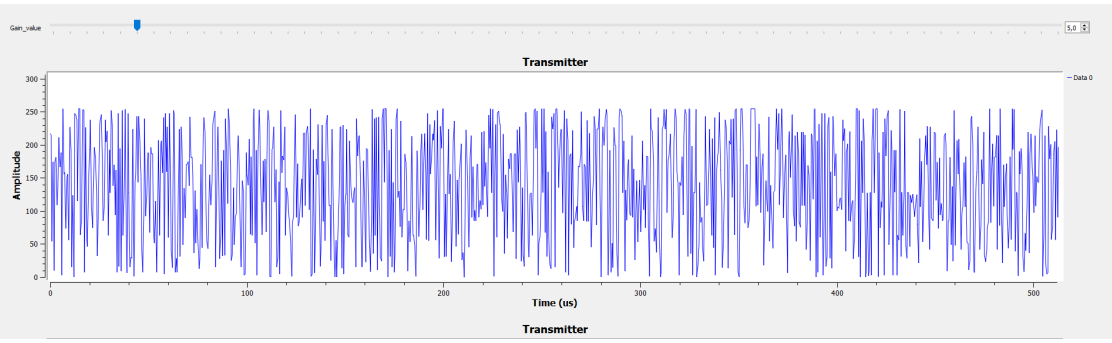

Figure 5.26: Time Display of Transmitted SPO2 signal.

is desirable for signal transmission, as it ensures the integrity of the signal strength throughout the communication process. This consistency in amplitude helps preserve the quality of the SPO2 signal, which is crucial for the accurate monitoring of oxygen saturation levels in medical applications.

On the other hand, the variation in phase indicates changes in the instantaneous frequency of the transmitted signal. This frequency modulation allows for efficient utilization of the available bandwidth and helps mitigate interference from other signals or noise sources. By dynamically adjusting the phase of the sig-

nal, the GMSK modulation technique enables effective signal transmission while minimizing the impact of channel impairments.

The absence of disruptions or interruptions in the phase, as observed in Figure 5.26, further demonstrates the reliability of the GMSK modulation technique. The consistent and smooth phase transitions indicate the robustness of the modulation scheme, ensuring the reliable transmission of the SPO2 signal without any significant distortions. The modulated signal's constellation diagram is displayed in Figure 5.27.

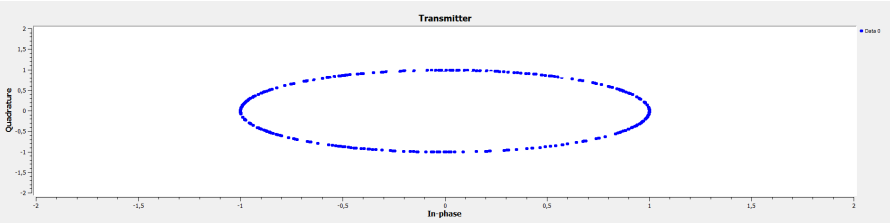

Figure 5.27: Constellation of Modulated SPO2 signal.

The demo of the Spo2 transceiver is illustrated in Figure 5.28. Overall, the analysis of the time-domain representation reinforces the advantages of using the GMSK modulation technique for the transmission of SPO2 signals. This technique maintains a constant amplitude, allows for frequency variation, and ensures the integrity of the phase, resulting in reliable and accurate communication of vital oxygen saturation information in medical applications.

- **Effect of Distance on Time Delay**

  In the implemented system, it has been observed that the distance between the transmitter and receiver antennas impacts both the time delay and the quality of the received SPO2 signal. Table 5.2 provides an overview of the effects of distance on time delay and signal quality.

  Figure 5.29 illustrates the SpO2 transmission performance using three metrics: Bit Error Rate (BER), Packet Error Rate (PER), and Symbol Error Rate (SER). As expected, all error rates decreased with an increase in Eb/No, which indicates that a higher signal-to-noise ratio leads to a more reliable transmission. As expected, all error rates decreased with an increase in Eb/No, which indicates that a higher signal-to-noise ratio leads to a more reliable transmission.

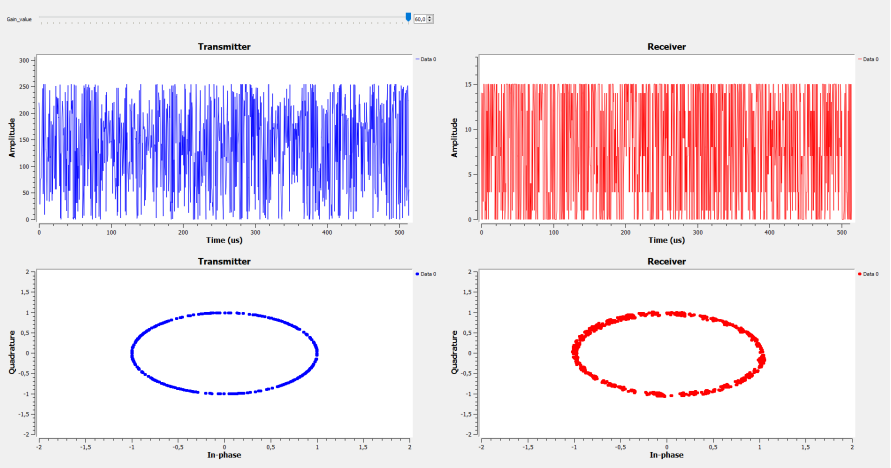

Figure 5.28: SPO2 transceiver.

Table 5.2: Effects of distance on signal quality.

Distance between Tx and Rx	**Time delay**	**Quality of the SPO2 received**
5 cm	3 Sec	Good Quality
15 cm	7 Sec	Moderate distortions
25 cm	9 Sec	High Distortions

- **Discussion**

  The performance of a SpO2 monitoring system is highly dependent on the Eb/No ratio, which is a critical parameter in wireless communication systems. The results show robust system performance, particularly considering the PER and SER metrics.

  – BER Performance: The BER performance indicates that, at lower Eb/No values, the system is susceptible to bit errors. However, the BER decreases significantly with modest increases in Eb/No, showing the system's capacity to correct bit errors effectively.

  – PER Robustness: The PER's consistently low rate suggests that packet-level protocols and error correction mechanisms are highly effective. Even when

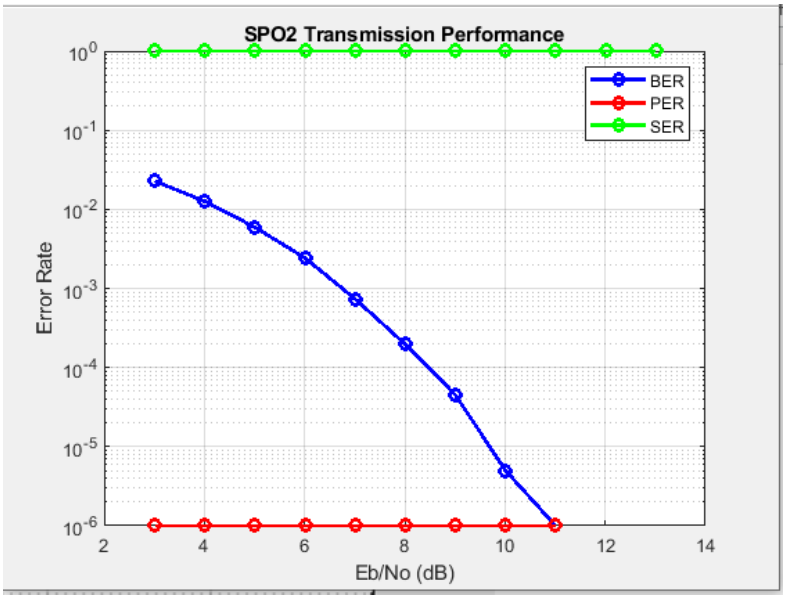

Figure 5.29: SPO2 transmission performance.

individual bits are erroneous, the overall packet integrity is maintained, which is crucial for reliable SpO2 data transmission in e-health applications.

– SER Consistency: Zero-error SER across the board is an outstanding feature of this system. This implies that the chosen symbol structure and error correction at the symbol level are more than adequate even under conditions of relatively low Eb/No.

– Implications for IoT e-health: In the context of IoT e-health, where power efficiency and reliable long-range communication are paramount, the results suggest that the system can operate reliably at lower power levels, thereby extending the battery life of wearable SpO2 sensors.

– Limitations: Although the results are promising, they are based on Eb/No levels that may not encompass extremely challenging communication environments, such as those with high levels of interference or multipath propagation effects. In conclusion, the transmission performance of the SpO2 monitoring system, as presented in the plot, is highly satisfactory, demonstrating the system's capability to provide reliable data transmission under various Eb/No conditions. This indicates a well-designed system that can be effectively deployed in IoT e-health applications with stringent reliability requirements.

Cross-layer design for monitor (SPO2) using commercial device

In this experiment, we implemented a cross-layer design (between the PHY, network, and application layers) for an IoT healthcare system that monitors a patient's vital signs (SPO2) using a commercial device. Figure 5.30 represent the implementation method.

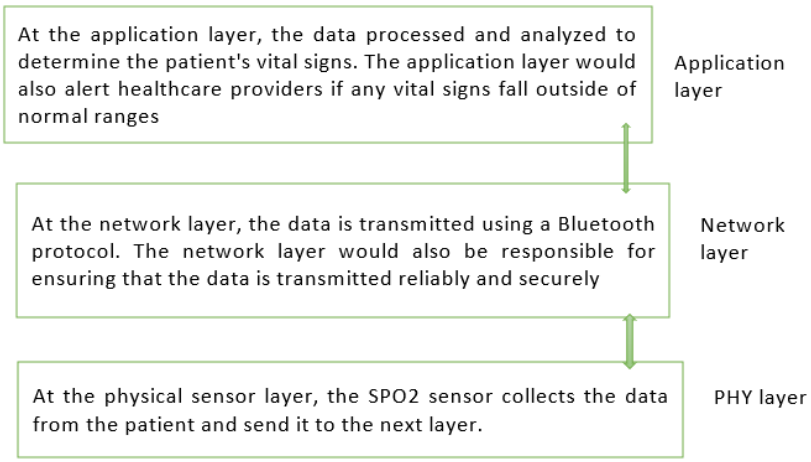

Figure 5.30: SPO2 using Commercial device.

The measurement range for this device ranged from 70% to 100%. The resolution of the measurements was set to 1%. The accuracy was within ± 3% for measurements between 70%and 100% .

The measurement method

The device continuously monitors the pulse rate (PR) and the oxygen saturation of the blood. Vital indicators appear in real-time on the system display, and alarms sound when PR or SpO2 moves outside the preset limits, which are customize to each patient's needs. Figure 5.31 shown the monitoring system using commercial device.

Result and discussion

The results were taken at different frequency ranges because Bluetooth uses frequency hopping technology. The channels are listened to to see which one is better to transmit. This is one of the important advantages of implementing IoT ap-

Figure 5.31: Monitoring system using commercial device.

Table 5.3: Analysis SpO2 Result

SpO2%	Bpm%	Observation
95% or more	40-100	Normal reading
91%-94%	101-109	Mild hypoxemia
86%-90%	110-130	Moderate hypoxemia
85% or less	131 or more	Severe hypoxemia

plications in healthcare. Figure 5.32. The experiment conducted in the laboratory environment, including active WiFi signals, demonstrated a notable peak at 2449.8 MHz within the Bluetooth frequency band, signifying successful SPO2 data transmission. The presence of WiFi introduces observable interference in the signal, as evidenced by the variability in the time-domain signal and spectral spread in the frequency domain. The spectral analysis validates the potential of using the 2449.8 MHz Bluetooth band for transmitting SPO2 data in an IoT e-health context. Despite the clear carrier signal, the interference from the lab's Wi-Fi signals underscores the challenges faced in a typical usage scenario. This interference may affect the SNR and, thus, the integrity of the SPO2 data. Mitigation techniques such as selective channel avoidance, adaptive frequency hopping, and the implementation of robust error correction codes should be considered to enhance transmission reliability in environments with competing wireless technologies.

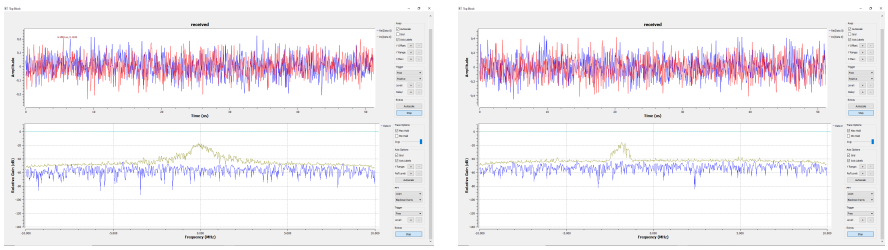

Figure 5.32: The SPO2 using Blutooth Spectrum

The figure 5.33 represents the signal transmit and received using GMSK modulation. As shown in Figure the transmission of SpO2 packets using Gaussian Minimum Shift Keying (GMSK) modulation has been successful, as evidenced by the clarity of the constellation diagram. This clarity indicates a low bit error rate

(BER) and suggests that the GMSK modulation scheme effectively preserved the integrity of the transmitted signal. Precise dot patterning within the constellation reflects a good signal-to-noise ratio and minimal phase distortion, which are critical for accurate and reliable SpO2 data communication in e-health applications.

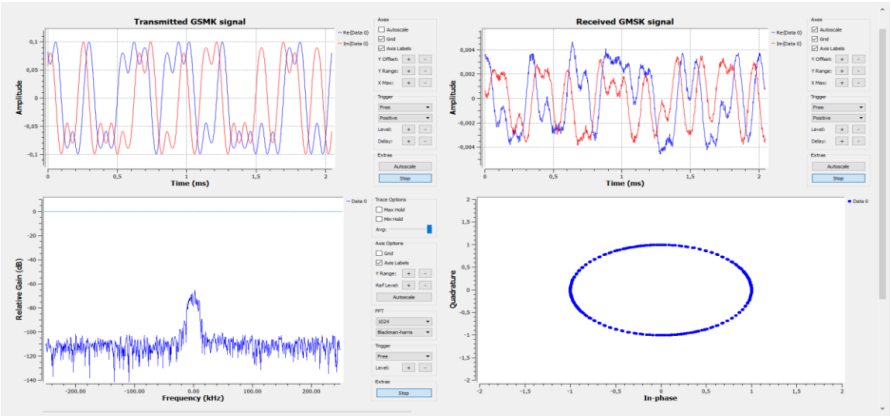

Figure 5.33: The SPO2 commercial device performance.

5.7 CONCLUSION

This chapter describes the implementation of a cross-layer design featuring Adaptive Modulation and Coding (AMC) for IEEE 802.11ah, a critical standard in the Internet of Things (IoT) for healthcare applications. Utilizing the Universal Software Radio Peripheral (USRP) and GNU Radio, an open-source toolkit, this work illustrates practical approaches to modulating and coding techniques, such as Binary Phase-Shift Keying (BPSK), Quadrature Phase-Shift Keying (QPSK), and Gaussian Minimum Shift Keying (GMSK), and conducts a comparative analysis to evaluate their performance in the context of IoT healthcare. Through this analysis, the chapter identifies prevailing challenges and provides future directions for research in this burgeoning field, ultimately contributing to the enhancement of e-health systems by using the IEEE 802.11ah protocol.

6

CONCLUSIONS AND PERSPECTIVES

Contents

6.1 CONCLUSIONS

This research focuses on enhancing IoT applications in healthcare by implementing cross-layer design Adaptive Modulation and Coding (AMC) for IEEE 802.11ah using USRP and GNU Radio. The study encompasses a thorough literature review and practical implementation using USRP and GNU Radio. It specifically addresses the challenges of body-path loss in healthcare scenarios.

The performance of the 802.11ah protocol with body path loss in indoor and outdoor environments was evaluated through theoretical analyses, simulations, and experiments. The analysis primarily examined Packet Error Rate (PER) and throughput. It is observed that the body path loss increases PER and decreases throughput owing to the absorption of electromagnetic signals by the human body.

To mitigate the impact of body path loss, a cross-layer algorithm was proposed. This algorithm detects the received power of the beacon and defers data transmission when body shadowing is likely to occur. The cross-layer method reduces the transmitted data compared with the non-cross-layer method by deferring transmission. Simulation models created using MATLAB demonstrate that the cross-layer method outperforms the non-cross-layer method in terms of PER while maintaining throughput, albeit with a reduction in the average throughput.

Experimental tests were conducted for body path loss scenarios and the attenuation caused by body path loss was also verifiedto validate the research findings. The implementation of 802.11ah PHY/MAC in Software-Defined Radio (SDR) is carried out because there are no off-the-shelf products available. .

To create a comprehensive IoT environment in healthcare, a proof-of-concept is implemented using SDR, sensors, a microcontroller, and an internet-connected server. This setup successfully enabled the observation of sensor data on the internet.

6.2 FUTURE RESEARCH DIRECTIONS

Future research in this field can explore several directions to further advance wireless communication systems for IoT in healthcare.

- Advanced Modulation Techniques
  Investigating more complex modulation schemes and coding techniques to further enhance the data rate and reliability of IoT healthcare devices while maintaining low power consumption.

- Investigating the Effects of Parameters:
  The effects of varying the packet size and transmission power on the performance of 802.11ah should be studied to optimize the system's efficiency and reliability.

- Addressing Hidden Terminal Problems
  The impact of hidden terminal problems, which are common in decentralized systems such as 802.11ah networks, needs to be addressed. Strategies to mitigate interference and improve network efficiency should be investigated.

- Machine Learning in AMC Exploring the use of machine learning algorithms in AMC design to dynamically adjust modulation and coding parameters in real-time, based on changing network conditions and device requirements.

- Integration with 5G and Beyond
  Examining how the IEEE 802.11ah standard and the developed cross-layer design can be integrated with emerging technologies such as 5G and beyond to create more robust, efficient, and scalable IoT networks.

- Energy Harvesting Technologies
  Investigating the integration of energy harvesting technologies with AMC to develop self-sustaining IoT devices is particularly critical in healthcare applications for uninterrupted monitoring.

- Security Enhancements
  Given the sensitivity of healthcare data, future research should also focus on enhancing security protocols within the AMC design to safeguard against data breaches and cyber threats.

- Interdisciplinary Collaboration
  Collaborating with healthcare professionals and industry experts to tailor communication solutions to specific medical needs and to ensure that the developed technologies align well with clinical workflows. By pursuing these future research directions, the field can continue to advance towards more efficient, reliable, and versatile wireless communication systems, supporting the ever-growing needs of the IoT in healthcare and beyond.

BIBLIOGRAPHY

[1] Mohammad Aminul Islam, Kazi Zehad Mostofa, Hamidreza Mohafez, Md Jakir Hossen, Foo Wah Low, Mikhail Vasiliev, Syed Mohammed Shamsul Islam, and Mohammad Nur-E-Alam. "17 Combination of Sensors-Based Monitoring System and Internet of Things (IoT)." In: *Non-Invasive Health Systems based on Advanced Biomedical Signal and Image Processing* (2024), p. 413.

[2] Stephanie B. Baker, Wei Xiang, and Ian Atkinson. "Internet of Things for Smart Healthcare: Technologies, Challenges, and Opportunities." In: *IEEE Access* 5 (2017), 26521–26544. ISSN: 2169-3536. DOI: 10.1109/access.2017.2775180. URL: http://dx.doi.org/10.1109/access.2017.2775180.

[3] Furqan Jameel, Shurjeel Wyne, Dushantha Nalin K. Jayakody, Georges Kaddoum, and Richard O'Kennedy. "Wireless Social Networks: A Survey of Recent Advances, Applications and Challenges." In: *IEEE Access* 6 (2018), 59589–59617. ISSN: 2169-3536. DOI: 10.1109/access.2018.2872686. URL: http://dx.doi.org/10.1109/access.2018.2872686.

[4] Hadda Ben Elhadj, Lamia Chaari, and Lotfi Kamoun. "A Survey of Routing Protocols in Wireless Body Area Networks for Healthcare Applications." In: *International Journal of E-Health and Medical Communications* 3.2 (Apr. 2012), 1–18. ISSN: 1947-3168. DOI: 10.4018/jehmc.2012040101. URL: http://dx.doi.org/10.4018/jehmc.2012040101.

[5] Mohammad Ghamari, Balazs Janko, R. Sherratt, William Harwin, Robert Piechockic, and Cinna Soltanpur. "A Survey on Wireless Body Area Networks for eHealthcare Systems in Residential Environments." In: *Sensors* 16.6 (June 2016), p. 831. ISSN: 1424-8220. DOI: 10.3390/s16060831. URL: http://dx.doi.org/10.3390/s16060831.

[6] Ian F Akyildiz and Mehmet Can Vuran. *Wireless sensor networks*. John Wiley & Sons, 2010.

[7] Lun-De Liao, Yuhling Wang, Yung-Chung Tsao, I-Jan Wang, De-Fu Jhang, Chiung-Cheng Chuang, and Sheng-Fu Chen. "Design and implementation of a multifunction wearable device to monitor sleep physiological signals." In: *Micromachines* 11.7 (2020), p. 672.

[8] Joel JPC Rodrigues, Dante Borges De Rezende Segundo, Heres Arantes Junqueira, Murilo Henrique Sabino, Rafael Maciel Prince, Jalal Al-Muhtadi, and Victor Hugo C De Albuquerque. "Enabling technologies for the internet of health things." In: *Ieee Access* 6 (2018), pp. 13129–13141.

[9] Bassam Al-Shargabi and Simak Abuarqoub. "IoT-Enabled Healthcare: Benefits, Issues and Challenges." In: *Proceedings of the 4th International Conference on Future Networks and Distributed Systems*. 2020, pp. 1–5.

[10] Anjali S Yeole and Dhananjay R Kalbande. "Use of Internet of Things (IoT) in healthcare: A survey." In: *Proceedings of the ACM Symposium on Women in Research 2016*. 2016, pp. 71–76.

[11] Unknown. *Internet of Medical Things in Healthcare*. Unknown. URL: https://www.helpwire.app/blog/internet-of-medical-things-healthcare/.

[12] Anjali S. Yeole and D. R. Kalbande. "Use of Internet of Things (IoT) in Healthcare: A Survey." In: *Proceedings of the ACM Symposium on Women in Research 2016*. WIR '16. ACM, Mar. 2016. DOI: 10.1145/2909067.2909079. URL: http://dx.doi.org/10.1145/2909067.2909079.

[13] Ning Zou, Shaobo Liang, and Daqing He. "Issues and challenges of user and data interaction in healthcare-related IoT: A systematic review." In: *Library Hi Tech* 38.4 (Mar. 2020), 769–782. ISSN: 0737-8831. DOI: 10.1108/lht-09-2019-0177. URL: http://dx.doi.org/10.1108/lht-09-2019-0177.

[14] Erdal Ozbay and Feyza Altunbey Ozbay. "Usage of Cloud Computing and Big data for Internet of Things." In: *International Journal of Computer Science and Mobile Computing* 9.11 (Nov. 2020), 38–48. ISSN: 2320-088X. DOI: 10.47760/ijcsmc.2020.v09i11.004. URL: http://dx.doi.org/10.47760/ijcsmc.2020.v09i11.004.

[15] Burhan Gulbahar. "Network Topology Modulation for Energy and Data Transmission in Internet of Magneto-Inductive Things." In: *2016 IEEE Globecom Workshops (GC Wkshps)*. IEEE, Dec. 2016. DOI: 10.1109/glocomw.2016.7848969. URL: http://dx.doi.org/10.1109/glocomw.2016.7848969.

[16] Ashwini Singh, Ajeet Kumar, and Pankaj Kumar. "Body sensor network: A modern survey & performance study in medical perspect." In: *Network and Complex Systems* 3.1 (2013), pp. 12–17.

[17] Sachi N Shah and Rutvij H Jhaveri. "Recent research on wireless body area networks: a survey." In: *Int. J. Comput. Appl* 975 (2016), pp. 8887–8894.

[18] Sana Ullah, Henry Higgins, Bart Braem, Benoit Latre, Chris Blondia, Ingrid Moerman, Shahnaz Saleem, Ziaur Rahman, and Kyung Sup Kwak.

"A comprehensive survey of wireless body area networks: On PHY, MAC, and network layers solutions." In: *Journal of medical systems* 36 (2012), pp. 1065–1094.

[19] Kyung Sup Kwak, Sana Ullah, and Niamat Ullah. "An overview of IEEE 802.15. 6 standard." In: *2010 3rd international symposium on applied sciences in biomedical and communication technologies (ISABEL 2010)*. IEEE. 2010, pp. 1–6.

[20] Samaneh Movassaghi, Mehran Abolhasan, Justin Lipman, David Smith, and Abbas Jamalipour. "Wireless Body Area Networks: A Survey." In: *IEEE Communications Surveys amp; Tutorials* 16.3 (2014), 1658–1686. ISSN: 1553-877X. DOI: 10.1109/surv.2013.121313.00064. URL: http://dx.doi.org/10.1109/surv.2013.121313.00064.

[21] "IEEE Draft Standard for Local and Metropolitan Area Networks - Specific Requirements - Part 11: Wireless LAN Medium Access Control (MAC) and Physical Layer (PHY) Specifications - Amendment 3: Enhancements for Very High Throughput in the 60 GHz Band." In: *IEEE P802.11ad/D6.0, March 2012 (Draft Amendment based on IEEE P802.11REVmb D12.0)* (2012), pp. 1–696.

[22] "IEEE Standard for Local and metropolitan area networks - Part 15.6: Wireless Body Area Networks." In: *IEEE Std 802.15.6-2012* (2012), pp. 1–271. DOI: 10.1109/IEEESTD.2012.6161600.

[23] Muhammad Sajjad Akbar, Zawar Hussain, Michael Sheng, and Rajan Shankaran. "Wireless body area sensor networks: Survey of mac and routing protocols for patient monitoring under ieee 802.15. 4 and ieee 802.15. 6." In: *Sensors* 22.21 (2022), p. 8279.

[24] Houssein Taleb, Abbass Nasser, Guillaume Andrieux, Nour Charara, and Eduardo Motta Cruz. "Wireless technologies, medical applications and future challenges in WBAN: A survey." In: *Wireless Networks* 27 (2021), pp. 5271–5295.

[25] Adrian Dance. *Bluetooth Low Energy (BLE) And The Internet Of Things*. 2022. URL: https://theiotpad.com/bluetooth-low-energy-and-internet-of-things/.

[26] Heikki Karvonen, Matti Hamalainen, Jari Iinatti, and Carlos Pomalaza-Raez. "Coexistence of wireless technologies in medical scenarios." In: *2017 European Conference on Networks and Communications (EuCNC)*. IEEE, June 2017. DOI: 10.1109/eucnc.2017.7980744. URL: http://dx.doi.org/10.1109/eucnc.2017.7980744.

[27] Peter S Hall and Yang Hao. "Antennas and propagation for body centric communications." In: *2006 First European Conference on Antennas and Propagation*. IEEE. 2006, pp. 1–7.

[28] Lisha Zhong, Shuling He, Jinzhao Lin, Jia Wu, Xi Li, Yu Pang, and Zhangyong Li. "Technological requirements and challenges in wireless body area networks for health monitoring: A comprehensive survey." In: *Sensors* 22.9 (2022), p. 3539.

[29] Aisha Bouani, Yann Ben Maissa, Rachid Saadane, Ahmed Hammouch, and Ahmed Tamtaoui. "A comprehensive survey of medium access control protocols for wireless body area networks." In: *Wireless Communications and Mobile Computing* 2021.1 (2021), p. 5561580.

[30] Yating Qu, Guoqiang Zheng, Huahong Ma, Xintong Wang, Baofeng Ji, and Honghai Wu. "A survey of routing protocols in WBAN for healthcare applications." In: *Sensors* 19.7 (2019), p. 1638.

[31] Anirudh Natarajan, Buddhika de Silva, Kok-Kiong Yap, and Mehul Motani. "Link layer behavior of body area networks at 2.4 GHz." In: *Proceedings of the 15th annual international conference on Mobile computing and networking*. 2009, pp. 241–252.

[32] Arifa Anwar and D Sridharan. "A performance comparison of routing protocols designed for body area networks." In: *2017 International Conference on Nextgen Electronic Technologies: Silicon to Software (ICNETS2)*. IEEE. 2017, pp. 108–111.

[33] Jyoti Anand and Deepak Sethi. "Comparative analysis of energy efficient routing in WBAN." In: *2017 3rd International Conference on Computational Intelligence & Communication Technology (CICT)*. IEEE. 2017, pp. 1–6.

[34] Samaneh Movassaghi, Mehran Abolhasan, Justin Lipman, David Smith, and Abbas Jamalipour. "Wireless body area networks: A survey." In: *IEEE Communications surveys & tutorials* 16.3 (2014), pp. 1658–1686.

[35] Reema Goyal, R. B. Patel, H. S. Bhaduria, and Devendra Prasad. "An Efficient Data Delivery Scheme in WBAN to Deal with Shadow Effect due to Postural Mobility." In: *Wireless Personal Communications* 117.1 (Dec. 2019), 129–149. ISSN: 1572-834X. DOI: 10.1007/s11277-019-06997-5. URL: http://dx.doi.org/10.1007/s11277-019-06997-5.

[36] Muhannad Quwaider and Subir Biswas. "DTN routing in body sensor networks with dynamic postural partitioning." In: *Ad Hoc Networks* 8.8 (Nov. 2010), 824–841. ISSN: 1570-8705. DOI: 10.1016/j.adhoc.2010.03.002. URL: http://dx.doi.org/10.1016/j.adhoc.2010.03.002.

[37] Arash Maskooki, Cheong Boon Soh, Erry Gunawan, and Kay Soon Low. "Opportunistic routing for body area network." In: *2011 IEEE Consumer*

Communications and Networking Conference (CCNC). IEEE, Jan. 2011. DOI: 10.1109/ccnc.2011.5766463. URL: http://dx.doi.org/10.1109/ccnc.2011.5766463.

[38] Xiaohui Liang, Xu Li, Qinghua Shen, Rongxing Lu, Xiaodong Lin, Xuemin Shen, and Weihua Zhuang. "Exploiting prediction to enable Secure and Reliable routing in Wireless Body Area Networks." In: *2012 Proceedings IEEE INFOCOM*. IEEE, Mar. 2012. DOI: 10.1109/infcom.2012.6195777. URL: http://dx.doi.org/10.1109/infcom.2012.6195777.

[39] Koushik Karmakar, Suparna Biswas, and Sarmistha Neogy. "MHRP: A novel mobility handling routing protocol in Wireless Body Area Network." In: *2017 International Conference on Wireless Communications, Signal Processing and Networking (WiSPNET)*. IEEE, Mar. 2017. DOI: 10.1109/wispnet.2017.8300099. URL: http://dx.doi.org/10.1109/wispnet.2017.8300099.

[40] Qinghui Tang, Naveen Tummala, Sandeep K. S. Gupta, and Loren Schwiebert. "TARA: Thermal-Aware Routing Algorithm for Implanted Sensor Networks." In: *Lecture Notes in Computer Science*. Springer Berlin Heidelberg, 2005, 206–217. ISBN: 9783540316718. DOI: 10.1007/11502593_17. URL: http://dx.doi.org/10.1007/11502593_17.

[41] Hadda Ben Elhadj, Lamia Chaari, and Lotfi Kamoun. "A survey of routing protocols in wireless body area networks for healthcare applications." In: *International Journal of E-Health and Medical Communications (IJEHMC)* 3.2 (2012), pp. 1–18.

[42] Wei Jiang, Zichun Wang, Meng Feng, and Tiantian Miao. "A survey of thermal-aware routing protocols in wireless body area networks." In: *2017 IEEE International Conference on Computational Science and En-*

gineering (CSE) and IEEE International Conference on Embedded and Ubiquitous Computing (EUC). Vol. 2. IEEE. 2017, pp. 17–21.

[43] Anirban Bag and Mostafa Bassiouni. "Energy Efficient Thermal Aware Routing Algorithms for Embedded Biomedical Sensor Networks." In: *2006 IEEE International Conference on Mobile Ad Hoc and Sensor Sysetems*. IEEE, Oct. 2006. DOI: 10.1109/mobhoc.2006.278619. URL: http://dx.doi.org/10.1109/mobhoc.2006.278619.

[44] Zahoor A. Khan, Shyamala Sivakumar, William Phillips, and Bill Robertson. "A QoS-aware Routing Protocol for Reliability Sensitive Data in Hospital Body Area Networks." In: *Procedia Computer Science* 19 (2013), 171–179. ISSN: 1877-0509. DOI: 10.1016/j.procs.2013.06.027. URL: http://dx.doi.org/10.1016/j.procs.2013.06.027.

[45] N. Javaid, Z. Abbas, M.S. Fareed, Z.A. Khan, and N. Alrajeh. "M-ATTEMPT: A New Energy-Efficient Routing Protocol for Wireless Body Area Sensor Networks." In: *Procedia Computer Science* 19 (2013), 224–231. ISSN: 1877-0509. DOI: 10.1016/j.procs.2013.06.033. URL: http://dx.doi.org/10.1016/j.procs.2013.06.033.

[46] Melody Moh, Benjamin Jack Culpepper, Lan Dung, Teng-Sheng Moh, Takeo Hamada, and Ching-Fong Su. "On data gathering protocols for in-body biomedical sensor networks." In: *GLOBECOM'05. IEEE Global Telecommunications Conference, 2005.* Vol. 5. IEEE. 2005, 6–pp.

[47] Benjamin J. Culpepper, Lan Dung, and Melody Moh. "Design and analysis of Hybrid Indirect Transmissions (HIT) for data gathering in wireless micro sensor networks." In: *ACM SIGMOBILE Mobile Computing and Communications Review* 8.1 (Jan. 2004), 61–83. ISSN: 1931-1222. DOI:

10.1145/980159.980169. URL: http://dx.doi.org/10.1145/980159.980169.

[48] Xuedong Liang and Ilangko Balasingham. "A QoS-aware Routing Service Framework for Biomedical Sensor Networks." In: *2007 4th International Symposium on Wireless Communication Systems*. IEEE, Oct. 2007. DOI: 10.1109/iswcs.2007.4392358. URL: http://dx.doi.org/10.1109/iswcs.2007.4392358.

[49] Deepak Sethi and Partha Pratim Bhattacharya. "A study on energy efficient and reliable data transfer (eerdt) protocol for wban." In: *2016 Second International Conference on Computational Intelligence & Communication Technology (CICT)*. IEEE. 2016, pp. 254–258.

[50] Djamel Djenouri and Ilangko Balasingham. "New QoS and Geographical Routing in Wireless Biomedical Sensor Networks." In: *Proceedings of the 6th International ICST Conference on Broadband Communications, Networks, and Systems*. BROADNETS. IEEE, 2009. DOI: 10.4108/icst.broadnets2009.7188. URL: http://dx.doi.org/10.4108/icst.broadnets2009.7188.

[51] Zahoor Khan, Nauman Aslam, Shyamala Sivakumar, and William Phillips. "Energy-aware Peering Routing Protocol for indoor hospital Body Area Network Communication." In: *Procedia Computer Science* 10 (2012), 188–196. ISSN: 1877-0509. DOI: 10.1016/j.procs.2012.06.027. URL: http://dx.doi.org/10.1016/j.procs.2012.06.027.

[52] Naveed Ahmad, Mohammad Daud Awan, Malik Sikander Hayat Khiyal, Muhammad Imran Babar, Abdelzahir Abdelmaboud, Hamza Awad Ibrahim, and Nadir O Hamed. "Improved QoS aware routing protocol (IM-QRP) for

WBAN based healthcare monitoring system." In: *IEEE Access* 10 (2022), pp. 121864–121885.

[53] Sultana Parween and Syed Zeeshan Hussain. "A Review on Cross-Layer Design Approach in WSN by Different Techniques." In: *Advances in Science, Technology and Engineering Systems Journal* 5.4 (2020), 741–754. ISSN: 2415-6698. DOI: 10.25046/aj050488. URL: http://dx.doi.org/10.25046/aj050488.

[54] Bo Fu, Yang Xiao, Hongmei Deng, and Hui Zeng. "A Survey of Cross-Layer Designs in Wireless Networks." In: *IEEE Communications Surveys amp; Tutorials* 16.1 (2014), 110–126. ISSN: 2373-745X. DOI: 10.1109/surv.2013.081313.00231. URL: http://dx.doi.org/10.1109/surv.2013.081313.00231.

[55] Wu Yaqin and Xiong Xiaoliang. "Sensor Deployment Distribution Effect on Intrusion Distance in Wireless Sensor Networks." In: *2011 Second International Conference on Innovations in Bio-inspired Computing and Applications*. IEEE, Dec. 2011. DOI: 10.1109/ibica.2011.30. URL: http://dx.doi.org/10.1109/ibica.2011.30.

[56] A. G. Ruzzelli, R. Jurdak, G. M.P O'Hare, and P. Van Der Stok. "Energy-efficient multi-hop medical sensor networking." In: *Proceedings of the 1st ACM SIGMOBILE international workshop on Systems and networking support for healthcare and assisted living environments*. Mobisys07. ACM, June 2007. DOI: 10.1145/1248054.1248064. URL: http://dx.doi.org/10.1145/1248054.1248064.

[57] Mung Chiang, Steven H. Low, A. Robert Calderbank, and John C. Doyle. "Layering as Optimization Decomposition: A Mathematical Theory of Network Architectures." In: *Proceedings of the IEEE* 95.1 (Jan. 2007),

255–312. ISSN: 0018-9219. DOI: 10.1109/jproc.2006.887322. URL: http://dx.doi.org/10.1109/jproc.2006.887322.

[58] Ian F. Akyildiz and Mehmet Can Vuran. *Wireless Sensor Networks*. Wiley, June 2010. ISBN: 9780470515181. DOI: 10.1002/9780470515181. URL: http://dx.doi.org/10.1002/9780470515181.

[59] Vineet Srivastava and Mehul Motani. *Cross-Layer Design and Optimization in Wireless Networks*. July 2007. DOI: 10.1002/9780470515143.ch6. URL: http://dx.doi.org/10.1002/9780470515143.ch6.

[60] Vijay T Raisinghani and Sridhar Iyer. "Cross-layer design optimizations in wireless protocol stacks." In: *Computer Communications* 27.8 (May 2004), 720–724. ISSN: 0140-3664. DOI: 10.1016/j.comcom.2003.10.011. URL: http://dx.doi.org/10.1016/j.comcom.2003.10.011.

[61] Robert Braden, Ted Faber, and Mark Handley. "From protocol stack to protocol heap: role-based architecture." In: *ACM SIGCOMM Computer Communication Review* 33.1 (Jan. 2003), 17–22. ISSN: 0146-4833. DOI: 10.1145/774763.774765. URL: http://dx.doi.org/10.1145/774763.774765.

[62] Sultana Parween, Syed Zeeshan Hussain, and Md Asdaque Hussain. "A Survey on Issues and Possible Solutions of Cross-Layer Design in Internet of Things." In: *International Journal of Computer Networks and Applications* 8.4 (Aug. 2021), p. 311. ISSN: 2395-0455. DOI: 10.22247/ijcna/2021/209699. URL: http://dx.doi.org/10.22247/ijcna/2021/209699.

[63] Davi Resner, Gustavo Medeiros de Araujo, and Antônio Augusto Fröhlich. "Design and implementation of a cross-layer IoT protocol." In: *Science of Computer Programming* 165 (Nov. 2018), 24–37. ISSN: 0167-6423. DOI:

10.1016/j.scico.2017.08.008. URL: http://dx.doi.org/10.1016/j.scico.2017.08.008.

[64] Hadda Ben Elhadj, Jocelyne Elias, Lamia Chaari, and Lotfi Kamoun. "A Priority based Cross Layer Routing Protocol for healthcare applications." In: *Ad Hoc Networks* 42 (May 2016), 1–18. ISSN: 1570-8705. DOI: 10.1016/j.adhoc.2015.10.007. URL: http://dx.doi.org/10.1016/j.adhoc.2015.10.007.

[65] Muhannad Quwaider and Subir Biswas. "On-body Packet Routing Algorithms for Body Sensor Networks." In: *2009 First International Conference on Networks amp; Communications*. IEEE, 2009. DOI: 10.1109/netcom.2009.54. URL: http://dx.doi.org/10.1109/netcom.2009.54.

[66] Olatinwo, Abu-Mahfouz, and Hancke. "A Survey on LPWAN Technologies in WBAN for Remote Health-Care Monitoring." In: *Sensors* 19.23 (Nov. 2019), p. 5268. ISSN: 1424-8220. DOI: 10.3390/s19235268. URL: http://dx.doi.org/10.3390/s19235268.

[67] Y.Z. Luan, G.L. Ren, and P.R. Zhang. "E-Health Cross Layer Design." In: *Proceedings of the 2015 International Conference on Artificial Intelligence and Industrial Engineering*. aiie-15. Atlantis Press, 2015. DOI: 10.2991/aiie-15.2015.71. URL: http://dx.doi.org/10.2991/aiie-15.2015.71.

[68] Ouchker Elmekki, Abderrahim Maizate, and Mohammed Ouzzif. "The Effects of Physical and Mac Parameters on the Routing by Cross-Layers Interaction Approach." In: *International Journal of Web-Based Learning and Teaching Technologies* 16.2 (Mar. 2021), 1–11. ISSN: 1548-1107. DOI:

10.4018/ijwltt.2021030101. URL: http://dx.doi.org/10.4018/ijwltt.2021030101.

[69] Abdellah Chehri. "Energy-efficient modified DCC-MAC protocol for IoT in e-health applications." In: *Internet of Things* 14 (June 2021), p. 100119. ISSN: 2542-6605. DOI: 10.1016/j.iot.2019.100119. URL: http://dx.doi.org/10.1016/j.iot.2019.100119.

[70] Hanumat Prasad and Suresh Babu. "A Survey on Network Routing Protocols in Internet of Things (IOT)." In: *International Journal of Computer Applications* 160.2 (Feb. 2017), 18–22. ISSN: 0975-8887. DOI: 10.5120/ijca2017912973. URL: http://dx.doi.org/10.5120/ijca2017912973.

[71] Farman Ullah, M. Zahid Khan, Gulzar Mehmood, Muhammad Shuaib Qureshi, and Muhammad Fayaz. "Energy Efficiency and Reliability Considerations in Wireless Body Area Networks: A Survey." In: *Computational and Mathematical Methods in Medicine* 2022 (Jan. 2022). Ed. by Shakeel Ahmad, 1–15. ISSN: 1748-670X. DOI: 10.1155/2022/1090131. URL: http://dx.doi.org/10.1155/2022/1090131.

[72] Moufida Maimour, Houda Zeghilet, and Francis Lepage. "Cluster-based Routing Protocols for Energy-Efficiency in Wireless Sensor Networks." In: *Sustainable Wireless Sensor Networks*. InTech, Dec. 2010. DOI: 10.5772/13274. URL: http://dx.doi.org/10.5772/13274.

[73] Boangoat Jarupan and Eylem Ekici. "A survey of cross-layer design for VANETs." In: *Ad Hoc Networks* 9.5 (July 2011), 966–983. ISSN: 1570-8705. DOI: 10.1016/j.adhoc.2010.11.007. URL: http://dx.doi.org/10.1016/j.adhoc.2010.11.007.

[74] Yufeng Chen, Zhengtao Xiang, Wei Jian, and Weirong Jiang. "A Cross-Layer AOMDV Routing Protocol for V2V Communication in Urban

VANET." In: *2009 Fifth International Conference on Mobile Ad-hoc and Sensor Networks*. IEEE, 2009. DOI: 10.1109/msn.2009.30. URL: http://dx.doi.org/10.1109/msn.2009.30.

[75] Jyoti Anand and Deepak Sethi. "Comparative analysis of energy efficient routing in WBAN." In: *2017 3rd International Conference on Computational Intelligence amp; Communication Technology (CICT)*. IEEE, Feb. 2017. DOI: 10.1109/ciact.2017.7977373. URL: http://dx.doi.org/10.1109/ciact.2017.7977373.

[76] Bart Braem, Benoit Latre, Ingrid Moerman, Chris Blondia, and Piet Demeester. "The Wireless Autonomous Spanning tree Protocol for Multihop Wireless Body Area Networks." In: *2006 Third Annual International Conference on Mobile and Ubiquitous Systems: Networking amp; Services*. IEEE, July 2006. DOI: 10.1109/mobiq.2006.340421. URL: http://dx.doi.org/10.1109/mobiq.2006.340421.

[77] Benoit Latre, Bart Braem, Ingrid Moerman, Chris Blondia, Elisabeth Reusens, Wout Joseph, and Piet Demeester. "A Low-delay Protocol for Multihop Wireless Body Area Networks." In: *2007 Fourth Annual International Conference on Mobile and Ubiquitous Systems: Networking Services (MobiQuitous)*. 2007, pp. 1–8. DOI: 10.1109/MOBIQ.2007.4451060.

[78] A.G. Ruzzelli, G.M.P O'Hare, M.J. O'Grady, and R. Tynan. "MERLIN: A Synergetic Integration of MAC and Routing Protocol for Distributed Sensor Networks." In: *2006 3rd Annual IEEE Communications Society on Sensor and Ad Hoc Communications and Networks*. IEEE, 2006. DOI: 10.1109/sahcn.2006.288431. URL: http://dx.doi.org/10.1109/sahcn.2006.288431.

[79] Anirban Bag and Mostafa A. Bassiouni. "Biocomm – a cross-layer medium access control (MAC) and routing protocol co-design for biomedical sensor networks." In: *International Journal of Parallel, Emergent and Distributed Systems* 24.1 (Feb. 2009), 85–103. ISSN: 1744-5779. DOI: 10.1080/17445760802335345. URL: http://dx.doi.org/10.1080/17445760802335345.

[80] Anirban Bag and Mostafa A Bassiouni. "Biocomm–A cross-layer medium access control (MAC) and routing protocol co-design for biomedical sensor networks." In: *International Journal of Parallel, Emergent and Distributed Systems* 24.1 (2009), pp. 85–103.

[81] Omar Ahmed, Min Hu, and Fuji Ren. "PEDTARA: Priority-Based Energy Efficient, Delay and Temperature Aware Routing Algorithm Using Multi-Objective Genetic Chaotic Spider Monkey Optimization for Critical Data Transmission in WBANs." In: *Electronics* 11.1 (Dec. 2021), p. 68. ISSN: 2079-9292. DOI: 10.3390/electronics11010068. URL: http://dx.doi.org/10.3390/electronics11010068.

[82] Annwesha Banerjee Majumder and Somsubhra Gupta. "An Energy-Efficient Congestion Avoidance Priority-Based Routing Algorithm for Body Area Network." In: *Industry Interactive Innovations in Science, Engineering and Technology*. Springer Singapore, July 2017, 545–552. ISBN: 9789811039539. DOI: 10.1007/978-981-10-3953-9_52. URL: http://dx.doi.org/10.1007/978-981-10-3953-9_52.

[83] Hadda Ben Elhadj, Jocelyne Elias, Lamia Chaari, and Lotfi Kamoun. "A priority based cross layer routing protocol for healthcare applications." In: *Ad Hoc Networks* 42 (2016), pp. 1–18.

[84] Xi Chen, Yixuan Xu, and Anfeng Liu. "Cross Layer Design for Optimizing Transmission Reliability, Energy Efficiency, and Lifetime in Body Sensor Networks." In: *Sensors* 17.4 (Apr. 2017), p. 900. ISSN: 1424-8220. DOI: 10.3390/s17040900. URL: http://dx.doi.org/10.3390/s17040900.

[85] Umer Fiaz Abbasi, Azlan Awang, and Nor Hisham Hamid. "Performance investigation of using direct transmission and opportunistic routing in wireless body area networks." In: *2013 IEEE Symposium on Computers amp; Informatics (ISCI)*. IEEE, Apr. 2013. DOI: 10.1109/isci.2013.6612376. URL: http://dx.doi.org/10.1109/isci.2013.6612376.

[86] Hongyun Zhang, Farzad Safaei, and Le Tran. "Joint Transmission Power Control and Relay Cooperation for WBAN Systems." In: *Sensors* 18.12 (Dec. 2018), p. 4283. ISSN: 1424-8220. DOI: 10.3390/s18124283. URL: http://dx.doi.org/10.3390/s18124283.

[87] Nedal Ababneh, Nicholas Timmons, and Jim Morrison. "Cross-layer optimization protocol for guaranteed data streaming over Wireless Body Area Networks." In: *2012 8th International Wireless Communications and Mobile Computing Conference (IWCMC)*. IEEE, Aug. 2012. DOI: 10.1109/iwcmc.2012.6314188. URL: http://dx.doi.org/10.1109/iwcmc.2012.6314188.

[88] GD Wang and KQ Guo. "A Cross-Layer Retransmission Strategy for the Body Shadowing Affect in IEEE 802.15. 6-Based WBAN." In: *Softw. Guide* 17 (2018), pp. 200–202.

[89] Wafa Badreddine, Nesrine Khernane, Maria Potop-Butucaru, and Claude Chaudet. "Convergecast in Wireless Body Area Networks." In: *Ad Hoc Networks* 66 (Nov. 2017), 40–51. ISSN: 1570-8705. DOI: 10.1016/j.

adhoc.2017.08.008. URL: http://dx.doi.org/10.1016/j.adhoc.2017.08.008.

[90] Benoît Latré, Bart Braem, Ingrid Moerman, Chris Blondia, and Piet Demeester. "A survey on wireless body area networks." In: *Wireless Networks* 17.1 (Nov. 2010), 1–18. ISSN: 1572-8196. DOI: 10.1007/s11276-010-0252-4. URL: http://dx.doi.org/10.1007/s11276-010-0252-4.

[91] Bart Braem, Benoit Latre, Ingrid Moerman, Chris Blondia, and Piet Demeester. "The wireless autonomous spanning tree protocol for multihop wireless body area networks." In: *2006 Third Annual International Conference on Mobile and Ubiquitous Systems: Networking & Services*. IEEE. 2006, pp. 1–8.

[92] Xi Chen, Yixuan Xu, and Anfeng Liu. "Cross layer design for optimizing transmission reliability, energy efficiency, and lifetime in body sensor networks." In: *Sensors* 17.4 (2017), p. 900.

[93] Javed Bangash, Abdul Abdullah, Mohammad Anisi, and Abdul Khan. "A Survey of Routing Protocols in Wireless Body Sensor Networks." In: *Sensors* 14.1 (Jan. 2014), 1322–1357. ISSN: 1424-8220. DOI: 10.3390/s140101322. URL: http://dx.doi.org/10.3390/s140101322.

[94] Arpan Pal, Hemant Kumar Rath, Samar Shailendra, and Abhijan Bhattacharyya. "IoT standardization: The road ahead." In: *Internet of Things-Technology, Applications and Standardization* (2018), pp. 53–74.

[95] Mohammed Aljubayri, Zhaohui Yang, and Mohammad Shikh-Bahaei. "Cross-layer multipath congestion control, routing and scheduling design in ad hoc wireless networks." In: *IET Communications* 15.8 (Mar. 2021), 1096–1108. ISSN: 1751-8636. DOI: 10.1049/cmu2.12145. URL: http://dx.doi.org/10.1049/cmu2.12145.

[96] P Sarwesh, N Shekar V Shet, and K Chandrasekaran. "Reliable Cross Layer Design for E-Health Applications—IoT Perspective." In: *Cognitive Computing for Big Data Systems Over IoT: Frameworks, Tools and Applications* (2018), pp. 97–113.

[97] D. P. Tobon, T. H. Falk, and M. Maier. "Context awareness in WBANs: a survey on medical and non-medical applications." In: *IEEE Wireless Communications* 20.4 (Aug. 2013), 30–37. ISSN: 1536-1284. DOI: 10.1109/mwc.2013.6590048. URL: http://dx.doi.org/10.1109/mwc.2013.6590048.

[98] Deying Yuan, Guoqiang Zheng, Huahong Ma, Jiaqing Shang, Jishun Li, et al. "An adaptive MAC protocol based on IEEE802. 15.6 for wireless body area networks." In: *Wireless Communications and Mobile Computing* 2019 (2019).

[99] Douma Ferdawss and Rafik Braham. "An Adaptive MAC Protocol for Wireless Body Area Networks." In: *International Conference on Intelligent Systems Design and Applications*. Springer. 2020, pp. 764–773.

[100] Benoit Latre, Bart Braem, Ingrid Moerman, Chris Blondia, Elisabeth Reusens, Wout Joseph, and Piet Demeester. "A Low-delay Protocol for Multihop Wireless Body Area Networks." In: *2007 Fourth Annual International Conference on Mobile and Ubiquitous Systems: Networking amp; Services (MobiQuitous)*. IEEE, 2007. DOI: 10.1109/mobiq.2007.4451060. URL: http://dx.doi.org/10.1109/mobiq.2007.4451060.

[101] In: *Regular Issue* 8.12 (Oct. 2019), 5414–5420. ISSN: 2278-3075. DOI: 10.35940/ijitee.l3790.1081219. URL: http://dx.doi.org/10.35940/ijitee.l3790.1081219.

[102] L. Tian, S. Santi, A. Seferagić, J. Lan, and J. Famaey. "Wi-Fi HaLow for the Internet of Things: An up-to-date survey on IEEE 802.11 ah research." In: *Journal of Network and Computer Applications* 182 (2021), p. 103036.

[103] IEEE Computer Society LAN/MAN Standards Committee et al. "IEEE Standard for Information technology-Telecommunications and information exchange between systems-Local and metropolitan area networks-Specific requirements Part 11: Wireless LAN Medium Access Control (MAC) and Physical Layer (PHY) Specifications." In: *IEEE Std 802.11^* (2007).

[104] Muhammad Qutab-ud din. "Enhancements And Challenges In Ieee 802.11 ah-A Sub-Gigahertz Wi-Fi For Iot Applications." MA thesis. 2015.

[105] Minyoung Park. "IEEE 802.11 ah: sub-1-GHz license-exempt operation for the internet of things." In: *IEEE Communications Magazine* 53.9 (2015), pp. 145–151.

[106] Weiping Sun, Munhwan Choi, Sunghyun Choi, et al. "IEEE 802.11 ah: a long range 802.11 wlan at sub 1 GHz." In: *J. ICT Stand.* 1.1 (2013), pp. 83–108.

[107] R D Vegt. "Potential compromise for 802.11 ah use case document." In: *IEEE 802.11-11/0457r0* (2011).

[108] Stefan Aust, R Venkatesha Prasad, and Ignas GMM Niemegeers. "IEEE 802.11 ah: Advantages in standards and further challenges for sub 1 GHz Wi-Fi." In: *2012 IEEE international conference on communications (ICC)*. IEEE. 2012, pp. 6885–6889.

[109] Sobia Arshad, Muhammad Awais Azam, Mubashir Husain Rehmani, and Jonathan Loo. "Recent advances in information-centric networking-based

Internet of Things (ICN-IoT).” In: *IEEE Internet of Things Journal* 6.2 (2018), pp. 2128–2158.

[110] Toni Adame, Albert Bel, Boris Bellalta, Jaume Barcelo, and Miquel Oliver. “IEEE 802.11 AH: the WiFi approach for M2M communications.” In: *IEEE Wireless Communications* 21.6 (2014), pp. 144–152.

[111] Minyoung Park. “Specification framework for TGah.” In: *IEEE802* (2013), pp. 11–11.

[112] Raja Karmakar, Sandip Chakraborty, and Samiran Chattopadhyay. “Impact of IEEE 802.11 n/ac PHY/MAC high throughput enhancements over transport/application layer protocols-a survey.” In: *arXiv preprint arXiv:1702.03257* (2017).

[113] Minho Cheong. “TGah functional requirements and evaluation methodology.” In: *IEEE 802.11-11/0905r5* (2012).

[114] Muhammad Shafiq, Maqbool Ahmad, Azeem Irshad, Moneeb Gohar, Muhammad Usman, Muhammad Khalil Afzal, Jin-Ghoo Choi, and Heejung Yu. “Multiple access control for cognitive radio-based IEEE 802.11 ah networks.” In: *Sensors* 18.7 (2018), p. 2043.

[115] Qinghua Chen, Zhengqiu Weng, Guolang Chen, et al. “A target wake time scheduling scheme for uplink multiuser transmission in IEEE 802.11 ax-based next generation WLANs.” In: *IEEE Access* 7 (2019), pp. 158207–158222.

[116] Víctor Hugo Baños González. “Contributions to IEEE 802.11-based long range communications.” In: (2020).

[117] Le Tian, Amina Šljivo, Serena Santi, Eli De Poorter, Jeroen Hoebeke, and Jeroen Famaey. “Extension of the IEEE 802.11 ah ns-3 Simulation Module.” In: *Proceedings of the 2018 Workshop on ns-3*. 2018, pp. 53–60.

[118] Nurzaman Ahmed, Debashis De, Ferdous Ahmed Barbhuiya, and Md Iftekhar Hussain. "MAC protocols for IEEE 802.11 ah-based Internet of Things: A survey." In: *IEEE Internet of Things Journal* 9.2 (2021), pp. 916–938.

[119] Le Tian, Serena Santi, Amina Seferagić, Julong Lan, and Jeroen Famaey. "Wi-Fi HaLow for the Internet of Things: An up-to-date survey on IEEE 802.11 ah research." In: *Journal of Network and Computer Applications* 182 (2021), p. 103036.

[120] Victor Baños-Gonzalez, M Shahwaiz Afaqui, Elena Lopez-Aguilera, and Eduard Garcia-Villegas. "Throughput and range characterization of IEEE 802.11 ah." In: *arXiv preprint arXiv:1604.08625* (2016).

[121] Bojan Domazetović and Enis Kočan. "Packet error rate in IEEE 802.11 ah use case scenarios." In: *2017 25th Telecommunication Forum (TELFOR)*. IEEE. 2017, pp. 1–4.

[122] R Porat. "TGah channel model." In: *IEEE 802.11-11/0968r2* (2011).

[123] Jangeun Jun, Pushkin Peddabachagari, and Mihail Sichitiu. "Theoretical maximum throughput of IEEE 802.11 and its applications." In: *Second IEEE International Symposium on Network Computing and Applications, 2003. NCA 2003.* IEEE. 2003, pp. 249–256.

[124] Julio Cesar Araiza Leon. "Evaluation of IEEE 802.11 ah Technology for Wireless Sensor Network Applications." MA thesis. 2015.

[125] Orod Raeesi, Juho Pirskanen, Ali Hazmi, Toni Levanen, and Mikko Valkama. "Performance evaluation of IEEE 802.11 ah and its restricted access window mechanism." In: *2014 IEEE international conference on communications workshops (ICC)*. IEEE. 2014, pp. 460–466.

[126] James R Norris. *Markov chains*. 2. Cambridge university press, 1998.

[127] Haitao Wu, Yong Peng, Keping Long, Shiduan Cheng, and Jian Ma. "Performance of reliable transport protocol over IEEE 802.11 wireless LAN: analysis and enhancement." In: *Proceedings. Twenty-first annual joint conference of the IEEE computer and communications societies*. Vol. 2. IEEE. 2002, pp. 599–607.

[128] Vu Khanh Quy and Nguyen Dinh Han Le Ngoc Hung. "CEPRM: A cloud-assisted energy-saving and performance-improving routing mechanism for MANETs." In: *Journal of Communications* 14 (2019), pp. 1211–1217.

[129] Ken Duffy, David Malone, and Douglas J Leith. "Modeling the 802.11 distributed coordination function in non-saturated conditions." In: *IEEE communications letters* 9.8 (2005), pp. 715–717.

[130] Linfeng Zheng, Juncheng Hu, and Yingjun Jiao. "A Cross-Layer Media Access Control Protocol for WBANs." In: *Sustainability* 15.14 (2023), p. 11381.

[131] Prasaja Wikanta. "Study and design of a new PHY/MAC Cross-Layer architecture for Wireless Sensor Networks Dedicated to Healthcare." PhD thesis. Université Polytechnique Hauts-de-France, 2021.

[132] Eugenia Cabot and Myles Capstick. *The effect of the human body on wireless microphone transmission*. 2015.

[133] Huan-Bang Li and Ryuji Kohno. "Body area network and its standardization at IEEE 802.15. BAN." In: *Advances in Mobile and Wireless Communications: Views of the 16th IST Mobile and Wireless Communication Summit*. Springer, 2008, pp. 223–238.

[134] H-BL Arthur Astrin and R Patro. *IEEE 802.15 WPAN Task Group 6 (TG6) Body Area Networks*. Tech. rep. IEEE 802.15, Tech. Rep, 2008.

[135] Elisabeth Reusens, Wout Joseph, Günter Vermeeren, and Luc Martens. "On-body measurements and characterization of wireless communication channel for arm and torso of human." In: *4th International Workshop on Wearable and Implantable Body Sensor Networks (BSN 2007) March 26–28, 2007 RWTH Aachen University, Germany*. Springer. 2007, pp. 264–269.

[136] Andrew Fort, Julien Ryckaert, Claude Desset, Philippe De Doncker, Piet Wambacq, and Leo Van Biesen. "Ultra-wideband channel model for communication around the human body." In: *IEEE Journal on Selected Areas in Communications* 24.4 (2006), pp. 927–933.

[137] Guido Dolmans and Andrew Fort. "Channel models wban-holst centre/imec-nl." In: *IEEE 802.15–08-0418-01-0006* (2008).

[138] T Kikuzuki, AS Andrenko, MGS Hossain, I Ida, K Kasai, and Y Ohashi. "A simple path loss model for body area network in the bed side monitoring applications." In: *Asia-Pacific Microwave Conference 2011*. IEEE. 2011, pp. 765–768.

[139] Arafat Al-Dweik, Youssef Iraqi, Hussam Mukhtar, Muhammad Naeem, Ekram Hossain, et al. "Hybrid automatic repeat request (HARQ) in wireless communications systems and standards: a contemporary survey." In: *Authorea Preprints* (2023).

[140] Victor Baños-Gonzalez, M Shahwaiz Afaqui, Elena Lopez-Aguilera, and Eduard Garcia-Villegas. "IEEE 802.11 ah: A technology to face the IoT challenge." In: *Sensors* 16.11 (2016), p. 1960.

[141] Dalei Wu and Song Ci. "Cross-layer design for combining adaptive modulation and coding with hybrid ARQ." In: *Proceedings of the 2006 inter-*

national conference on wireless communications and mobile computing. 2006, pp. 147–152.

[142] David Haccoun and Guy Begin. "High-rate punctured convolutional codes for Viterbi and sequential decoding." In: *IEEE transactions on communications* 37 (1989), pp. 1113–1125.

[143] Harri Holma and Antti Toskala. *WCDMA for umts: hspa evolution and lte*. john Wiley & sons, 2007.

[144] M Pursley and D Taipale. "Error probabilities for spread-spectrum packet radio with convolutional codes and Viterbi decoding." In: *IEEE Transactions on communications* 35.1 (1987), pp. 1–12.

[145] Jeffery M Torrance and Lajos Hanzo. "Upper bound performance of adaptive modulation in a slow Rayleigh-fading channel." In: *Electronics letters* 32.8 (1996), pp. 718–719.

[146] Maruf Mohammad and R Michael Buehrer. "On the impact of SNR estimation error on adaptive modulation." In: *IEEE communications letters* 9.6 (2005), pp. 490–492.

[147] Paul Ferrand, Jean-Marie Gorce, and Claire Goursaud. "Approximations of the packet error rate under slow fading in direct and relayed links." PhD thesis. INRIA, 2013.

[148] Qingwen Liu, Shengli Zhou, and Georgios B Giannakis. "Cross-layer combining of adaptive modulation and coding with truncated ARQ over wireless links." In: *IEEE Transactions on wireless communications* 3.5 (2004), pp. 1746–1755.

[149] IEEE 802.11 g Working Group et al. "Draft amendment to IEEE Std 802.11-1999 Part 11: Wireless LAN Medium Access Control (MAC) and

Physical Layer (PHY) specification: Further higher data rate extension in the 2.4 GHz band." In: *IEEE Std 802.11 g-2003* (2003).

[150] Dustin Maas, Mohammad H. Firooz, Junxing Zhang, Neal Patwari, and Sneha K. Kasera. "Channel Sounding for the Masses: Low Complexity GNU 802.11b Channel Impulse Response Estimation." In: *IEEE Transactions on Wireless Communications* 11.1 (Jan. 2012), 1–8. ISSN: 1536-1276. DOI: 10.1109/twc.2011.111611.091774. URL: http://dx.doi.org/10.1109/twc.2011.111611.091774.

[151] Scott Biddlestone and Keith A. Redmill. "A GNU Radio based testbed implementation with IEEE 1609 WAVE functionality." In: *2009 IEEE Vehicular Networking Conference (VNC)*. IEEE, Oct. 2009. DOI: 10.1109/vnc.2009.5416372. URL: http://dx.doi.org/10.1109/vnc.2009.5416372.

[152] Bastian Bloessl, Michele Segata, Christoph Sommer, and Falko Dressler. "An IEEE 802.11a/g/p OFDM receiver for GNU radio." In: *Proceedings of the second workshop on Software radio implementation forum*. SIGCOMM'13. ACM, Aug. 2013. DOI: 10.1145/2491246.2491248. URL: http://dx.doi.org/10.1145/2491246.2491248.

[153] Zheng RUAN, Rong-Jie GU, and Dong-Li WANG. "Establishing IEEE802.11p Test Platform Based on GNU Radio and USRP." In: *DEStech Transactions on Computer Science and Engineering* aice-ncs (Mar. 2017). ISSN: 2475-8841. DOI: 10.12783/dtcse/aice-ncs2016/5725. URL: http://dx.doi.org/10.12783/dtcse/aice-ncs2016/5725.

[154] Prasaja Wikanta, Andy Triwinarko, Iyad Dayoub, and El Hadj Dogheche. "A Cross Layer Protocol PHY/MAC for Body Pathloss in IEEE 802.11ah IoT Networks." In: *2020 IEEE SENSORS*. IEEE, Oct. 2020. DOI: 10.1109/

sensors47125.2020.9278825. URL: http://dx.doi.org/10.1109/sensors47125.2020.9278825.

[155] Wikipedia contributors. *Software-defined radio*. https://en.wikipedia.org/wiki/Software-defined_radio. Accessed: January 12, 2024. 2024.

[156] Nader Daneshfar. "Performance enhancement mechanism of ieee 802.11 ah machine communication system." MA thesis. 2015.

[157] Hicham Anouar and Christian Bonnet. "Optimal Constant-Window Back-off Scheme for IEEE 802.11 DCF in Single-Hop Wireless Networks Under Finite Load Conditions." In: *Wireless Personal Communications* 43.4 (July 2007), 1583–1602. ISSN: 1572-834X. DOI: 10.1007/s11277-007-9329-5. URL: http://dx.doi.org/10.1007/s11277-007-9329-5.

[158] Bastian Bloessl, Michele Segata, Christoph Sommer, and Falko Dressler. "Performance Assessment of IEEE 802.11p with an Open Source SDR-Based Prototype." In: *IEEE Transactions on Mobile Computing* 17.5 (May 2018), 1162–1175. ISSN: 1536-1233. DOI: 10.1109/tmc.2017.2751474. URL: http://dx.doi.org/10.1109/tmc.2017.2751474.

[159] Bastian Bloessl, Michele Segata, Christoph Sommer, and Falko Dressler. "Towards an Open Source IEEE 802.11 p stack: A full SDR-based transceiver in GNU Radio." In: *2013 IEEE Vehicular Networking Conference*. IEEE. 2013, pp. 143–149.

[160] Michael Rice and F Harris. "Polyphase filterbanks for symbol timing synchronization in sampled data receivers." In: *MILCOM 2002. Proceedings*. Vol. 2. IEEE. 2002, pp. 982–986.

[161] Ryan Reed. “Implementation of a BPSK Transceiver for use with the University of Kansas Agile Radio.” MA thesis. University of Kansas, 2006.

[162] Ping He, T.T. Tjhung, and L.K. Rasmussen. “Constant modulus algorithm (CMA) for CDMA communications systems.” In: *VTC ’98. 48th IEEE Vehicular Technology Conference. Pathway to Global Wireless Revolution (Cat. No.98CH36151)*. VETEC-98. IEEE. DOI: 10.1109/vetec.1998.686380. URL: http://dx.doi.org/10.1109/vetec.1998.686380.

****